BIOMATERIALS FOR CELL-BASED THERAPY

EDITED BY: Liyuan Zhang, Huanan Wang and Xuetao Shi
PUBLISHED IN: Frontiers in Bioengineering and Biotechnology and Frontiers in Materials

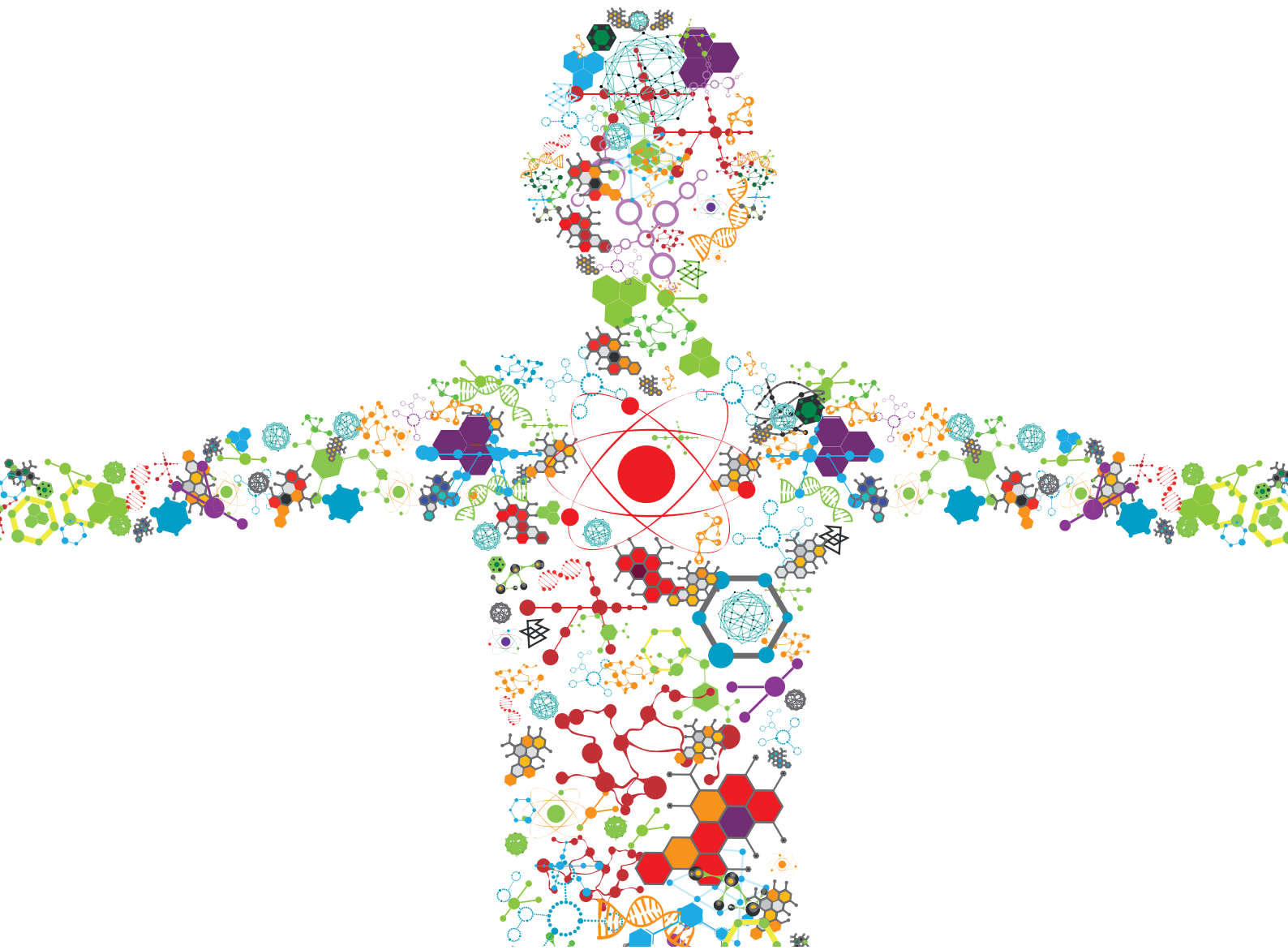

frontiers Research Topics

ISSN 1664-8714
ISBN 978-2-88974-296-7
DOI 10.3389/978-2-88974-296-7

About Frontiers

Frontiers is more than just an open-access publisher of scholarly articles: it is a pioneering approach to the world of academia, radically improving the way scholarly research is managed. The grand vision of Frontiers is a world where all people have an equal opportunity to seek, share and generate knowledge. Frontiers provides immediate and permanent online open access to all its publications, but this alone is not enough to realize our grand goals.

Frontiers Journal Series

The Frontiers Journal Series is a multi-tier and interdisciplinary set of open-access, online journals, promising a paradigm shift from the current review, selection and dissemination processes in academic publishing. All Frontiers journals are driven by researchers for researchers; therefore, they constitute a service to the scholarly community. At the same time, the Frontiers Journal Series operates on a revolutionary invention, the tiered publishing system, initially addressing specific communities of scholars, and gradually climbing up to broader public understanding, thus serving the interests of the lay society, too.

Dedication to Quality

Each Frontiers article is a landmark of the highest quality, thanks to genuinely collaborative interactions between authors and review editors, who include some of the world's best academicians. Research must be certified by peers before entering a stream of knowledge that may eventually reach the public - and shape society; therefore, Frontiers only applies the most rigorous and unbiased reviews.
Frontiers revolutionizes research publishing by freely delivering the most outstanding research, evaluated with no bias from both the academic and social point of view. By applying the most advanced information technologies, Frontiers is catapulting scholarly publishing into a new generation.

What are Frontiers Research Topics?

Frontiers Research Topics are very popular trademarks of the Frontiers Journals Series: they are collections of at least ten articles, all centered on a particular subject. With their unique mix of varied contributions from Original Research to Review Articles, Frontiers Research Topics unify the most influential researchers, the latest key findings and historical advances in a hot research area! Find out more on how to host your own Frontiers Research Topic or contribute to one as an author by contacting the Frontiers Editorial Office: frontiersin.org/about/contact

BIOMATERIALS FOR CELL-BASED THERAPY

Topic Editors:
Liyuan Zhang, Harvard University, United States
Huanan Wang, Dalian University of Technology, China
Xuetao Shi, South China University of Technology, China

Citation: Zhang, L., Wang, H., Shi, X., eds. (2022). Biomaterials for Cell-Based Therapy. Lausanne: Frontiers Media SA. doi: 10.3389/978-2-88974-296-7

Table of Contents

frontiers in Materials

EDITORIAL
published: 16 September 2021
doi: 10.3389/fmats.2021.752277

Editorial: Biomaterials for Cell-Based Therapy

Liyuan Zhang[1]* *and Huanan Wang*[2]*

[1]School of Engineering and Applied Sciences, Harvard University, Cambridge, MA, United States, [2]School of Life Science and Biotechnology, Dalian University of Technology, Dalian, China

Keywords: cell encapsulation, biomaterials, MSC, stem cell therapy, IPS

Editorial on the Research Topic

Biomaterials for Cell-Based Therapy

Cells are becoming one of the most important and promising forms of therapy. The use of cells as therapeutics has stimulated numerous new therapeutic companies that have reached valuations of billions of dollars. Stem cells, such as embryonic stem cells, iPSCs (pluripotent stem cells), and adult stem cells, are being used to regenerate human tissue for autologous and allogeneic therapy and for autoimmune disease. It offers the perfect solution when there is a need for tissue and organ shortage or organ transplantation, differentiating into specific cell types that are required for tissue repair. Immune cells can be collected directly from patients, engineered for new functionality, and injected into patients as a key component of immunotherapy. For instance, the use of hematopoietic stem cell transplantation can broadly be broken down into autologous cell transplants, represented by ~2,000 patients per year and ~8,000 for allogeneic transplants in the US. Cells directly injected into the body are not very effective in performing their tasks and are instead rapidly degraded, making the process very inefficient. Moreover, this often induces graft versus host disease (GVHD), a highly morbid complication that kills allogeneic transplant patients, making this an even more complex process. Thus, researchers are constantly searching for new strategies that are stable, safe, and easily accessible for stem cells, maintaining their potential to differentiate into several lineages.

Encapsulating cells in biodegradable micron-scale hydrogels offers numerous attractive features for tissue engineering, such as a highly hydrated tissue-like environment for cell and tissue repair, and the ability to form *in vivo*. The efficacy of cell-based therapies depends on materials science. Many materials properties have to be considered for the design of a hydrogel-based scaffold that mimics the extracellular matric, such as mechanical properties, degradation, and mass transfer and diffusion. Moreover, the fabrication process is critical for maintaining cell function and also is closely linked to the crosslinked structure of the hydrogel. All these considerations have posed a deep barrier for selectively choosing suitable materials for cell encapsulation. The main biopolymers that can be used to form a gel that mimics the extra-cellular matrix are alginate, gelatin, collagen, and fibrin. Most of these biopolymers need to be functionalized before forming a delivery vehicle for cells, which could potentially largely damaged cell viability. Furthermore, large quantities are essential for clinical application, where the amount required gram of cell-laden microgels that are not easy to fabricate under the current strategy. All these hindrances need to be removed before the broad application of cell-laden microgel for cell therapy.

In this Research Topic, we present a state-of-the-art study for the investigation of the therapeutic effect of various stem-cell-based therapy for various diseases treatment. There are totally three main subjects on cell-based therapy. First, we have materials, which are mainly hydrogels or their derived materials for encapsulating, delivering, and regulating the cell and

OPEN ACCESS

Edited and reviewed by:
Hasan Uludag,
University of Alberta, Canada

***Correspondence:**
Liyuan Zhang
liyuanzhang1987@gmail.com
Huanan Wang
huananwang@dlut.edu.cn

Specialty section:
This article was submitted to Biomaterials, a section of the journal Frontiers in Materials

Received: *02 August 2021*
Accepted: *24 August 2021*
Published: *16 September 2021*

Citation:
Zhang L and Wang H (2021) Editorial: Biomaterials for Cell-Based Therapy. Front. Mater. 8:752277. doi: 10.3389/fmats.2021.752277

cell behavior. For example, Sivaraj et al. have summarized the current hydrogel-based materials. Yang et al. have introduced an injectable glycol chitosan/dibenzaldehyde terminated PEG for cartilage defect repair. Lewicka et al. has employed silk protein matrices to regulate the differentiation of neural stem cells. Xu et al. have shown the hDPSCs for pancreatic disease, Second, there is the new encapsulation approach. Shao et al. have introduced a microfluidic-based technique for cell encapsulation. Third, there is the new delivery system; Li and Liu have engineered bacterial outer membrane vesicles as the new delivery platform. We also present the importance of considering designing biodegradable biomaterials for cell encapsulation and highlight recent advances in hydrogel design and their application. We are confident that the studies collected in this issue establish a new benchmark for the solution and new technologies for reprogramming stem cells as well as immune cells for a deeper understanding of stem cell differentiation, stem-cell-based tissue regeneration, and their stem cell recovery mechanisms.

AUTHOR CONTRIBUTIONS

All authors listed have made a substantial, direct, and intellectual contribution to the work and approved it for publication.

Conflict of Interest: The authors declare that the research was conducted in the absence of any commercial or financial relationships that could be construed as a potential conflict of interest.

frontiers in Bioengineering and Biotechnology

REVIEW
published: 31 March 2020
doi: 10.3389/fbioe.2020.00247

Advances of Stem Cell-Laden Hydrogels With Biomimetic Microenvironment for Osteochondral Repair

Bingbing Xu[1†], Jing Ye[1†], Fu-Zhen Yuan[1], Ji-Ying Zhang[1], You-Rong Chen[1], Bao-Shi Fan[2], Dong Jiang[1], Wen-Bo Jiang[3], Xing Wang[4,5] and Jia-Kuo Yu[1*]*

[1] Knee Surgery Department of the Institute of Sports Medicine, Peking University Third Hospital, Beijing, China, [2] School of Clinical Medicine, Weifang Medical University, Weifang, China, [3] Clinical Translational R&D Center of 3D Printing Technology, Shanghai Ninth People's Hospital, Shanghai Jiao Tong University School of Medicine, Shanghai, China, [4] Beijing National Laboratory for Molecular Sciences, State Key Laboratory of Polymer Physics & Chemistry, Institute of Chemistry, Chinese Academy of Sciences, Beijing, China, [5] University of Chinese Academy of Sciences, Beijing, China

OPEN ACCESS

Edited by:
Xuetao Shi,
South China University of Technology, China

Reviewed by:
Chao Liu,
Kyoto University, Japan
Weizhi Chen,
Nanjing University, China

***Correspondence:**
Xing Wang
wangxing@iccas.ac.cn
Jia-Kuo Yu
yujiakuo@126.com

[†]These authors have contributed equally to this work

Specialty section:
This article was submitted to Biomaterials, a section of the journal Frontiers in Bioengineering and Biotechnology

Received: 23 January 2020
Accepted: 10 March 2020
Published: 31 March 2020

Citation:
Xu B, Ye J, Yuan F-Z, Zhang J-Y, Chen Y-R, Fan B-S, Jiang D, Jiang W-B, Wang X and Yu J-K (2020) Advances of Stem Cell-Laden Hydrogels With Biomimetic Microenvironment for Osteochondral Repair. Front. Bioeng. Biotechnol. 8:247. doi: 10.3389/fbioe.2020.00247

Osteochondral damage from trauma or osteoarthritis is a general joint disease that can lead to an increased social and economic burden in the modern society. The inefficiency of osteochondral defects is mainly due to the absence of suitable tissue-engineered substrates promoting tissue regeneration and replacing damaged areas. The hydrogels are becoming a promising kind of biomaterials for tissue regeneration. The biomimetic hydrogel microenvironment can be tightly controlled by modulating a number of biophysical and biochemical properties, including matrix mechanics, degradation, microstructure, cell adhesion, and intercellular interactions. In particular, advances in stem cell-laden hydrogels have offered new ideas for the cell therapy and osteochondral repair. Herein, the aim of this review is to underpin the importance of stem cell-laden hydrogels on promoting the development of osteochondral regeneration, especially in the field of manipulation of biomimetic microenvironment and utilization growth factors with various delivery methods.

Keywords: stem cell-laden hydrogels, microenvironment, extracellular matrix, osteochondral tissue engineering, regenerative medicine

INTRODUCTION

Osteochondral interface defects generally involve lesions in articular cartilage and subchondral cartilage. Cartilage is essentially avascular and less cellular, and lacks the ability to repair itself (Abdel-Sayed and Pioletti, 2015). Meanwhile, if cartilage defects are not treated, joints will gradually and irrevocably deteriorate, leading to severe osteoarthritis and eventually disability (Chen et al., 2011). Current treatment strategies for osteochondral defects mainly include the microfracture (bone marrow stimulation) (Dasar et al., 2016), auto-transplantation and allografts of osteochondral (VanTienderen et al., 2017), and autologous chondrocyte implantation (Beck et al., 2018). Despite their widespread usage in the actual clinic, there are still obvious and inevitable limitations and shortcomings. For example, microfracture treatment may cause the formation of fibrocartilage with poor biological function (Steinwachs and Kreuz, 2007; Becher et al., 2019). Autologous chondrocyte implantation has been applied for 20 years in clinic, but there are still disadvantages like shortage source and long harvest time of chondrocyte, periosteal hypertrophy

and ablation (Lohan et al., 2013), and low effectiveness for elderly patients (Giannoni et al., 2005). Allografts are plagued by limited supply, immune rejection, insufficient integration, and low cell viability. Autologous transplantation lacks integration and tissue sources, and requires additional surgery that may induce the potential disease at the donor site (Bal et al., 2010; Sartori et al., 2017). Compared to the above-mentioned strategies, osteochondral tissue engineering has been proposed and approved for more effective treatment, among which the stem cell research has been of great importance in the biomedical and tissue regenerations.

Tissue engineering, consisting of scaffolds, cells and favorable growth factors, has evolved into the most promising therapeutic strategy for cartilage tissue reconstruction (Huang et al., 2018; Wang et al., 2018). In order to achieve perfect regeneration of damaged cartilage, biodegradable scaffolds must be provided to simulate local characteristics of specific tissues, transport growth factors and tissue cells for newly formed tissues (Polo-Corrales et al., 2014). In the best case, cartilage tissue-engineered scaffolds should be characterized by porous, non-toxic, biodegradable, biocompatible, and promoted cell differentiation and tissue regeneration. In order to construct an ideal tissue-engineering program, it is important to design a functional biomaterial that essentially mimics the natural extracellular matrix (ECM) component of cartilage. Traditional methods typically include the precise incorporation of bioactive growth factors into target tissue, the use of cell-free scaffold biomaterials, and mimic natural ECM with the use of cell-laden building scaffolds, especially for three-dimensional (3D) porous scaffolds, which are the most commonly used biomaterials to facilitate cell organization into ECM during reconstruction (Ansboro et al., 2014; Du et al., 2014; Bernhard and Vunjak-Novakovic, 2016).

As a most promise of future tissue engineering and regeneration, stem cells with multidirectional differentiation potentials can be used to promote tissue growth, metabolism, repair and microenvironmental stability. Stem cells are characterized by their ability to self-renew and differentiate into various mature cells, which have inspired the development of biomedical science (Madl and Heilshorn, 2018), including the applications of regenerative medicine methods, repair or replacement of damaged tissues, disease modeling, and pharmacology screening platforms. However, simulating the unique biological functions of articular cartilage remains a challenge, because the composition and regional structure of these joints is highly complex. Tissue engineering methods offer appropriate biomaterials as artificial ECM to promote stem cell growth, proliferation and differentiation at defect sites, leaving the regeneration of articular cartilage to the involved natural biological processes that stem cells can interact with soluble factors. Stem cells reside in a specialized microenvironment *in vivo*, called the stem cell niche which is both dynamic and complex (Li and Xie, 2005; McClenahan et al., 2016). Biophysical and biochemical factors form the niche that guides the fate of resident stem cells. Many of these factors are provided by the microstructure, biochemical composition and mechanical properties of the ECM. In the field of tissue engineering, it is a popular strategy to control engineered niches by using the characteristics of scaffold materials to guide the differentiation and maturation of stem cells into functional tissue constructs.

Hydrogels are consisting of natural or synthetic hydrophilic polymer chains connected to each other at the crosslinking point, which have a unique 3D crosslinked polymer network covering a wide range of chemical compositions and physical properties (Paschos et al., 2015; Liu et al., 2016). The natural hydrophilicity of polymer chains enables hydrogels to absorb a certain amount of water and be applied in various technical biomaterials for drug delivery and tissue regeneration. Especially, *in situ* hydrogels have the advantages of simple drug preparation and strong ability to deliver drugs, peptides and cells. Hydrogels have a unique combination similar to natural ECM and are attractive biomaterials for the osteochondral tissue engineering. The hydrogel microenvironment can be strictly controlled through the adjustment of many biophysical and biochemical properties, such as the matrix mechanics, degradability, microstructure, cell adhesion, and cell-cell interactions (Brown and Anseth, 2017; Jekhmane et al., 2019). These properties can be easily manipulated to suit for a variety of biomedical applications (Sun et al., 2018). Therefore, stem cell-hydrogel constructs could be personalized for patients using the advanced technology. Hydrogels that combine stem cells and growth factors have great potential to challenge regeneration of osteochondral defects. In the past decade, basic research on osteochondral tissue engineering of stem cell-laden hydrogels systems with biomimetic microenvironment has achieved remarkable success, bringing promise for osteochondral tissue repair (Li et al., 2018; Xu et al., 2019).

This review will focus on the importance and development of biomimetic microenvironment using the engineering cell-laden hydrogels on promotion of osteochondral tissue engineering and regeneration medicine fields, mainly including extracellular matrix, engineered matrix degradation, microarchitecture, cell-adhesive ligands, and cell-cell interactions. We also summarize the strategies for repairing cartilage defects by stem cell-laden hydrogels and discuss how various growth factors and delivery methods affect stemness maintenance and differentiation to facilitate the chondrogenesis or osteogenesis within the hydrogels. Finally, we provide some suggestions and prospects on developing stem cell-laden hydrogels via tailoring of their biomimetic microenvironment (e.g., physicochemical and mechanical properties) for effective osteochondral tissue engineering. Understanding medical needs and concurrently lessening the difficulty of hydrogel construction should therefore be the goal for future research in regeneration medicine fields.

EFFECTS OF BIOMIMETIC MICROENVIRONMENT ON THE ENGINEERING HYDROGELS

The stem cell niche consists of a myriad of interacting ECM components, which can provide many biophysical and biochemical inputs to regulate the stem cell functions such as cell populations, self-recovery, quiescence, differentiation, etc. (Xie and Spradling, 2000). The most important factors are the

interactions among the stem cells, neighboring differentiated cells and ECM (Morrison et al., 1997). Additionally, other factors like oxygen level, ion concentration, growth factors, and cytokines also play important roles (Drueke, 2006; Scadden, 2006; Hsu and Drummond-Barbosa, 2009; Eliasson and Jonsson, 2010). In this section, we will focus on the effects of matrix mechanics, on-demand degradation, microstructure, cell-adhesive ligands and cell-cell interactions for maintaining and regulating stem cells in the engineering hydrogels (Fuchs et al., 2004).

Extracellular Mechanics

ECM, mainly including geometry, elasticity and mechanical signals, provides the necessary stimuli to control the shape, activity, and migration of stem cell (Lv et al., 2015). Especially, mechanical forces from the ECM and subsequent alterations in intracellular tension can regulate stem cell differentiation via the cytoskeletal tension and RhoA-ROCK pathway activation (Shah et al., 2014). As for the tissue engineering, extracellular mechanics like stiffness and viscoelasticity play important roles in the signal pathways between cells to tailor the stem cell proliferation behaviors and regenerative qualities (Hoben et al., 2008; Chang and Knothe Tate, 2011).

Extracellular Stiffness

Stiffness is typically described by an elastic or Young's modulus, which is defined as the ratio of applied stress (i.e., force per area) to strain (i.e., relative deformation) for small perturbations. ECM can be recognized as a cross-linked polymer network, possessing the time-independent stiffness behavior. This mechano-sensing ability can affect the fundamental cellular functions. With this understanding, development of stiffness hydrogels is useful for researching the mechanical interactions between stem cells and extracellular environments. For example, Kim et al. developed a linear stiffness gradient hydrogel via tailoring the polymerization of gelatin methacryloyl (GelMA) with a gradient UV photomask for stem cell mechano-sensation and differentiation abilities (**Figure 1**; Kim et al., 2020). Furthermore, they also found human adipose-derived stem cells (hADSCs) could increase chondrogenic roles *in vivo* by controlling the stiffness of cell-free and cell-embedded fibrin hydrogel; in this case, optimal scaffolds could promote both cell survival and chondrogenic potential for cartilage tissue engineering (Jung et al., 2010).

Extracellular Viscoelasticity

Besides for the commonly used elastic hydrogel systems to tailor stem cell mechanobiology and activity, natural ECM components are also viscoelastic materials with stress-relaxation behavior (Levental et al., 2007; Geerligs et al., 2008). Hydrogels composed of reconstituted ECM proteins like collagen and fibrin exhibit stress relaxation in response to a constant load pressure (Isono and Nishitake, 1995), because polymer chains within the network can rearrange in order to dissipate the applied force from the molecular level. Thus, recent efforts have been directed toward designing hydrogels with tuneable viscoelasticity to recapitulate the ECM and cell interactions (Haugh and Heilshorn, 2016). Li et al. synthesized a kind of GG/PEGDA DN hydrogel through the linkage of gellan gum (GG) with polyethylene glycol diacrylate (PEGDA) to offer physical environment for mesenchymal stem cells (MSCs) proliferation, spreading, chondrogenic differentiation and cartilage tissue engineering (**Figure 2**; Li et al., 2020). Xie et al. also found that viscoelasticity played a significant role in expanding seed cells for articular cartilage tissue engineering and regeneration (Xie et al., 2019).

Matrix Degradation

Matrix degradation of the ECM affects stem cell proliferation, self-recovery, quiescence and differentiation through the integrins (Daley et al., 2008), because the cell-secreted enzymes

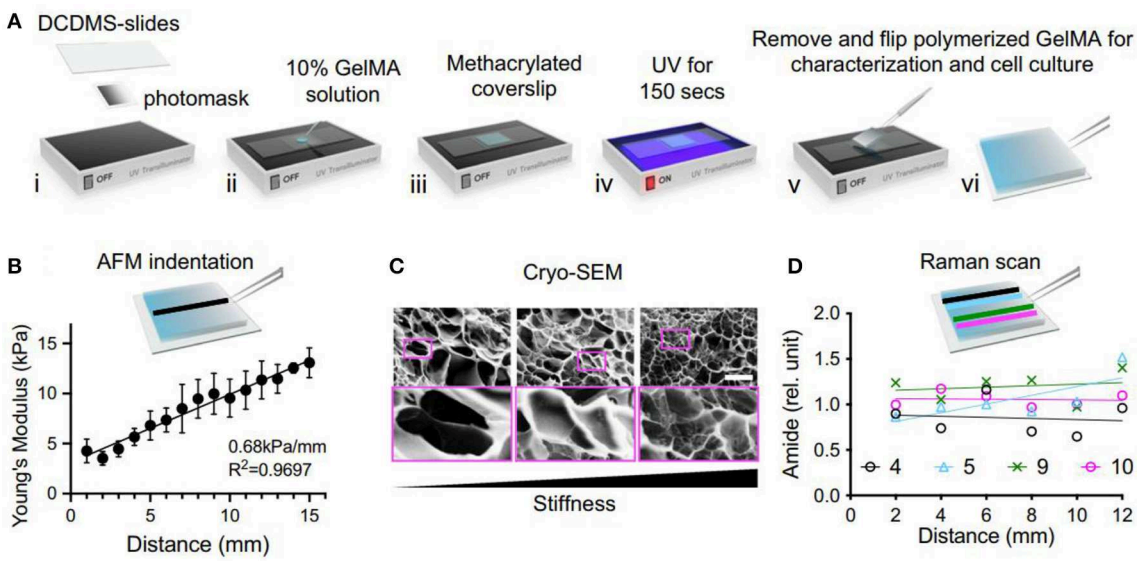

FIGURE 1 | The fabrication and characterization of GelMA stiffness gradient hydrogel. **(A)** Schematic of UV polymerization. **(B)** Atomic force microscopy (AFM) measurement. **(C)** Images from cryo-Scanning electron microscopy (SEM) showed an inverse correlation to stiffness. **(D)** Raman scanning does not show a significant change in amide amount on the stiffness gradient. Reproduced with permission from Kim et al. (2020).

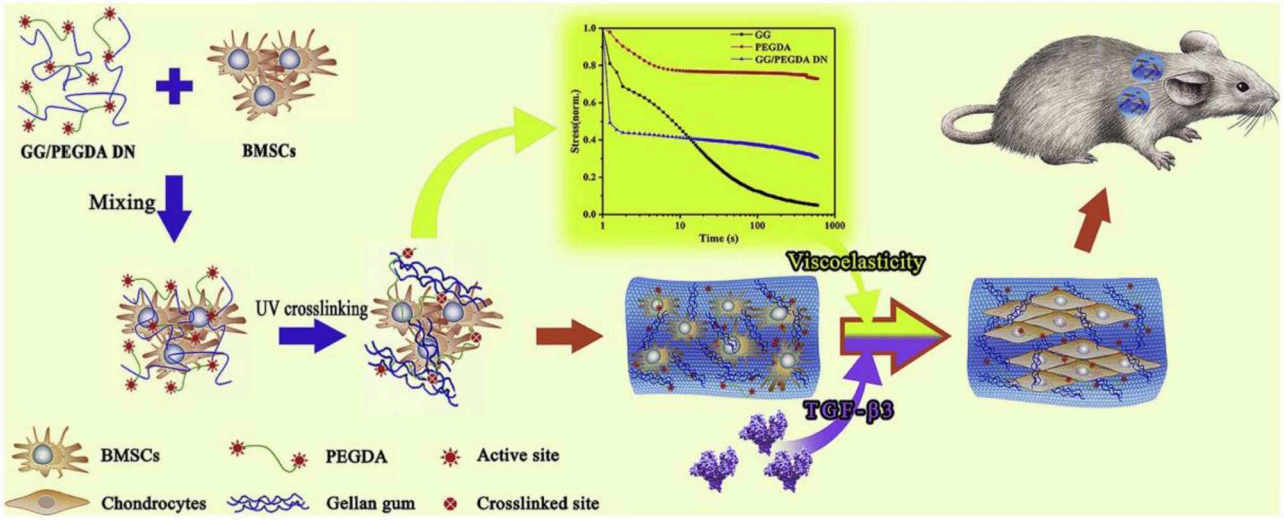

FIGURE 2 | Schematic illustration of experimental approach of bone marrow-derived mesenchymal stem cells (BM-MSCs) encapsulated in GG/PEGDA DN hydrogels and chondrogenic differentiation *in vivo*. Reproduced with permission from Li et al. (2020).

can degrade the native ECM to upgrade the cell spreading and migration capacities through the matrix. By mimicking this dynamic matrix degradation for 3D cell culture, engineered hydrogel had been well-developed by passive hydrolysis of ester crosslinkers for polyethylene glycol (PEG) hydrogels (Sawhney et al., 1994; Bryant et al., 2004). In addition, introduction of enzyme can significantly promote the degradation behaviors to permit cell-mediated remodeling. Lutolf et al. prepared a kind of PEG hydrogels with peptides susceptible to cleavage by matrix metalloproteinases (MMPs). Altering the amino acid sequence of peptide cause the various affinity of MMPs for the peptides, thus controlling the hydrogel degradation kinetics (Park et al., 2004). Kloxin et al. developed a photodegradable PEG hydrogel system that possessed the selective degradation behavior with spatial and temporal material resolution; in this case, mechanics, mesh size and swelling property of hydrogels were necessarily tailored similar to modulating 3D stiffness methods (Kloxin et al., 2009).

Microarchitecture

The innate hierarchical structure and composition distribution of the musculoskeletal tissue interface is destroyed and replaced by fibrotic tissue in the case of disease and degeneration. The focus of the tissue-engineering strategy is to restore the transitional complexity found at the junction of regenerative medicine. For bio-mimicking the 3D contexts, strategies for generating biomimetic fibrous topographies are urgently needed by designing the substrates with well-defined engineered features like grooves, pits and pillars with the order of hundreds of nanometers to tens of micrometers (Lu et al., 2016). Common techniques for producing macroporous hydrogels contain microparticle template, freeze dry, and gas foam (Kuo and Ma, 2011), which represents a class of 3D materials with engineered topographical variation. In addition, cross-linking of hydrogel microribbons (Han et al., 2013) and self-assembly of microgels (Griffin et al., 2015) have also been recognized as alternative techniques to gain architecture hydrogels. Due to limitations in material fabrication techniques, pore size is known as a key factor for cells to interact with the implanted hydrogel materials, thereby 3D architecture can modify the transport properties of cellular microenvironments and endow an additional mechanism to modulate the stem cell microenvironment (Wolf et al., 2014). For example, Zhu et al. constructed an injectable continuous stratified scaffold and designed multiple cell systems to enhance the osteochondral regeneration. The biomimetic constructs of structure and function not only stimulated the regeneration of hyalcartilage and subchondral bone, but also promoted integration of newly formed tissue with the host tissue (Zhu et al., 2019).

Cell-Adhesive Ligands

Specific cell-matrix adhesion is required for cell spreading, migration and mechano-sensing via cell surface receptors. In particular, a class of heterodimeric receptors as integrins link the intracellular cytoskeleton to the specific cell-adhesive ligands on ECM proteins (Barczyk et al., 2010). Tripeptide arginine-glycine-aspartic acid (RGD) is found in multiple ECM proteins and binds to several different integrin dimers, which facilitates cell spreading and migration (Cao et al., 2016) and has been incorporated into hydrogel systems to construct the adhesion of various cell types (Hersel et al., 2003; Cipriani et al., 2019). Besides, combinations of other ligands with RGD are also necessary to elicit the desired behaviors. In order to solve the difficulty in the ligand interactions, ligand concentrations, identity and nanoscale spacing of cell-adhesive ligands should be optimized to regulate the cell activity (Jongpaiboonkit et al., 2008; Lam et al., 2015). Therefore, strategies to pattern adhesive ligands in hydrogels have been developed to control cellular access to adhesive cues by cell-matrix adhesion (Luo and Shoichet, 2004; Ekerdt et al., 2013). An alternative strategy had been to incorporate photocaged adhesive peptides into the hydrogels that were initially inaccessible for cell binding (Wirkner et al., 2011). In these systems, many photochemical approaches to hydrogel

modification above have been employed to temporally control ligand availability (**Figure 3**; Lee et al., 2015). Kloxin et al. used the photoreactive methods to control the hydrogel degradation for selectively releasing the RGD peptides and decreasing the adhesivity after a defined culture interval (Kloxin et al., 2009). Boekhoven et al. applied the host-guest interactions to display RGD peptides from alginate surfaces. Surfaces initially presenting cell-adhesive RGD peptides could be rendered non-adhesive by addition of a control peptide with a stronger host-guest binding partner (Boekhoven et al., 2013). Other self-assembly approaches have also been employed complementary leucine zipper peptides (Liu et al., 2010) and complementary DNA strands to achieve dynamic control over ligand presentation dynamics (Zhang et al., 2013).

Cell-Cell Interactions

Differentiated progeny and heterologous cells communicate with direct cell-cell contact and the secretion of soluble factors, thus continuously exchanging signals related to stem cell fate, activity and differentiation. Among them, direct cell-cell contact was usually achieved through three main types of cellular junctions: gap junctions, tight junctions and adherent junctions (**Figure 4A**; Paschos et al., 2015). Optimized co-culture of stem cells with other cell types allows stem cells to remain pluripotent or trigger differentiation into the desired lineage (Kaji et al., 2011; Paschos et al., 2015).

The natural ECM components contain the binding motifs of various soluble signals, for instance, the growth factors. These natural interactions inspired the desired engineering bioactivity of artificial stem cell niches. Earlier studies have shown that growth factors immobilized on solid substrates kept the biological activity of stem cells (Kaji et al., 2011) and more effective than their soluble counterparts in some cases (Tamama et al., 2006). It is more biomimetic for localizing cell-secreted factors to incorporate charged polysaccharides to sequester growth factors (Hortensius and Harley, 2013) or peptide sequences binding the secreted ECM proteins (Cook et al., 2017). Instead, growth factors are designed to increase the effectiveness of these factors by increasing their longer-term interaction with natural ECM (Martino et al., 2014). Many biological processes, e.g., cell migration and tissue morphogenesis, are more sensitive to the concentration gradient of soluble factors than

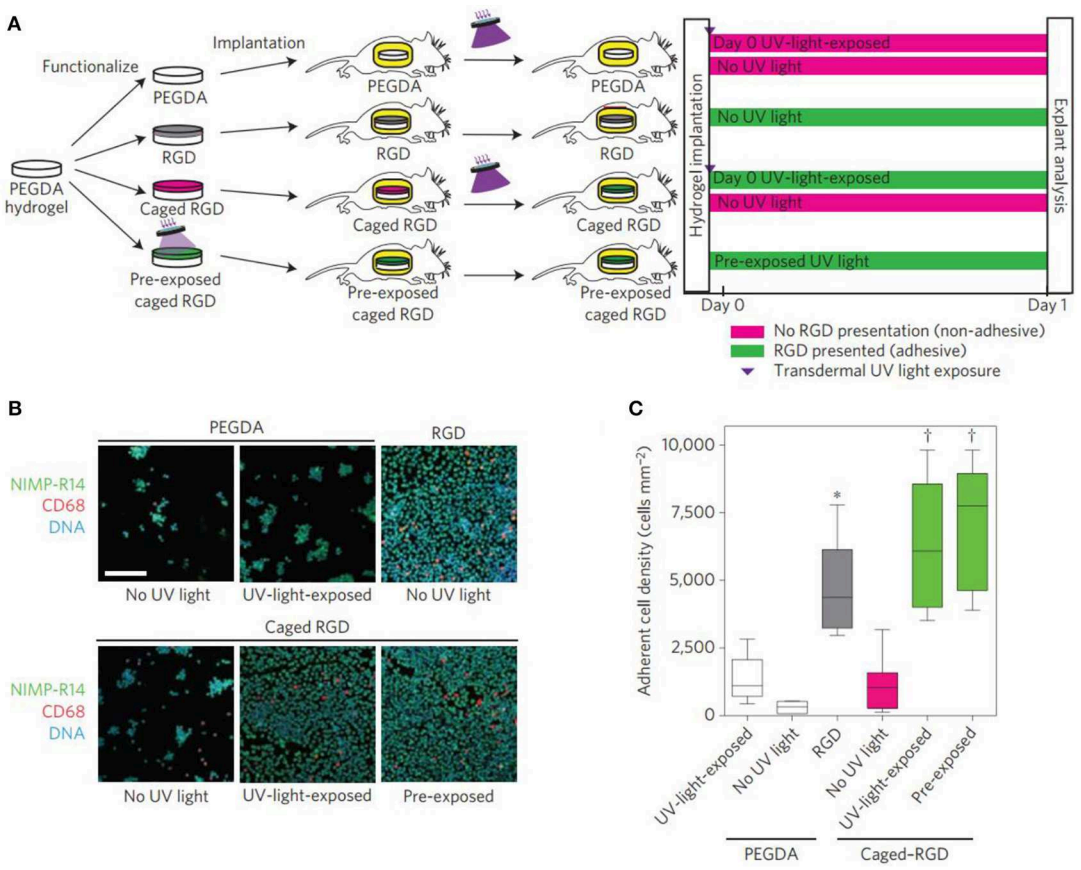

FIGURE 3 | Transdermal activation of *in vivo* inflammatory cell adhesion. **(A)** Schematic representation of the time line for *in vivo* activation of cell adhesion using transdermal UV light exposure. **(B)** Photographs of explanted hydrogels stained for adherent inflammatory cells (green, NIMP-R14 (neutrophil); magenta, CD68 (macrophage); blue, DAPI (DNA); scale bar = 80 μm). Reproduced with permission from Lee et al. (2015). **(C)** Adherent cell density, box-whisker plot for 6–8 mice per group, demonstrating light-based triggering of inflammatory cell adhesion to caged RGD-presenting implants. ANOVA $p < 0.0001$, $^{***}p < 0.05$ vs. UV-light-exposed PEGDA, $^{\dagger}p < 0.001$ vs. no-UV-light caged RGD.

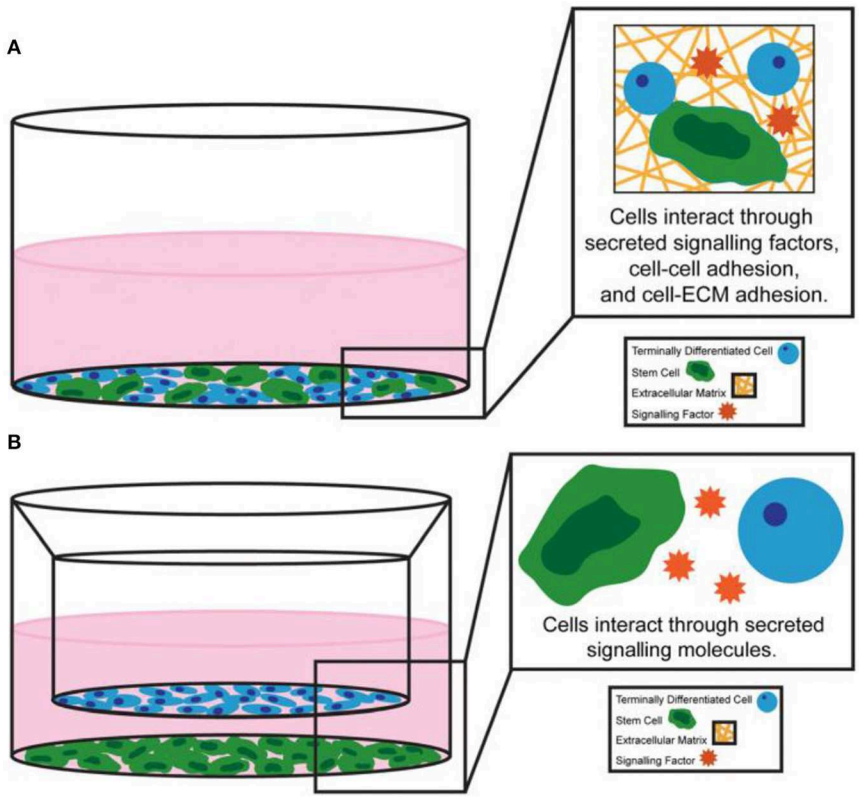

FIGURE 4 | Examples of **(A)** direct co-culture system and **(B)** indirect co-culture system. Reproduced with permission from Paschos et al. (2015).

to their uniform expression. Various engineering strategies have been applied to generate gradients in hydrogel systems, such as microfluidic devices and spatial patterns of growth factor-chelating molecules (Kim et al., 2014).

In addition, stem cells can interact with other niche cells by the indirect cell-cell contact (**Figure 4B**; Paschos et al., 2015). Cell adhesion molecules were immobilized to the surface by fusing immunoglobulin Fc domain of the e-cadherin cell outfield in the early engineering system experiments (Miki et al., 2008). Recently, HAVDI peptides have been conjugated to hyaluronic acid (HA) hydrogels through the mediation of n-cadherin (Nagaoka et al., 2002). In addition to cadherin-mediated contact, peptide sequences that simulate the activity of neural cell adhesion molecule were incorporated into engineered elastin like protein materials (You et al., 2015).

BIOLOGICAL REGULATORY FACTORS FOR CHONDROGENESIS AND THEIR DELIVERY METHODS OF MSCs-LADEN HYDROGELS

Biological Regulatory Factors for Chondrogenesis

The native ECMs could separate biological regulatory factors for promoting cell proliferation and differentiation. These biological regulatory factors include multiple signaling pathways, including transforming growth factor beta (TGF-β)/bone morphogenic proteins (BMPs), fibroblast growth factors (FGFs), hedgehog, notch, Wnt/β-catenin, angiogenic, and hypoxia signaling pathways. Many biomodulators of chondrogenesis provide multiple methods to induce chondrogenic formation and differentiation in MSCs (**Figure 5**; Green et al., 2015). Current research indicates that TGF-β proteins were the most effective inducers of chondrogenesis in human mesenchymal stem cells (hMSCs) among regulatory factors involved in regulating chondrogenesis (Stevens et al., 2004; Jin et al., 2007; Zhao and Hantash, 2011).

Delivery of Biological Regulatory Factors

There are five ways to deliver biological regulators: freeform in medium, physical mixing in hydrogel, microencapsulation, covalent bond with hydrogel, and gene delivery.

Freeform in Medium

Free-form biomodulator delivery in culture medium is an effective method for culture of engineered cell-laden hydrogel osteochondral constructs *in vitro*. During the monolayer expansion process before hydrogel encapsulation, it was found that MSCs exposed to TGF-β3 in culture medium can form chondrocyte populations of different maturities at 7 and 14 days (Lam et al., 2014). The specially designed two-chamber well-provides both osteogenic and chondrogenic stimulation by

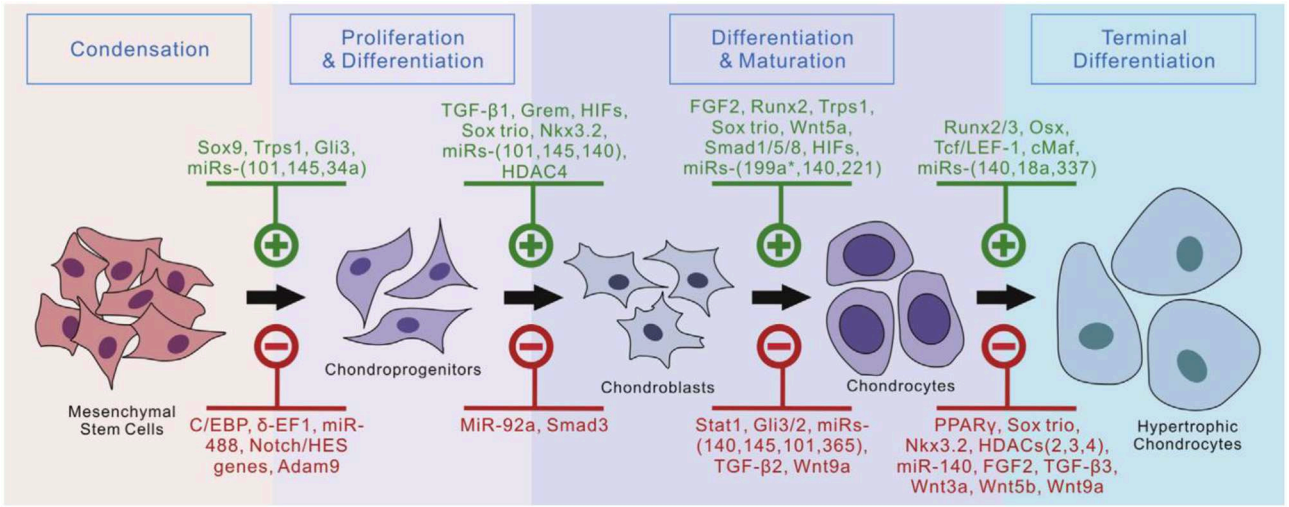

FIGURE 5 | Currently identified regulators of chondrogenic differentiation from MSCs. Reproduced with permission from Green et al. (2015).

freeform biomodulator in medium to rabbit BM-MSCs located in different areas of the scaffold (Chen et al., 2016). However, the need for frequent administration to maintain the concentration and biological activity of biological regulators in the medium is not best for the long-term culture of tissue-engineering.

Physical Mixing in Hydrogel

Encapsulating biological regulatory factors into the hydrogels is a simple and efficacious way for sustained release. BMP-2 can be delivered through MMP-based sensitive hydrogels to promote osteochondral repair *in vivo* (Holloway et al., 2014). Oligo [poly(ethylene glycol) fumarate] hydrogel composites containing TGF-β1-loaded gelatin microparticles and MSCs were implanted in osteochondral defects and facilitated subchondral bone formation (Guo et al., 2010). α2β1 integrin-specific peptide (GFOGER)-functionalized hydrogels with MSCs can continuously release low doses of BMP-2 around the periphery and enhance bone repair capabilities (Shekaran et al., 2014). Delivering biological regulators through encapsulation in hydrogels may require no multiple dosages and may keep release for several weeks, which was beneficial for osteochondral tissue engineering. And the delivery could apply to the formation of cartilage *in vivo*. However, the efficiency of chondrogenic induction may be limited by the fact that the amount of biological regulator from hydrogels significantly decreases over time.

Microencapsulation

The controlled local delivery of growth factors is another applicable strategy for cultivating engineered osteochondral constructs by MSCs. For this purpose, chondrocyte cells growth factors could be loaded into microencapsulation and further embedded in different regions of the constructs (Kim et al., 2016). In order to investigate the use of transplantable constructs for cartilage repair, Bian et al. studied the co-encapsulation of TGF-β3 containing alginate microspheres and hMSCs in HA hydrogels. HA hydrogel constructs inoculated with MSCs and microspheres containing TGF-β3 had comparable mechanical properties and cartilage matrix content compared to those continuously added TGF-β3 in the medium, while those directly encapsulated in a gel containing no microspheres had poor performance (**Figure 6**; Bian et al., 2011). The constructs including TGF-β3 microspheres also formed excellent cartilage matrix after implanted subcutaneously in nude mice. Moshaverinia et al. develop a novel co-delivery system based on TGF-β1 loaded RGD-coupled alginate microspheres encapsulating dental MSCs. And ectopic cartilage tissue regeneration has been observed inside and around the transplanted microspheres in animal studies (Moshaverinia et al., 2013). Although this approach is very useful to control release speed and improve delivery efficiency, the process may add complexity to the preparation and design of scaffolds.

Covalent Bond With Hydrogel

Hydrogel systems allow chelating biological regulatory factors through covalent binding, which has advantages over other delivery ways. Since the diffusion of small molecular weight proteins in hydrogels is very rapid, the strategy of immobilizing growth factors in the bioactive, physiologically related hydrogel-microenvironment is an important step in guiding cells to regenerate cartilage tissue. Benoit et al. first controlled the induction of multiple hMSC lineages purely by interacting with small molecular chemical functional groups bound to the hydrogel materials (Benoit et al., 2008). The proliferation of encapsulated cells and the production of cartilage ECM were increased by immobilizing TGF-β1 to thiol-ene PEG hydrogel by covalent bounds over a period of 28 day (Sridhar et al., 2014), which levels exceeded those of cells in hydrogels in culture medium with dosed TGF-β1 or untreated. Such growth factor delivery methods by simple chemistry to control high levels of cell proliferation and differentiation would be particularly powerful because they are simpler, cheaper and easier to control.

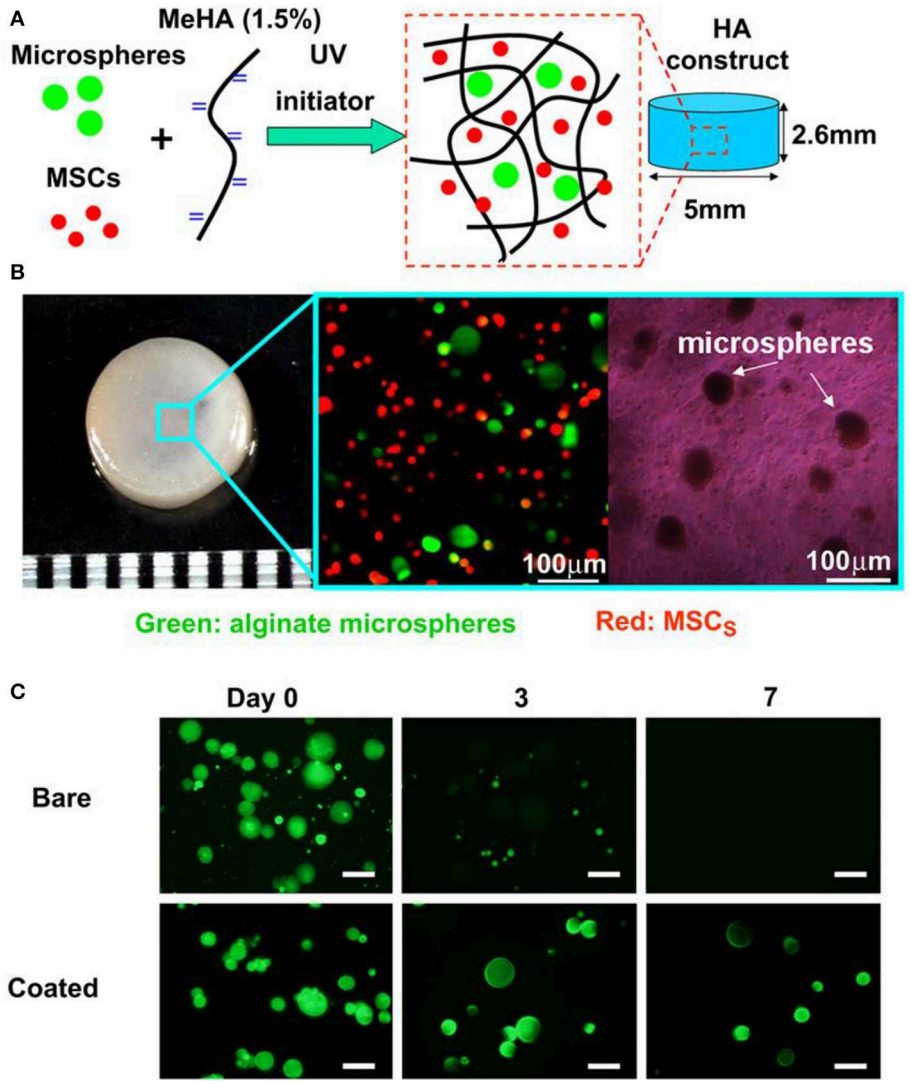

FIGURE 6 | Microencapsulation preparation and *in vitro* culture. Photoencapsulation of alginate microspheres and MSCs into Methacrylated HA (MeHA) hydrogel disks **(A)**; fabricated HA hydrogel disk and fluorescent and bright field microscopic images of MSCs (membrane labeled with red dye) and alginate microspheres (containing FITC-labeled protein) encapsulated in HA gels **(B)**; release of encapsulated BSA-FITC from bare and coated alginate microspheres over 7 days in PBS **(C)**, scale bar = 50 μm. Reproduced with permission from Bian et al. (2011).

Gene Delivery

Integrating therapeutic genes into biomaterials is a new method of delivering regulatory factors that promote tissue regeneration. Non-viral gene therapy may provide more physiological, long-lasting and cost-effective alternatives (Meinel et al., 2006). Compared with pre-synthesized recombinant proteins, the expression of gene products guarantees true post-translational modification, which reduced possible immunogenicity and increased the biological activity. There are two kinds of gene delivery vehicles: viral vectors and non-viral vectors. Viral vectors have a highly evolved mechanism for delivering DNA to cells, but could induce an effective immune response in host cells (Franceschi et al., 2004). Non-viral vector delivery is a promising gene therapy way, including cationic polymers, cationic polypeptides, and cationic liposomes (Yang et al., 2018). In tissue engineering applications, gene therapy can be combined with biomaterials to extend, persist and locally deliver the target protein *in situ*. Tomas et al. have developed and identified a novel nanohydroxyapatite (nHA)-mediated plasmid DNA (pDNA) encoding-activated alginate hydrogel that can direct the fate of MSCS toward either a chondrogenic or osteogenic phenotype by delivering TGF-β3 and/or BMP-2 (Gonzalez-Fernandez et al., 2016), which may be important to the clinical treatment of osteochondral defects. Non-viral dual delivery of VEGF and BMP2 in a collagen-nanohydroxyapatite scaffold accelerates the bone regeneration of MSCs *in vitro* and vascularization and bone repair by host cells *in vivo* (Curtin et al., 2015). However, compared to viral vectors, non-viral vectors are often disregarded due to their relatively inefficient.

CARTILAGE DEFECTS REPAIR OF STEM CELL-LADEN HYDROGELS

The production of functional substitutes for autogenous cartilage and the development of new therapeutic strategies for cartilage defects are significant challenges that can be addressed through the field of tissue engineering. MSCs have become the most widely used stem cell in regenerative medicine due to their abundant cell sources, low immunogenicity, no ethical issues and minimal risk of teratomas (Wang et al., 2016). Cell therapy and tissue engineering have been combined in the repair of cartilage defects. MSC has the ability to multidirectionally differentiate into a variety of cells, including the chondrogenesis. Treatment combining MSCs and hydrogel are being applied in cartilage tissue engineering. The "medical signaling cell" properties associated with their immunomodulatory and anti-inflammatory effects induce the establishment of regenerative microenvironments in injured tissues. These nutritional effects, along with the long-established cartilage generator capacity, can be used for tissue-engineered constructs for articular cartilage repair. This section will focus on the cell therapy and tissue engineering of various MSCs for articular cartilage damage.

Bone Marrow-Derived Mesenchymal Stem Cells (BM-MSCs)

BM-MSCs reside in bone marrow have been widely used in animal models and some clinical cases to study their chondrogenic potential for the treatment of OA (Zhang et al., 2019). Erickson et al. studied that the pre-maturation of MSC-seeded HA hydrogels *in vitro* could improve cartilage repair (Erickson et al., 2012). Vishal et al. studied MSC-seeded HA neocartilage and anatomic MSC-seeded HA constructs crosslinked by ammonium persulfate and N,N,N'N'-tetramethylethylenediamine for hMSC chondrogenesis in chondral defects (**Figure 7**; Ansboro et al., 2014). Meng et al. designed a composite scaffold combining affinity peptide-modified demineralized bone matrix particles with chitosan hydrogels for cartilage engineering, exhibiting appropriate porosity and providing a microenvironment for cell adhesion and proliferation. The functional composite of demineralized bone matrix particles and chitosan hydrogels (DBM-E7/CS) scaffold increased matrix production and improved the cartilage differentiation ability of BM-MSCs *in vitro*, which was a choice for repairing irregularly shaped cartilage defects (Meng et al., 2015). In clinical cases, the use of BM-MSCs in cartilage

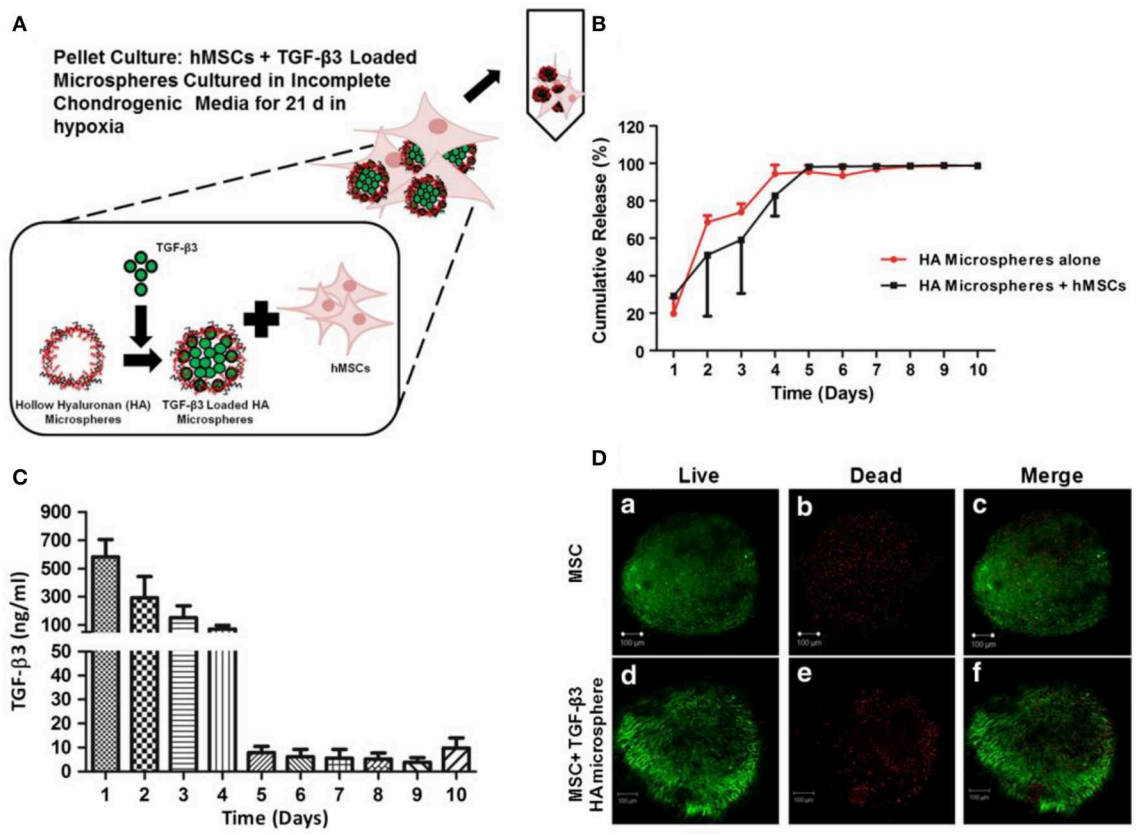

FIGURE 7 | Loading, viability, and release of TGF-β3 from hollow HA microspheres. **(A)** An illustration of an HA microsphere pellet culture system loading TGF-β3. **(B)** Cumulative release profile of TGF-β3 from microspheres with/without hMSCs. **(C)** The release of TGF-β3 from HA microspheres cultured with hMSCs. **(D)** Viability of chondrogenic pellets cultured for 21 d with (d–f) and without (a–c) microspheres loading TGF-β3. Scale bar = 100 μm. Reproduced with permission from Ansboro et al. (2014).

repair circumvented limitations of autologous chondrocyte implantation (ACI). BM-MSCs implantation for cure of cartilage defects achieved the equivalent clinical results as the first-generation ACI over a period of up to 10 years, with no significant increased risk of tumor formation (Teo et al., 2019).

Adipose-Derived Stem Cells (ADSCs)

Adipose tissue as a rich source of MSCs has aroused great interest in cartilage tissue engineering. ADSCs are easily obtained in high yields through minimally invasive surgery (such as liposuction) (Tapp et al., 2008). Popa et al. proposed κ-carrageenan as a potential hydrogel that can be used for cell transport and for further application in cartilage regeneration. ADSCs encapsulated in κ-carrageenan hydrogel can still survive, proliferate and differentiate into cartilage cells (Popa et al., 2013). Rizk et al. evaluated that TGF-β1-fixed scaffolds prepared by incorporating TGF-β1-loaded gelatin microspheres into the poly(lactic-co-glycolic acid) (PLGA) framework enhanced the differentiation of ADSCs into chondrocytes (Yin et al., 2015). Furthermore, hADSCs can be mixed with sodium alginate and gelatin, combination with 3D bioprinting technology, to form a 3D bioprinted body of hADSCs-sodium alginate-gelatin mixture, which had the ability of ectopic bone formation in nude mice (Song et al., 2016). Huang et al. showed that the biomimetic matrix from chitosan-HA provided a suitable environment to support the differentiation of chondrocytes from ADSCs to the cartilage matrix (Huang et al., 2019). Fan et al. corroborated that an injectable bioorthogonal dextran-based hydrogel can support the chondrogenesis of ADSCs *in vitro* and *in vivo*, highlighting the role of bioorthogonal hydrogels for stem cell-based cartilage regeneration (Fan et al., 2018).

Umbilical Cord Blood-Derived Mesenchymal Stem Cells (UCB-MSCs)

UCB-MSCs have attracted wide interest as a promising source of regenerative medicine cells due to their non-invasive collection, high expansion capacity, availability, and low immunogenicity. These cells have been identified and found phenotypic similarities to BM-MSCs and embryonic stem cells. Chung et al. explored the feasibility and efficacy of repairing articular cartilage using a composite of hUCB-MSCs and four different hydrogels in a rat model. The results showed that group with 4% HA hydrogel can significantly improve cartilage histologically and achieved the cellular arrangement and collagen tissue pattern mimicking adjacent undamaged articular cartilage (**Figure 8**; Chung et al., 2014). Park et al. demonstrated that treatment with undifferentiated vs. chondrogenic predifferentiated hUCB-MSCs and 4% HA hydrogel resulted in more approving cartilage repair than the control groups with chondro-MSCs in a rat model (Park et al., 2019). From the clinical trial for safety and proof-of-concept with 7 years of extended follow-up, Park et al. reported that the hUCB-MSCs-based HA hydrogels appeared to be safe and effective for cartilage regeneration in osteoarthritic patients (Park et al., 2017).

Autologous Activated Peripheral Blood Stem Cells (AAPBSCs)

AAPBSCs contain MSCs with chondrocyte precursor potential to initiate hyaline cartilage remodeling (Duff et al., 2003; Turajane et al., 2014). The clinical trial studied by Saw's groups showed that, arthroscopic cartilage can be regenerated with arthroscopic subchondral drilling followed by injecting autologous PBPCs and HA into postoperative intra-articularly (IA) autologous (Saw et al., 2011). The combination of AAPBSC and HA on the autologous cancellous bone scaffold initiated the chondrocyte differentiation. And the addition of platelet-rich plasma (PRP) and human granulocyte colony stimulating factor (hG-CSF) further stimulated the proliferation of cells to the chondrocyte phenotype with enhanced Sox9 transcription. The above processes led to the continuous increase of col-2 and aggrecan mRNA, which ultimately resulted in the histologically confirmed proteoglycan and glycosaminoglycan contents increase in newly formed in transparent cartilage (Turajane et al., 2014). The combination of AAPBSCs with growth factor addition/preservation with HA and arthroscopic microdrilling MCSs can improve cartilage regeneration in early knee disease that failed conservative treatment (Turajane et al., 2013).

SUMMARY AND PERSPECTIVES

This paper reviews the latest progress in the design and preparation of stem cell-laden hydrogel for osteochondral tissue engineering applications in terms of engineering hydrogel properties, biomimetic microenvironment, and growth factor delivery. Stem cell-based therapies have recently opened up new opportunities for clinical applications to treat diseases that cannot be effectively treated with conventional chemotherapy. MSCs are isolated from different tissues, such as bone marrow, adipose tissue, placenta, umbilical cord blood, and peripheral blood. Stem cells can sustainably release of therapeutic small molecules that are important for cell survival and tissue regeneration, which has been acknowledged as an essential treatment for effective treatment of various diseases. Despite the considerable potential of these stem cell therapies, the reduced viability of transplanted stem cells after transplantation often leads to unsatisfactory results in *in vivo* studies. The microenvironment of damaged tissue, such as reactive oxygen species and host immune responses, is unfavorable for growth of stem cells. In addition, the absence of cell support signals around damaged tissues can also result in the ultimate death of the transplanted stem cells. Therefore, it is important for the research focusing on the stem cell transplantation in combination with substances supporting cell survival, inducing cell bioactivity, and enhancing cell retention at managed sites. Especially, hydrogels supplying a tissue-like environment have been widely studied as a vehicle for delivering stem cells.

Hydrogel materials afford control over critical regulators of stem cell fate, including matrix mechanics and biochemistry, microscale structure, and cell-cell interactions. With the development of tissue engineering and the regenerative medicine,

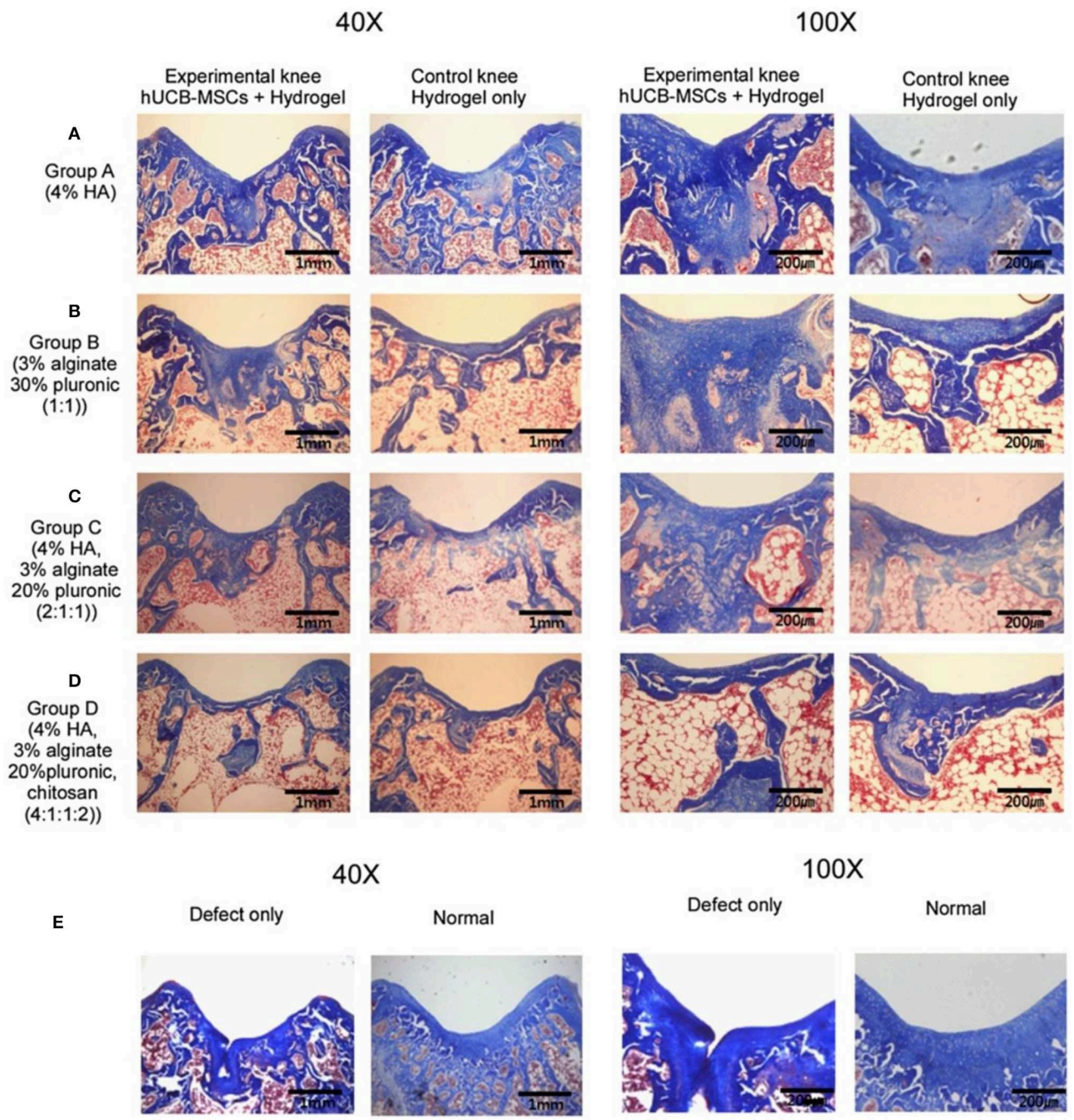

FIGURE 8 | Masson's trichrome staining at 16 weeks post-transplantation. **(A)** Group A with/without hUCB-MSCs + 4% HA hydrogel composites; **(B)** Group B with/without hUCB-MSCs + 3% alginate:30% pluronic (1:1, v/v) composites; **(C)** Group C with/without hUCB-MSCs + 4% HA: 3% alginate: 20% pluronic (2:1:1, v/v) composites; **(D)** Group D with/without hUCB-MSCs + 4% HA: 3% alginate: 20% pluronic: chitosan (4:1:1:2, v/v); **(E)** Defect only and normal cartilage. Reproduced with permission from Chung et al. (2014).

it is found that tissue regeneration and reconstruction require a multifunctional scaffold to load and delivery tissue-specific cells. In this sense, hydrogel scaffolds are recognized as ideal biomaterials for the tissue engineering of cartilage, bone, skin, heart valves, nerves, tendons, etc., due to their composition, structure, morphology, function, and mechanics are closely similar to the natural tissue extracellular matrix. The hydrogels and 3D architecture scaffolds combined with various bioactive molecules, genes and cells as well as the tunable mechanical properties have capacity to guide and promote the *in vivo* implantation and development of multifunctional engineered tissues. Thus, these hydrogels

scaffolds with customized morphologies and suitable mechanical behaviors bring the prospect of cartilage tissue engineering through the tailorable retention, and delivery abilities of cells and growth factors in the injury site.

Chondrocytes can successfully repair focal cartilage, however, the problems including the limited supply of them, long expansion time, and may be differentiated into fibroblasts. On the other hand, stem cells have more application prospects due to their rich in source and potential to differentiate into chondrocytes. Various types of stem cells encapsulated in hydrogels can differentiate into chondrocytes or osteoblasts under the induction of growth factors. Delivery of growth factors via microencapsulation, covalent bond with hydrogel and gene delivery is attractive for the localized release of inducers.

Even though, it should be noted that it is still a major challenge to fully restore cartilage to its original composition, architecture, mechanics, and biofunction. For example, simultaneous achievement of integrating cartilage and subchondral bone regeneration has been a critical challenge in tissue engineering. The difference of structure and modulus in two distinct types of tissues should be carefully considered for overcoming the difficulties in simulating the structures and functions by the hybrid or bi-phase hydrogel scaffolds. Wherein, the part of cartilage repair exhibited highly elastic modulus to bear the pressure and resist the friction to facilitate the extracellular matrix, enhance the chondrogenesis of MSCs, inhibit the hypertrophic differentiation, and contribute to the chondrocyte mineralization. While another part of subchondral bone repair could effectively contribute to the formation of blood vessel network within the hydrogels to facilitate nutrient transports, stimulate osteoblast proliferations and provide great supports for regenerative cartilage. More importantly, integration of the surrounding cartilage and the implants should possess strong interfacial adhesion that can be significantly enhanced for regenerated cartilage. Additionally, smart incorporations of intelligence or self-guided features also played the essential roles in the fabrication and development of a new kind of cell-laden hydrogels to obtain the fully cartilage regeneration in biomedical applications.

It should be also further noted that although there have been some limited clinically approved tissue-engineered products for the clinical trials status quo in recent years, a rapid progress toward more advanced and targeted therapies is still particularly noticed by promoting microfabrication techniques and developing the cellular scaffold-based approaches. It is concluded that an ideal stem cell-laden hydrogel for achieving the cartilage tissue engineering should synchronously possess the following characterizations: (1) biological activity and biomimetic function; (2) mechanical reinforcement; (3) integration of cartilage with bone tissue; and (4) transport of drugs and growth factors. Therefore, the intelligent and hybrid hydrogel scaffolds with complex architectures should be well-fabricated for realizing the customized clinic treatments. And the corresponding researches on the mechanical and biological behaviors of hydrogel scaffolds should also be emphasized to ensure the powerful tissue interactions, resorption and hierarchical architecture for enabling the tissue engineering implants. With this understanding, the future work should forcefully focus on identifying the secondary, tertiary and higher order architectures of the hybrid hydrogels, quantifying their composition, morphology and function, characterizing their binding pockets and interactions with cell surface receptors and finally turning them into a clinically tissue engineering biomaterial for effective cartilage tissue engineering. In this sense, in the future we should establish such a methodology or criteria on the design and development of final biological tissue engineering products for regenerative medicine, which makes the cell-laden hydrogel satisfy more advantages on adjustable structure, better strength, adequate immune response, adhesive interfacial binding force and good biodegradability for enabling the real applications in human patients.

We are strongly convinced that with the help of continuous developments of cell-laden hydrogels and exquisite adjustment of their physicochemical and mechanical properties for effective osteochondral tissue engineering, more advanced multi-responsive histological engineering products with optimized architectures and functions will be eventually created to obtain the greater manipulation and higher availability for various biomedical applications. The compositions, structures and mechanical properties of newly responsive hydrogels are hopefully to be continually developed, and thus we will further obtain smart biomaterials with topological complexity for tissue engineering of regenerative medicine.

AUTHOR CONTRIBUTIONS

BX and JY contributed equally to this review paper. XW and J-KY conceived and designed the content of the paper. BX, JY, F-ZY, J-YZ, Y-RC, and B-SF collected the researched literatures. J-YZ arranged the outline of collected documents. BX and JY wrote the article. DJ and W-BJ made important suggestions and helped revising the paper. All authors reviewed and commented on the entire manuscript.

FUNDING

This research was funded by the National Natural Science Foundation of China (NSFC, 51920105006, 81630056, 51973226 and 51773004) and the National Key Research and Development Program of China (Grant No. 2016YFC1100704).

REFERENCES

Abdel-Sayed, P., and Pioletti, D. P. (2015). Strategies for improving the repair of focal cartilage defects. *Nanomedicine* 10, 2893–2905. doi: 10.2217/nnm.15.119

Ansboro, S., Hayes, J. S., Barron, V., Browne, S., Howard, L., Greiser, U., et al. (2014). A chondromimetic microsphere for in situ spatially controlled chondrogenic differentiation of human mesenchymal stem cells. *J. Control. Release* 179, 42–51. doi: 10.1016/j.jconrel.2014.01.023

Bal, B. S., Rahaman, M. N., Jayabalan, P., Kuroki, K., Cockrell, M. K., Yao, J. Q., et al. (2010). *In vivo* outcomes of tissue-engineered osteochondral grafts. *J. Biomed. Mater. Res. Part B Appl. Biomater.* 93, 164–174. doi: 10.1002/jbm.b.31571

Barczyk, M., Carracedo, S., and Gullberg, D. (2010). Integrins. *Cell Tissue Res.* 339, 269–280. doi: 10.1007/s00441-009-0834-6

Becher, C., Malahias, M. A., Ali, M. M., Maffulli, N., and Thermann, H. (2019). Arthroscopic microfracture vs. arthroscopic autologous matrix-induced chondrogenesis for the treatment of articular cartilage defects of the talus. *Knee Surg. Sports Traumatol. Arthrosc.* 27, 2731–2736. doi: 10.1007/s00167-018-5278-7

Beck, J. J., Sugimoto, D., and Micheli, L. (2018). Sustained results in long-term follow-up of autologous chondrocyte implantation (ACI) for distal femur juvenile osteochondritis dissecans (JOCD). *Adv. Orthopedi.* 2018:7912975. doi: 10.1155/2018/7912975

Benoit, D. S., Schwartz, M. P., Durney, A. R., and Anseth, K. S. (2008). Small functional groups for controlled differentiation of hydrogel-encapsulated human mesenchymal stem cells. *Nat. Mater.* 7, 816–823. doi: 10.1038/nmat2269

Bernhard, J. C., and Vunjak-Novakovic, G. (2016). Should we use cells, biomaterials, or tissue engineering for cartilage regeneration. *Stem Cell Res. Ther.* 7:56. doi: 10.1186/s13287-016-0314-3

Bian, L., Zhai, D. Y., Tous, E., Rai, R., Mauck, R. L., and Burdick, J. A. (2011). Enhanced MSC chondrogenesis following delivery of TGF-beta3 from alginate microspheres within hyaluronic acid hydrogels *in vitro* and *in vivo*. *Biomaterials* 32, 6425–6434. doi: 10.1016/j.biomaterials.2011.05.033

Boekhoven, J., Rubert Perez, C. M., Sur, S., Worthy, A., and Stupp, S. I. (2013). Dynamic display of bioactivity through host-guest chemistry. *Angewand. Chem.* 52, 12077–12080. doi: 10.1002/anie.201306278

Brown, T. E., and Anseth, K. S. (2017). Spatiotemporal hydrogel biomaterials for regenerative medicine. *Chem. Soc. Rev.* 46, 6532–6552. doi: 10.1039/C7CS00445A

Bryant, S. J., Bender, R. J., Durand, K. L., and Anseth, K. S. (2004). Encapsulating chondrocytes in degrading PEG hydrogels with high modulus: engineering gel structural changes to facilitate cartilaginous tissue production. *Biotechnol. Bioeng.* 86, 747–755. doi: 10.1002/bit.20160

Cao, Y., Lee, B. H., Peled, H. B., and Venkatraman, S. S. (2016). Synthesis of stiffness-tunable and cell-responsive gelatin-poly(ethylene glycol) hydrogel for three-dimensional cell encapsulation. *J. Biomed. Mater. Res. Part A* 104, 2401–2411. doi: 10.1002/jbm.a.35779

Chang, H., and Knothe Tate, M. L. (2011). Structure-function relationships in the stem cell's mechanical world B: emergent anisotropy of the cytoskeleton correlates to volume and shape changing stress exposure. *Mol. Cell. Biomech.* 8, 297–318.

Chen, H., Hoemann, C. D., Sun, J., Chevrier, A., McKee, M. D., Shive, M. S., et al. (2011). Depth of subchondral perforation influences the outcome of bone marrow stimulation cartilage repair. *J. Orthopaed. Res.* 29, 1178–1184. doi: 10.1002/jor.21386

Chen, K., Ng, K. S., Ravi, S., Goh, J. C., and Toh, S. L. (2016). *In vitro* generation of whole osteochondral constructs using rabbit bone marrow stromal cells, employing a two-chambered co-culture well design. *J. Tissue Eng. Regen. Med.* 10, 294–304. doi: 10.1002/term.1716

Chung, J. Y., Song, M., Ha, C. W., Kim, J. A., Lee, C. H., and Park, Y. B. (2014). Comparison of articular cartilage repair with different hydrogel-human umbilical cord blood-derived mesenchymal stem cell composites in a rat model. *Stem Cell Res. Ther.* 5:39. doi: 10.1186/scrt427

Cipriani, F., Bernhagen, D., Garcia-Arevalo, C., de Torre, I. G., Timmerman, P., and Rodriguez-Cabello, J. C. (2019). Bicyclic RGD peptides with high integrin alpha v beta 3 and alpha 5 beta 1 affinity promote cell adhesion on elastin-like recombinamers. *Biomed. Mater.* 14:035009. doi: 10.1088/1748-605X/aafd83

Cook, C. D., Hill, A. S., Guo, M., Stockdale, L., Papps, J. P., Isaacson, K. B., et al. (2017). Local remodeling of synthetic extracellular matrix microenvironments by co-cultured endometrial epithelial and stromal cells enables long-term dynamic physiological function. *Integrat. Biol.* 9, 271–289. doi: 10.1039/c6ib00245e

Curtin, C. M., Tierney, E. G., McSorley, K., Cryan, S. A., Duffy, G. P., and O'Brien, F. J. (2015). Combinatorial gene therapy accelerates bone regeneration: non-viral dual delivery of VEGF and BMP2 in a collagen-nanohydroxyapatite scaffold. *Adv. Healthcare Mater.* 4, 223–227. doi: 10.1002/adhm.201400397

Daley, W. P., Peters, S. B., and Larsen, M. (2008). Extracellular matrix dynamics in development and regenerative medicine. *J. Cell Sci.* 121, 255–264. doi: 10.1242/jcs.006064

Dasar, U., Gursoy, S., Akkaya, M., Algin, O., Isik, C., and Bozkurt, M. (2016). Microfracture technique versus carbon fibre rod implantation for treatment of knee articular cartilage lesions. *J. Orthopaed. Surg.* 24, 188–193. doi: 10.1177/1602400214

Drueke, T. B. (2006). Haematopoietic stem cells-role of calcium-sensing receptor in bone marrow homing. *Nephrol. Dialysis Transplant.* 21, 2072–2074. doi: 10.1093/ndt/gfl206

Du, M., Liang, H., Mou, C., Li, X., Sun, J., Zhuang, Y., et al. (2014). Regulation of human mesenchymal stem cells differentiation into chondrocytes in extracellular matrix-based hydrogel scaffolds. *Colloids Surfaces B Biointerf.* 114, 316–323. doi: 10.1016/j.colsurfb.2013.10.001

Duff, S. E., Li, C., Garland, J. M., and Kumar, S. (2003). CD105 is important for angiogenesis: evidence and potential applications. *FASEB* 17, 984–992. doi: 10.1096/fj.02-0634rev

Ekerdt, B. L., Segalman, R. A., and Schaffer, D. V. (2013). Spatial organization of cell-adhesive ligands for advanced cell culture. *Biotechnol. J.* 8, 1411–1423. doi: 10.1002/biot.201300302

Eliasson, P., and Jonsson, J. I. (2010). The hematopoietic stem cell niche: low in oxygen but a nice place to be. *J. Cell. Physiol.* 222, 17–22. doi: 10.1002/jcp.21908

Erickson, I. E., Kestle, S. R., Zellars, K. H., Dodge, G. R., Burdick, J. A., and Mauck, R. L. (2012). Improved cartilage repair via in vitro pre-maturation of MSC-seeded hyaluronic acid hydrogels. *Biomed. Mater.* 7:024110. doi: 10.1088/1748-6041/7/2/024110

Fan, L., Lin, C., Zhao, P., Wen, X., and Li, G. (2018). An Injectable bioorthogonal dextran hydrogel for enhanced chondrogenesis of primary stem cells. *Tissue Eng. Part C Methods* 24, 504–513. doi: 10.1089/ten.tec.2018.0085

Franceschi, R. T., Yang, S., Rutherford, R. B., Krebsbach, P. H., Zhao, M., and Wang, D. (2004). Gene therapy approaches for bone regeneration. *Cells Tissues Organs* 176, 95–108. doi: 10.1159/000075031

Fuchs, E., Tumbar, T., and Guasch, G. (2004). Socializing with the neighbors: stem cells and their niche. *Cell* 116, 769–778. doi: 10.1016/S0092-8674(04)00255-7

Geerligs, M., Peters, G. W. M., Ackermans, P. A. J., Oomens, C. W. J., and Baaijens, F. P. T. (2008). Linear viscoelastic behavior of subcutaneous adipose tissue. *Biorheology* 45, 677–688. doi: 10.3233/BIR-2008-0517

Giannoni, P., Pagano, A., Maggi, E., Arbico, R., Randazzo, N., Grandizio, M., et al. (2005). Autologous chondrocyte implantation (ACI) for aged patients: development of the proper cell expansion conditions for possible therapeutic applications. *Osteoarthritis Cartilage* 13, 589–600. doi: 10.1016/j.joca.2005.02.015

Gonzalez-Fernandez, T., Tierney, E. G., Cunniffe, G. M., O'Brien, F. J., and Kelly, D. J. (2016). Gene delivery of TGF-β3 and BMP2 in an MSC-laden alginate hydrogel for articular cartilage and endochondral bone tissue engineering. *Tissue Eng. Part A* 22, 776–787. doi: 10.1089/ten.tea.2015.0576

Green, J. D., Tollemar, V., Dougherty, M., Yan, Z., Yin, L., Ye, J., et al. (2015). Multifaceted signaling regulators of chondrogenesis: Implications in cartilage regeneration and tissue engineering. *Genes Dis.* 2, 307–327. doi: 10.1016/j.gendis.2015.09.003

Griffin, D. R., Weaver, W. M., Scumpia, P. O., Di Carlo, D., and Segura, T. (2015). Accelerated wound healing by injectable microporous gel scaffolds assembled from? Annealed building blocks. *Nat. Mater.* 14, 737–744. doi: 10.1038/nmat4294

Guo, X., Park, H., Young, S., Kretlow, J. D., van den Beucken, J. J., Baggett, L. S., et al. (2010). Repair of osteochondral defects with biodegradable hydrogel composites encapsulating marrow mesenchymal stem cells in a rabbit model. *Acta Biomater.* 6, 39–47. doi: 10.1016/j.actbio.2009.07.041

Han, L. H., Yu, S., Wang, T., Behn, A. W., and Fan, Y. (2013). Microribbon-like elastomers for fabricating macroporous and highly flexible scaffolds that support cell proliferation in 3D. *Adv. Funct. Mater.* 23, 346–358. doi: 10.1002/adfm.201201212

Haugh, M. G., and Heilshorn, S. C. (2016). Integrating concepts of material mechanics, ligand chemistry, dimensionality and degradation to control differentiation of mesenchymal stem cells. *Curr Opin. Solid State Mater. Sci.* 20, 171–179. doi: 10.1016/j.cossms.2016.04.001

Hersel, U., Dahmen, C., and Kessler, H. (2003). RGD modified polymers: biomaterials for stimulated cell adhesion and beyond.

Biomaterials 24, 4385–4415. doi: 10.1016/S0142-9612(03)00343-0

Hoben, G. M., Koay, E. J., and Athanasiou, K. A. (2008). Fibrochondrogenesis in two embryonic stem cell lines: effects of differentiation timelines. *Stem Cells* 26, 422–430. doi: 10.1634/stemcells.2007-0641

Holloway, J. L., Ma, H., Rai, R., and Burdick, J. A. (2014). Modulating hydrogel crosslink density and degradation to control bone morphogenetic protein delivery and *in vivo* bone formation. *J. Control. Release* 191, 63–70. doi: 10.1016/j.jconrel.2014.05.053

Hortensius, R. A., and Harley, B. A. (2013). The use of bioinspired alterations in the glycosaminoglycan content of collagen-GAG scaffolds to regulate cell activity. *Biomaterials* 34, 7645–7652. doi: 10.1016/j.biomaterials.2013.06.056

Hsu, H. J., and Drummond-Barbosa, D. (2009). Insulin levels control female germline stem cell maintenance via the niche in Drosophila. *Proc. Natl. Acad. Sci. U.S.A.* 106, 1117–1121. doi: 10.1073/pnas.0809144106

Huang, K., Li, Q., Li, Y., Yao, Z., Luo, D., Rao, P., et al. (2018). Cartilage tissue regeneration: the roles of cells, stimulating factors and scaffolds. *Curr. Stem Cell Res. Therap.* 13, 547–567. doi: 10.2174/1574888X12666170608080722

Huang, Y., Seitz, D., Konig, F., Muller, P. E., Jansson, V., and Klar, R. M. (2019). Induction of articular chondrogenesis by chitosan/hyaluronic-acid-based biomimetic matrices using human adipose-derived stem cells. *Int. J. Mol. Sci.* 20:4487. doi: 10.3390/ijms20184487

Isono, Y., and Nishitake, T. (1995). Stress relaxation and change in entanglement structure of polyisobutylene in large shearing deformations. *Polymer* 36, 1635–1638. doi: 10.1016/0032-3861(95)99009-J

Jekhmane, S., Prachar, M., Pugliese, R., Fontana, F., and Medeiros-Silva, J. (2019). Design parameters of tissue-engineering scaffolds at the atomic scale. *Angew. Chem. Int. Edn.* 58, 16943–16951. doi: 10.1002/anie.201907880

Jin, X., Sun, Y., Zhang, K., Wang, J., Shi, T., Ju, X., et al. (2007). Ectopic neocartilage formation from predifferentiated human adipose derived stem cells induced by adenoviral-mediated transfer of hTGF beta2. *Biomaterials* 28, 2994–3003. doi: 10.1016/j.biomaterials.2007.03.002

Jongpaiboonkit, L., King, W. J., Lyons, G. E., Paguirigan, A. L., Warrick, J. W., Beebe, D. J., et al. (2008). An adaptable hydrogel array format for 3-dimensional cell culture and analysis. *Biomaterials* 29, 3346–3356. doi: 10.1016/j.biomaterials.2008.04.040

Jung, S. N., Rhie, J. W., Kwon, H., Jun, Y. J., Seo, J.-W., Yoo, G., et al. (2010). *In vivo* cartilage formation using chondrogenic-differentiated human adipose-derived mesenchymal stem cells mixed with fibrin glue. *J. Craniofac. Surg.* 21, 468–472. doi: 10.1097/SCS.0b013e3181cfea50

Kaji, H., Camci-Unal, G., Langer, R., and Khademhosseini, A. (2011). Engineering systems for the generation of patterned co-cultures for controlling cell-cell interactions. *Biochim. Biophys. Acta* 1810, 239–250. doi: 10.1016/j.bbagen.2010.07.002

Kim, B. S., Jang, J., Chae, S., Gao, G., Kong, J. S., Ahn, M., et al. (2016). Three-dimensional bioprinting of cell-laden constructs with polycaprolactone protective layers for using various thermoplastic polymers. *Biofabrication* 8:035013. doi: 10.1088/1758-5090/8/3/035013

Kim, C., Young, J. L., Holle, A. W., Jeong, K., Major, L. G., Jeong, J. H., et al. (2020). Stem cell mechanosensation on gelatin methacryloyl (GelMA) stiffness gradient hydrogels. *Ann. Biomed. Eng.* 48, 893–902. doi: 10.1007/s10439-019-02428-5

Kim, D., Wu, X., Young, A. T., and Haynes, C. L. (2014). Microfluidics-based *in vivo* mimetic systems for the study of cellular biology. *Acc. Chem. Res.* 47, 1165–1173. doi: 10.1021/ar4002608

Kloxin, A. M., Kasko, A. M., Salinas, C. N., and Anseth, K. S. (2009). Photodegradable hydrogels for dynamic tuning of physical and chemical properties. *Science* 324, 59–63. doi: 10.1126/science.1169494

Kuo, C. K., and Ma, P. X. (2011). Controlling diffusion of solutes through ionically crosslinked alginate hydrogels designed for tissue engineering. *Biomater. Drug Deliv. Tissue Eng.* 662:LL1.5. doi: 10.1557/PROC-662-LL1.5

Lam, J., Carmichael, S. T., Lowry, W. E., and Segura, T. (2015). Hydrogel design of experiments methodology to optimize hydrogel for iPSC-NPC culture. *Adv. Healthcare Mater.* 4, 534–539. doi: 10.1002/adhm.201400410

Lam, J., Lu, S., Meretoja, V. V., Tabata, Y., Mikos, A. G., and Kasper, F. K. (2014). Generation of osteochondral tissue constructs with chondrogenically and osteogenically predifferentiated mesenchymal stem cells encapsulated in bilayered hydrogels. *Acta Biomater.* 10, 1112–1123. doi: 10.1016/j.actbio.2013.11.020

Lee, T. T., Garcia, J. R., Paez, J. I., Singh, A., Phelps, E. A., Weis, S., et al. (2015). Light-triggered *in vivo* activation of adhesive peptides regulates cell adhesion, inflammation and vascularization of biomaterials. *Nat. Mater.* 14, 352–360. doi: 10.1038/nmat4157

Levental, I., Georges, P. C., and Janmey, P. A. (2007). Soft biological materials and their impact on cell function. *Soft Matter* 3, 299–306. doi: 10.1039/B610522J

Li, F., Truong, V. X., Fisch, P., Levinson, C., Glattauer, V., Zenobi-Wong, M., et al. (2018). Cartilage tissue formation through assembly of microgels containing mesenchymal stem cells. *Acta Biomater.* 77, 48–62. doi: 10.1016/j.actbio.2018.07.015

Li, L., and Xie, T. (2005). Stem cell niche: structure and function. *Ann. Rev. Cell Dev. Biol.* 21, 605–631. doi: 10.1146/annurev.cellbio.21.012704.131525

Li, W., Wu, D., Hu, D., Zhu, S., Pan, C., Jiao, Y., et al. (2020). Stress-relaxing double-network hydrogel for chondrogenic differentiation of stem cells. *Mater. Sci. Eng. C Mater. Biol. App.* 107:110333. doi: 10.1016/j.msec.2019.110333

Liu, B., Liu, Y., Riesberg, J. J., and Shen, W. (2010). Dynamic presentation of immobilized ligands regulated through biomolecular recognition. *J. Am. Chem. Soc.* 132, 13630–13632. doi: 10.1021/ja1054669

Liu, Y., Xu, L., Liu, J. S., Liu, X. Y., Chen, C. H., Li, G. Y., et al. (2016). Graphene oxides cross-linked with hyperbranched polyethylenimines: preparation, characterization and their potential as recyclable and highly efficient adsorption materials for lead(II) ions. *Chem. Eng. J.* 285, 698–708. doi: 10.1016/j.cej.2015.10.047

Lohan, A., Marzahn, U., El Sayed, K., Bock, C., Haisch, A., Kohl, B., et al. (2013). Heterotopic and orthotopic autologous chondrocyte implantation using a minipig chondral defect model. *Ann. Anatomy* 195, 488–497. doi: 10.1016/j.aanat.2013.04.009

Lu, Y., Huang, J., Yu, G., Cardenas, R., and Guo, Z. (2016). Coaxial electrospun fibers: applications in drug delivery and tissue engineering. *Wiley Interdiscip. Rev. Nanomed. Nanobiotechnol.* 8, 654–677. doi: 10.1002/wnan.1391

Luo, Y., and Shoichet, M. S. (2004). Light-activated immobilization of biomolecules to agarose hydrogels for controlled cellular response. *Biomacromolecules* 5, 2315–2323. doi: 10.1021/bm0495811

Lv, H., Li, L., Zhang, Y., Chen, Z., Sun, M., Xu, T., et al. (2015). Union is strength: matrix elasticity and microenvironmental factors codetermine stem cell differentiation fate. *Cell Tissue Res.* 361, 657–668. doi: 10.1007/s00441-015-2190-z

Madl, C. M., and Heilshorn, S. C. (2018). Engineering hydrogel microenvironments to recapitulate the stem cell niche. *Ann. Rev. Biomed. Eng.* 20, 21–47. doi: 10.1146/annurev-bioeng-062117-120954

Martino, M. M., Briquez, P. S., Guc, E., Tortelli, F., Kilarski, W. W., Metzger, S., et al. (2014). Growth factors engineered for super-affinity to the extracellular matrix enhance tissue healing. *Science* 343, 885–888. doi: 10.1126/science.1247663

McClenahan, F. K., Sharma, H., Shan, X., Eyermann, C., and Colognato, H. (2016). Dystroglycan suppresses notch to regulate stem cell niche structure and function in the developing postnatal subventricular zone. *Dev. Cell* 38, 548–566. doi: 10.1016/j.devcel.2016.07.017

Meinel, L., Hofmann, S., Betz, O., Fajardo, R., Merkle, H. P., Langer, R., et al. (2006). Osteogenesis by human mesenchymal stem cells cultured on silk biomaterials: comparison of adenovirus mediated gene transfer and protein delivery of BMP-2. *Biomaterials* 27, 4993–5002. doi: 10.1016/j.biomaterials.2006.05.021

Meng, Q., Man, Z., Dai, L., Huang, H., Zhang, X., Hu, X., et al. (2015). A composite scaffold of MSC affinity peptide-modified demineralized bone matrix particles and chitosan hydrogel for cartilage regeneration. *Sci. Rep.* 5:17802. doi: 10.1038/srep17802

Miki, R., Tatsumi, N., Matsumoto, K., and Yokouchi, Y. (2008). New primary culture systems to study the differentiation and proliferation of mouse fetal hepatoblasts. *Am. J. Physiol. Gastrointest. Liver Physiol.* 294, G529–G539. doi: 10.1152/ajpgi.00412.2007

Morrison, S. J., Shah, N. M., and Anderson, D. J. (1997). Regulatory mechanisms in stem cell biology. *Cell* 88, 287–298. doi: 10.1016/S0092-8674(00)81867-X

Moshaverinia, A., Xu, X., Chen, C., Akiyama, K., Snead, M. L., and Shi, S. (2013). Dental mesenchymal stem cells encapsulated in an alginate hydrogel co-delivery microencapsulation system for cartilage regeneration. *Acta Biomater.* 9, 9343–9350. doi: 10.1016/j.actbio.2013.07.023

Nagaoka, M., Ise, H., and Akaike, T. (2002). Immobilized E-cadherin model can enhance cell attachment and differentiation of primary hepatocytes but not proliferation. *Biotechnol. Lett.* 24, 1857–1862. doi: 10.1023/A:1020905532227

Park, Y., Lutolf, M. P., Hubbell, J. A., Hunziker, E. B., and Wong, M. (2004). Bovine primary chondrocyte culture in synthetic matrix metalloproteinase-sensitive poly(ethylene glycol)-based hydrogels as a scaffold for cartilage repair. *Tissue Eng.* 10, 515–522. doi: 10.1089/107632704323061870

Park, Y. B., Ha, C. W., Kim, J. A., Kim, S., and Park, Y. G. (2019). Comparison of undifferentiated versus chondrogenic predifferentiated mesenchymal stem cells derived from human umbilical cord blood for cartilage repair in a Rat model. *Am. J. Sports Med.* 47, 451–461. doi: 10.1177/0363546518815151

Park, Y. B., Ha, C. W., Lee, C. H., Yoon, Y. C., and Park, Y. G. (2017). Cartilage regeneration in osteoarthritic patients by a composite of allogeneic umbilical cord blood-derived mesenchymal stem cells and hyaluronate hydrogel: results from a clinical trial for safety and proof-of-concept with 7 years of extended follow-up. *Stem Cells Transl. Med.* 6, 613–621. doi: 10.5966/sctm.2016-0157

Paschos, N. K., Brown, W. E., Eswaramoorthy, R., Hu, J. C., and Athanasiou, K. A. (2015). Advances in tissue engineering through stem cell-based co-culture. *J. Tissue Eng. Regen. Med.* 9, 488–503. doi: 10.1002/term.1870

Polo-Corrales, L., Latorre-Esteves, M., and Ramirez-Vick, J. E. (2014). Scaffold design for bone regeneration. *J. Nanosci. Nanotechnol.* 14, 15–56. doi: 10.1166/jnn.2014.9127

Popa, E. G., Caridade, S. G., Mano, J. F., Rui, L. R., and Gomes, M. E. (2013). Chondrogenic potential of injectable κ-carrageenan hydrogel with encapsulated adipose stem cells for cartilage tissue-engineering applications. *J. Tissue Eng. Regen. Med.* 9, 550–563. doi: 10.1002/term.1683

Sartori, M., Pagani, S., Ferrari, A., Costa, V., Carina, V., Figallo, E., et al. (2017). A new bi-layered scaffold for osteochondral tissue regeneration: *in vitro* and *in vivo* preclinical investigations. *Mater. Sci. Eng. C* 70, 101–111. doi: 10.1016/j.msec.2016.08.027

Saw, K. Y., Anz, A., Merican, S., Tay, Y. G., Ragavanaidu, K., Jee, C. S., et al. (2011). Articular cartilage regeneration with autologous peripheral blood progenitor cells and hyaluronic acid after arthroscopic subchondral drilling: a report of 5 cases with histology. *Arthroscopy* 27, 493–506. doi: 10.1016/j.arthro.2010.11.054

Sawhney, A. S., Pathak, C. P., van Rensburg, J. J., Dunn, R. C., and Hubbell, J. A. (1994). Optimization of photopolymerized bioerodible hydrogel properties for adhesion prevention. *J. Biomed. Mater. Res.* 28, 831–838. doi: 10.1002/jbm.820280710

Scadden, D. T. (2006). The stem-cell niche as an entity of action. *Nature* 441, 1075–1079. doi: 10.1038/nature04957

Shah, N., Morsi, Y., and Manasseh, R. (2014). From mechanical stimulation to biological pathways in the regulation of stem cell fate. *Cell Biochem. Funct.* 32, 309–325. doi: 10.1002/cbf.3027

Shekaran, A., Garcia, J. R., Clark, A. Y., Kavanaugh, T. E., Lin, A. S., Guldberg, R. E., et al. (2014). Bone regeneration using an alpha 2 beta 1 integrin-specific hydrogel as a BMP-2 delivery vehicle. *Biomaterials* 35, 5453–5461. doi: 10.1016/j.biomaterials.2014.03.055

Song, Y., Wang, X. F., Wang, Y. G., Sun, Y. C., and Lv, P. J. (2016). Osteogenesis of human adipose-derived mesenchymal stem cells-biomaterial mixture *in vivo* after 3D bio-printing. *J. Peking Univer. Health Sci.* 48, 45–50.

Sridhar, B. V., Doyle, N. R., Randolph, M. A., and Anseth, K. S. (2014). Covalently tethered TGF-beta1 with encapsulated chondrocytes in a PEG hydrogel system enhances extracellular matrix production. *J. Biomed. Mater. Res. Part A* 102, 4464–4472. doi: 10.1002/jbm.a.35115

Steinwachs, M., and Kreuz, P. C. (2007). Autologous chondrocyte implantation in chondral defects of the knee with a type I/III collagen membrane: a prospective study with a 3-year follow-up. *Arthroscopy* 23, 381–387. doi: 10.1016/j.arthro.2006.12.003

Stevens, M. M., Marini, R. P., Martin, I., Langer, R., and Prasad Shastri, V. (2004). FGF-2 enhances TGF-beta1-induced periosteal chondrogenesis. *J. Orthopaed. Res.* 22, 1114–1119. doi: 10.1016/j.orthres.2003.12.021

Sun, M., Sun, X., Wang, Z., Guo, S., Yu, G., and Yang, H. (2018). Synthesis and properties of gelatin methacryloyl (GelMA) hydrogels and their recent applications in load-bearing tissue. *Polymers* 10:1290. doi: 10.3390/polym10111290

Tamama, K., Fan, V. H., Griffith, L. G., Blair, H. C., and Wells, A. (2006). Epidermal growth factor as a candidate for *ex vivo* expansion of bone marrow-derived mesenchymal stem cells. *Stem Cells* 24, 686–695. doi: 10.1634/stemcells.2005-0176

Tapp, H., Hanley, E. N., Patt, J. C., and Gruber, H. E. (2008). Adipose-derived stem cells: characterization and current application in orthopaedic tissue repair. *Exp. Biol. Med.* 234, 1–9. doi: 10.3181/0805-MR-170

Teo, A. Q. A., Wong, K. L., Shen, L., Lim, J. Y., Toh, W. S., Lee, E. H., et al. (2019). Equivalent 10-year outcomes after implantation of autologous bone marrow-derived mesenchymal stem cells versus autologous chondrocyte implantation for chondral defects of the knee. *Am. J. Sports Med.* 47, 2881–2887. doi: 10.1177/0363546519867933

Turajane, T., Chaweewannakorn, U., Larbpaiboonpong, V., Aojanepong, J., Thitiset, T., Honsawek, S., et al. (2013). Combination of intra-articular autologous activated peripheral blood stem cells with growth factor addition/preservation and hyaluronic acid in conjunction with arthroscopic microdrilling mesenchymal cell stimulation improves quality of life and regenerates articular cartilage in early osteoarthritic knee disease. *J. Med. Assoc. Thailand.* 96, 580–588.

Turajane, T., Thitiset, T., Honsawek, S., Chaveewanakorn, U., Aojanepong, J., and Papadopoulos, K. I. (2014). Assessment of chondrogenic differentiation potential of autologous activated peripheral blood stem cells on human early osteoarthritic cancellous tibial bone scaffold. *Musculoskel. Surg.* 98, 35–43. doi: 10.1007/s12306-013-0303-y

VanTienderen, R. J., Dunn, J. C., Kusnezov, N., and Orr, J. D. (2017). Osteochondral allograft transfer for treatment of osteochondral lesions of the talus: a systematic review. *Arthroscopy* 33, 217–222. doi: 10.1016/j.arthro.2016.06.011

Wang, L., Huang, J., Huang, C., Li, Q., Liu, L., Luo, S., et al. (2018). Adult stem cells and hydrogels for cartilage regeneration. *Curr. Stem Cell Res. Therapy* 13, 533–546. doi: 10.2174/1574888X12666170511142917

Wang, L. T., Ting, C. H., Yen, M. L., Liu, K. J., Sytwu, H. K., Wu, K. K., et al. (2016). Human mesenchymal stem cells (MSCs) for treatment towards immune- and inflammation-mediated diseases: review of current clinical trials. *J. Biomed. Sci.* 23:76. doi: 10.1186/s12929-016-0289-5

Wirkner, M., Weis, S., San Miguel, V., Alvarez, M., Gropeanu, R. A., Salierno, M., et al. (2011). Photoactivatable caged cyclic RGD peptide for triggering integrin binding and cell adhesion to surfaces. *Chembiochem* 12, 2623–2629. doi: 10.1002/cbic.201100437

Wolf, M. T., Dearth, C. L., Ranallo, C. A., LoPresti, S. T., Carey, L. E., Daly, K. A., et al. (2014). Macrophage polarization in response to ECM coated polypropylene mesh. *Biomaterials* 35, 6838–6849. doi: 10.1016/j.biomaterials.2014.04.115

Xie, T., and Spradling, A. C. (2000). A niche maintaining germ line stem cells in the Drosophila ovary. *Science* 290, 328–330. doi: 10.1126/science.290.5490.328

Xie, Y., Liu, X., Wang, S., Wang, M., and Wang, G. (2019). Proper mechanical stimulation improve the chondrogenic differentiation of mesenchymal stem cells: improve the viscoelasticity and chondrogenic phenotype. *Biomed. Pharmacother.* 115:108935. doi: 10.1016/j.biopha.2019.108935

Xu, J., Feng, Q., Lin, S., Yuan, W., Li, R., Li, J., et al. (2019). Injectable stem cell-laden supramolecular hydrogels enhance in situ osteochondral regeneration via the sustained co-delivery of hydrophilic and hydrophobic chondrogenic molecules. *Biomaterials* 210, 51–61. doi: 10.1016/j.biomaterials.2019.04.031

Yang, W., Wang, F., Feng, L., Yan, S., and Guo, R. (2018). Applications and prospects of non-viral vectors in bone regeneration. *Curr. Gene Therapy* 18, 21–28. doi: 10.2174/1566523218666180227154232

Yin, F., Cai, J., Zen, W., Wei, Y., Zhou, W., Yuan, F., et al. (2015). Cartilage regeneration of adipose-derived stem cells in the TGF-β3-immobilized PLGA-gelatin scaffold. *Stem Cell Rev. Rep.* 11, 453–459. doi: 10.1007/s12015-014-9561-9

You, J., Raghunathan, V. K., Son, K. J., Patel, D., Haque, A., Murphy, C. J., et al. (2015). Impact of nanotopography, heparin hydrogel microstructures, and encapsulated fibroblasts on phenotype of primary hepatocytes. *ACS Appl. Mater. Interfaces* 7, 12299–12308. doi: 10.1021/am504614e

Zhang, R., Ma, J., Han, J., Zhang, W., and Ma, J. (2019). Mesenchymal stem cell related therapies for cartilage lesions and osteoarthritis. *Am. J. Transl. Res.* 11, 6275–6289.

Zhang, Z., Li, S., Chen, N., Yang, C., and Wang, Y. (2013). Programmable display of DNA-protein chimeras for controlling cell-hydrogel interactions via reversible intermolecular hybridization. *Biomacromolecules* 14, 1174–1180. doi: 10.1021/bm400096z

Zhao, L., and Hantash, B. M. (2011). TGF-beta1 regulates differentiation of bone marrow mesenchymal stem cells. *Vitamins Hormones* 87, 127–141. doi: 10.1016/B978-0-12-386015-6.00042-1

Zhu, Y., Kong, L., Farhadi, F., Xia, W., Chang, J., He, Y., et al. (2019). An injectable continuous stratified structurally and functionally biomimetic construct for enhancing osteochondral regeneration. *Biomaterials* 192, 149–158. doi: 10.1016/j.biomaterials.2018.11.017

Conflict of Interest: The authors declare that the research was conducted in the absence of any commercial or financial relationships that could be construed as a potential conflict of interest.

frontiers in Bioengineering and Biotechnology

ORIGINAL RESEARCH
published: 26 June 2020
doi: 10.3389/fbioe.2020.00636

The Higher Inherent Therapeutic Potential of Biomaterial-Based hDPSCs and hEnSCs for Pancreas Diseases

Bingbing Xu[1], Fu-Zhen Yuan[1], Lin Lin[1], Jing Ye[1], Bao-Shi Fan[2], Ji-Ying Zhang[1], Meng Yang[2], Dong Jiang[1], Wen-Bo Jiang[3], Xing Wang[4,5] and Jia-Kuo Yu[1]**

[1] Knee Surgery Department of the Institute of Sports Medicine, Peking University Third Hospital, Beijing, China, [2] School of Clinical Medicine, Weifang Medical University, Weifang, China, [3] Clinical Translational R&D Center of 3D Printing Technology, Shanghai Ninth People's Hospital, Shanghai Jiao Tong University School of Medicine, Shanghai, China, [4] Beijing National Laboratory for Molecular Sciences, State Key Laboratory of Polymer Physics & Chemistry, Institute of Chemistry, Chinese Academy of Sciences, Beijing, China, [5] University of Chinese Academy of Sciences, Beijing, China

OPEN ACCESS

Edited by:
Xuetao Shi,
South China University of Technology, China

Reviewed by:
Chuang Li,
Washington University School of Medicine in St. Louis, United States
Jian Song,
Sun Yat-sen University, China
Mingshun Sun,
Westlake Institute for Advanced Study (WIAS), China

***Correspondence:**
Xing Wang
wangxing@iccas.ac.cn
Jia-Kuo Yu
yujiakuo@126.com

Specialty section:
This article was submitted to Biomaterials, a section of the journal Frontiers in Bioengineering and Biotechnology

Received: 09 April 2020
Accepted: 26 May 2020
Published: 26 June 2020

Citation:
Xu B, Yuan F-Z, Lin L, Ye J, Fan B-S, Zhang J-Y, Yang M, Jiang D, Jiang W-B, Wang X and Yu J-K (2020) The Higher Inherent Therapeutic Potential of Biomaterial-Based hDPSCs and hEnSCs for Pancreas Diseases. Front. Bioeng. Biotechnol. 8:636. doi: 10.3389/fbioe.2020.00636

Human endometrial stem cells (hEnSCs), dental pulp stem cells (hDPSCs) and adipose tissue-derived stem cells (hADSCs) are considered to be the promising candidates for the treatment of pancreas diseases. The prognosis is better with *in situ* injection of mesenchymal stem cells (MSCs) to the damaged pancreas compared with intravenous injection. However, the clinical application of these cells are limited, due to poor engraftment of transplanted cells after delivery. On the other hand, understanding the role of the biomaterials in cell therapy is essential to promote the therapeutic effects of MSCs. Matrigel, a basement membrane matrix biomaterial, is rich in laminin and collagen IV. The aim of this study is to investigate the difference of biological characteristics of hEnSCs, hDPSCs and hADSCs *in vitro* and their survival situation with Matrigel post intrapancreatic transplantation *in vivo*. Our findings showed, firstly, there was no significant difference in morphology and immunophenotype of these MSCs. Secondly, the biological properties, including cell proliferation, the ability of adipogenic and osteogenic differentiation and the mRNA expression levels of pancreas development-related genes, have been showed distinct difference among these MSCs. Thirdly, Matrigel can improve the survival of MSCs *in vivo*, especially for Matrigel-based hDPSCs and Matrigel-based hEnSCs in pancreas parenchyma of SD rats. These results suggest that hDPSCs and hEnSCs are with the greater inherent therapeutic potential for pancreas diseases compared with hADSCs.

Keywords: hEnSCs, hDPSCs, hADSCs, biomaterial, orthotopic transplantation

INTRODUCTION

Type 1 diabetes, characterized by insulin deficiency caused by autoimmune destruction of pancreatic beta-cells (American Diabetes Association, 2013), results in an enormous burden on global health and economy. An elegant solution to reintroduce functional insulin-secreting cells in patients is to derive islets, β-cells or pancreatic progenitor cells *in vitro* from human pluripotent stem cells (Pagliuca et al., 2014), which would provide an alternative cell source for cell transplantation therapy in diabetes. Of particular interest is the application of autologous

mesenchymal stem cells (MSCs) with the low risk of tumorigenesis (Domínguez-Bendala et al., 2012), no immune rejection and little ethical concerns. Among them, human endometria, dental pulp and adipose tissue–derived MSCs are considered to be the attractive sources for potential clinical application, because of their easy accessibility, high clonogenicity and minimal economic burden and discomfort for donors (Prianishnikov, 1978; Gronthos et al., 2000; Zuk et al., 2002).

The endometrium is highly dynamic and experienced 400 menstrual cycles during a woman's lifetime. In 1978, Prianishnikov first observed that stem cells were present in the endometrium (Prianishnikov, 1978). Human endometrial stem cells (hEnSCs) have specific stem or progenitor cells that have long been believed to be critical for cyclic growth and regeneration (Gargett and Masuda, 2010). Human dental pulp stem cells (hDPSCs) are located in the pulp tissue in the central cavity of the tooth, and are particularly interesting because although tooth is small but still a source of abundant cells for clinical applications. These cells were firstly reported in 2000 by Gronthos and characterized with high clonogenicity, regenerative capacity, and the ability to generate densely calcified nodules (Gronthos et al., 2000). Human adipose tissue-derived stem cells (hADSCs) were firstly isolated from subcutaneous adipose tissue and introduced as a multipotent, undifferentiated and self-renewing cell population by Zuk et al. (2002). ADSCs can be acquired easily from adipose tissue through a minimally invasive method, and the quality and proliferation of ADSCs do not decline with the donor's age (Beane et al., 2014).

Previous studies have demonstrated that MSCs derived from various tissue sources are different in gene expression profile, growth pattern and propensity toward specific lineage (Nekanti et al., 2010). Therefore, it is reasonable that various MSCs producing different cytokines and growth factors that might be more suitable for specific clinical applications. Similarly, we assumed that gene expressions determining the cells development pathway are different among MSCs derived from various sources. Moriscot et al. found that native human bone marrow MSCs constitutively express NKX6.1 at a low level but lack all other transcription factors implicated in β-cell differentiation (Moriscot et al., 2005). In addition, umbilical cord blood contains a subpopulation of cells that are very similar in phenotype to endocrine cell precursors in transition to β-cells (Pessina et al., 2004), but the related gene expression of hEnSCs, hDPSCs and hADSCs in β-cell differentiation remains poorly understood.

A pattern of orderly activation and extinction of many genes during development control the formation of the pancreas and their subsequent differentiation into mature cell types including different exocrine and endocrine cell types. Expression of these related genes is regulated by a hierarchy of key transcription factors, such as SRY-box 17 (Sox17), forkhead box A2 (Foxa2), C-X-C motif chemokine receptor 4 (Cxcr4), pancreatic and duodenal homeobox 1(Pdx1), neuronal differentiation 1 (Neurod1), neurogenin 3 (Ngn3), paired box 4 (Pax4), which control the embryonic formation of pancreatic islets (Jensen, 2004).

On the other hand, the direct injection of MSCs into the damaged pancreas may improve the therapeutic effects compared with intravenous injection. However, these cells are not always function efficiently after injection, due to poor engraftment of transplanted cells, which prevents its wider application. Biomaterials have experienced steady and strong growth over its history and attracted increasing attention for tissue restoration and regeneration (Zhu et al., 2019; Xu et al., 2020b). However, the role of the biomaterials in cell therapy remains unclear. Matrigel is a biomaterial basement membrane matrix, which is derived from mouse sarcoma, and is mainly composed of laminin and collagen IV.

To better understand the inherent therapeutic potential for pancreas diseases of hEnSCs, hDPSCs and hADSCs and the role of biomaterials post intrapancreatic transplantation *in vivo*, first we compared and confirmed that these cells exhibit typical MSC morphology, have high proliferation and multipotency, and express the phenotypic surface marker characteristics of MSCs. Subsequently, we compared the different expression levels of key transcription factors implicated in pancreatic development and function in MSCs by reverse transcription-quantitative polymerase chain reaction (RT-qPCR). Finally, our initial experiments show that the three types of Matrigel-based MSCs can survive differently under pancreatic microenvironment conditions after local injection into pancreatic parenchyma in living SD rats (**Figure 1**).

MATERIALS AND METHODS

Materials

Dulbecco's modified Eagle's medium/nutrient mixture F-12 (DMEM-F12), penicillin/streptomycin and fetal bovine serum (FBS) were obtained from Gibco. Collagenase P were obtained from Roche. Anti-human CD34-PE, CD45-FITC, HLA-DR-FITC, CD44-FITC, CD73-PE, CD90-FITC, and were purchased from BD Biosciences. Adipogenic and osteogenic inducing medium from Cyagen. Matrigel were obtained from Corning. Trizol Reagent were purchased by Invitrogen. All-In-One RT MasterMix Kit, EvaGreen qPCR MasterMix Kit were obtained from abmGood. Cell-tracker dye CM-DiI were purchased from Invitrogen.

Isolation and Culture of hEnSCs, hDPSCs and hADSCs

Endometrium tissues were collected from menstrual blood of 5 donors (ages 24–30 year olds females). Adipose tissues were obtained from 5 donors (ages 24–30 year olds females) through liposuction procedures. Intact deciduous tooth were obtained from 5 children (aged 8–12 years) who were undergoing continuous occlusal treatment with tooth extraction. All the donors and guardians provided written informed consents and experiments involving human tissue were approved by Peking University Third Hospital.

The endometrial sliced tissue was digested with 0.1% (w/v) collagenase P for 30 min and followed by the shaking with DNase I (15 U/mL) for another 30 min (37°C, 180 rpm), finally kept in DMEM-F12, adding with 1% (v/v) penicillin/ streptomycin and

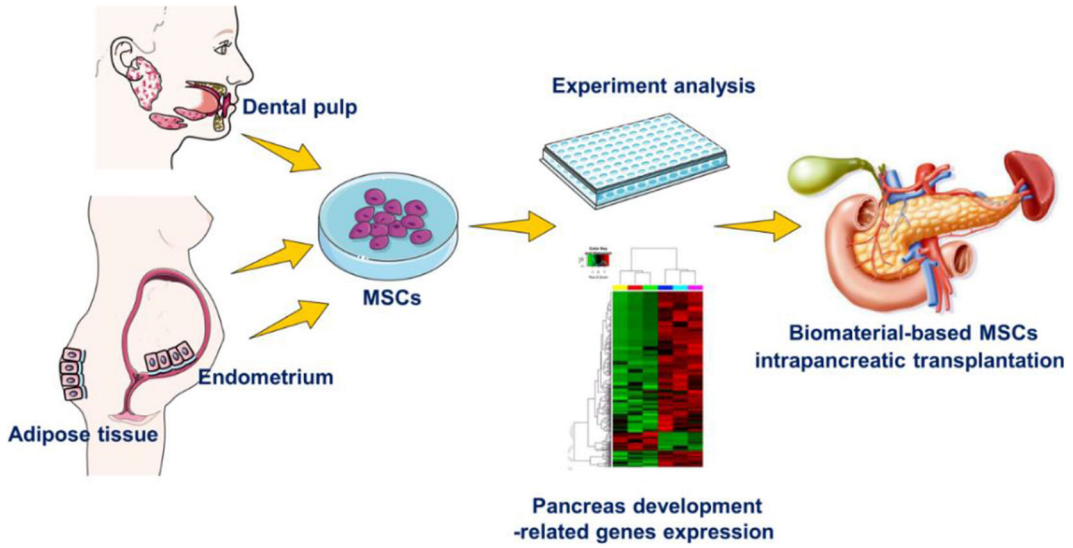

FIGURE 1 | Experimental design. The differences in hEnSCs, hDPSCs and hADSCs in the aspects of biological characteristics *in vitro* and their survival situation with Matrigel biomaterial post intrapancreatic transplantation *in vivo*.

10% (v/v) FBS. Nonadherent cells were removed 48 h after initial plating by intensely washing the flasks.

The dental pulp was expose, chopped into small pieces, minced, and digested in a 0.04% (w/v) collagenase solution. Culture conditions and medium were the same as hEnSCs.

The adipose tissue was washed and centrifuged. The adipose tissue in the middle was left and washed. The next procedures, culture conditions and medium were the same as hDPSCs.

Growth Characteristics Analysis

To compare the growth characteristics of the MSCs at P4, the growth rate and population doubling time (PDT) were measured. The cells in 6-well plates were counted for 7 consecutive days to measure the growth rate by digesting 3 wells and counting the cells. For PDT measure, the cells were counted until they reached 100% confluency. The PDT was calculated using the following formula: PDT = (CT × ln2)/ln(Nf/Ni), where CT is the cell culture time, Ni is the initial number of cells, and Nf is the final number of cells (Chen et al., 2015).

Flow Cytometry Analysis

For phenotypic identification of the MSCs at P4, cells were stained with the following antibodies (1: 200) for 15 min at room temperature: anti-human CD44-FITC, CD73-PE, CD90-FITC, CD34-PE, CD45-FITC, and HLA-DR-FITC. No antibody is added to the negative control group. The MSCs were washed twice with PBS, resuspended and analyzed by flow cytometry.

In vitro Differentiation Assay

The MSCs at P4 were induced to differentiate into adipocytes and osteoblasts. Briefly, hADSCs were exposed to adipogenic induc medium for 7 days, and hDPSCs and hEnSCs were exposed for 28 days. Then, all MSCs were induced in osteogenic induction medium for 28 days. MSCs were stained with oil red O and alizarin red for adipogenic and osteogenic differentiation evaluation, respectly.

TABLE 1 | Primers sequences used in quantitative polymerase chain reaction.

Gene	Sequence (5′ to 3′)	Product length (bp)
Sox17	F: GGCGCAGCAGAATCCAGA R: CCACGACTTGCCCAGCAT	61
Foxa2	F: AAGACCTACAGGCGCAGCTA R: CCTTCAGGAAACAGTCGTTGA	214
Cxcr4	F: AACTGAGAAGCATGACGGACAAGTAC R: GCTGTAGAG GTTGACTGTGTAGATGAG	164
Pdx1	F: TGATACTGGATTGGCGTTGT R: GAATGGCTTTATGGCAGATTA	191
Ngn3	F: GGCTGTGGGTGCTAAGGGTA R: CAGGGAGAAGCAGAAGGAACAA	104
Neurod1	F: GACGACCTCGAAGCCATGAACG R: CCTCCTCTTCCTCTTCTTCCTCCTC	106
Pax4	F: GTATGGCTTGGAATGAGGCAGGAG R: GCAATCACAGGAAGGAGGAAGGAG	125
Insulin	F: CAGCCGCAGCCTTTGTGA R: GTGTAGAAGAAGCCTCGTTCC	91
GAPDH	F: CAGGAGGCATTGCTGATGAT R: GAAGGCTGGGGCTCATTT	138

RNA Isolation and RT-qPCR Analysis

Total cellular RNA of MSCs at P4 was extracted with Trizol Reagent. cDNA was synthesized from RNA by using All-In-One RT MasterMix Kit and qPCR assay was performed with gene specific primers and EvaGreen qPCR MasterMix kit. The primer sequences of qPCR were shown in **Table 1**.

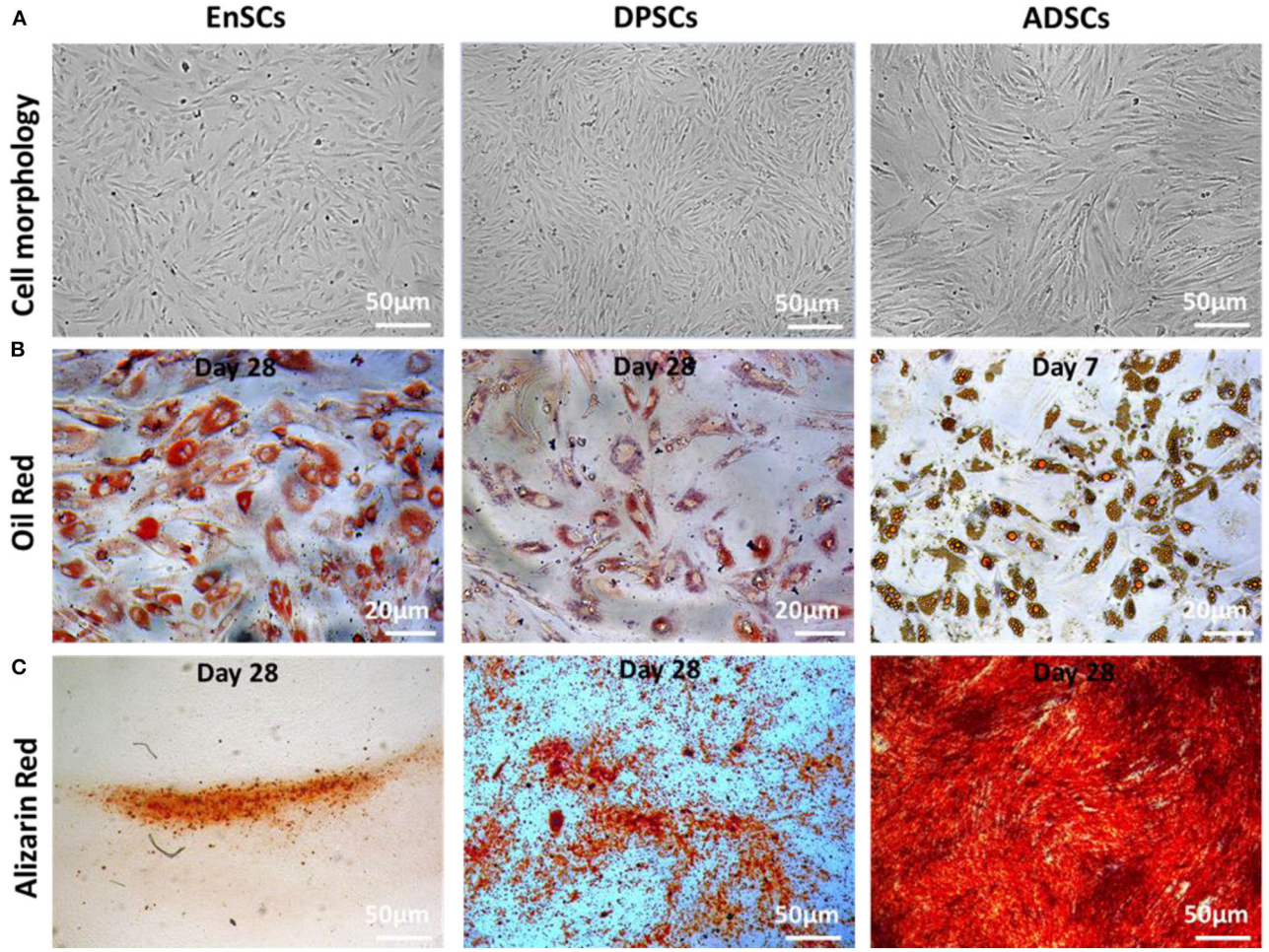

FIGURE 2 | Morphology and multilineage differentiation of MSCs derived from different tissues. All MSCs exhibited spindle-shaped morphology (**A**, scale bar = 50 μm). The differentiation of adipocytes and osteoblasts were verified by Oil Red O (**B**, scale bar = 20 μm) and Alizarin Red (**C**, scale bar = 50 μm), respectively. The representative picture is captured from one of 3 independent experiments.

In vivo Studies of MSCs

The MSCs (about 1×10^6 cells) were labeled with membrane-bound cell-tracker dye CM-DiI (Invitrogen). Matrigel physical embedded and not embedded MSCs were orthotopically transplanted into pancreatic parenchyma of SD rats ($n = 5$ in each group) by local injection, respectively. The survival of the SD rats in each group were observed. The fasting blood glucose levels of the tail tip were monitored at 30 min and day 1 post-implantation and followed by every three other days using a standard blood glucose meter. SD rats were sacrificed 14 days post transplantation, the pancreatic tissues were harvested for cryo-section. The slides with nuclear staining (DAPI) were evaluated to examine the survival of MSCs under pancreatic microenvironment conditions. All animal experiments were approved by Peking University Third Hospital.

Statistical Analysis

The statistical data are analyzed by GraphPad Prism 5.0 (California, USA). The data are presented as the means ± standard deviation (SD). Bilateral unpaired *t*-test is performed for comparisons between the two groups.

RESULTS AND DISCUSSION

Morphology and Multilineage Differentiation Potential

We found no significant differences in the morphology of three MSCs. All MSCs exhibited typical MSC morphology, including fibroblast-like, spindle shape (**Figure 2**, top panel). To examine the differentiation potential of the MSCs, the cells at P4 were induced to differentiate into the osteogenic and adipogenic lineages (**Figure 2**). Lipid droplets began to appear in hADSCs, hEnSCs and hDPSCs on about day 2, 16, and 21, respectively. The accumulation of cytoplasmic lipid vacuoles was obvious in the hADSCs on day 7, whereas only very small lipid granules were detected in hEnSCs and hDPSCs on day 28 and the adipogenic differentiation of hDPSCs were lower than hEnSCs (**Figure 2B**). In addition, hADSCs exhibited significant

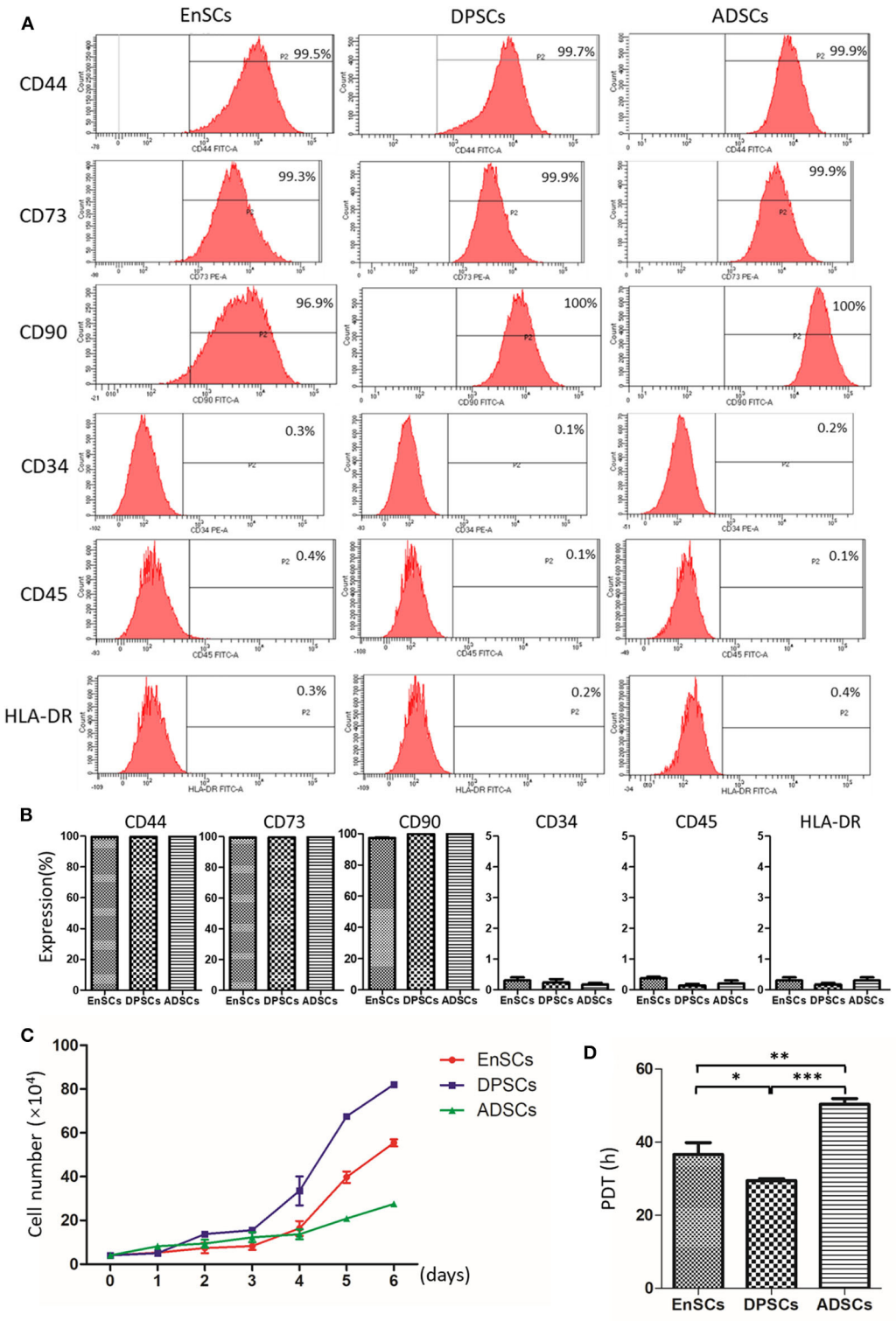

FIGURE 3 | Immunophenotype and proliferative potential of hEnSCs, hDPSCs and hADSCs. **(A,B)** Flow cytometric analysis of the expression of surface markers on MSCs. Shown **(A)** is one representative of 3 independent experiments. **(C)** Growth curves of MSCs ($n = 3$ donors). **(D)** PDT of MSCs from different types were analyzed and compared ($^{*}p < 0.05$, $^{**}p < 0.01$, $^{***}p < 0.0001$).

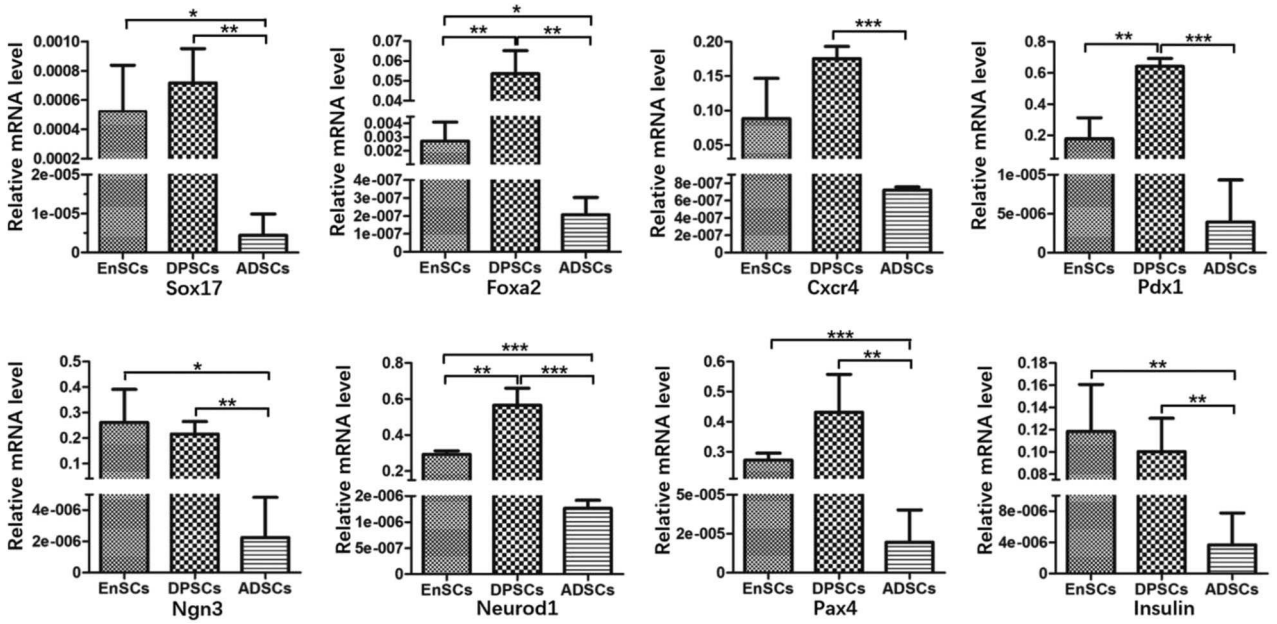

FIGURE 4 | Gene expression analysis of hEnSCs, hDPSCs and hADSCs. The expression levels relative to the housekeeping gene (GAPDH) are shown. The data are presented as the means ± standard deviation (SD) of 3 experiments; $^{*}p < 0.05$, $^{**}p < 0.01$, $^{***}p < 0.0001$.

osteogenic phenotypes, and the osteogenic differentiation in hEnSCs were only a little positive (**Figure 2C**).

Our results suggested that hEnSCs and hDPSCs show delayed adipogenic and osteogenic differentiation compared with hADSCs; the adipogenic differentiation of hDPSCs and the osteogenic differentiation of hEnSCs was lower than other MSCs in this study. Our findings, for the first time, revealed that hEnSCs had greater adipogenic competence. hADSCs showed significant osteogenic phenotypes in previous study (Zuk et al., 2002), and our data further demonstrated that hADSCs exhibited higher osteogenic differentiation compared with hEnSCs and hDPSCs. Additionally, hDPSCs showed more remarkable osteogenic potential compared with hEnSCs as well, which was consistent with the previous publication (Tabatabaei and Torshabi, 2017).

Immunophenotype

The International Society for Cellular Therapy (ISCT) criteria (Dominici et al., 2006) defined the classical MSCs phenotypic markers. All of these MSCs were highly expressed with MSC-specific surface markers (CD44, CD73, and CD90), and lowly expressed with hematopoietic cell marker (CD34), leucocyte marker (CD45), and monocyte/macrophage marker (HLA-DR). Our results showed there was no significant difference of immunophenotype in the MSCs ($n = 3$) (**Figures 3A,B**).

Growth Characteristics of MSCs

The growth curves of hEnSCs, hDPSCs and hADSCs at P4 show that the proliferation ability of the MSCs was hDPSCs > hEnSCs > hADSCs (**Figure 3C**). Furthmore, the cell PDT of the hEnSCs, hDPSCs and hADSCs were 36.62 ± 3.19 h, 29.45 ± 0.54 h, 50.34 ± 1.56 h, respectively (**Figure 3D**). The previous study showed the proliferation rate of hEnSCs were greater than that of hDPSCs from adult teeth (Tabatabaei and Torshabi, 2017), which was not contradictory with our results because hDPSCs from deciduous teeth in our study showed higher proliferation rate than hDPSCs from adult teeth (Wang et al., 2018). Meanwhile, hDPSCs from adult teeth were highly proliferative compared with hADSCs (Abu Kasim et al., 2015), which was consistent with our results.

Gene Expression Analysis

Relative mRNA expression levels of pancreas development-related genes in MSCs were analyzed using RT-qPCR (**Figure 4**). The results showed that hEnSCs, hDPSCs and hADSCs all expressed these genes. The mRNA expression levels of *Sox17*, *Foxa2*, *Ngn3*, *Neurod1*, *Pax4*, and *Insulin* from hADSCs were markedly lower than hEnSCs and hDPSCs. High expressions of *Foxa2*, *Pdx1*, and *Neurod1* were observed in hDPSCs compared with hEnSCs, but there were no significant differences in the expression of *Sox17*, *Cxcr4*, *Ngn3*, *Pax4*, and *Insulin* among these MSCs. Interestingly, the mRNA expressions of *Foxa2*, *Pdx1*, and *Neurod1* in hDPSCs were at least twenty times, three times, twice as high as in hEnSCs, respectively. hADSCs expressed significantly lower level of *Cxcr4* and *Pdx1* than hDPSCs, and no significant difference in the expression of *Cxcr4* was observed compared with hEnSCs.

In our study, MSCs all naturally express *Sox17*, *Foxa2*, *Cxcr4*, *Pdx1*, *Neurod1*, *Ngn3*, *Pax4*, and *Insulin*, and the mRNA expression levels of these genes showed great variation. Govindasamy et al. revealed that the gene variations of the stem cells determine the lineage propensity toward a specific destination (Govindasamy et al., 2010). It has been demonstrated that MSCs from dental pulp and adipose tissue can differentiate

into functional insulin-producing cells by using the same three-step protocol, but the yield of PDX-1^+ cells and C-peptide-positive cells from hDPSCs were 44.92 ± 0.9% and 30.56 ± 2%, respectively; and that from murine epididymal ADSCs were 57–71% and 47–51%, respectively (Chandra et al., 2010; Govindasamy et al., 2011). The different yield of PDX-1^+ cells and C-peptide-positive cells may be related to the inherent expressions of pancreas development-related genes.

In previous studies, researchers succeeded in obtaining islet-like cell aggregates using a stepwise method, from MSCs to endoderm-like cells, pancreatic progenitor-like cells, and β cells (Chandra et al., 2010; Govindasamy et al., 2011; Li et al., 2014). *Sox17*, *Foxa2*, and *Cxcr4*, three relatively specific marker genes for definitive endoderm (Li et al., 2014). We found that the expression of *Sox17* in the hADSCs was obviously lower compared with the other two kinds of MSCs and there were no significant differences between hDPSCs and hEnSCs. *Sox17* drives human pluripotent stem cells toward an endodermal or mesendodermal fate (Guo and Hebrok, 2009). For another two endodermal markers, hDPSCs expressed the highest level of *Foxa2* but expression of Cxcr4 only higher than hADSCs. hADSCs expressed significantly less *Foxa2* than hEnSCs. *Foxa2* is essential for the cell type–specific transcription of the *Pdx1* gene in the differentiation of the pancreas (Lee et al., 2002). *Cxcr4* is essential for pancreatic endocrine progenitor cells proliferation and maturation (Guo and Hebrok, 2009). Based on these results, it is possible that the potential of MSCs reprograming into definitive endoderm-like cells was as follows: hDPSCs > hEnSCs > hADSCs.

Pdx1, one specific marker gene for pancreatic progenitors; *Ngn3* and *Neurod1,* two endocrine progenitor marker genes (Li et al., 2014). *Pdx1* is the only transcription factor specific of the endocrine pathway (Moriscot et al., 2005). *Ngn3* is crucial for the induction of differentiation from pancreatic progenitor cells into endocrine cells and switches off before the final differentiation into β cells (Watada, 2004). *Neurod1* plays a crucial role in endocrine cell survival and *Insulin* gene transcription (Watada, 2004). In this study, strong expressions of *Pdx1* and Neurod1 were observed in hDPSCs compared to that of hEnSCs. The expression levels of *Ngn3* and *Neurod1* in hADSCs were the lowest in the three MSCs, but the expression of *Pdx1* only less than hEnSCs. These results were surprising in that *Pdx1* could control *Ngn3* in activating the expression of other differentiation factors for endocrine cells, while *Neurod1* is activated by *Ngn3* (Pessina et al., 2004; Watada, 2004). Furthermore, it is of possibility as well that the potential of MSCs from definitive endoderm-like cells into pancreatic progenitors-like cells was as follows: hDPSCs > hEnSCs > hADSCs.

Pax4 is essential to initiate pancreatic cell differentiation (Guo and Hebrok, 2009). Furthermore, we observed that expression levels of *Pax4 and Insulin* in hADSCs were the lowest as compared with hEnSCs and hDPSCs, while no significant differences in the expressions of *Pax4* and *Insulin* were observed in hDPSCs compared to that of hEnSCs. Most importantly, the *Insulin* mRNA is expressed in all the MSCs, but undifferentiated hEnSCs, hDPSCs and hADSCs can't release *Insulin* in response to

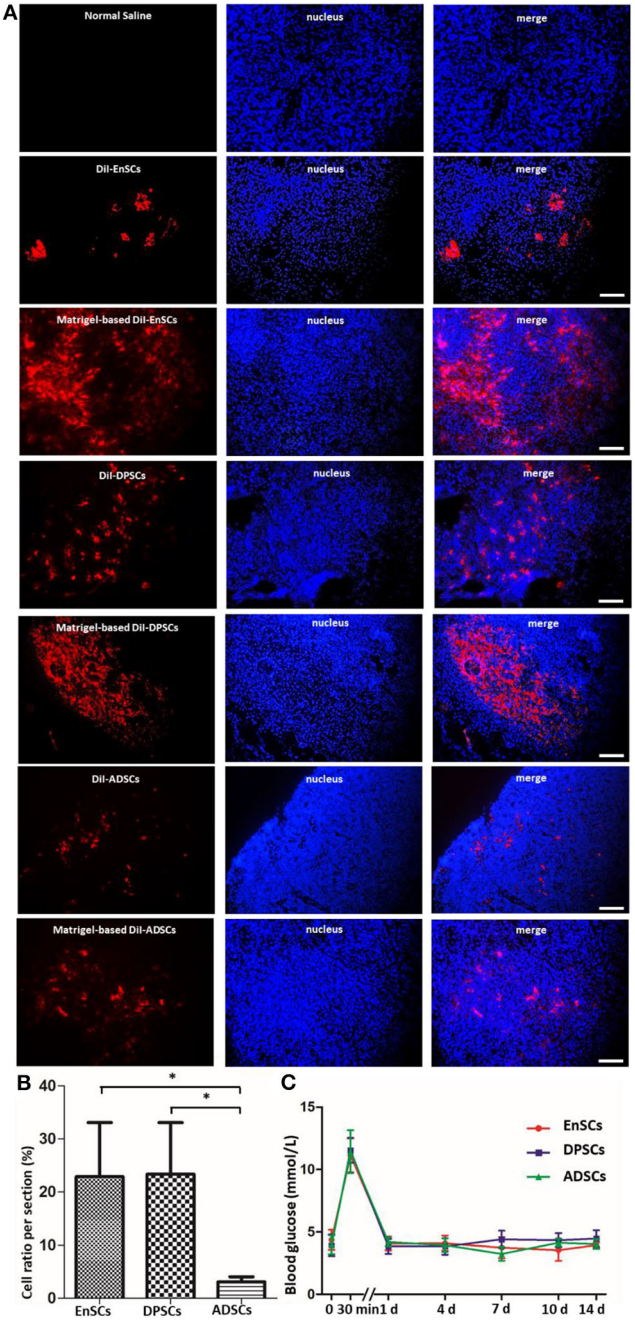

FIGURE 5 | MSCs from three sources at day 14 post orthotopic injection into pancreatic parenchyma of SD rats. **(A)** Representative fluorescence micrographs of cryo-sections in the EnSCs (upper panel), DPSCs (middle panel) and ADSCs (bottom panel) engraftment groups 14 days after orthotopical transplantation into pancreatic parenchyma of SD rats, respectively. Dil fluorescence, red; DAPI fluorescence, blue. Scale bar = 20 μm. **(B)** The average ratios of Matrigel-based CM-Dil-labeled cells counted in the pancreatic cryo-sections. Shown in the histogram were the percentages of Matrigel-based CM-Dil-labeled MSCs in the three groups compared to the total nuclei. $^*p < 0.05$. **(C)** Blood glucose levels in SD rats transplanted orthotopically with Matrigel-based hEnSCs, Matrigel-based hDPSCs, and Matrigel-based hADSCs. Shown are the average blood glucose levels of the tail tip measured and plotted for each time point.

glucose *in vitro* (Chandra et al., 2010; Govindasamy et al., 2011; Santamaria et al., 2011). All the mRNA expression levels of these pancreas development-related genes suggest that potential post-transcriptional regulating mechanisms may block the protein expression of some key transcription factors implicated in pancreatic development. And it can be hypothesized that the silent genes reside in the three MSCs in a standby state, and the activation of the genes are restricted by their natural environment.

The Survival of Matrigel-Based MSCs Post Transplantation and the Effects of Matrigel-Based MSCs to SD Rats

Direct check of cryo-section under a Immunofluorescence microscope showed that all the CM-DiI-labeled MSCs could be detected in the pancreatic tissues on day 14 post-transplanation (**Figure 5A**). The average ratios of CM-DiI-labeled cells in Matrigel-based hDPSCs (23.4 ± 5.58%) and Matrigel-based hEnSCs (22.88 ± 5.89%) counted per pancreatic section were significantly higher than Matrigel-based hADSCs (3.09 ± 0.57%) ($p < 0.05$) (**Figure 5B**). These results indicated that Matrigel could improve the survival of MSCs and Matrigel-based hDPSCs, and Matrigel-based hEnSCs had higher survival rates than Matrigel-based hADSCs in pancreas parenchyma of SD rats, which was consistent with the mRNA expression levels of pancreas development-related genes. It is suggested that mRNA expressions of these genes may reflect the survival of MSCs in pancreas.

The blood glucose levels of the rats were increased instantaneously at 30 min after the implantation of Matrigel-based MSCs and then decreased to normal levels at day 1 post-implantation. There were no significant difference among these MSCs (**Figure 5C**). These results suggested that the pancreatic orthotopic engraftment of MSCs did little damage to the pancreas, and pancreatic orthotopic engraftment of hDPSCs and hEnSCs could be used for clinical treatment.

These data indicate that Matrigel-based hDPSCs, Matrigel-based hEnSCs and Matrigel-based hADSCs could survive in the pancreatic parenchyma of SD rats. Low-temperature Matrigel suspension and injection was effective for establishing an orthotopic mouse model of pancreatic cancer (Jiang et al., 2014). The three-dimensional culture of hDPSCs in Matrigel promotes the differentiation of DPSCs into insulin-producing Cells (Xu et al., 2020a). Matrigel could also be used for the renal subcapsular transplant of native mouse islets and pancreatic progenitor-like cells (Li et al., 2014). However, there is no research on the role of biomaterials in pancreas transplantation of MSCs. Our findings, for the first time, revealed that Matrigel can improve the survival of MSCs, and Matrigel-based hDPSCs and Matrigel-based hEnSCs had higher survival rates than Matrigel-based hADSCs in pancreas.

CONCLUSION

In summary, our novel and unexpected finding is a step forward in evaluating the high inherent therapeutic potential of hDPSCs and hEnSCs for pancreas diseases. Nevertheless, further investigations are needed to identify the ability of MSCs derived from the two sources differentiating into insulin-producing β-cells.

DATA AVAILABILITY STATEMENT

The raw data supporting the conclusions of this article will be made available by the authors, without undue reservation.

ETHICS STATEMENT

The studies involving animal and human participants were reviewed and approved by Peking University Third Hospital. Written informed consent to participate in this study was provided by the participants' legal guardian/next of kin.

AUTHOR CONTRIBUTIONS

XW and J-KY conceived the research. BX, F-ZY, JY, J-YZ, MY, and B-SF isolated and cultured the MSCs. J-YZ analyzed the growth characteristics. BX and LL performed the Flow cytometry. BX and B-SF did the RT-qPCR analysis and transplantation experiment. BX wrote the manuscript. DJ and W-BJ helped revising the paper. All authors contributed to the article and approved the submitted version.

FUNDING

This research was funded by the National Natural Science Foundation of China (NSFC, 51920105006, 81630056, 51973226, and 51773004) and the National Key Research and Development Program of China (Grant No. 2016YFC1100704).

ACKNOWLEDGMENTS

We thank Dr. Chao Liu for critical comments on the manuscript.

REFERENCES

Abu Kasim, N. H., Govindasamy, V., Gnanasegaran, N., Musa, S., Pradeep, P. J., Srijaya, T. C., et al. (2015). Unique molecular signatures influencing the biological function and fate of post-natal stem cells isolated from different sources. *J. Tissue Eng. Regenerative Med.* 9, E252–E266. doi: 10.1002/term.1663

American Diabetes Association (2013). Diagnosis and classification of diabetes mellitus. *J. Sci. Diabetes Care.* 36, S67–S74. doi: 10.2337/dc13-S067

Beane, O. S., Fonseca, V. C., Cooper, L. L., Koren, G., and Darling, E. M. (2014). Impact of aging on the regenerative properties of bone marrow-, muscle-, and adipose-derived mesenchymal stem/stromal cells. *PLoS ONE* 9:e115963. doi: 10.1371/journal.pone.0115963

Chandra, V., G, S., Phadnis, S., Nair, P. D., and Bhonde, R. R. (2010). Generation of pancreatic hormone-expressing islet-like cell aggregates from murine adipose tissue-derived stem cells. *Stem Cells* 27, 1941–1953. doi: 10.1002/stem.117

Chen, G., Yue, A., Ruan, Z., Yin, Y., Wang, R., Ren, Y., et al. (2015). Comparison of biological characteristics of mesenchymal stem cells derived

from maternal-origin placenta and Wharton's jelly. *Stem Cell Res. Therapy*. 6:228. doi: 10.1186/s13287-015-0219-6

Domínguez-Bendala, J., Lanzoni, G., Inverardi, L., and Ricordi, C. (2012). Concise review: mesenchymal stem cells for diabetes. *Stem Cells Transl. Med*. 1, 59–63. doi: 10.5966/sctm.2011-0017

Dominici, M. L. B. K., Le Blanc, K., Mueller, I., Slaper-Cortenbach, I., Marini, F. C., Krause, D. S., et al. (2006). Minimal criteria for defining multipotent mesenchymal stromal cells. The International Society for Cellular Therapy position statement. *Cytotherapy* 8, 315–317. doi: 10.1080/14653240600855905

Gargett, C., and Masuda, H. (2010). Adult stem cells in the endometrium. *J. Sci. Mol Hum Reprod*. 16, 818–834. doi: 10.1093/molehr/gaq061

Govindasamy, V., Abdullah, A. N., Ronald, V. S., Musa, S., Ab Aziz, Z. A., Zain, R. B., et al. (2010). Inherent differential propensity of dental pulp stem cells derived from human deciduous and permanent teeth. *J. Endodontics* 36, 1504–1515. doi: 10.1016/j.joen.2010.05.006

Govindasamy, V., Ronald, V. S., Abdullah, A. N., Nathan, K. R., Ab Aziz, Z. A., Abdullah, M., et al. (2011). Differentiation of dental pulp stem cells into islet-like aggregates. *J. Dental Res*. 90, 646–652. doi: 10.1177/0022034510396879

Gronthos, S., Mankani, M., Brahim, J., Robey, P. G., and Shi, S. (2000). Postnatal human dental pulp stem cells (DPSCs) *in vitro* and *in vivo*. *Proc Natl Acad Sci USA*. 97, 13625–13630. doi: 10.1073/pnas.240309797

Guo, T., and Hebrok, M. (2009). Stem cells to pancreatic beta-cells: new sources for diabetes cell therapy. *Endocrine Rev*. 30:214. doi: 10.1210/er.2009-0004

Jensen, J. (2004). Gene regulatory factors in pancreatic development. *Dev Dyn*. 229, 176–200. doi: 10.1002/dvdy.10460

Jiang, Y. J., Lee, C. L., Wang, Q., Zhou, Z. W., Yang, F., Jin, C., et al. (2014). Establishment of an orthotopic pancreatic cancer mouse model: Cells suspended and injected in Matrigel. *World J. Gastroenterol*. 28, 9476–9485. doi: 10.3748/wjg.v20.i28.9476

Lee, C. S., Sund, N. J., Vatamaniuk, M. Z., Matschinsky, F. M., Stoffers, D. A., and Kaestner, K. H. (2002). Foxa2 controls Pdx1 gene expression in pancreatic beta-cells *in vivo*. *Diabetes* 51, 2546–2551. doi: 10.2337/diabetes.51.8.2546

Li, K., Zhu, S., Russ, H. A., Xu, S., Xu, T., Zhang, Y., et al. (2014). Small molecules facilitate the reprogramming of mouse fibroblasts into pancreatic lineages. *Cell Stem Cell* 14, 228–236. doi: 10.1016/j.stem.2014.01.006

Moriscot, C., De Fraipont, F., Richard, M. J., Marchand, M., Savatier, P., Bosco, D., et al. (2005). Human bone marrow mesenchymal stem cells can express insulin and key transcription factors of the endocrine pancreas developmental pathway upon genetic and/or microenvironmental manipulation *in vitro*. *Stem Cells*. 23, 594–603. doi: 10.1634/stemcells.2004-0123

Nekanti, U., Rao, V. B., Bahirvani, A. G., Jan, M., Totey, S., and Ta, M. (2010). Long-term expansion and pluripotent marker array analysis of Wharton's Jelly-derived mesenchymal stem cells. *Stem Cells Dev*. 19, 117–130. doi: 10.1089/scd.2009.0177

Pagliuca, F. W., Millman, J. R., Gürtler, M., Segel, M., Van Dervort, A., Ryu, J. H., et al. (2014). Generation of functional human pancreatic beta cells *in vitro*. *Cell*. 159, 428–439. doi: 10.1016/j.cell.2014.09.040

Pessina, A., Eletti, B., Croera, C., Savalli, N., Diodovich, C., and Gribaldo, L. (2004). Pancreas developing markers expressed on human mononucleated umbilical cord blood cells. *Biochem. Biophys. Res. Commun*. 323, 315–322. doi: 10.1016/j.bbrc.2004.08.088

Prianishnikov, V. A. (1978). On the concept of stem cell and a model of functional-morphological structure of the endometrium. *Contraception* 8, 213–223. doi: 10.1016/S0010-7824(78)80015-8

Santamaria, X., Massasa, E. E., Feng, Y., Wolff, E., and Taylor, H. S. (2011). Derivation of insulin producing cells from human endometrial stromal stem cells and use in the treatment of murine diabetes. *Mol. Ther*. 19, 2065–2071. doi: 10.1038/mt.2011.173

Tabatabaei, F. S., and Torshabi, M. (2017). In vitro proliferation and osteogenic differentiation of endometrial stem cells and dental pulp stem cells. *Cell Tissue Banking* 18, 1–9. doi: 10.1007/s10561-017-9620-y

Wang, H., Zhong, Q., Yang, T., Qi, Y., Fu, M., Yang, X., et al. (2018). Comparative characterization of SHED and DPSCs during extended cultivation *in vitro*. *Mol. Med. Rep*. 17, 6551–6559. doi: 10.3892/mmr.2018.8725

Watada, H. (2004). Neurogenin 3 is a key transcription factor for differentiation of the endocrine pancreas. *Endocr. J*. 51, 55–64. doi: 10.1507/endocrj.51.255

Xu, B., Fan, D., Zhao, Y., Li, J.,Wang, Z.,Wang, J., et al. (2020a). Three-dimensional culture promotes the differentiation of human dental pulp mesenchymal stem cells into insulin-producing cells for improving the diabetes therapy. *Front. Pharmacol*. 10:1576. doi: 10.3389/fphar.2019.01576

Xu, B., Ye, J., Yuan, F. Z., Zhang, J. Y., Chen, Y. R., Fan, B. S., et al. (2020b). Advances of stem cell-laden hydrogels with biomimetic microenvironment for osteochondral repair. *Front. Bioeng. Biotechnol*. 8:247. doi: 10.3389/fbioe.2020.00247

Zhu, C., Xia, Y., Zai, Y., Dai, Y., Liu, X., Bian, J., et al. (2019). Adsorption and desorption behaviors of HPEI and thermoresponsive HPEI based gels on anionic and cationic dyes. *Chem. Eng. J*. 369, 863–873. doi: 10.1016/j.cej.2019.03.169

Zuk, P. A., Zhu, M., Ashjian, P., De Ugarte, D. A., Huang, J. I., Mizuno, H., et al. (2002). Human adipose tissue is a source of multipotent stem cells. *Mol. Biol. Cell*. 13, 4279–4295. doi: 10.1091/mbc.e02-02-0105

Conflict of Interest: The authors declare that the research was conducted in the absence of any commercial or financial relationships that could be construed as a potential conflict of interest.

frontiers in Materials

REVIEW
published: 10 July 2020
doi: 10.3389/fmats.2020.00202

Engineered Bacterial Outer Membrane Vesicles as Multifunctional Delivery Platforms

Ruizhen Li[1] *and Qiong Liu*[1,2]*

[1] Department of Medical Microbiology, School of Medicine, Nanchang University, Nanchang, China, [2] Key Laboratory of Tumor Pathogenesis and Molecular Pathology, School of Medicine, Nanchang University, Nanchang, China

Outer membrane vesicles (OMVs) are valued for their unique, convenient, and amendable functions. They are flexible, controllable nanoparticles, which can be modified in different ways, for use in a wide array of applications like adjuvants, vaccines, drug presentation, and fluorescence tracking. Attempts have been made to alter the nanoparticles in liposomes and bacterial ghosts using traditional methods. However, it has not been highly successful owing to certain unavoidable disadvantages. OMVs have unique advantages and are considered novel platforms for heterologous protein presentation. Although previous reviews have described this to some extent, owing to the rapid development in this field, there is a need for the regular update of the reviews. This review focuses on few novel applications of engineered OMVs, and redefines the significance of OMVs as novel multifunctional delivery platforms. Additionally, this review also supplements and provides an update on the OMV transformation methods.

Keywords: genetic engineering, multifunctional delivery platform, outer membrane vesicles (OMVs), LPS, ClyA, AT

OPEN ACCESS

Edited by:
Huanan Wang,
Dalian University of Technology, China

Reviewed by:
David Wibowo,
Griffith University, Australia
Michihiro Nakamura,
Yamaguchi University, Japan

***Correspondence:**
Qiong Liu
qiongliu@ncu.edu.cn

Specialty section:
This article was submitted to Biomaterials, a section of the journal Frontiers in Materials

Received: *28 January 2020*
Accepted: *03 June 2020*
Published: *10 July 2020*

Citation:
Li R and Liu Q (2020) Engineered Bacterial Outer Membrane Vesicles as Multifunctional Delivery Platforms. Front. Mater. 7:202. doi: 10.3389/fmats.2020.00202

INTRODUCTION

Outer membrane vesicle (OMV), naturally secreted by Gram-negative bacteria, is a spherical nanostructure with a diameter of 30–200 nm (**Figure 1**) (Liu et al., 2016). Bacteria can produce OMVs in solid and liquid media, or in biofilms and intracellular infections under *in vitro* conditions (Unal et al., 2011; Klimentová and Stulík, 2014; Caruana and Walper, 2020). The generation of OMVs is considered a stress response. Various stress factors, such as temperature, nutrient consumption, and exposure to harmful chemicals, may cause accumulation and aggregation of misfolded proteins in the periplasm. Packing these pressure products to the outer membrane and releasing them, OMVs are formed (Klimentová and Stulík, 2014). Quantitative analysis showed that *Escherichia coli* packages ∼0.2–0.5% of outer membrane and periplasmic protein into OMV (Kesty and Kuehn, 2004). Approximately 1% of the outer membrane material could be incorporated into the vesicles of *Pseudomonas aeruginosa*, while the logarithmic phase culture of *Neisseria meningitidis* incorporates 8–12% of its total protein and endotoxin into vesicles (Devoe and Gilchrist, 1973; Bauman and Kuehn, 2006). Most of the components of OMVs are lipopolysaccharide (LPS), glycerophospholipids, and proteins including periplasmic proteins (Ellis and Kuehn, 2010; Underhill and Goodridge, 2012). The various components on OMVs serve different functions. LPS of OMVs gives its adjuvant function, which is useful for vaccine formulation, and some other antigen components that can be used for vaccine development. In addition, other components on OMVs also play roles that cannot be ignored. OMVs have been found to function as a multifaceted delivery system with intra- and inter-species

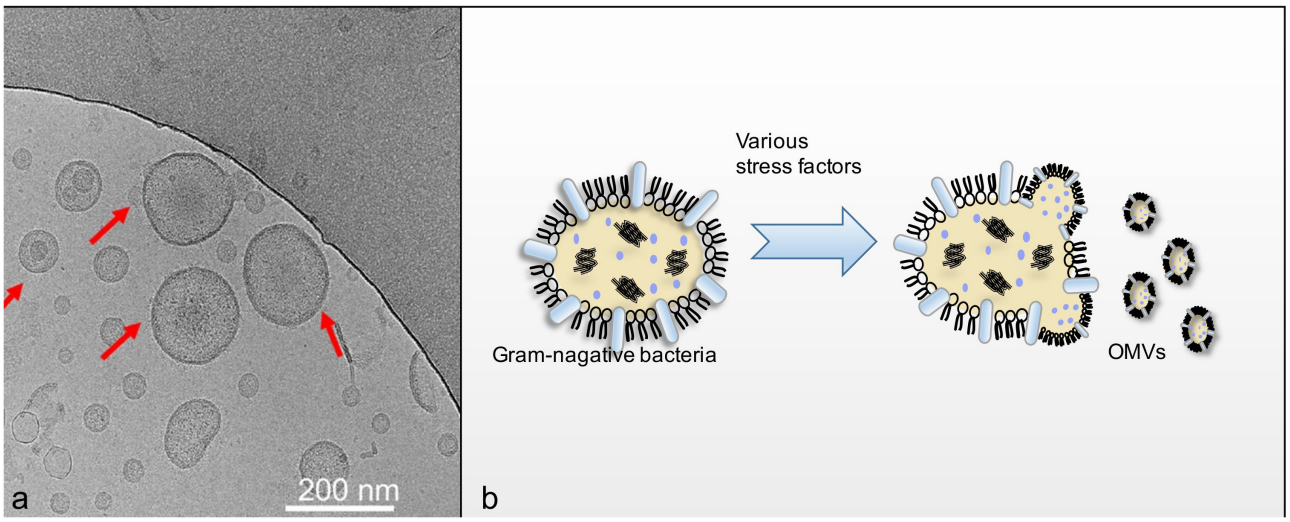

FIGURE 1 | (a) Showed that Cryo-EM imaging of OMVs (Liu et al., 2016). OMVs derived from the flagellin-deficient *S.typhimurium* were visualized using cryo-EM. The red arrows indicate the visible OMVs; **(b)** showed schematic diagram of OMVs secretion process.

interactions through membrane proteins (Ellis and Kuehn, 2010). The OMVs produced by *Mycobacterium tuberculosis* carries the iron-carrier mold, mycomycin, which transports this essential nutrient over long distances in a hostile host environment (Prados–Rosales et al., 2014). Regarding the interspecies interactions of OMVs, multiple studies have indicated the use of OMVs by many bacterial pathogens to deliver virulent determinants to host cells, at proximal and distal sites, thereby impairing the host defense system and promoting infection. In contrast, OMVs from various mucosal pathogens show numerous pathogen-associated molecular patterns including LPS, lipoproteins, DNA, and RNA. Their interaction with the pattern recognition receptors (PRR) on host epithelial cells stimulates the production of cytokines and chemokines on the mucosal epithelial surface, their interactions with immune cells, and regulates pathology in a variety of ways (Yoon, 2016). The virulence factors contained in OMVs can be distributed over long distances, and also transferred onto the plasma membranes of the host cells (Ellis and Kuehn, 2010).

Schulz et al. (2018) characterized the morphology of OMVs by electron microscopy and found that OMVs are biocompatible with epithelial cells and differentiated macrophages (Schulz et al., 2018). They showed low endotoxin activity compared to control samples, indicating low acute inflammation potential. At the same time, OMVs also showed good biodegradability, and it has been proven that OMV in the lysosome can be completely degraded after 48 h of endocytosis (Kim et al., 2012). Bioengineering can be used to increase OMV output, and may be used in conjunction with specific production processes to obtain a large number of well-defined, stable, and unified OMV particle vaccine products (van der Pol et al., 2015). Commercially available *N. meningitidis* serotype B OMV vaccine indicates the use of OMVs for disease prevention and treatment (Mirlashari et al., 2010; Collins, 2011; Santos et al., 2012). Currently, research has been focused on the use of OMVs in vaccine transformation platforms; different heterologous proteins can be efficiently added to achieve the use of such nanoparticles in multiple applications (Chen et al., 2010; Bartolini et al., 2013; Alves et al., 2015).

Although previous reviews have described OMVs in vaccine transformation platforms, since this is a rapidly growing area of research, the reviews need to be updated frequently (Gerritzen et al., 2017). This review mainly describes the applications of the most recently engineered OMVs, and gives an update on few novel engineering methods. Additionally, the advantages and disadvantages of the different engineering methods have been compared, and few prospective applications of the engineered OMVs have been described.

PURIFICATION, THE KEY STEP IN OMV USAGE IN VACCINE APPLICATIONS

Some bacterial nanoparticles have gradually gaining interest and are being developed with antigen-related functions. However, compared with OMV, the production process is more complicated and expensive, and it is difficult to ensure its safety in living organisms (**Table 1**) (Carita et al., 2018; Hu et al., 2019; Lee et al., 2019; Sánchez et al., 2020). Presently, there have been a variety of bacterial OMVs used in vaccine production attempts, such as *E. coli, P. aeruginosa, Shigella, Salmonella, Helicobacter pylori* (*H. pylori*), *Campylobacter jejuni, Borrelia burgdorferi, Vibrio,* and *Neisseria* spp. (Bauman and

Abbreviations: OMVs, Outer membrane vesicles; LPS, lipopolysaccharide; PRR, pattern recognition receptors; GFP, green fluorescent protein; ClyA, Cytosolic A; AT, Autotransport; GST, glutathione-S-transferase; OVA, Ovalbumin; β-stem, β-helix core structure; AA, amino acid; PTE, phosphodiesterase; Scaf3, trivalent scaffold; geOMVs, Glycosylation-modified OMVs; KGF-2, keratinocyte growth factor 2; Nluc, nano-luciferase; OMV Mel, biopolymer-melanin OMV.

TABLE 1 | The advantages and disadvantages of OMVs and other bacterial small molecules.

Bacterially produced carriers	Particle size	Material properties	Advantages	Disadvantages	References
Liposomes	10 nm–hundreds nm	Phospholipid vesicles	More extensive research; High biocompatibility; Low immunogenicity	Drug leakage; Incomplete loading function; Cumbersome quality control system	Carita et al., 2018
Bacterial ghosts	40–200 nm	Empty envelopes of Gram-negative bacteria	High security	Low efficiency; Complex production; Unclear effects of human application	Hu et al., 2019
Biologically synthesized polyester	100–500 nm	Polyester particles	Ensure antigen integrity; High biocompatibility; Non-toxic metabolism	Complex purification; Unstable production; Difficult to control the particle size of the host cell	Lee et al., 2019
Inclusion Bodies (IBs)	50 nm–hundreds nm	Inactive protein particles	Dense structure, hard to hydrolyze; Complete biocompatibility; Highly expressed protein	Purification is complex; Hard to produce large batches; Complex and Inconsistent production	Sánchez et al., 2020
OMVs	30–200 nm	Outer membrane of Gram-negative bacteria	Clinical use; High biocompatibility; Good biodegradability; Large-scale production; Simple purification steps; Unified production process; Convenient antigen presentation platform	Multiple antigen presentation efficiency is not high	Kesty and Kuehn, 2004; Ellis and Kuehn, 2010

Kuehn, 2006; Chatterjee and Chaudhuri, 2011; Elmi et al., 2012; Schwechheimer and Kuehn, 2015; Turner et al., 2015; Elhenawy et al., 2016). In the making of vaccines of different strains, some components on OMVs (such as LPS) could affect the safety of the vaccine. Purification can remove some unnecessary or harmful components, thereby making OMVs more in line with needs. Purification is the first and the most important step in the use of OMVs and impurities can have a large impact, resulting in extremely unfavorable on experimental outcomes. Thus, the purification of OMVs using traditional methods has been summarized, and the latest approaches for the purification of OMVs using genetic modifications have been elaborated.

Purification of OMVs Using Traditional Methods

Traditional methods of OMV purification include ultracentrifugation, density gradient separation, precipitation, and gel filtration techniques (Kataoka et al., 2014; Klimentová and Stulík, 2014; Cecil et al., 2016; Kim et al., 2017a,b). Density gradient centrifugation and gel filtration are commonly used methods for OMV purification (Kulp and Kuehn, 2010), while ultracentrifugation and precipitation are the primary methods to obtain OMVs. Although ultracentrifugation methods have been widely used in the preparation of OMVs, this method has certain shortcomings. The primary problem is the complexity of the operation process. It is time consuming, and requires skilled labor, owing to the complexity of the process. In addition, the high cost of the purification equipment makes it difficult to commercialize. Although sedimentation is relatively inexpensive, it also has certain unavoidable disadvantages. The preparation of the salt solution required for precipitation is difficult, and the steps are complicated. Also, the proteins on the OMVs are easily damaged, thereby allowing for a negative impact on experimental results (Qing et al., 2019). Additionally, considering the impact of LPS on the experiment, researchers have attempted certain special methods. Initially, detergent was added during the extraction process to attenuate LPS. However, studies have shown that LPS is a potential endotoxin, and acts as a powerful adjuvant for specific antigens (Mitra et al., 2013). Consequently, the complete removal of LPS from OMVs was required, rather than LPS attenuation with detergent, which proved unsuitable for the betterment of vaccine performance (Mitra et al., 2016). Therefore, researchers proposed the use of EDTA extraction (chelating agent) to obtain high quality OMVs, by accurately controlling the pH and collection point (van de Waterbeemd et al., 2012). However, this method demands stringent extraction conditions, and has a complex operation process. If the purification methods do not meet the research requirements, the development and application of OMVs in the biomedical field will be limited. Therefore, the development of a simpler and more feasible method is very crucial.

Genetic Engineering Used for Attenuating Toxicity of OMVs

Generally, major pathogenic Gram-negative bacteria can secrete OMVs and interact with the host through OMVs (Kuehn and Kesty, 2005). Although OMVs can be obtained by extraction with detergents, the improper use of chemicals can result in the loss of lipoproteins and enzymes, and their activity, which impairs the ability of OMVs to stimulate cross-protective immunity. In order to obtain OMVs with low toxicity and high safety, the genetic modification, and purification of OMVs has been proposed. Genetic modification is primarily aimed at the attenuation of the OMVs, and improvement of its yield. An established method is the knock out of the *msbB* gene, which regulates LPS in bacteria. The inactivation of *msbB* leads to a significant decrease

in the level of LPS endotoxin (Kim et al., 2009; Ranallo et al., 2010). This method has been widely used in the preparation of OMVs (Leitner et al., 2015). Latest research has combined a new modification scheme with the genetic modification of the *msbB* gene, and has helped to obtain good results. At the same time, the Dutch vaccine research institute found that the deletion of the *lpxL1* gene attenuated LPS toxicity while retaining the adjuvant activity required for the immune response (van der Ley et al., 2001; Fisseha et al., 2005; Koeberling et al., 2008). Engineered OMVs obtained from *Bordetella pertussis* expressing the *pagL* gene of *Bordetella bronchiseptica*, had lower endotoxin activity and better adjuvant performance. Attenuated OMVs are considered as prospective candidates in the development of novel vaccines targeting multiple antigens (Asensio et al., 2011).

Compared to the traditional methods, genetically engineered bacterial strains not only possess exclusively attenuated LPS, but also have the ability to induce pathogen-specific immune responses to OMVs, which is more suitable for the non-endotoxin conversion of OMVs (Shim et al., 2017). These pivotal genes attracted attention, and their knockout lead to a decrease in immunogenicity. Consequently, researchers have gradually started to explore more novel methods such as using non-pathogenic symbiotic bacteria as the source of OMVs, which can overcome the risks of gene knockout and render a certain degree of safety (Carvalho et al., 2019). Now, OMVs can be mass-produced through optimized purification methods, and for reference, Gerritzen et al. (2019) has summarized various purification methods of OMV (Gerritzen et al., 2019).

Genetic Engineering in the Increasing Production of OMVs

The Tol-Pal system continues to attract attention since its functioning affects the OMV production (Shrivastava et al., 2017). The five proteins of the Tol-Pal system includes three inner membrane proteins (TolA, TolQ, and TolR), a periplasmic protein (TolB), and a peptidoglycan-related lipoprotein (Pal) associated with the outer membrane proteins (Derouiche et al., 1995). The *tolB* mutant shows increased OMV release in many bacteria like *E. coli*, *Salmonella typhimurium*, and *H. pylori* (Deatherage et al., 2009; Nevermann et al., 2019). Interestingly, *tol* mutants can often be introduced into the bacteria of interest by means of electrotransportation (Turner et al., 2015). Additionally, the *rmpM* gene deletion mutant was found to have a loosely attached outer membrane, which increased OMV release (Maharjan et al., 2016). Theoretically, the combination of the *lpxL1* and *rmpM* mutations can address toxicity and resolve issues associated with the detergent-free OMV vaccines. Both gene mutations have been reported to have beneficial effects, making the detergent-free method a better alternative to the traditional detergent-based OMV purification methods (van de Waterbeemd et al., 2010). With gradual improvement in genetically engineered OMVs, multiple genes have been modified for the purification of OMVs. For example, few studies have attempted to incorporate a non-natural histidine amino acid. The sequence (His-tag) has been used to purify the bacterial OMVs by affinity chromatography (Alves et al., 2015). Additionally, genetic engineering has also been used to produce a high-yield of bacteria lacking the *OmpA* gene, which has been widely used in OMV engineering (Moon et al., 2012; Kulp et al., 2015).

Studies in *E. coli* have shown that the stability of the envelope comes from three major cross-links: OmpA, LppAB, and the Tol-Pal complex (Mizushima, 1984; Yeh et al., 2010; Park et al., 2012). When there is a decrease in these cross-links, the yield of OMV increases, and vice versa. Thus, *S. typhimurium* mutants lacking OmpA, LppAB, Pal, TolA, or TolB show increased OMV production (Deatherage et al., 2009). Similarly, gene deletion can have a negative impact on immunogenicity. For example, the TolA gene can increase the resistance of *S. typhimurium* to bile (Lahiri et al., 2011). The *tolR* gene encodes proteins with exercise-related functions in *S. typhimurium* and *E. coli* (Santos et al., 2014). Deletion of these genes will inevitably have a negative impact on the function of OMVs, like reduced immunogenicity. Consequently, the question of balancing yield and the immune efficacy remains unsolved.

UPDATE ON THE APPLICATION OF OMVS AS ANTIGEN PRESENTATION PLATFORMS USING GENETIC ENGINEERING

Increasing evidence exists for the delivery of antigens by OMVs, to proximal host cells and distal host cells, which in turn stimulates the immune system and triggers immune response in the host (Shen et al., 2012). The antigens in OMVs can be distributed over long distances and are not damaged by dynamic physical and biochemical stresses. In addition, they can be transferred to the plasma membrane of the host cell (Sharpe et al., 2011; Yoon et al., 2011). Moreover, some transmembrane proteins on OMVs can be used as anchoring proteins, and play a role in presenting heterologous proteins in engineering transformation. To design a safer and a more efficient antigen delivery system, the naturally occurring OMVs have been modified by genetic engineering to obtain a multifunctional antigen delivery platform (Kim et al., 2009). By summarizing existing transformation methods, we hope to highlight the systematic processes of engineering OMVs (**Figure 2**).

Presentation of Heterologous Proteins

The modification of OMVs, in terms of the presentation of heterologous antigens, is an established method. Since this modification alters the communication between the cells and the bacteria to a certain extent, it affects the functionality of OMVs as vaccines. Most of the heterologous antigens are heterologous proteins.

Intrinsic Antigens

The expression of intrinsic antigens in OMVs is widely used, and is closely associated with the development of vaccines. The symbiotic bacteria *Neisseria gonorrhoeae* and *N. meningitidis* share a tendency to overproduce the bacterial outer membrane, leading to the formation and release of OMVs during growth.

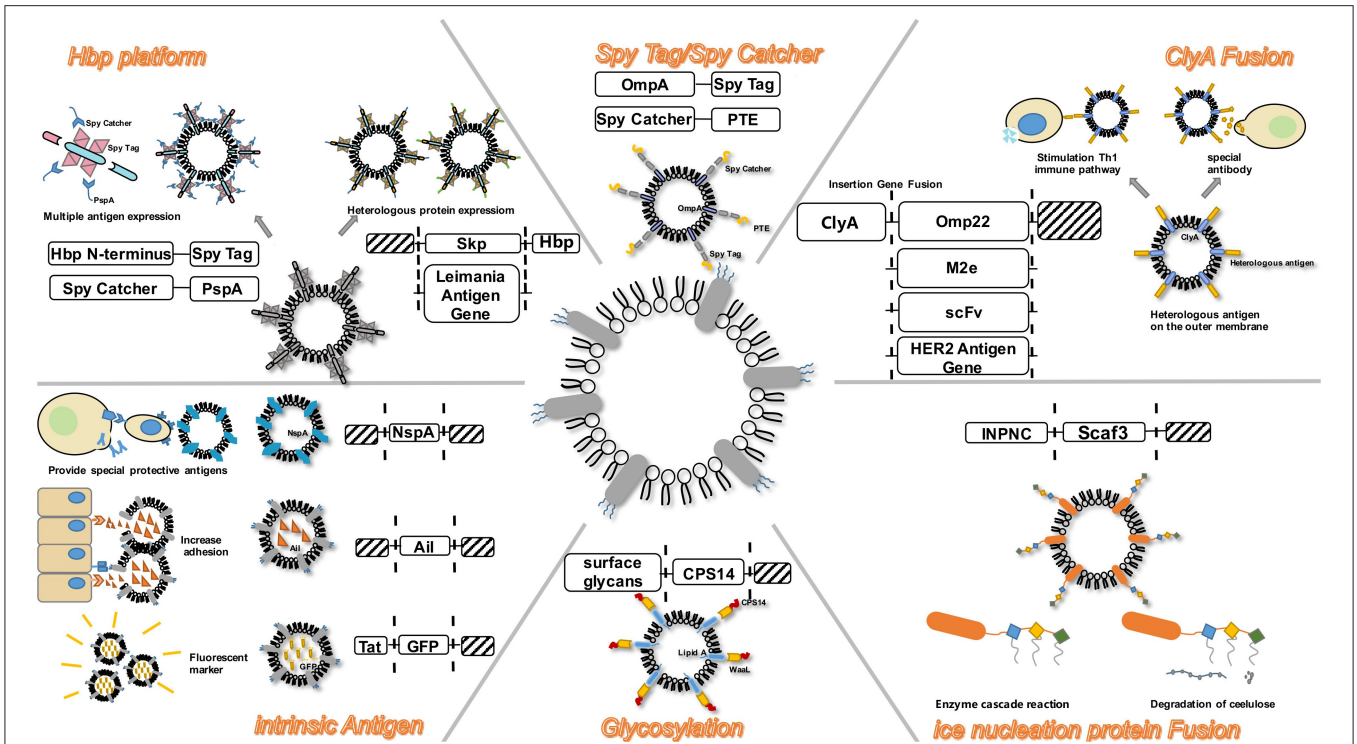

FIGURE 2 | OMV serves as a versatile transformation platform. Engineering methods include: ClyA Fusion; Spy Tag/Spy Catcher; Hbp platform; intrinsic antigen; Glycosylation; Ice nucleation protein Fusion.

OMVs from the meningococcal and commensal intima have been reported to function as a vaccine against meningococcal disease (Mirlashari et al., 2010). The *nspA* gene has been shown to be highly conserved in a variety of meningococcal strains, and has been extensively studied as a potential antigen for vaccines (Lewis et al., 2010, 2012; Echenique–Rivera et al., 2011; Giuntini et al., 2011). However, this method is difficult to commercialize. Previous studies have reported that recombinant *E. coli* was not suitable for the expression of other meningococcal OMV vaccine components, owing to its ability to genetically up-regulate certain outer membrane proteins in meningococcus, and separately engineer OMVs (O'dwyer et al., 2004). Ail is an outer membrane adhesin and invasin from *Yersinia enterocolitica*. Following genetic engineering, the OMVs of the *E. coli* DH5α strain carrying Ail can be internalized in the eukaryotic cells. The presence of Ail enabled non-invasive strains to invade the CHO cells (Kesty and Kuehn, 2004).

Moreover, green fluorescent protein (GFP) fused with the Tat signal sequence, was secreted into the periplasm by the double arginine transporter (Tat) in the *E. coli* DH5α strain. Pronase-resistant fluorescence was detected in the vesicles of the Tat-GFP transformed strain, demonstrating the presence of GFP in intact vesicles (Kesty and Kuehn, 2004). The inclusion of GFP cargo increased the vesicle density, but did not bring about any morphological changes in the vesicles. More than 60 membrane proteins have been detected in the OMVs (Molloy et al., 2000; Tokuda and Matsuyama, 2004; Lee et al., 2007). These proteins continue to be identified as anchoring proteins in the engineered OMVs. With further study of OMVs, more proteins with important functions will be identified.

Fusion of *ClyA*

Cytosolic A (*ClyA*), a 34-kDa cytosolic protein encoded by the *ClyA* gene (also known as *sheA* and *hlyE*), is located on the K-12 chromosome of *E. coli* (Westermark et al., 2000). Lately, researchers have favored the genetic fusion of *ClyA*. *ClyA* acts as a leading sequence and aids in the localization of heterologous proteins in the outer membranes where OMVs are secreted, resulting in the display of functional proteins on the surface of the OMVs (Kim et al., 2008). The gene for the heterologous protein expresses a recombinant outer membrane protein by fusion with the *ClyA* gene. Since *ClyA* is anchored to the outer membrane, the heterologous antigen can be expressed in an extracellular manner. Experiments on the heterologous protein presentation of *ClyA*-OMVs have been gradually extended. For example, expression of the Omp22 protein using the *E. coli* DH5α strain and the Fv fragment of the presenting antibody, the HER2 antibody, and the influenza virus M2e antibody, and so on (Kesty and Kuehn, 2004; Kim et al., 2008; Gujrati and Sangyong, 2014; Garrett Rappazzo et al., 2016; Huang et al., 2016).

Vesicles produced by bacterial pathogens promote the direct delivery of antigens into the host cells. In this regard, the recombinant *ClyA*-OMV increases the antigen delivery efficiency by 8-fold (Wai et al., 2003). Further research shows that the protein fusion on *ClyA* has different effects. Fusion with the

N-terminal of *ClyA* produces heterologous antigens that are inconsistent, while C-terminal fusions always produce well-displayed proteins which retain their biological functions (Kim et al., 2008). This may be due to the fact that the C-terminus of *ClyA* is closer to the outer surface compared to the distance between the N-terminus of *ClyA* and the outer membrane, and is therefore more likely to extend into the extracellular environment (Tzokov et al., 2006; Eifler et al., 2014). Additionally, the physiological state of *ClyA* also affects its localization in the OMVs. According to experiments, the redox state of *ClyA* is pivotal in regulating its localization in the OMVs (Kim et al., 2008).

AT Platform

Autotransport (AT) is a large virulence factor (usually over 100 kDa) secreted by Gram-negative bacteria. The AT system is simple, and is hypothesized to carry all information concerning the inner periplasm, and the outer membrane translocation of the protein itself. AT is synthesized as a large precursor protein containing three domains: first, the N-terminal signal peptide, which targets the protein to the Sec translocator and initiates the transfer through the intima; second, the passenger domain; third, the C-terminal beta-domain, which integrates into the outer membrane and plays a crucial role in passenger translocation into the extracellular space (Eifler et al., 2012). The AT system has been used as a transport vehicle for many heterologous fusion partners in Gram-negative bacteria (Kjaergaard et al., 2000; Junker et al., 2019). In most cases, variants of the *Neisseria* IgA protease and the endogenous *E. coli* AT AIDA-I are used to engineer antigens specifically for surface display (Junker et al., 2007). Two model antigens of *Leishmania* were successfully expressed using this method (Schroeder and Aebischer, 2009). Recently, the skp protein of ETEC has been successfully loaded into OMVs through AT, which fused with the glutathione-S-transferase (GST) epitope and combined with cholera toxin to prepare an ideal vaccine (Hays et al., 2018). OspA has been extensively studied as a vaccine component against Lyme disease (Wressnigg et al., 2014; Comstedt et al., 2015). The OspA antigen has been successfully expressed in OMVs but has not been exposed on the surface of OMVs. The improved method uses a meningococcal surface protein, fHbp, as the anchor protein. By connecting OspA to the N-terminus of fHbp, the strong immune response elicited by the engineered OMVs was successfully detected (Salverda et al., 2016; Zhang et al., 2016). Ovalbumin (OVA) hemoglobin protease has also been successfully expressed on the surface of engineered OMVs through the AT platform, and has been shown to have the ability to induce antigen-specific CD8 + T cell responses (Schetters et al., 2019). Unlike *ClyA*, the AT system can successfully present multiple antigens using a slightly different approach. Using the crystal structure of the AT passenger, five passenger side domains were selected and replaced with the *M. tuberculosis* antigen ESAT6 sequentially, while the β-helix core structure (β-stem) remained intact (Otto et al., 2005). The resulting Hbp-ESAT6 chimera was efficiently and stably secreted into the medium of *E. coli*. The Hbp-ESAT6 display variant was constructed by disrupting the cleavage site between the passenger and the β-domain, which maintains cell correlation and promotes efficient surface exposure of ESAT6 (Eifler et al., 2012). Compared to the *ClyA* fusion system, the AT system has multiple sites for the insertion of heterologous sequences that can simultaneously bind multiple antigens. This enables the formation of a multivalent recombinant live vaccine. This is of high value because multivalent vaccines are a key requirement for the prevention of infectious diseases such as tuberculosis (Aagaard et al., 2011). Importantly, since the passenger side domains have Hbp function, their replacement with antigenic proteins automatically eliminates potential toxic effects, making the proposed Hbp platform safe for antigen delivery (van Bloois et al., 2011). Thus, the AT system has been found to be more efficient, convenient, and safer than the engineered OMVs associated with *ClyA*.

Spy Tag/Spy Catcher System

The SpyCatcher is a genetically encoded protein designed to spontaneously form a covalent bond with its peptide partner SpyTag (Brune et al., 2016). Studies have demonstrated the ability of this bioconjugate system to deliver antigens, which can be linked to an antigen delivery system via common cell-linking proteins (Alves et al., 2015). It has been found that this system can be used as a modification of the autotransport system (Jong et al., 2010). In the AT system, although antigen delivery has been successfully accomplished, their density on the OMVs has been found to be affected (Jong et al., 2010). The SpyCatcher/SpyTag protein ligation technology can enzymatically attach the antigen to the high-density Hbp in OMVs, without being hampered by the membrane environment, as verified by recent experiments. This protein ligation system is based on the fibronectin of *Streptococcus pyogenes,* and forms an intramolecular isopeptide bond between the adjacent lysine and aspartate residues by an autocatalytic mechanism (Zakeri et al., 2012). The domain was split into a 13 amino acid (AA) peptide called the SpyTag, and a 138-AA fragment called the SpyCatcher, to create a SpyCatcher/SpyTag pair for coupling with heterologous proteins and autotransporters. When fused to different proteins, the SpyTag and the SpyCatcher recombine with the domain following mixing and form stable intermolecular covalent bonds under certain conditions (Fierer et al., 2014). Additionally, a similar structure, the orthogonal SnoopTag/SnoopCatcher system, can also couple multiple antigenic modules to Hbp by a sequential ligation strategy without affecting antigenic display (Veggiani et al., 2016). Spy ligation can be easily performed by gene fusion to the end of the Hbp display vector, and directional loading onto the OMVs. OMV display technology, combined with protein linkages, constitutes a plug-and-play system designed for customized antigen delivery. As a "mediating" protein system, the Spy Tag/Spy Catcher can also link other anchoring proteins such as OmpA, to deliver the corresponding antigen. This has been verified in the presentation of the active enzyme phosphodiesterase (PTE) (Alves et al., 2015). Therefore, the Spy Tag/Spy Catcher system can be used for modifying anchoring proteins, allowing engineered OMVs to perform antigen delivery more efficiently.

Ice Nucleation Protein

To display multiple functional proteins on OMVs, a trivalent scaffold (Scaf3) plasmid was constructed to express the protein of interest (Tsai et al., 2009). Park et al. (2014) used an enzyme scaffold to express the protein in bacteria, and immobilized it on the outer membrane using a truncated ice nucleation protein anchor. The plasmid pINP was constructed by amplification using a truncated ice nucleation protein gene from pPNC20 (Bae et al., 2002). High levels of INP-scaf3 were successfully detected on engineered *E. coli* OMVs, by binding Scf3 to INP by primers (Park et al., 2014). This provides a simple and convenient way to express different enzymes on OMVs. The assembled enzyme complex not only retains full activity, but also leads to the hydrolysis of cellulose, 23 times faster than the conventional enzymes. This method can thus be used as a simple platform for the efficient functioning of multiple enzymes as nano-biocatalysts (Park et al., 2014). The flexibility to design scaffolds using various specific binding domains allows for the display of unlimited number of functional proteins on OMVs.

Similar to the AT system, the enzyme scaffold is also a high-performance system that can simultaneously load multiple heterologous proteins. However, the AT system has certain inevitable shortcomings, like a truncated passenger structure used in the loading of multiple antigens (Jong et al., 2010). Similar to the AT system, the enzyme scaffold also binds the target protein in an orderly manner, forming a multi-functional system independently. Therefore, it is expected to demonstrate more applications.

Glycosylation Linkage

Glycosylation-modified OMVs (geOMVs), as seen in *Streptococcus pneumoniae* capsules and *C. jejuni* N-linked glycans, have been shown to produce a good immune response (Price et al., 2016). The geOMV platform utilizes the loose glycan structure of the O-antigen ligase. Specifically, they are delivered to the lipid A-core molecule in the inner membrane (Kaniuk et al., 2004; Han et al., 2012). First, glycans were customized using the initial glycosyltransferase, WecA, and a specific glycosyltransferase encoded on a plasmid. The flip enzyme Wzx subsequently moved the glycans to the periplasmic surface of the inner membrane, and the enzyme Wzy polymerized the glycan subunits into a high-molecular-weight form of the surface glycans. The WaaL ligase then attached the glycan to the lipid A-core molecule. Finally, these customized LPS molecules were transported to the outer membrane and flipped into the extracellular space through the Lpt protein complex (Kaniuk et al., 2004; Simpson et al., 2015). When bacteria formed the OMVs, LPS as well as proteins and lipids were packaged into OMVs, resulting in the formation of mature geOMVs. The *S. pneumoniae* capsules were expressed in *E. coli* cells lacking the relevant O antigen, and the relevant plasmid was constructed and introduced into *E. coli* to secrete the corresponding OMVs. The immunological potency was confirmed using animal experiments (Price et al., 2016). Glycosylated conjugate vaccines are valuable. However, technical challenges exist with respect to the attachment of glycan chains (Jones, 2005; Wacker et al., 2006; Bottomley et al., 2012). The glycol-engineered *E. coli*-expressing OMVs can express the glycans required for binding to the vaccine, and thus can complement the current conjugate vaccines, particularly for serotypes corresponding to glycan structures that have not been resolved. The studies of glycans were less than those of proteins, lipids, and nucleic acids (Williams et al., 2018). The successful validation of glycosylated OMVs provides an inspiring platform for future engineered glycosylation efforts (Liang et al., 2014; Shimoda et al., 2017).

OTHER APPLICATIONS OF OMVs USING GENETIC ENGINEERING

In addition to presenting antigens for vaccine application, the transformation of OMVs has now embraced more functions, including drug delivery, bioimaging, nanogenerators, and new adjuvants (**Table 2**). OMVs are being developed for more applications due to their flexible retrofit characteristics.

Drug Delivery

In addition to serving as a platform for surface antigen presentation, the function of OMVs to encapsulate small molecule particles in the lumen for presentation is also of interest. Recent studies have found that OMVs have a great potential in the transport of small molecule drugs (**Table 3**). The method of loading drugs into the lumen of OMVs by electroporation has been proven. For relatively hydrophobic and positively charged small molecule drugs that easily interact with lipophilic membranes, passive diffusion can be used. However, for hydrophilic molecules, the bilayer lipid membrane may constitute an obstacle, in which case electroporation may be the method of choice (Gujrati et al., 2014) (**Figure 3**). Although OMVs can only encapsulate about 15% of KSP-siRNA, the amount is sufficient to exert cytotoxicity. This electrotransport method is convenient and easy to implement, and has been widely used in loading small molecular substances (Turner et al., 2015). Recently, scientists have tried to use bioengineering methods to successfully upload cancer treatment drugs on OMVs. OMVs from the non-pathogenic commensal bacteria were used to deliver keratinocyte growth factor 2 (KGF-2), a small molecule with the potential to treat inflammatory bowel disease (Baumgart and Sandborn, 2007). Adding intact KGF-2 OMVs to epithelial cell culture promoted cell proliferation and accelerated wound healing, in a safe manner (Carvalho et al., 2019). Melanin, a specific agent for photothermia therapy in cancer treatment, was presented through OMVs, and almost all the cancer cells in the animal model were destroyed (Gujrati et al., 2019) (**Figure 4**). Another loading method is the incorporation of drugs into OMVs during their biological generation through parental bacteria. Further to cancer treatment, drug delivery by OMVs has also been confirmed. Allan and Beveridge (2003) have demonstrated that the incorporation of gentamicin during the growth of *P. aeruginosa* PAO1 strains produced gentamicin-containing OMVs, which can deliver drugs to the target, *Burkholderia*

TABLE 2 | Application and performance of engineered OMVs.

Application	Lumen/outer membrane	Anchor protein	Results and efficacy	References
Nanopolymer bioreactor	Outer membrane	Ice Nucleation Protein (INP)	Provide synergistic cellulose hydrolysis; Increase glucose production by 23 times compared with free enzyme	Park et al., 2014
Multifunctional imaging and detection platforms	Lumen	None	Easily customize through genetic engineering; Create a wide range of applications including live cell imaging	Chen et al., 2017
Drug delivery	Lumen	None	Slowly release drugs under specific environmental conditions; Reduce non-specific toxicity caused by drug leakage into the circulatory system	Gujrati et al., 2014
Vaccine adjuvant	Lumen / Outer membrane	ClyA; Autotransport (AT); Ice nucleation protein; Glycosylation	Safe and effective vaccine platform	Kesty and Kuehn, 2004; Junker et al., 2007; Park et al., 2014; Price et al., 2016

TABLE 3 | Engineering OMVs delivering drugs and corresponding efficacy of diseases.

Bacterial strain	Disease	Drugs	Effect and characteristic	References
Bteroides thetaiotaomicron VPI-5482	Colitis	keratinocyte growth factor-2 (KGF-2)	Control colitis clinically and pathologically; Reduce colon atrophy and length reduction caused by treatment; Reduce epithelial damage and inflammatory infiltration	Carvalho et al., 2019
Escherichia coli strain that exhibits reduced endotoxicity toward human cells	Cancer	Therapeutic siRNA	Complete biodegradability; Very rigid and stable nanostructure; Reduced drug leakage and non-specific toxicity	Gujrati et al., 2014
Escherichia coli K12	Cancer	Naturally occurring melanin	Tumor growth is reduced by about 43%; High safety, non-toxic to normal cells	Gujrati et al., 2019
Pseudomonas aeruginosa PAO1 strain	Cystic fibrosis, Cepacia syndrome	Gentamicin	Thermodynamic stability and will not decompose in suspension	Allan and Beveridge, 2003
Streptococcus flexi serotype 5 (M90T)	Parasitic disease	Gentamicin	Drug stability	Kadurugamuwa and Beveridge, 1998

cepacia (Allan and Beveridge, 2003). This was also confirmed in *Shigella flexneri* OMVs (Kadurugamuwa and Beveridge, 1998).

As a drug presentation tool, OMVs have the advantage of being small, stable, well-tolerated, and highly specific. OMVs can slowly release drugs under specific Physiological conditions, reducing non-specific toxicity caused by drug leakage into the circulatory system. In addition, this slow-release property can provide sufficient time for siRNA to reach its target cancer cells in areas with abnormal blood supply (Gujrati et al., 2014). OMVs have thermodynamic stability and will not decompose in suspension, while ordinary liposomes have the disadvantages of drug leakage and easy degradation of circulation. Although the packaging efficiency is not ideal, it is sufficient to exert drug efficacy.

Multifunctional Imaging and Detection Platforms

Complex, multi-antigen-bound engineered OMVs have begun to evolve and grow. Based on this technology, scientists have proposed a "one-pot synthesis" model (Chen et al., 2017). According to the mutual binding between proteins, the nano-luciferase (Nluc) and the Z domain recruits antibodies which exists in OMVs at the same time (Tashiro et al., 1997). Experiments have confirmed the feasibility of imaging cancer cells by multifunctional OMVs (Ferreira et al., 2006). Currently, multifunctional OMVs can be customized with ease through genetic engineering, creating an almost unlimited combination of "capture" and "report," for a wide range of applications including live cell imaging (Chen et al., 2017) (**Figure 5**). At the same time, the photoacoustic imaging method has proven to be feasible to produce encapsulated biopolymer-melanin OMV (OMV Mel), using bacterial strains expressing the tyrosinase transgenes. The OMV Mel is generated under near-infrared light, and is suitable for imaging applications. The strong photoacoustic signal non-invasively monitors tumor-associated OMV Mel distribution *in vivo* (Gujrati et al., 2019). This experiment represents the rationale on the use of bioengineered OMVs as effective alternatives to synthetic particles in photoacoustic imaging, for image enhancement and photo-thermal applications (**Figure 4**).

OMVs have been reported to possess excellent sensitivity. When used in thrombin detection, the detection limit of

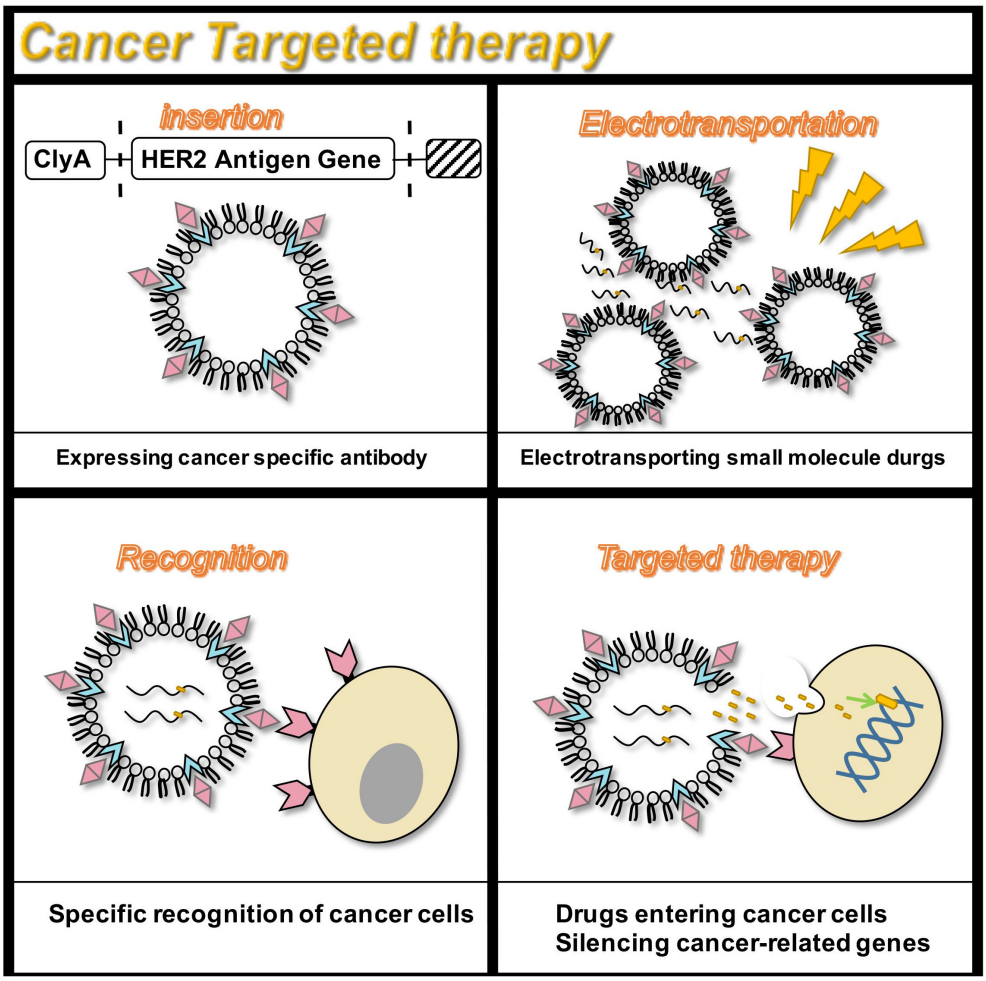

FIGURE 3 | Targeted therapy for the HER2 receptor. OMVs are genetically engineered to carry siRNA that silence cancer genes, and specifically target cancer cells that express the HER2 antigen to exert anti-cancer effects.

thrombin by OMVs was found to be 0.5 nm (Chen et al., 2017). Additionally, the preparatory method is simple, and a high yield of OMVs can be successfully obtained with ease only through a simple fermentation process. Furthermore, since more than 60 membrane-anchoring proteins have been detected in OMVs, a variety of modified enzymes can be presented by OMVs. Therefore, OMVs can flexibly modify electrochemical-based detection or colorimetric detection of enzymes. Owing to these advantages, OMVs can be applied in immunoassays, *in vivo* imaging, and cancer cell detection.

Nanopolymer Bioreactor

Multi-step enzyme pathways play a key role in cell metabolism. Enzyme cascade reactions are highly complex systems. A key feature of a highly efficient enzymatic pathway is the synergistic and spatial organization of the enzyme to ensure sequential transformation of the substrate (Agapakis et al., 2012). OMV is relatively stable in the surrounding environment and can be manufactured cost-effectively, and is considered to have the potential of a bioreactor. A novel study by Park et al. (2014) identified a single protein scaffold based on the Coh-Doc interaction, which can be used to sequentially assemble multiple enzymes onto the surface of OMVs, thereby resulting in a nanoreactor capable of complex biocatalysis (Park et al., 2014) (**Figure 6**). By genetically engineering enzyme scaffolds into OMVs, scientists have succeeded in obtaining an enzyme system with an enzyme cascade. Recently, the expression of organophosphate hydrolase in *E. coli* OMVs has also been successful, and engineered OMVs have enhanced thermal stability and pH stability (Su et al., 2017). After 15 reaction cycles, at least 83% of the OMVs initial activity is retained. After 40 days, about 20–30% of initial activity is retained (Su et al., 2017). In addition, phosphotriesterase was displayed in OMVs through the outer membrane porin OmpA of *E. coli* (Alves et al., 2018).

In recent decades, various methods have been developed to create artificial multi-enzyme complexes, including OMVs, polyhydroxyalkanoate (PHA) particles, virus-like particles (VLP), enzyme-derived nanoparticles (EZPs), and

magnetosomes (Parlane et al., 2017; Yan et al., 2017; Wilkerson et al., 2018; Schmid-Dannertand and López-Gallego, 2019). However, in terms of its wider application, there are still some obstacles. For example, due to steric hindrance, the encapsulation rate of large proteins is low, and the substrate cannot fully enter the enzyme assembly and the vesicle shell (Wong et al., 2020). These nanoparticles are difficult to challenge for long-term storage and have poor biocompatibility. The enzyme system expressed through the outer membrane vesicles has been proven stable for long-term storage and has the potential to be used as a carrier for industrial production of enzyme systems.

As a Vaccine Adjuvant

An adjuvant is defined as a molecule that aids an antigen in eliciting an immune response. Adjuvants improve the immune response in people with poor immune response, expand cross-protection, induce a shift in the specific T cell-assisted response, and reduce the amount of antigen required for vaccine development (Maisonneuve et al., 2014). OMVs have been considered as potential vaccine adjuvants since their inception (**Figure 7**). However, due to the toxicity of wild-type LPS, such as flagellin, lipoprotein, and other OMPs, they may trigger allergic reactions such as excessive inflammation (Arigita et al., 2005; Thompson et al., 2005). Therefore, the OMV endotoxins are removed manually following production. Another disadvantage is that the LPS-deficient OMVs generally exhibit lower immunogenicity compared to the immunogenicity of the wild-type OMVs containing wild-type LPS (Gnopo et al., 2017). Therefore, the appropriate modification of LPS is necessary to obtain an optimal balance between low-toxicity and high-immunogenicity. The latest method of LPS modification involves the synthetic assembly or genetic modification of bacteria (Arenas et al., 2010). Further, OMVs with *LpxL* gene deletion and *PagL* gene expression have been proven to possess good adjuvant ability and show significantly better abilities compared to that of the wild type (Arenas et al., 2010; van de Waterbeemd et al., 2010; Asensio et al., 2011). Further comparison has revealed that the *PagL* gene expression possesses higher endotoxic activity compared to that of the *LpxL* gene, which was also supported by animal studies. The *PagL* gene is considered to have a better adjuvant effect (Asensio et al., 2011).

Recent studies have shown that the adjuvant ability of engineered OMVs continues to attract the attention of researchers. Engineered OMVs carrying the Ail antigen have been shown to increase adhesion to the CHO cells, and non-invasive vesicles have been modified to invade the CHO cells (Kesty and Kuehn, 2004). Recent developments in vaccine research involve the use of more antigen profiles, expressing

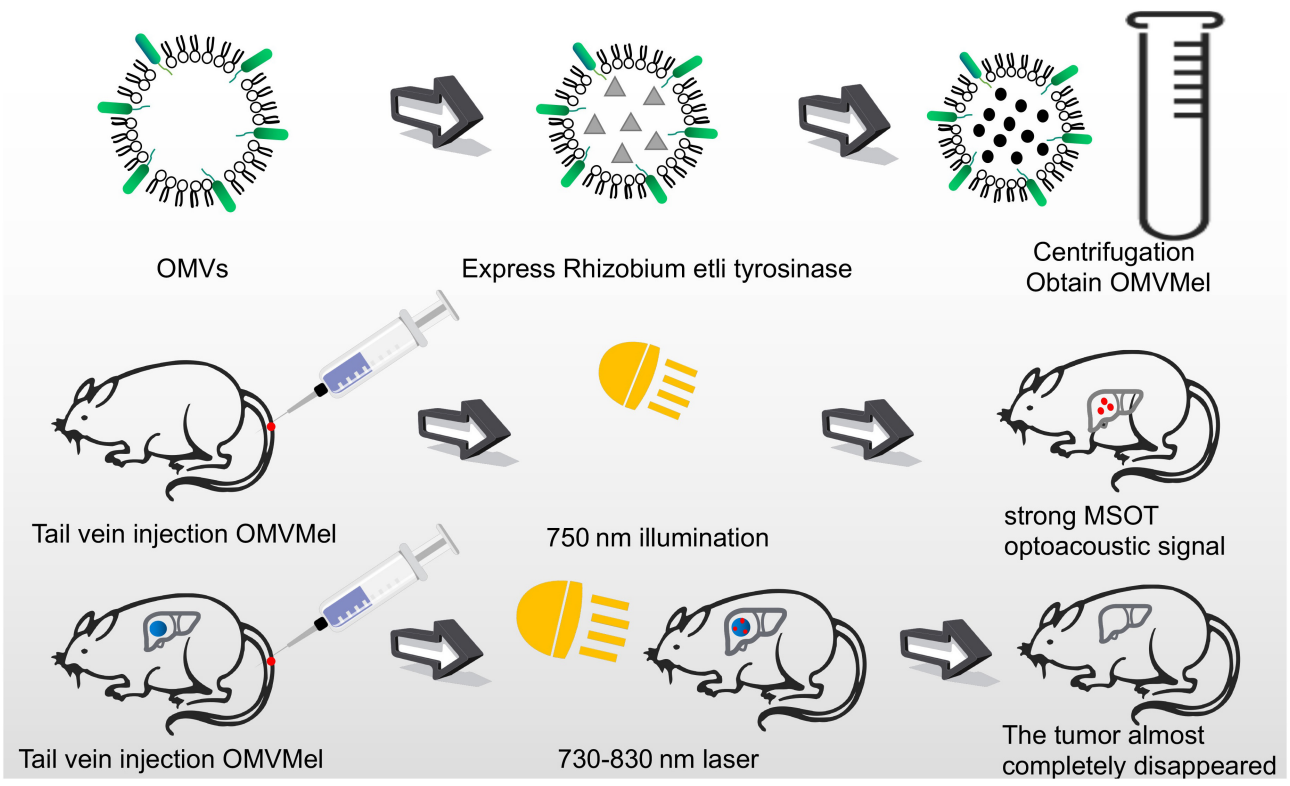

FIGURE 4 | OMVs loaded with melanin were injected into mice through the tail vein. After irradiating at 750 nm, a strong photoacoustic signal of MSOT was generated. The tumor cells were almost completely killed by laser irradiation at 730–830 nm for several minutes.

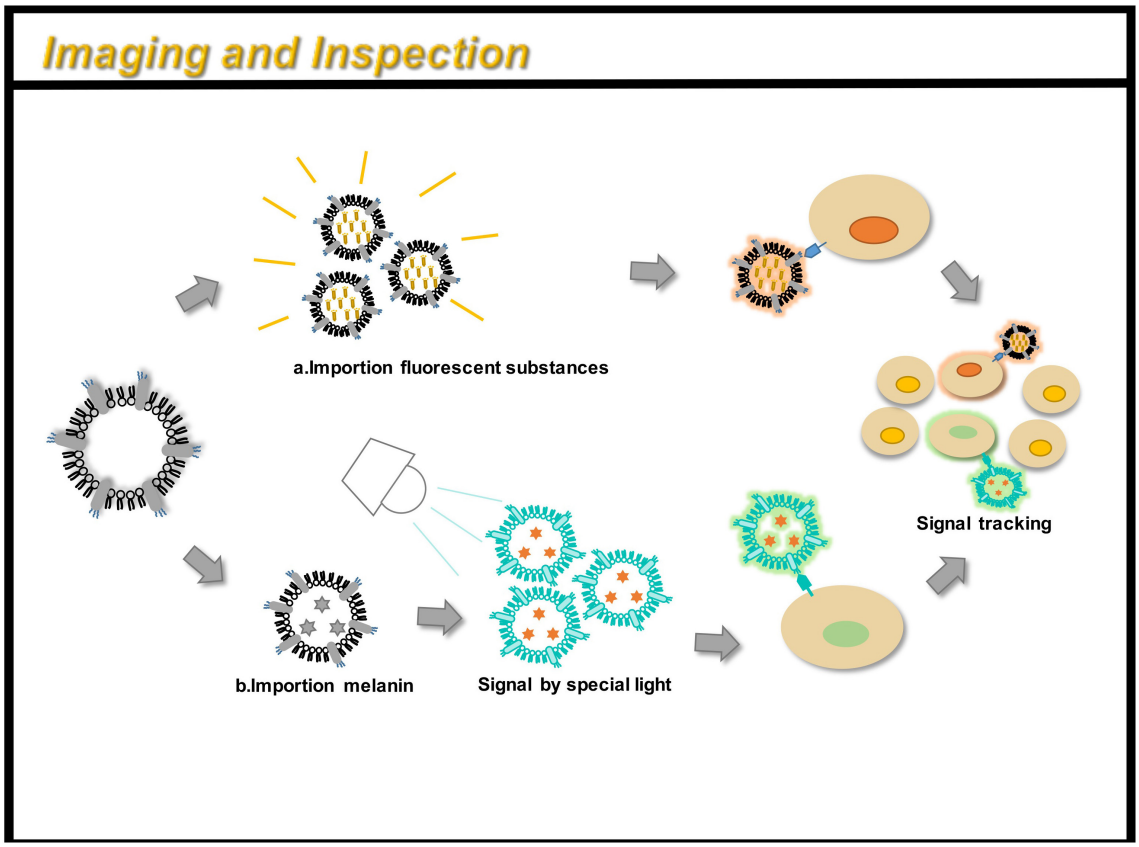

FIGURE 5 | OMVs can be engineered for immunoimaging and cell detection. There are two main methods: (a) directly loading a fluorescent substance; (b) indirectly loading a small molecular substance (such as melanin), and a signal can be obtained under a specific light. By taking OMV preparation, you can track the path of action of the drug in the body and monitor its efficacy.

mutant forms of HlaH35L, SpAKKAA, LukE, LukD/E, one of the two components of the interleukin Csa1A, and the iron binding protein, FhuD2, on meningococcal OMVs, have proven to possess good immunogenicity (Falugi et al., 2013; Gasanov et al., 2013; Spaan et al., 2017). The OMVs produced in *Salmonella* carrying pneumococcal protein antigens have shown promising results in a murine model (Kuipers et al., 2015). This allows glycans and proteins to synergistically enhance the immunogenicity of vaccines (Price et al., 2016). In contrast, the currently existing and the most successful antimicrobial vaccine glycoconjugates face multiple problems like complex preparation, slow development, insufficient safety, instability, and batch-to-batch variability. In addition, glycoconjugates do not contain multiple serotypes. OMVs can be genetically modified with flexibility and ease to produce geOMVs with the perfect balance between reduced toxicity and optimal adjuvant properties.

FUTURE RESEARCH DIRECTIONS

Compared to conventional adjuvants, OMVs show a clear advantage in terms of future development (Tan et al., 2018). As a platform for the convenient implementation of genetic modification, OMVs have received attention in the field of precision medicine, in addition to a wide range of vaccine applications (Wang et al., 2019). For example, OMVs have become a potential choice for the targeted delivery of cancer drugs. As an easily engineered nanoparticle, OMVs can transport a variety of small molecules with different characteristics, thereby involving in important applications such as immunoimaging, enzyme-linked reaction polymers, etc. Further research will help to unveil the undiscovered aspects and future applications of the engineered OMVs.

Targeted Cancer Therapy Delivery Platform

Targeted therapy continues to receive attention owing to its fewer side effects. Bio-nanocarriers derived from a variety of natural resources like pathogens and mammalian cells have been identified to be well-suited for drug delivery (Yoo et al., 2011), and nanomaterials have been widely studied as drug delivery vehicles in the treatment of cancer (Petros and DeSimone, 2010; Shi et al., 2010). Designing OMVs to target specific cell types makes them an attractive treatment option. In addition, engineering OMVs offers several advantages. The outer

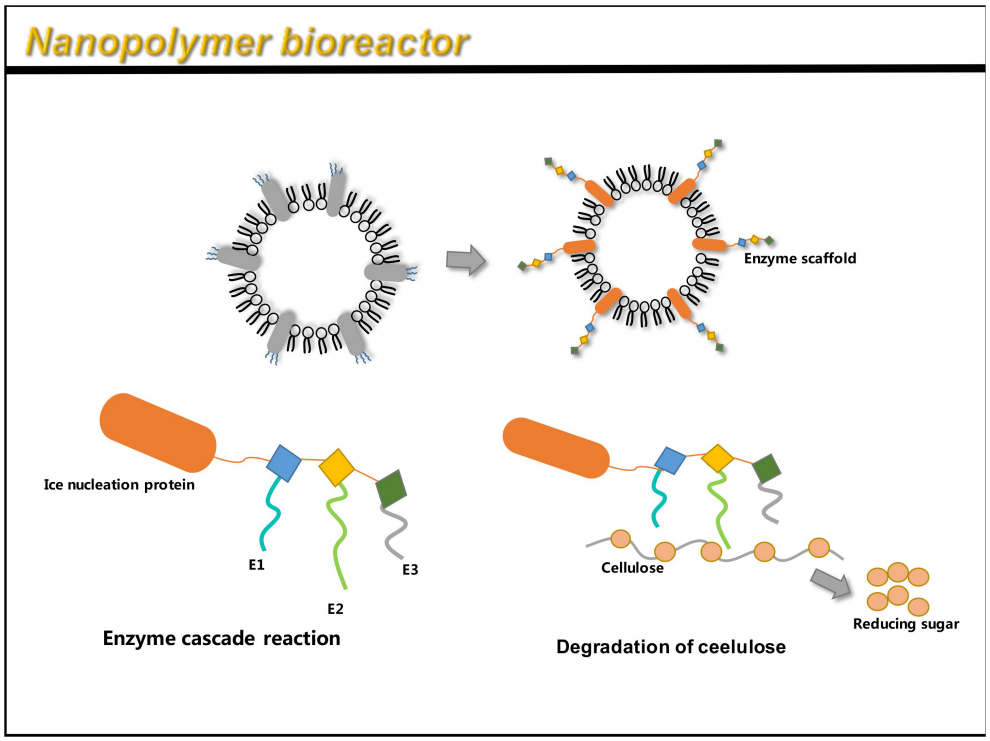

FIGURE 6 | OMV can be linked to an enzyme scaffold through gene functions to connect three enzyme molecules that can complete a complete set of reactions. Through the action of enzymes, cellulose is successfully hydrolyzed to reduce sugars.

membrane protects the OMV contents such as chemotherapeutic agents, from protease or nuclease degradation, thereby increasing the circulating half-life of the drug. Recent studies have successfully designed tumor-targeted OMVs carrying an anti-tumor siRNA (Gujrati and Sangyong, 2014; Gujrati et al., 2014). The transmembrane receptor HER2, chosen as the cell-specific target, was found to be overexpressed in a range of cancers, including breast, ovarian, and gastric cancers (Weaver and Cleveland, 2005). By binding HER2 antibody to ClyA, OMVs targeting cancer cells were obtained. *In vitro* studies by Gujrati et al. (2014) have demonstrated the ability of the siRNA-loaded OMVs to deliver siRNA in ovarian and breast cancer cell lines, subsequently inducing cancer cell death (Gujrati et al., 2014). Multiple forms of cancer treatment have been proven feasible. By presenting melanin, a substance with good light-to-heat conversion rate, a treatment can be achieved that can kill tumor cells by selectively irradiating the melanin-containing tissues, thereby inducing local heating (Liu et al., 2013). Animal studies have shown that almost all tumor cells in the body were eliminated. Furthermore, this photothermal therapy monitors the effect of local treatment by photoacoustic imaging (Gujrati et al., 2019). Additionally, recent studies have shown that engineered OMVs, which transport OVA hemoglobin protease using the AT system, have a mediatory function in the induction of antigen-specific $CD8^+$ T cell response (Schetters et al., 2019). $CD8^+$ T cells control viral replication and tumor growth. This property of OMVs also hints at its powerful potential in cancer treatment.

OMVs deliver heterologous proteins thus, acting as tools for delivering targeted drugs. Such vesicles are expected to be further developed in the near future. The advent of nanobiotechnology, and advances in genomics, immunology, microbiology, and vaccine needs, alone and in combination, have made OMVs a novel choice for precision therapies and targeted-drug therapies.

Multifunctional Delivery Platform

In addition to the widely known function of antigen presentation, OMVs have been used in a wide array of applications. For example, OMVs can be used as bioreactors for enzyme cascade reactions. By carrying anchor proteins which load multiple heterologous proteins such as ice nucleating proteins, OMVs can combine multiple related enzymes to complete a more complex set of biological reactions (Park et al., 2014). Additionally, engineered OMVs have also been used in the field of immune bioimaging. OMVs can be directly tagged with fluorescent substances that can be easily detected, such as GFP, and perform functions such as *in vivo* imaging and remote tracking (Chen et al., 2017). Indirect detection methods have also been confirmed. OMVs carrying melanin generate strong photoacoustic signals suitable for imaging applications under near-infrared light (Gujrati et al., 2019). This method has also proven to be therapeutically effective. For rendering OMVs

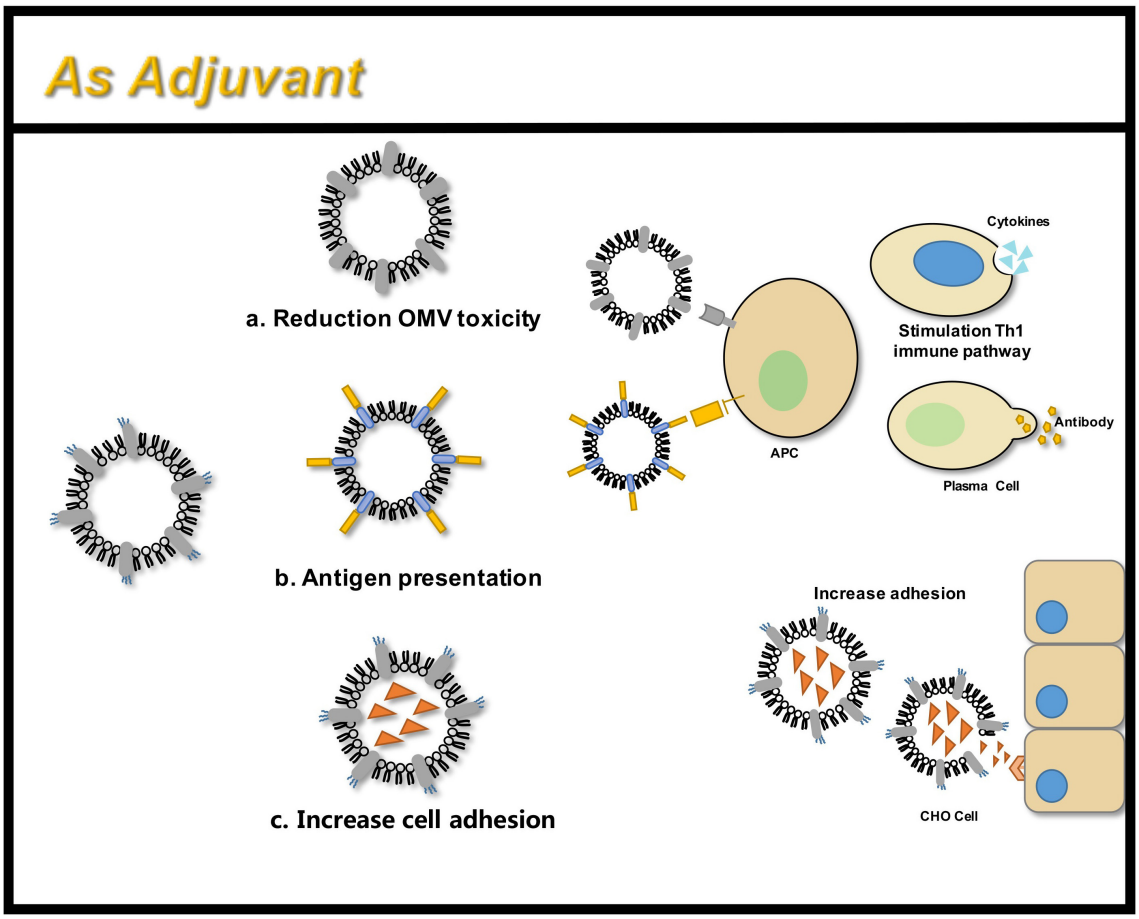

FIGURE 7 | OMVs function as an adjuvant through three main areas: **(a)** attenuated antigen stimulation; **(b)** presentation of heterologous antigens; **(c)** increased adhesion to tissue cells.

in various platforms, secure performance is a pre-requisite. In addition to existing methods for attenuating gene knockouts, the use of non-pathogenic symbiotic bacteria as a source of OMVs has also received attention (Carvalho et al., 2019). Reconstruction of these OMVs can easily produce engineered OMVs with high safety.

With further study of OMVs, it has been shown that this bio-nanoparticle has a variety of functions not limited to vaccine adjuvants. Relying on flexible genetic modifications, OMVs perform multiple functions by carrying small molecules with multiple functions. OMVs are expected to demonstrate more applications in the fields of immunology, diagnostics, and so on.

CONCLUSION

OMVs have attracted attention as a new engineering platform for vaccine development. Through research on the engineering of OMVs, we find that the applications of OMVs are not limited to vaccines. As a convenient bio-nanoparticle, OMV has the potential to function as a multi-functional delivery platform, and thus can be applied in many fields such as immunology, clinical medicine, diagnostics, and biochemistry. However, there are still some problems in the application of OMVs: (i) the toxicity of LPS on OMVs is still a major concern, especially when applied in the human body; (ii) in biological engineering, OMVs load heterologous proteins and the efficiency of small molecular substances is not high; (iii) in large-scale production, the size of OMVs is not easy to control, and the difference between batches is large. At the same time, the lack of understanding of the exact assembly mechanism of OMVs leads to poor programmability of the particles. In future research, attention should be paid to other problems of modifying OMVs such as: (i) increasing the load rate; (ii) improving safety and reduce costs when large-scale production is required; and (iii) delineating the mechanism of OMVs germination for a better understanding of the mechanism of its functions. This review focuses on some of the latest advances in the application of engineered OMVs such as drugs for cancer treatment, immune imaging, etc. It is anticipated that the functions of OMVs may be better manipulated through genetic engineering in subsequent studies.

AUTHOR CONTRIBUTIONS

RL wrote the manuscript. QL and RL revised the manuscript for integrity and accuracy. QL approved the final version of the manuscript and takes responsibility for its content. All authors contributed to the article and approved the submitted version.

FUNDING

This study was supported by the National Natural Science Foundation of China (31760261), the Science and Technology Research Project of Jiangxi Provincial Education Department (60224), and Key Research and Development Projects of Jiangxi Natural Science Foundation (20192BBG70067).

REFERENCES

Aagaard, C., Hoang, T., Dietrich, J., Cardona, P.-J., Izzo, A., Dolganov, G., et al. (2011). A multistage tuberculosis vaccine that confers efficient protection before and after exposure. *Nat. Med.* 17, 189–194. doi: 10.1038/nm.2285

Agapakis, C. M., Boyle, P. M., and Silver, P. A. (2012). Natural strategies for the spatial optimization of metabolism in synthetic biology. *Nat. Chem. Biol.* 8, 527–535. doi: 10.1038/nchembio.975

Allan, N. D., and Beveridge, T. J. (2003). Gentamicin delivery to Burkholderia cepacia group IIIa strains via membrane vesicles from *Pseudomonas aeruginosa* PAO1. *Antimicrob. Agents Chemother*. 47, 2962–2965. doi: 10.1128/AAC.47.9.2962-2965.2003

Alves, N. J., Moore, M., Johnson, B. J., Dean, S. N., Turner, K. B., Medintz, I. L., et al. (2018). Environmental decontamination of a chemical warfare simulant utilizing a membrane vesicle-encapsulated phosphotriesterase. *ACS Appl. Mater. Interfaces* 10, 15712–15719. doi: 10.1021/acsami.8b02717

Alves, N. J., Turner, K. B., Daniele, M. A., Oh, E., Medintz, I. L., and Walper, S. A. (2015). Bacterial nanobioreactors-directing enzyme packaging into bacterial outer membrane vesicles. *ACS Appl. Mater. Interfaces* 7, 24963–24972. doi: 10.1021/acsami.5b08811

Arenas, J., van Dijken, H., Kuipers, B., Hamstra, H. J., Tommassen, J., and van der Ley, P. (2010). Coincorporation of LpxL1 and PagL mutant lipopolysaccharides into liposomes with *Neisseria meningitidis* opacity protein: influence on endotoxic and adjuvant activity. *Clin. Vaccine Immunol.* 17, 487–495. doi: 10.1128/CVI.00423-09

Arigita, C., Luijkx, T., Jiskoot, W., Poelen, M., Hennink, W. E., Crommelin, D. J. A., et al. (2005). Well-defined and potent liposomal meningococcal B vaccines adjuvated with LPS derivatives. *Vaccine* 23, 5091–5098. doi: 10.1016/j.vaccine.2005.06.001

Asensio, C. J. A., Gaillard, M. E., Moreno, G., Bottero, D., Zurita, E., Rumbo, M., et al. (2011). Outer membrane vesicles obtained from *Bordetella pertussis* tohama expressing the lipid A deacylase PagL as a novel acellular vaccine candidate. *Vaccine* 29, 1649–1656. doi: 10.1016/j.vaccine.2010.12.068

Bae, W., Mulchandani, A., and Chen, W. (2002). Cell surface display of synthetic phytochelatins using ice nucleation protein for enhanced heavy metal bioaccumulation. *J. Inorg. Biochem.* 88, 223–227. doi: 10.1016/S0162-0134(01)00392-0

Bartolini, E., Ianni, E., Frigimelica, E., Petracca, R., Galli, G., Scorza, F. B., et al. (2013). Recombinant outer membrane vesicles carrying chlamydia muridarum HtrA induce antibodies that neutralize chlamydial infection *in vitro*. *J. Extracell. Vesicles* 2:20181. doi: 10.3402/jev.v2i0.20181

Bauman, S. J., and Kuehn, M. J. (2006). Purification of outer membrane vesicles from *Pseudomonas aeruginosa* and their activation of an IL-8 response. *Microb. Infect.* 8, 2400–2408. doi: 10.1016/j.micinf.2006.05.001

Baumgart, D. C., and Sandborn, W. J. (2007). Inflammatory bowel disease: clinical aspects and established and evolving therapies. *Lancet* 369, 1641–1657. doi: 10.1016/S0140-6736(07)60751-X

Bottomley, M. J., Serruto, D., Sáfadi, M. A. P., and Klugman, K. P. (2012). Future challenges in the elimination of bacterial meningitis. *Vaccine* 30, B78–B86. doi: 10.1016/j.vaccine.2011.12.099

Brune, K. D., Leneghan, D. B., Brian, I. J., Ishizuka, A. S., Bachmann, M. F., Draper, S. J., et al. (2016). Plug-and-display: decoration of virus-like particles via isopeptide bonds for modular immunization. *Sci. Rep*. 6:19234. doi: 10.1038/srep19234

Carita, A. C., Eloy, J. O., Chorilli, M., Lee, R. J., and Leonardi, G. R. (2018). Advances, and perspectives in liposomes for cutaneous drug delivery. *Curr. Med. Chem.* 25, 606–635. doi: 10.2174/0929867324666171009120154

Caruana, J. C., and Walper, S. A. (2020). Bacterial membrane vesicles as mediators of microbe - microbe and microbe - host community interactions. *Front. Microbiol.* 11:432. doi: 10.3389/fmicb.2020.00432

Carvalho, A. L., Fonseca, S., Miquel-Clopés, A., Cross, K., Kok, K.-S., Wegmann, U., et al. (2019). Bioengineering commensal bacteria-derived outer membrane vesicles for delivery of biologics to the gastrointestinal and respiratory tract. *J. Extracell. Vesicles* 8:1632100. doi: 10.1080/20013078.2019.1632100

Cecil, J. D., O'Brien-Simpson, N. M., Lenzo, J. C., Holden, J. A., Chen, Y.-Y., et al. (2016). Differential responses of pattern recognition receptors to outer membrane vesicles of three periodontal pathogens. *PLoS ONE* 11:e0151967. doi: 10.1371/journal.pone.0151967

Chatterjee, D., and Chaudhuri, K. (2011). Association of cholera toxin with vibrio cholerae outer membrane vesicles which are internalized by human intestinal epithelial cells. *FEBS Lett*. 585, 1357–1362. doi: 10.1016/j.febslet.2011.04.017

Chen, D. J., Osterrieder, N., Metzger, S. M., Buckles, E., Doody, A. M., DeLisa, M. P., et al. (2010). Delivery of foreign antigens by engineered outer membrane vesicle vaccines. *Proc. Natl. Acad. Sci. U.S.A*. 107, 3099–3104. doi: 10.1073/pnas.0805532107

Chen, Q., Rozovsky, S., and Chen, W. (2017). Engineering multi-functional bacterial outer membrane vesicles as modular nanodevices for biosensing and bioimaging. *Chem. Commun*. 53, 7569–7572. doi: 10.1039/C7CC04246A

Collins, B. S. (2011). Gram-negative outer membrane vesicles in vaccine development. *Discov. Med.* 12, 7–15.

Comstedt, P., Hanner, M., Schüler, W., Meinke, A., Schlegl, R., and Lundberg, U. (2015). Characterization and optimization of a novel vaccine for protection against lyme borreliosis. *Vaccine* 33, 5982–5988. doi: 10.1016/j.vaccine.2015.07.095

Deatherage, B. L., Lara, J. C., Bergsbaken, T., Barrett, S. L. R., Lara, S., and Cookson, B. T. (2009). Biogenesis of bacterial membrane vesicles. *Mol. Microbiol.* 72, 1395–1407. doi: 10.1111/j.1365-2958.2009.06731.x

Derouiche, R., Bénédetti, H., Lazzaroni, J. C., Lazdunski, C., and Lloubès, R. (1995). Protein complex within *Escherichia coli* inner membrane. TolA N-terminal domain interacts with TolQ and TolR proteins. *J. Biol. Chem*. 270, 11078–11084. doi: 10.1074/jbc.270.19.11078

Devoe, I. W., and Gilchrist, J. E. (1973). Release of endotoxin in the form of cell wall blebs during *in vitro* growth of *Neisseria meningitidis*. *J. Exp. Med.* 138, 1156–1167. doi: 10.1084/jem.138.5.1156

Echenique–Rivera, H., Muzzi, A., Del Tordello, E., Seib, K. L., Francois, P., Rappuoli, R., et al. (2011). Transcriptome analysis of *Neisseria meningitidis* in human whole blood and mutagenesis studies identify virulence factors involved in blood survival. *PLoS Pathog.* 7:e1002027. doi: 10.1371/journal.ppat.1002027

Eifler, N., Vetsch, M., Gregorini, M., Ringler, P., Chami, M., Philippsen, A., et al. (2012). A structurally informed autotransporter platform for efficient heterologous protein secretion and display. *Microbiol. Cell. Fact.* 11:85. doi: 10.1186/1475-2859-11-85

Eifler, N., Vetsch, M., Gregorini, M., Ringler, P., Chami, M., Philippsen, A., et al. (2014). Cytotoxin ClyA from *Escherichia coli* assembles to a 13-meric pore independent of its redox-state. *EMPO J.* 25, 2652–2661. doi: 10.1038/sj.emboj.7601130

Elhenawy, W., Bording–Jorgensen, M., Valguarnera, E., Haurat, M. F., Wine, E., and Feldman, M. F. (2016). LPS remodeling triggers formation

of outer membrane vesicles in salmonella. *mBio* 7, e00940–e00916. doi: 10.1128/mBio.00940-16

Ellis, T. N., and Kuehn, M. J. (2010). Virulence and immunomodulatoary roles of bacterial outer membrane vesicles. *Microbiol. Mol. Biol. Rev.* 74, 81–94. doi: 10.1128/MMBR.00031-09

Elmi, A., Watson, E., Sandu, P., Gundogdu, O., Mills, D. C., Inglis, N. F., et al. (2012). *Campylobacter jejuni* outer membrane vesicles play an important role in bacterial interactions with human intestinal epithelial cells. *Infect. Immun.* 80, 4089–4098. doi: 10.1128/IAI.00161-12

Falugi, F., Kim, H. K., Missiakas, D. M., and Schneewind, O. (2013). Role of protein A in the evasion of host adaptive immune responses by Staphylococcus aureus. *mBio* 4:e00575. doi: 10.1128/mBio.00575-13

Ferreira, C. S. M., Matthews, C. S., and Missailidis, S. (2006). DNA aptamers that bind to MUC1 tumour marker: design and characterization of MUC1-binding single-stranded DNA aptamers. *Tumour Biol.* 27, 289–301. doi: 10.1159/000096085

Fierer, J. O., Veggiani, G., and Howarth, M. (2014). SpyLigase peptide-peptide ligation polymerizes affibodies to enhance magnetic cancer cell capture. *Proc. Natl. Acad. Sci. U.S.A.* 111, E1176–E1181. doi: 10.1073/pnas.1315776111

Fisseha, M., Chen, P., Brandt, B., Kijek, T., Moran, E., and Zollinger, W. (2005). Characterization of native outer membrane vesicles from lpxL mutant strains of *Neisseria meningitidis* for use in parenteral vaccination. *Infect. Immun.* 73, 4070–4080. doi: 10.1128/IAI.73.7.4070-4080.2005

Garrett Rappazzo, C., Watkins, H. C., Guarino, C. M., Chau, A., Lopez, J. L., DeLisa, M. P., et al. (2016). Recombinant M2e outer membrane vesicle vaccines protect against lethal influenza A challenge in BALB/c mice. *Vaccine* 34, 1252–1258. doi: 10.1016/j.vaccine.2016.01.028

Gasanov, A. G., Mamedbeili, E. G., Guseinov, N. S., Ayubov, I. G., and Gasanov Kh, I. (2013). Dienes from the C5 pyrolyzate fraction in thermal and catalytic [4 + 2]-cycloaddition reactions. *Petroleum Chem.* 53, 54–58. doi: 10.1134/S0965544113010052

Gerritzen, M. J. H., Martens, D. E., Wijffels, R. H., van der Poland, L., and Stork, M. (2017). Bioengineering bacterial outer membrane vesicles as vaccine platform. *Biotechnol. Adv.* 35, 565–574. doi: 10.1016/j.biotechadv.2017.05.003

Gerritzen, M. J. H., Salverda, M. L. M., Martens, D. E., Wijffels, R. H., and Stork, M. (2019). Spontaneously released *Neisseria meningitidis* outer membrane vesicles as vaccine platform: production and purification. *Vaccine* 37, 6978–6986. doi: 10.1016/j.vaccine.2019.01.076

Giuntini, S., Reason, D. C., and Granoff, D. M. (2011). Complement-mediated bactericidal activity of anti-factor H binding protein monoclonal antibodies against the meningococcus relies upon blocking factor H binding. *Infect. Immun.* 79, 3751–3759. doi: 10.1128/IAI.05182-11

Gnopo, Y. M. D., Watkins, H. C., Stevenson, T. C., DeLisa, M. P., and Putnam, D. (2017). Designer outer membrane vesicles as immunomodulatory systems - reprogramming bacteria for vaccine delivery. *Adv. Drug Deliv. Rev.* 114, 132–142. doi: 10.1016/j.addr.2017.05.003

Gujrati, V., Kim, S., Kim, S.-H., Min, J. J., Choy, H. E., Kim, S. C., et al. (2014). Bioengineered bacterial outer membrane vesicles as cell-specific drug-delivery vehicles for cancer therapy. *ACS Nano* 8, 1525–1537. doi: 10.1021/nn405724x

Gujrati, V., Prakash, J., Malekzadeh–Najafabadi, J., Stiel, A., Klemm, U., Mettenleiter, G., et al. (2019). Bioengineered bacterial vesicles as biological nano-heaters for optoacoustic imaging. *Nat. Commun.* 10:1114. doi: 10.1038/s41467-019-09034-y

Gujrati, V. B., and Sangyong, J. (2014). Bioengineered bacterial outer membrane vesicles: what is their potential in cancer therapy? *Nanomedicine* 9, 933–935. doi: 10.2217/nnm.14.56

Han, W., Wu, B., Li, L., Zhao, G., Woodward, R., Pettit, N., et al. (2012). Defining function of lipopolysaccharide O-antigen ligase WaaL using chemoenzymatically synthesized substrates. *J. Biol. Chem.* 287, 5357–5365. doi: 10.1074/jbc.M111.308486

Hays, M. P., Houben, D., Yang, Y., Luirink, J., and Hardwidge, P. R. (2018). Immunization with Skp delivered on outer membrane vesicles protects mice against enterotoxigenic *Escherichia coli* challenge. *Front. Cell. Infect. Microbiol.* 8:132. doi: 10.3389/fcimb.2018.00132

Hu, J., Zuo, J., Chen, Z., Fu, L., Lv, X., Hu, S., et al. (2019). Use of a modified bacterial ghost lysis system for the construction of an inactivated avian pathogenic *Escherichia coli* vaccine candidate. *Vet. Microbiol.* 229, 48–58. doi: 10.1016/j.vetmic.2018.12.020

Huang, W., Wang, S., Yao, Y., Xia, Y., Yang, X., Li, K., et al. (2016). Employing *Escherichia coli*-derived outer membrane vesicles as an antigen delivery platform elicits protective immunity against *Acinetobacter baumannii* infection. *Sci. Rep.* 6:37242. doi: 10.1038/srep37242

Jones, C. (2005). Vaccines based on the cell surface carbohydrates of pathogenic bacteria. *An. Acad. Bras. Cienc.* 77, 293–324. doi: 10.1590/S0001-37652005000200009

Jong, W. S. P., Saurí, A., and Luirink, J. (2010). Extracellular production of recombinant proteins using bacterial autotransporters. *Curr. Opin. Biotechnol.* 21, 646–652. doi: 10.1016/j.copbio.2010.07.009

Junker, M., Besingi, R. N., and Clark, P. L. (2007). The autodisplay story, from discovery to biotechnical and biomedical applications. *Microbiol. Mol. Biol. Rev.* 71, 600–619. doi: 10.1128/MMBR.00011-07

Junker, M., Besingi, R. N., and Clark, P. L. (2019). Vectorial transport, and folding of an autotransporter virulence protein during outer membrane secretion. *Mol. Microbiol. 96:*333a. doi: 10.1016/j.bpj.2008.12.1677

Kadurugamuwa, J. L., and Beveridge, T. J. (1998). Delivery of the non-membrane-permeative antibiotic gentamicin into mammalian cells by using *Shigella flexneri* membrane vesicles. *Antimicrob. Agents Chemother.* 42, 1476–1483. doi: 10.1128/AAC.42.6.1476

Kaniuk, N. A., Vinogradov, E., and Whitfield, C. (2004). Investigation of the structural requirements in the lipopolysaccharide core acceptor for ligation of O antigens in the genus salmonella: WaaL "ligase" is not the sole determinant of acceptor specificity. *J. Biol. Chem.* 279, 36470–36480. doi: 10.1074/jbc.M401366200

Kataoka, M., Yamaoka, A., Kawasaki, K., Shigeri, Y., and Watanabe, K. (2014). Extraordinary denaturant tolerance of keratinolytic protease complex assemblies produced by meiothermus ruber H328. *Appl. Microbiol. Biotechnol.* 98, 2973–2980. doi: 10.1007/s00253-013-5155-8

Kesty, N. C., and Kuehn, M. J. (2004). Incorporation of heterologous outer membrane and periplasmic proteins into *Escherichia coli* outer membrane vesicles. *J. Biol. Chem.* 279, 2069–2076. doi: 10.1074/jbc.M307628200

Kim, J.-Y., Doody, A. M., Chen, D. J., Cremona, G. H., Shuler, M. L., Putnam, D., et al. (2008). Engineered bacterial outer membrane vesicles with enhanced functionality. *J. Mol. Biol.* 380, 51–66. doi: 10.1016/j.jmb.2008.03.076

Kim, O. Y., Hong Dinh, N. T., Park, H. T., Choi, S. J., Hong, K., and Gho, Y. S. (2017a). Bacterial protoplast-derived nanovesicles for tumor targeted delivery of chemotherapeutics. *Biomaterials* 113, 68–79. doi: 10.1016/j.biomaterials.2016.10.037

Kim, O. Y., Park, H. T., Hong Dinh, N. T., Choi, S. J., Lee, J., Kim, J. H., et al. (2017b). Bacterial outer membrane vesicles suppress tumor by interferon-γ-mediated antitumor response. *Nat. Commun.* 8, 626–626. doi: 10.1038/s41467-017-00729-8

Kim, S., Kim, D., Jung, H. H., Lee, I.-H., Kim, J. I., Suh, J.-Y., et al. (2012). Bio-inspired design and potential biomedical, applications of a novel class of high-affinity peptides. *Angew. Chem. Int. Ed. Engl.* 51, 1890–1894. doi: 10.1002/anie.201107894

Kim, S.-H., Kim, K.-S., Lee, S.-R., Kim, E., Kim, M.-S., Lee, E.-Y., et al. (2009). Structural modifications of outer membrane vesicles to refine them as vaccine delivery vehicles. *Biochim. Biophys. Acta* 1788, 2150–2159. doi: 10.1016/j.bbamem.2009.08.001

Kjaergaard, K., Schembri, M. A., Hasman, H., and Klemm, P. (2000). Antigen 43 from *Escherichia coli* induces inter- and intraspecies cell aggregation and changes in colony morphology of *Pseudomonas fluorescens*. *J. Bacteriol.* 182, 4789–4796. doi: 10.1128/JB.182.17.4789-4796.2000

Klimentová, J., and Stulík, J. (2014). Methods of isolation and purification of outer membrane vesicles from gram-negative bacteria. *Microbiol. Res.* 170, 1–9. doi: 10.1016/j.micres.2014.09.006

Koeberling, O., Seubert, A., and Granoff, D. M. (2008). Bactericidal antibody responses elicited by a meningococcal outer membrane vesicle vaccine with overexpressed factor H–binding protein and genetically attenuated endotoxin. *J. Infect. Dis.* 198, 262–270. doi: 10.1086/589308

Kuehn, M. J., and Kesty, N. C. (2005). Bacterial outer membrane vesicles and the host-pathogen interaction. *Genes Dev.* 19, 2645–2655. doi: 10.1101/gad.1299905

Kuipers, K., Daleke-Schermerhorn, M. H., Jong, W. S. P., ten Hagen-Jongman, C. M., van Opzeeland, F., Simonetti, E., et al. (2015). Salmonella outer

membrane vesicles displaying high densities of pneumococcal antigen at the surface offer protection against colonization. *Vaccine* 33, 2022–2029. doi: 10.1016/j.vaccine.2015.03.010

Kulp, A., and Kuehn, M. J. (2010). Biological functions and biogenesis of secreted bacterial outer membrane vesicles. *Annu. Rev. Microbiol.* 64, 163–184. doi: 10.1146/annurev.micro.091208.073413

Kulp, A. J., Sun, B., Ai, T., Manning, A. J., Orench–Rivera, N., Schmid, A. K., et al. (2015). Genome-wide assessment of outer membrane vesicle production in *Escherichia coli*. *PLoS ONE* 10:e0139200. doi: 10.1371/journal.pone.0139200

Lahiri, A., Ananthalakshmi, T. K., Nagarajan, A. G., Ray, S., and Chakravortty, D. (2011). TolA mediates the differential detergent resistance pattern between the salmonella enterica subsp. enterica serovars typhi and typhimurium. *Microbiology* 157, 1402–1415. doi: 10.1099/mic.0.046565-0

Lee, E.-Y., Bang, J. Y., Park, G. W., Choi, D.-S., Kang, J. S., Kim, H.-J., et al. (2007). Global proteomic profiling of native outer membrane vesicles derived from *Escherichia coli*. *Proteomics* 7, 3143–3153. doi: 10.1002/pmic.200700196

Lee, Y., Cho, I. J., Choi, S. Y., and Lee, S. Y. (2019). Systems metabolic engineering strategies for non-natural microbial polyester production. *Biotechnol. J.* 14:e1800426. doi: 10.1002/biot.201800426

Leitner, D. R., Lichtenegger, S., Temel, P., Zingl, F. G., Ratzberger, D., Roier, S., et al. (2015). A combined vaccine approach against *Vibrio cholerae* and ETEC based on outer membrane vesicles. *Front. Microbiol.* 6:823. doi: 10.3389/fmicb.2015.00823

Lewis, L. A., Carter, M., and Ram, S. (2012). The relative roles of factor H binding protein, neisserial surface protein A, and lipooligosaccharide sialylation in regulation of the alternative pathway of complement on meningococci. *J. Immunol.* 188, 5063–5072. doi: 10.4049/jimmunol.1103748

Lewis, L. A., Ngampasutadol, J., Wallace, R., Reid, J. E. A., Vogel, U., and Ram, S. (2010). The meningococcal vaccine candidate neisserial surface protein A (NspA) binds to factor H and enhances meningococcal resistance to complement. *PLoS Pathog.* 6:e1001027. doi: 10.1371/journal.ppat.1001027

Liang, Y., Eng, W. S., Colquhoun, D. R., Dinglasan, R. R., Graham, D. R., and Mahal, L. K. (2014). Complex N-linked glycans serve as a determinant for exosome/microvesicle cargo recruitment. *J. Biol. Chem.* 289, 32526–32537. doi: 10.1074/jbc.M114.606269

Liu, Q., Yi, J., Liang, K., Hu, B., Zhang, X., Curtiss, R. III., et al. (2016). Outer membrane vesicles from flagellin-deficient Salmonella enterica serovar Typhimurium induce cross-reactive immunity and provide cross-protection against heterologous Salmonella challenge. *Sci. Rep.* 6:34776. doi: 10.1038/srep34776

Liu, Y., Ai, K., Liu, J., Deng, M., He, Y., and Lu, L. (2013). Dopamine-melanin colloidal nanospheres: an efficient near-infrared photothermal therapeutic agent for *in vivo* cancer therapy. *Adv. Mater.* 25, 1353–1359. doi: 10.1002/adma.201204683

Maharjan, S., Saleem, M., Feavers, I. M., Wheeler, J. X., Care, R., and Derrick, J. P. (2016). Dissection of the function of the RmpM periplasmic protein from *Neisseria meningitidis*. *Microbiology* 162, 364–375. doi: 10.1099/mic.0.000227

Maisonneuve, C., Bertholet, S., Philpott, D. J., and De Gregorio, E. (2014). Unleashing the potential of NOD- and Toll-like agonists as vaccine adjuvants. *Proc. Natl. Acad. Sci. U.S.A.* 111, 12294–12299. doi: 10.1073/pnas.1400478111

Mirlashari, M. R., Høiby, E. A., Holst, J., and Lyberg, T. (2010). Outer membrane vesicles from *Neisseria meningitidis*. *Cytokine* 110, 193–204. doi: 10.1034/j.1600-0463.2002.100301.x

Mitra, S., Chakrabarti, M. K., and Koley, H. (2013). Multi-serotype outer membrane vesicles of shigellae confer passive protection to the neonatal mice against shigellosis. *Vaccine* 31, 3163–3173. doi: 10.1016/j.vaccine.2013.05.001

Mitra, S., Sinha, R., Mitobe, J., and Koley, H. (2016). Development of a cost-effective vaccine candidate with outer membrane vesicles of a tolA-disrupted shigella boydii strain. *Vaccine* 34, 1839–46. doi: 10.1016/j.vaccine.2016.02.018

Mizushima, S. (1984). Post-translational modification and processing of outer membrane prolipoproteins in *Escherichia coli*. *Mol. Cell. Biochem.* 60, 5–15. doi: 10.1007/BF00226297

Molloy, M. P., Herbert, B. R., Slade, M. B., Rabilloud, T., Nouwens, A. S., Williams, K. L., et al. (2000). Proteomic analysis of the *Escherichia coli* outer membrane. *Eur. J. Biochem.* 267, 2871–2881. doi: 10.1046/j.1432-1327.2000.01296.x

Moon, D. C., Choi, C. H., Lee, J. H., Choi, C.-W., Kim, H.-Y., Park, J. S., et al. (2012). *Acinetobacter baumannii* outer membrane protein a modulates the biogenesis of outer membrane vesicles. *J. Microbiol.* 50, 155–160. doi: 10.1007/s12275-012-1589-4

Nevermann, J., Silva, A., Otero, C., Oyarzún, D. P., Barrera, B., Gil, F., et al. (2019). Identification of genes involved in biogenesis of outer membrane vesicles (OMVs) in salmonella enterica serovar typhi. *Front. Microbiol.* 10:104. doi: 10.3389/fmicb.2019.00104

O'dwyer, C. A., Reddin, K., Martin, D., Taylor, S. C., Gorringe, A. R., Hudson, M. J., et al. (2004). Expression of heterologous antigens in commensal Neisseria spp.: preservation of conformational epitopes with vaccine potential. *Infect. Immun.* 72, 6511–6518. doi: 10.1128/IAI.72.11.6511-6518.2004

Otto, B. R., Sijbrandi, R., Luirink, J., Oudega, B., Heddle, J. G., Mizutani, K., et al. (2005). Crystal structure of hemoglobin protease, a heme binding autotransporter protein from pathogenic *Escherichia coli*. *J. Biol. Chem.* 280, 17339–17345. doi: 10.1074/jbc.M412885200

Park, J. S., Lee, W. C., Yeo, K. J., Ryu, K.-S., Kumarasiri, M., Hesek, D., et al. (2012). Mechanism of anchoring of OmpA protein to the cell wall peptidoglycan of the gram-negative bacterial outer membrane. *FASEB J.* 26, 219–228. doi: 10.1096/fj.11-188425

Park, M., Sun, Q., Liu, F., DeLisa, M. P., and Chen, W. (2014). Positional assembly of enzymes on bacterial outer membrane vesicles for cascade reactions. *PLoS ONE* 9:e97103. doi: 10.1371/journal.pone.0097103

Parlane, N. A., Gupta, S. K., Rubio–Reyes, P., Chen, S., Gonzalez–Miro, M., Wedlock, D. N., et al. (2017). Self-assembled protein-coated polyhydroxyalkanoate beads: properties and biomedical applications. *ACS Biomater. Sci. Eng.* 3, 3043–3057. doi: 10.1021/acsbiomaterials.6b00355

Petros, R. A., and DeSimone, J. M. (2010). Strategies in the design of nanoparticles for therapeutic applications. *Nat. Rev. Drug Discov.* 9, 615–627. doi: 10.1038/nrd2591

Prados–Rosales, R., Weinrick, B. C., Piqué, D. G., Jacobs, W. R. Jr., Casadevall, A., and Rodriguez, M. G. (2014). Role for *Mycobacterium tuberculosis* membrane vesicles in iron acquisition. *J. Bacteriol.* 196, 1250–1256. doi: 10.1128/JB.01090-13

Price, N. L., Goyette–Desjardins, G., Nothaft, H., Valguarnera, E., Szymanski, C. M., Segura, M., et al. (2016). Glycoengineered outer membrane vesicles: a novel platform for bacterial vaccines. *Sci. Rep.* 6:24931. doi: 10.1038/srep24931

Qing, G., Gong, N., Chen, X., Chen, J., Zhang, H., Wang, Y., et al. (2019). Natural and engineered bacterial outer membrane vesicles. *Biophys. Rep.* 5, 184–198. doi: 10.1007/s41048-019-00095-6

Ranallo, R. T., Kaminski, R. W., George, T., Kordis, A. A., Chen, Q., Szabo, K., et al. (2010). Virulence, inflammatory potential, and adaptive immunity induced by *Shigella flexneri* msbB mutants. *Infect. Immun.* 78, 400–412. doi: 10.1128/IAI.00533-09

Salverda, M. L. M., Meinderts, S. M., Hamstra, H.-J., Wagemakers, A., Hovius, J. W. R., van der Ark, A., et al. (2016). Surface display of a borrelial lipoprotein on meningococcal outer membrane vesicles. *Vaccine* 34, 1025–1033. doi: 10.1016/j.vaccine.2016.01.019

Sánchez, J. M., López-Laguna, H., Álamo, P., Serna, N., Sánchez-Chardi, A., Nolan, V., et al. (2020). Artificial inclusion bodies for clinical development. *Adv. Sci.* 7:1902420. doi: 10.1002/advs.201902420

Santos, S., de Arauz, L. J., Baruque–Ramos, J., Lebrun, I., Carneiro, S. M., Barreto, S. A., et al. (2012). Outer membrane vesicles (OMV) production of *Neisseria meningitidis* serogroup B in batch process. *Vaccine* 30, 6064–6069. doi: 10.1016/j.vaccine.2012.07.052

Santos, T. M. A., Lin, T.-Y., Rajendran, M., Anderson, S. M., and Weibel, D. B. (2014). Polar localization of *Escherichia coli* chemoreceptors requires an intact Tol-Pal complex. *Mol. Microbiol.* 92, 985–1004. doi: 10.1111/mmi.12609

Schetters, S. T. T., Jong WSP, Horrevorts, S. K., Kruijssen, L. J. W., Engels, S., Stolk, D., et al. (2019). Outer membrane vesicles engineered to express membrane-bound antigen program dendritic cells for cross-presentation to CD8+ T cells. *Acta Biomater.* 91, 248–257. doi: 10.1016/j.actbio.2019.04.033

Schmid-Dannertand, C., and López-Gallego, F. (2019). Advances and opportunities for the design of self-sufficient and spatially organized cell-free biocatalytic systems. *Curr. Opin. Chem. Biol.* 49, 97–104. doi: 10.1016/j.cbpa.2018.11.021

Schroeder, J., and Aebischer, T. (2009). Recombinant outer membrane vesicles to augment antigen-specific live vaccine responses. *Vaccine* 27, 6748–6754. doi: 10.1016/j.vaccine.2009.08.106

Schulz, E., Goes, A., Garcia, R., Panter, F., Koch, M., Müller, R., et al. (2018). Biocompatible bacteria-derived vesicles show inherent antimicrobial activity. *J. Control. Release* 290, 46–55. doi: 10.1016/j.jconrel.2018.09.030

Schwechheimer, C., and Kuehn, M. J. (2015). Outer-membrane vesicles from gram-negative bacteria: biogenesis and functions. *Nat. Rev. Microbiol.* 13, 605–619. doi: 10.1038/nrmicro3525

Sharpe, S. W., Kuehn, M. J., and Mason, K. M. (2011). Elicitation of epithelial cell-derived immune effectors by outer membrane vesicles of nontypeable *Haemophilus influenzae*. *Infect. Immun.* 79, 4361–4369. doi: 10.1128/IAI.05332-11

Shen, Y., Torchia, M. L. G., Lawson, G. W., Karp, C. L., Ashwell, J. D., and Mazmanian, S. K. (2012). Outer membrane vesicles of a human commensal mediate immune regulation and disease protection. *Cell Host Microbe* 12, 509–520. doi: 10.1016/j.chom.2012.08.004

Shi, J., Votruba, A. R., Farokhzad, O. C., and Langer, R. (2010). Nanotechnology in drug delivery and tissue engineering: from discovery to applications. *Nano Lett.* 10, 3223–3230. doi: 10.1021/nl102184c

Shim, S.-M., Song, E.-J., Song, D., Lee, T.-Y., Kim, D.-J., Nam, J.-H., et al. (2017). Nontoxic outer membrane vesicles efficiently increase the efficacy of an influenza vaccine in mice and ferrets. *Vaccine* 35, 3741–3748. doi: 10.1016/j.vaccine.2017.05.053

Shimoda, A., Tahara, Y., Sawada, S.-I., Sasaki, Y., and Akiyoshi, K. (2017). Glycan profiling analysis using evanescent-field fluorescence-assisted lectin array: importance of sugar recognition for cellular uptake of exosomes from mesenchymal stem cells. *Biochem. Biophys. Res. Commun.* 491, 701–707. doi: 10.1016/j.bbrc.2017.07.126

Shrivastava, R., Jiang, X., and Chng, S.-S. (2017). Outer membrane lipid homeostasis via retrograde phospholipid transport in *Escherichia coli*. *Mol. Microbiol.* 106, 395–408. doi: 10.1111/mmi.13772

Simpson, B. W., May, J. M., Sherman, D. J., Kahne, D., and Ruiz, N. (2015). Lipopolysaccharide transport to the cell surface: biosynthesis and extraction from the inner membrane. *Philos. Trans. R Soc. Lond. B Biol. Sci.* 370, 209–211. doi: 10.1098/rstb.2015.0029

Spaan, A. N., van Strijp, J. A. G., and Torres, V. J. (2017). Leukocidins: staphylococcal bi-component pore-forming toxins find their receptors. *Nat. Rev. Microbiol.* 15, 435–447. doi: 10.1038/nrmicro.2017.27

Su, F.-H., Tabañag, I. D. F., Wu, C.-Y., and Tsai, S.-L. (2017). Decorating outer membrane vesicles with organophosphorus hydrolase and cellulose binding domain for organophosphate pesticide degradation. *Chem. Eng. J.* 308, 1–7. doi: 10.1016/j.cej.2016.09.045

Tan, K., Li, R., Huang, X., and Liu, Q. (2018). Outer membrane vesicles: current status,and future direction, of these novel vaccine adjuvants. *Front. Microbiol.* 9:783. doi: 10.3389/fmicb.2018.00783

Tashiro, M., Tejero, R., Zimmerman, D. E., Celda, B., Nilsson, B., and Montelione, G. T. (1997). High-resolution solution NMR structure of the Z domain of staphylococcal protein A. *J. Mol. Biol.* 272, 573–590. doi: 10.1006/jmbi.1997.1265

Thompson, B. S., Chilton, P. M., Ward, J. R., Evans, J. T., and Mitchell, T. C. (2005). The low-toxicity versions of LPS, MPL® adjuvant and RC529, are efficient adjuvants for CD4+ T cells. *J. Leukoc. Biol.* 78, 1273–1280. doi: 10.1189/jlb.0305172

Tokuda, H., and Matsuyama, S. (2004). Sorting of lipoproteins to the outer membrane in *E. coli*. *Biochim. Biophys. Acta* 1693, 5–13. doi: 10.1016/j.bbamcr.2004.02.005

Tsai, S.-L., Oh, J., Singh, S., Chen, R., and Chen, W. (2009). Functional assembly of minicellulosomes on the *Saccharomyces cerevisiae* cell surface for cellulose hydrolysis and ethanol production. *Appl. Environ. Microbiol.* 75, 6087–6093. doi: 10.1128/AEM.01538-09

Turner, L., Praszkier, J., Hutton, M. L., Steer, D., Ramm, G., Kaparakis–Liaskos, M., et al. (2015). Increased outer membrane vesicle formation in a *Helicobacter pylori* tolB mutant. *Helicobacter* 20, 269–283. doi: 10.1111/hel.12196

Tzokov, S. B., Wyborn, N. R., Stillman, T. J., Jamieson, S., Czudnochowski, N., Artymiuk, P. J., et al. (2006). Structure of the hemolysin E (HlyE, ClyA, and SheA) channel in its membrane-bound form. *J. Biol. Chem.* 281, 23042–23049. doi: 10.1074/jbc.M602421200

Unal, C. M., Schaar, V., and Riesbeck, K. (2011). Bacterial outer membrane vesicles in disease and preventive medicine. *Semin. Immunopathol.* 33, 395–408. doi: 10.1007/s00281-010-0231-y

Underhill, D. M., and Goodridge, H. S. (2012). Information processing during phagocytosis. *Nat. Rev. Immunol.* 12, 492–502. doi: 10.1038/nri3244

van Bloois, E., Winter, R. T., Kolmar, H., and Fraaije, M. W. (2011). Decorating microbes: surface display of proteins on *Escherichia coli*. *Trends Biotechnol.* 29, 79–86. doi: 10.1016/j.tibtech.2010.11.003

van de Waterbeemd, B., Streefland, M., van der Ley, P., Zomer, B., van Dijken, H., Martens, D., et al. (2010). Improved OMV vaccine against *Neisseria meningitidis* using genetically engineered strains and a detergent-free purification process. *Vaccine* 28, 4810–4816. doi: 10.1016/j.vaccine.2010.04.082

van de Waterbeemd, B., Streefland, M., van Keulen, L., van den Ijssel, J., de Haan, A., Eppink, M. H., et al. (2012). Identification and optimization of critical process parameters for the production of NOMV vaccine against *Neisseria meningitidis*. *Vaccine* 30, 3683–3690. doi: 10.1016/j.vaccine.2012.03.028

van der Ley, P., Steeghs, L., Hamstra, H. J., ten Hove, J., Zomer, B., and van Alphen, L. (2001). Modification of lipid A biosynthesis in *Neisseria meningitidis* lpxL mutants: influence on lipopolysaccharide structure, toxicity, and adjuvant activity. *Infect. Immun.* 69, 5981–5990. doi: 10.1128/IAI.69.10.5981-5990.2001

van der Pol, L., Stork, M., and van der Ley, P. (2015). Outer membrane vesicles as platform vaccine technology. *Biotechnol. J.* 10, 1689–1706. doi: 10.1002/biot.201400395

Veggiani, G., Nakamura, T., Brenner, M. D., Gayet, R. V., Yan, J., Robinson, C. V., et al. (2016). Programmable polyproteams built using twin peptide superglues. *Proc. Natl. Acad. Sci. U.S.A.* 113, 1202–1207. doi: 10.1073/pnas.1519214113

Wacker, M., Feldman, M. F., Callewaert, N., Kowarik, M., Clarke, B. R., Pohl, N. L., et al. (2006). Substrate specificity of bacterial oligosaccharyltransferase suggests a common transfer mechanism for the bacterial and eukaryotic systems. *Proc. Natl. Acad. Sci. U.S.A.* 103, 7088–7093. doi: 10.1073/pnas.0509207103

Wai, S. N., Lindmark, B., Söderblom, T., Takade, A., Westermark, M., Oscarsson, J., et al. (2003). Vesicle-mediated export and assembly of pore-forming oligomers of the enterobacterial clya cytotoxin. *Cell* 115, 25–35. doi: 10.1016/S0092-8674(03)00754-2

Wang, S., Gao, J., and Wang, Z. (2019). Outer membrane vesicles for vaccination and targeted drug delivery. *Wiley Interdiscip. Rev. Nanomed. Nanobiotechnol.* 11:e1523. doi: 10.1002/wnan.1523

Weaver, B. A. A., and Cleveland, D. W. (2005). Decoding the links between mitosis, cancer, and chemotherapy: the mitotic checkpoint, adaptation, and cell death. *Cancer Cell* 8, 7–12. doi: 10.1016/j.ccr.2005.06.011

Westermark, M., Oscarsson, J., Mizunoe, Y., Urbonaviciene, J., and Uhlin, B. E. (2000). Silencing and activation of ClyA cytotoxin expression in *Escherichia coli*. *J. Bactorial.* 182, 6347–6357. doi: 10.1128/JB.182.22.6347-6357.2000

Wilkerson, J. W., Yang, S.-O., Funk, P. J., Stanley, S. K., and Bundy, B. C. (2018). Nanoreactors: strategies to encapsulate enzyme biocatalysts in virus-like particles. *N. Biotechnol.* 44, 59–63. doi: 10.1016/j.nbt.2018.04.003

Williams, C., Royo, F., Aizpurua–Olaizola, O., Pazos, R., Boons, G.-J., Reichardt, N.-C., et al. (2018). Glycosylation of extracellular vesicles: current knowledge, tools and clinical perspectives. *J. Extracell. Vesicles* 7:1442985. doi: 10.1080/20013078.2018.1442985

Wong, J. X., Ogura, K., Chen, S., and Rehm, B. H. A. (2020). Bioengineered polyhydroxyalkanoates as immobilized enzyme scaffolds for industrial applications. *Front. Bioeng. Biotechnol.* 8:156. doi: 10.3389/fbioe.2020.00156

Wressnigg, N., Barrett, P. N., Pöllabauer, E.-M., O'Rourke, M., Portsmouth, D., Schwendinger, M. G., et al. (2014). A Novel multivalent OspA vaccine against Lyme borreliosis is safe and immunogenic in an adult population previously infected with *Borrelia burgdorferi* sensu lato. *Clin. Vaccine Immunol.* 21, 1490–1499. doi: 10.1128/CVI.00406-14

Yan, L., Da, H., Zhang, S., López, V. M., and Wang, W. (2017). Bacterial magnetosome and its potential application. *Microbiol. Res.* 203, 19–28. doi: 10.1016/j.micres.2017.06.005

Yeh, Y.-C., Comolli, L. R., Downing, K. H., Shapiro, L., and McAdams, H. H. (2010). The caulobacter Tol-Pal complex is essential for outer membrane integrity and the positioning of a polar localization factor. *J. Bacteriol.* 192, 4847–4858. doi: 10.1128/JB.00607-10

Yoo, J.-W., Irvine, D. J., Discher, D. E., and Mitragotri, S. (2011). Bio-inspired, bioengineered and biomimetic drug delivery carriers. *Nat. Rev. Drug Discov.* 10, 521–535. doi: 10.1038/nrd3499

Yoon, H. (2016). Bacterial outer membrane vesicles as a delivery system for virulence regulation. *J. Microbiol. Biotechnol.* 26, 1343–7. doi: 10.4014/jmb.1604.04080

Yoon, H., Ansong, C., Adkins, J. N., and Heffron, F. (2011). Discovery of salmonella virulence factors translocated via outer membrane vesicles to murine macrophages. *Infect. Immun.* 79, 2182–2192. doi: 10.1128/IAI.01277-10

Zakeri, B., Fierer, J. O., Celik, E., Chittock, E. C., Schwarz–Linek, U., Moy, V. T., et al. (2012). Peptide tag forming a rapid covalent bond to a protein, through engineering a bacterial adhesin. *Proc. Natl. Acad. Sci. U.S.A.* 109, E690–E697. doi: 10.1073/pnas.1115485109

Zhang, L., Wen, Z., Lin, J., Xu, H., Herbert, P., Wang, X.-M., et al. (2016). Improving the immunogenicity of a trivalent *Neisseria meningitidis* native outer membrane vesicle vaccine by genetic modification. *Vaccine* 34, 4250–4256. doi: 10.1016/j.vaccine.2016.05.049

Conflict of Interest: The authors declare that the research was conducted in the absence of any commercial or financial relationships that could be construed as a potential conflict of interest.

frontiers in Bioengineering and Biotechnology

ORIGINAL RESEARCH
published: 14 October 2020
doi: 10.3389/fbioe.2020.583065

Microfluidic Encapsulation of Single Cells by Alginate Microgels Using a Trigger-Gellified Strategy

Fei Shao[1†], Lei Yu[1†], Yang Zhang[2†], Chuanfeng An[1], Haoyue Zhang[1], Yujie Zhang[1], Yi Xiong[2] and Huanan Wang[1]*

[1] Key State Laboratory of Fine Chemicals, School of Bioengineering, Dalian University of Technology, Dalian, China, [2] Laboratory of Regenerative Biomaterials, Department of Biomedical Engineering, Health Science Center, Shenzhen University, Shenzhen, China

Microfluidics-based alginate microgels have shown great potential to encapsulate cells in a high-throughput and controllable manner. However, cell viability and biological functions are substantially compromised due to the harsh conditions for gelation, which remains a major challenge for cell encapsulation. Herein, we presented an efficient and biocompatible method by on-chip triggered gelation to generate microfluidic alginate microgels for single-cell encapsulation. Two calcium complexes of calcium–ethylenediaminetetraacetic acid (Ca-EDTA) and calcium–nitrilotriacetic (Ca-NTA) as crosslinkers for triggered gelation of alginate were compared and investigated for feasible application. By triggered release of Ca^{2+} ions from the calcium complex via adding acetic acid in the oil phase, the alginate precursor in the aqueous droplets can be crosslinked to form alginate microgels. Although using Ca-EDTA and Ca-NTA both achieved on-chip gelation, Ca-NTA led to significantly higher cell viability since the dissociation of Ca^{2+} ions from Ca-NTA can be obtained using less concentration of acid compared to Ca-EDTA. We further demonstrated the functionality of encapsulated mesenchymal stem cells (MSCs) in alginate microgels prepared using Ca-NTA, as evidenced by the osteogenesis of encapsulated MSCs upon inductive culture. In summary, our study provided a biocompatible strategy to prepare alginate microgels for single-cell encapsulation which can be further used for applications in tissue engineering and cell therapies.

Keywords: microfluidics, alginate microgels, cell encapsulation, calcium complexes, on-chip gelation, biocomatability

OPEN ACCESS

Edited by:
Nihal Engin Vrana, Sparta Medical, France

Reviewed by:
Gonzalo Hortelano, Nazarbayev University, Kazakhstan
Mingqiang Li, Sun Yat-sen University, China

***Correspondence:**
Huanan Wang
Huananwang@dlut.edu.cn

† These authors have contributed equally to this work

Specialty section:
This article was submitted to Biomaterials, a section of the journal Frontiers in Bioengineering and Biotechnology

Received: *14 July 2020*
Accepted: *16 September 2020*
Published: *14 October 2020*

Citation:
Shao F, Yu L, Zhang Y, An C, Zhang H, Zhang Y, Xiong Y and Wang H (2020) Microfluidic Encapsulation of Single Cells by Alginate Microgels Using a Trigger-Gellified Strategy. Front. Bioeng. Biotechnol. 8:583065. doi: 10.3389/fbioe.2020.583065

INTRODUCTION

Constructing cell carriers has become a powerful way to address biomedical questions, such as screening and delivery of drugs (Holloway et al., 2014; Yeung et al., 2016; Kang et al., 2020), cell therapy (Lim and Sun, 1980; Burdick et al., 2016), and tissue regeneration (Caiazzo et al., 2016; An et al., 2020). Hydrogels containing hydrophilic polymeric networks are widely used as matrix materials to construct cell carriers because it resembles a natural extracellular matrix (ECM) and can be further functionalized to offer physiologically relevant environmental cues (Borenstein et al., 2007; Mao et al., 2017). However, conventional bulk hydrogels have limited diffusion efficiency, which may hamper efficient nutrition and oxygen transfer, thus resulting in restricted intercellular

communication and inaccurate control of cell behavior. With this aim, micrometer-sized hydrogels (microgels) were extensively studied as cell vehicles. Moreover, cell transplantation in uniform microgels can offer administration by injection in a minimally invasive manner, which enables the promotion of cell viability and leveraged therapeutic activities of encapsulated cells (Velasco et al., 2012; Wan, 2012). Besides, due to the tight microenvironment control of cells, cells encapsulated in microgels can be served as a tissue engineering module for constructing large tissues and organs.

To produce such microgel modules containing cells in a high-throughput manner, several microfabrication techniques such as micro-molding, photolithography, and flow lithography have been developed (Selimovic et al., 2012; Yun et al., 2013; Kang et al., 2014). However, most of them are limited for further application due to relatively low throughput and impaired cell viability and activity during processing (Franco et al., 2011; Choi et al., 2016). To this end, microfluidic technology has been considered as a practical method to obtain microgels given its controllable and biocompatible generation process.

Alginate microgels have been mostly used for cell encapsulation (Moyer et al., 2010; Hu et al., 2017), drug delivery (Somo et al., 2017; Uyen et al., 2019), and tissue engineering (Goh et al., 2012; Kumar Meena et al., 2019) due to its biocompatibility and ease of gelation. Lim and Sun (1980) firstly used alginate microgels to encapsulate islet cells to escape from the immune clearance and prolong retention time after implantation. It was also used as a vesicle to deliver MSCs' (Mao et al., 2017; Campiglio et al., 2020), chondrocytes (Markstedt et al., 2015; An et al., 2020), and murine pre-adipocyte cells (Mao et al., 2017) for tissue regeneration. Regarding the microfluidic fabrication of cell-laden alginate microgels, a typical process involved (i) emulsification of cell-laden aqueous suspension in an immiscible, non-polar liquid (continuous phase) and (ii) the formation of droplets containing alginate precursor solution which can be subsequently gelled. Alginate microgels can be crosslinked by divalent ions such as calcium ions (Moyer et al., 2010; Yao et al., 2012; Pereira et al., 2013). The gelation of alginate relies on the crosslinking reaction that occurs rapidly between calcium ions and the α-L-guluronic (G) fragment of the polymer chain (Goh et al., 2012). Two gelation strategies of alginate microfluidic microgels are commonly adopted, i.e., external gelation in which crosslinkers are diffused outside of the droplets (Tan and Takeuchi, 2007; Zhang et al., 2007; Utech et al., 2015; Hati et al., 2016) and internal gelation in which crosslinkers are loaded within the aqueous phase and trigger-gellified upon stimuli (Huang et al., 2006). The external approach was widely used for the preparation of alginate beads with a size ranging from several hundreds of microns to millimeters. These methods were reported to lead to an exposure of cells to potential cytotoxicity of a high concentration of Ca^{2+} and compromised injectability due to their large size (Kang et al., 2014). Instead, the method of internal gelation can be triggered by the release of Ca^{2+} ions upon the diffusion of acetic acid from the continuous phase into the aqueous phase using calcium sources such as $CaCO_3$ (Tan and Takeuchi, 2007) or $CaSO_4$ (Kong, 2003) particles. This method, however, suffers from problematic issues such as inhomogeneous hydrogel network formation and high cytotoxicity upon prolonged exposure to surfactants or crosslinkers (Tan and Takeuchi, 2007; Zhang et al., 2007; Choi et al., 2016). To overcome these problems, the introduction of soluble calcium complexes was recently developed as a more promising strategy for rapid and uniform gelation upon Ca^{2+} ion release triggered by the acid. For instance, calcium chelated with ethylenediaminetetraacetic acid (EDTA) to form a calcium complex was used as a crosslinker for alginate to enable the release of Ca^{2+} ions at an acidic environment (pH $<$ 5.0) (Utech et al., 2015). Since alginate and Ca-EDTA are both water soluble, Ca^{2+} ions can be uniformly dispersed in the alginate precursor solution to allow further internal gelation to form a uniform hydrogel network. However, the cell viability and activities can be substantially compromised due to extensive exposure to the acidic condition during the fabrication process (more than a few minutes) (Utech et al., 2015). To solve the problem, Hati et al. (2016) proposed a method of on-chip triggered gelation at pH 6.7. Zn^{2+} ions are able to exchange between ethylenediamine-*N*,*N*'-diacetic acid (EDDA) and EDTA due to the difference in dissociation constant, thus resulting in the release of Ca^{2+} ions at a relatively neutral pH (Hati et al., 2016). It is promising to exploit calcium complexes with a high equilibrium dissociation constant for precisely controlled on-chip gelation and high cell viability by introducing a rather mild crosslinking condition for cell encapsulation. With this aim, a comprehensive evaluation of different calcium complexes as crosslinking agents for the microfluidic preparation of cell-laden alginate microgels is desired.

Herein, we reported a biocompatible microfluidic approach for on-chip gelation of alginate microgels using calcium complexes that can be released in a more physiologically relevant condition. We introduced nitrilotriacetic calcium (Ca-NTA) with a relatively high dissociation constant as the calcium source and compared it with Ca-EDTA by evaluating the dissociation energy and gelation time for on-chip microgel formation. We further demonstrated the viability of encapsulated fibroblasts and the biofunctionality of encapsulated MSCs using an osteogenic differentiation model.

MATERIALS AND METHODS

Isothermal Titration Calorimetry (ITC)

To evaluate the dissociation constant of calcium complexes, an ITC (MicroCal iTC200, United States) method was used as previously reported (Rafols et al., 2016). Specifically, calcium chloride ($CaCl_2$, Sigma, United States) solution was titrated into the EDTA or NTA solution which was buffered to a defined pH (pH 6.5 and pH 7) using 4-morpholineethanesulfonic acid hydrate (MES, Solarbio, China) or *N*-2-hydroxyethylpiperazine-*N*-2-ethane sulfonic acid (HEPES, Solarbio, China). Both $CaCl_2$ and EDTA (Sigma, United States) were configured using buffers. The concentrations of $CaCl_2$ and EDTA/NTA were 10^{-2} and

10^{-3} M, respectively. All solutions were degassed before the test. To carry out the titration, the syringe was loaded with the $CaCl_2$ solution, and the sample cuvette was filled with EDTA (or NTA) solution. The identical $CaCl_2$ solution was used in the buffer as background titration to determine the dilution heat which was subtracted from the sample value. The solution in the cuvette was stirred at 1,000 rpm by the syringe to ensure a rapid mixing. Typically, 2 μl of titrants was injected into a known volume of samples placed in the cuvette during 60 s. The number of additions was 19 with an adequate interval of 150 s between injections to allow complete equilibrations. All ITC titrations were carried out at 37°C.

Cell Isolation and Culture

Fibroblasts (NIH3T3, ATCC, China) were cultured in DMEM (HyClone, United States) with 10% of fetal bovine serum (FBS, Gibco, United States) and 1% of penicillin/streptomycin at 37°C and 5% CO_2. Primary rat bone marrow-derived MSCs were isolated from 3-week-old male Sprague-Dawley (SD) rats. In brief, cells were flushed out of the marrow cavity and sieved through a 70-μm-mesh strainer and then collected by centrifugation (300 *g* for 5 min). Cells were then cultured in α-Minimum Essential Medium (α-MEM) with 10% of FBS and 1% of penicillin/streptomycin (Gibco, United States). Non-adherent cells were removed after 36 h before fresh medium was added. MSCs were cultured and passaged when cells reached 80% confluency, and MSCs at passages of 3–5 were collected for further experiments.

Fabrication of PDMS Microfluidic Devices

PDMS microfluidic devices were fabricated by soft lithography protocol (Qin et al., 2010). In brief, a negative photoresist SU-8 (MicroChem, United States) was spin-coated onto a clean silicon wafer to a thickness of 50 μm and baked at 65°C for 3 min and then 95°C for 8 min. Subsequently, through a transparency photomask (Newway, China) designed by CAD (Art Service, United States), an exposure energy of 200 mJ/cm^2 was used for UV exposure. Then the postexposure bake was carried out at 65°C for 1.5 min and further at 95°C for 6 min. To develop the microstructure, the sample was immersed in a photoresist developer for 5 min and washed three times by isopropyl alcohol. All chips were then dried with filtered nitrogen before being baked for 2 min at 150°C to ensure the stability of SU-8. After the microstructure fabrication, poly(dimethylsiloxane) (PDMS) and crosslinker (base/crosslinker = 10/1) were poured onto the pattern and solidified overnight at 85°C. PDMS molds were peeled off the silicon plate, and channel inlets and outlets were made by a biopsy punch of 1-mm diameter (Wenhan, China). The obtained PDMS replica was bonded to a glass slide after oxygen-plasma treatment and cured for 1 h at 85°C. To render the channel surface hydrophobic, all chips were treated with the Aquapel (a hydrophobic silane, PPG Industries, Pittsburgh, PA, United States). All microfluidic chips were finally dried by the filtered nitrogen before being baked at 85°C.

Microfluidics Generation of Alginate Microgels

A homogeneous hydrogel precursor solution containing 1% (w/v) alginate and 50 mM calcium complex was prepared. $CaCl_2$ solution and Na-EDTA (Na-NTA) solution were mixed at a 1:1 molar ratio to obtain Ca-EDTA (Ca-NTA) solution, followed by the neutralization to pH 7.4 using sodium hydroxide (potassium hydroxide solution). Fluorinated carbon oil (HFE7100, 3M, United States) containing 0.5 v/v% Krytox-polyethylene glycol (PEG)-Krytox surfactants (DragonDrop, China) and acetic acid (0.05–1 v/v‰) was used as the continuous phase, and HFE7100 containing 20 v/v% PFO (Aladdin, China) was used as the washing phase to disturb the stability of the water/oil interface for de-emulsification. All liquids were separately added into syringes for injection into the chip. Polyethylene tubes with an inner diameter of 0.38 μm were used to connect the syringes and the PDMS devices. The flow rates were individually controlled by syringe pumps. The flow rate of the aqueous phase was kept constant at 100 μl/h to avoid cell damage from the shearing force during the injection, and the flow rates of the continuous phase and PFO oil phase were both set at 1,000 μ l/h.

The gelation time of microgels was determined by the crosslink density of the hydrogel. To calculate the gelation time of microgels in the microfluidics channel, microfluidic chips with channels of different lengths were fabricated to estimate the gelation time of microgel within the chip. Specifically, all microfluidic chips contained two flow-focusing junctions which were connected using a straight microchannel of different lengths (between 1 mm and 4 cm). Droplets containing alginate precursor were generated by the first flow-focusing junction and were trigger-gellified within the downstream straight channel where acetic acid from the oil phase diffuses into the aqueous droplets to initiate the gelation process. Upon converging into the second flow-focusing junction, a buffering phase containing 25 mM HEPES (pH 7.4) to neutralize the pH was introduced; this will quench the crosslinking reaction. Here, the flow rate of the aqueous phase was kept constant at 100 μl/h, while those of the oil phase and washing phase were set at 1,000 μl/h. If the in-drop gelation of alginate can be finalized, spherical solid-like hydrogel particles can be collected from the outputting solution. Otherwise, no spherical microparticles or even no microparticles can be collected since the time for the droplets to finalize alginate crosslinking was not enough. We denoted the latter phenomenon as "uncrosslinked droplets." The morphology of the resulting microgels characterized by different degrees of roundness further provided quantitative information of the crosslinking degree. For the resulting microgels with a high degree of roundness, we considered them as "completely crosslinked microgels." In contrast, microgels showing poor roundness or particle aggregation can be considered as "incompletely crosslinked microgels." Subsequently, the real-time detection of microgel flow was collected by a high-speed camera (i-SPEED 221, iX

Cameras, United Kingdom), and the flow time of completely crosslinked microgels can be determined.

Microfluidic Generation of Cell-Laden Microgels

Arg-Gly-Asp (RGD)-modified sodium alginate was synthesized by the carbodiimide chemistry according to our published work (An et al., 2020). In brief, 1 g sodium alginate (BioReagent, Sigma, United States) was completely dissolved in 100 ml MES buffer solution (0.1 M MES, 0.3 M NaCl, pH 6.5). Then, sequentially added into the sodium alginate solution were 48.42 mg of EDC (Aladdin, China), 27.4 mg of sulfo-NHS (Aladdin, China), and 16.7 mg of peptide motif G4RGDY (Wuhan Holder, China), which were reacted at least 20 h with stirring and finally stopped by adding 18 mg of hydroxylamine hydrochloride. To obtain purified RGD-alginate, the resulting solution was dialyzed with a dialysis tube (MWCO 3500, Solarbio, China) over 3 days. Afterward, the dialyzed solution was sterilized by a 0.22-μm filter and then lyophilized to obtain sodium alginate powder.

Cells were dispersed in alginate solution with a final cell density of 3×10^6 cells/ml in 1 w/v% alginate and 50 mM Ca-EDTA/Ca-NTA. The composition of the continuous phase and the aqueous phase was described above, but 0.4 and 0.2 v/v‰ acetic acid were used in the Ca-EDTA system and Ca-NTA system, respectively. The flow rate of the aqueous phase was kept constant at 100 μl/h, and the flow rates of the continuous phase and PFO were both set at 1,000 μl/h. The collection solution to retreat the encapsulated cells was composed of α-MEM plus 25 mM HEPES (pH 7.4) to neutralize the pH of the aqueous phase. The cell-laden microgels were finally collected by centrifugation (300 *g* for 5 min) before being redispersed in the medium.

Cell Viability

To assess the biocompatibility of the encapsulation process, 3×10^6 fibroblasts were mixed with 1 ml alginate precursor solution and kept in the syringe for 1 and 4 h, respectively. Fibroblasts were subsequently collected and washed three times with PBS to remove the alginate. The remaining fibroblasts were centrifuged (300 *g* for 5 min) and counted in the tissue culture plates. To evaluate the biocompatibility of produced alginate microgels, cell-laden microgels were also collected by centrifuge (300 *g* for 5 min) after 1 day of culture and seeded in tissue culture plates. Fibroblast were further stained with 2 mM calcein-AM (Invitrogen, China) and 4 mM ethidium homodimer (Invitrogen, China) for 15 min at room temperature. Samples were then observed using a confocal laser scanning microscope (OLYMPUS FV3000, Japan), and the cell viability was analyzed.

Cell Metabolism Activity

Cell metabolism activity was determined using a CCK-8 assay (Yisheng, China) according to the instruction of the manufacturer. In brief, cell-laden microgels were collected by centrifugation (300 *g* for 5 min) after 1 day of culture, and then 1 ml of CCK-8 work solution was added and incubated for 2 h at 37°C. After that, cell-laden microgels were centrifuged, and 200 μl of supernatant was transferred into 96-well plates. The absorbance at 450 nm was measured using a microplate reader (Bio-Rad iMark, United States). The final values of each group were determined by subtracting the value of the blank control.

Nuclear Staining

Nuclear staining of encapsulated cells was determined according to the instruction of a SYTO 9 green-fluorescent nucleic acid kit (Invitrogen, China). In brief, microgels were collected by centrifugation (300 *g* for 5 min) after 1, 4, 7, 14, and 21 days of culture, and the medium was refreshed. SYTO 9 dyes of 5 μM were subsequently added and incubated for 10 min at room temperature before being observed using a confocal laser scanning microscope (OLYMPUS FV3000, Japan).

Differentiation of Stem Cells in Microgels

Into six-well non-adherent plates were placed 1×10^5 MSC-laden microgels (NEST, China). After 3 days of culture in the growth medium, MSC-laden microgels were cultured in the osteogenic medium (α-MEM supplemented with 100 nM dexamethasone (Sigma, United States), 10 mM β-glycerophosphate (Sigma, United States), and 50 μM ascorbic acid (Sinopharm, China), and the medium was refreshed every 3 days. After 1, 4, 7, 14, and 21 days, microgels were collected and digested with 500 μl of EDTA solution at 37°C until the microgels were completely degraded. Afterward, samples were centrifuged (300 *g* for 5 min) and washed three times with PBS and then suspended in 250 μl of RIPA lysis buffer (Solarbio, China) for 15 min. The DNA content of encapsulated cells was quantified using the PicoGreen dsDNA Quantitation Reagent (Yisheng, China) per the manufacturer's instruction. A 4-nitrophenyl phosphate-based method was applied to assess the alkaline phosphatase (ALP) activity of encapsulated cells according to the instruction of an Alkaline Phosphatase Assay Kit (Beyotime, China). ALP activity was further normalized to the dsDNA content.

Mineralized of MSC-Laden Microgels

The mineralization of microgels was quantified by the opacity of microgels. In brief, after 1, 4, 7, 14, and 21 days of culture, cell-laden microgels were observed with a phase contrast microscope (Motic AE2000, China), and the gray value of microgels was evaluated using ImageJ. The mineralization of cell-laden alginate microgels was also characterized with the Alizarin Red S staining (Solarbio, China). In brief, after 21 days of culture in the osteogenic medium, microgels were collected and washed with PBS and then fixed with 4% PFA for 15 min; microgels were then stained with 0.1% Alizarin Red S for 15 min before being observed with the phase contrast microscope.

Statistical Analysis

All data are presented as means ± SD. To determine the significant difference, comparisons between Ca-NTA and Ca-EDTA were performed by Student's *t*-test, and other comparisons between different groups were performed by a one-way ANOVA with a Tukey *post-hoc* multiple comparison. Levels of statistical significance were set at $^*p < 0.05$, $^{**}p < 0.01$, and $^{***}p < 0.001$.

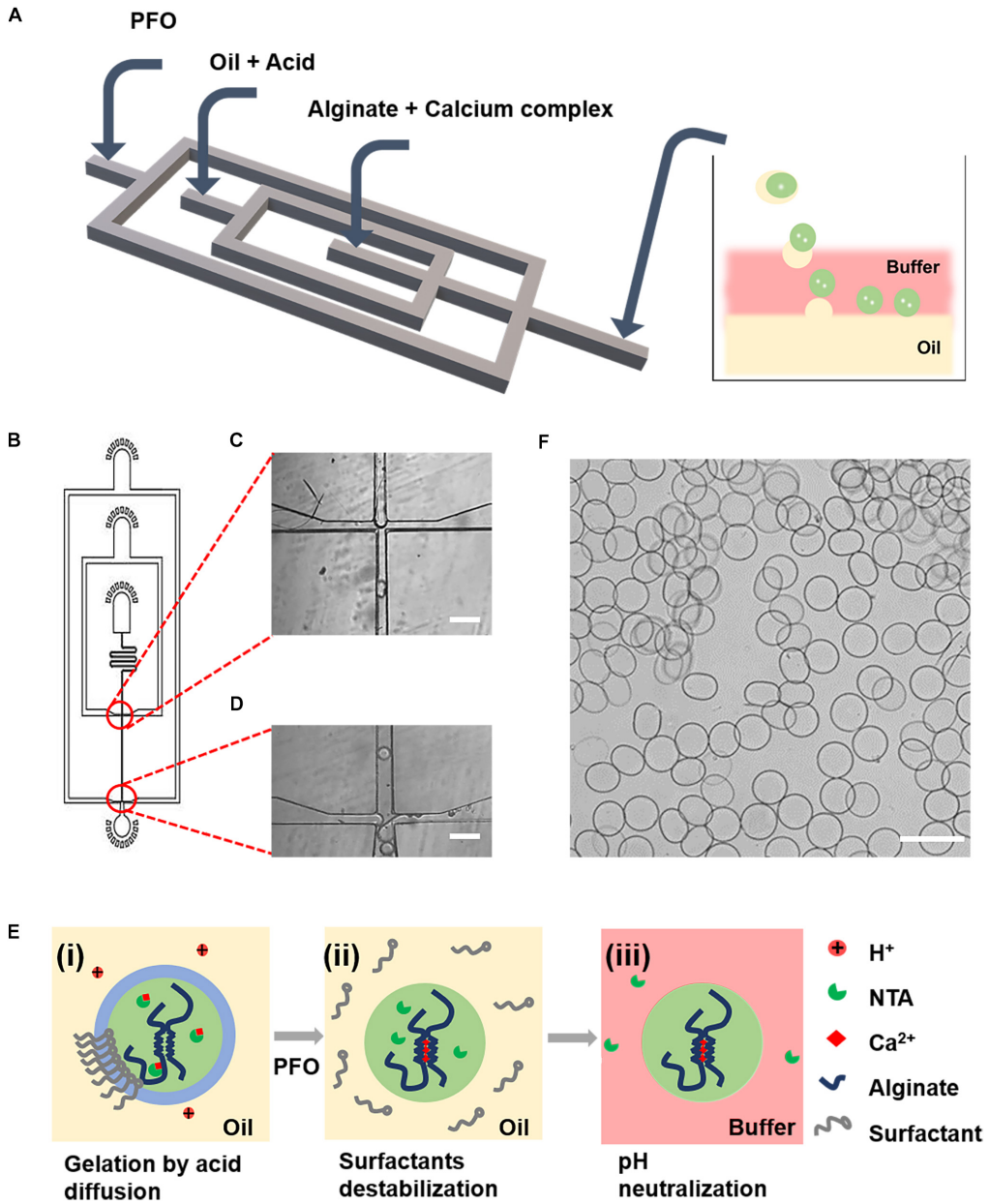

FIGURE 1 | Microfluidic generation of alginate gelation by on-chip release of calcium ions from a water-soluble calcium complex as the crosslinker. **(A)** Schematic illustration of the design of the PDMS device for the generation of cell-laden alginate microgels. **(B)** AutoCAD design of the microfluidic device for continuous generation of cell-laden microgels. **(C,D)** Microscopic images of the microchannels showing the flow-focusing drop-maker **(C)** and the cross-junction for adding of PFO **(D)**. **(E)** Schematics showing the formation mechanism of alginate microgels. (i) Flow-focusing junction breaking up the lamellar flow into droplets. The acetic acid in the oil phase diffused into the aqueous droplet, which triggered the release of Ca^{2+} ions from calcium complex conjugates and induced the gelation of alginate. (ii) The stability of the oil–water interface was broken by PFO. (iii) Microgels were immediately transferred from the oil to an aqueous phase consisting the buffer until the pH of microgels was neutralized. **(F)** Microscopic image showing the resulting alginate microgels. Scale bar is 100 μm.

RESULTS AND DISCUSSION

Formation of On-Chip Gelation in Microfluidic Droplets

To generate alginate microgels, a microfluidic device (**Figures 1A,B**) integrating functions of droplet formation (**Figure 1C**), in-drop gelation, and de-emulsification (**Figure 1D**) was used (Zhang et al., 2018; An et al., 2020). To trigger the gelation of alginate, we used calcium complexes, i.e., Ca-EDTA and Ca-NTA, as the crosslinker, which can chelate with calcium ions and remain soluble in the aqueous phase without reacting with alginate molecules. After the formation of droplets, alginate gelation was induced by the addition

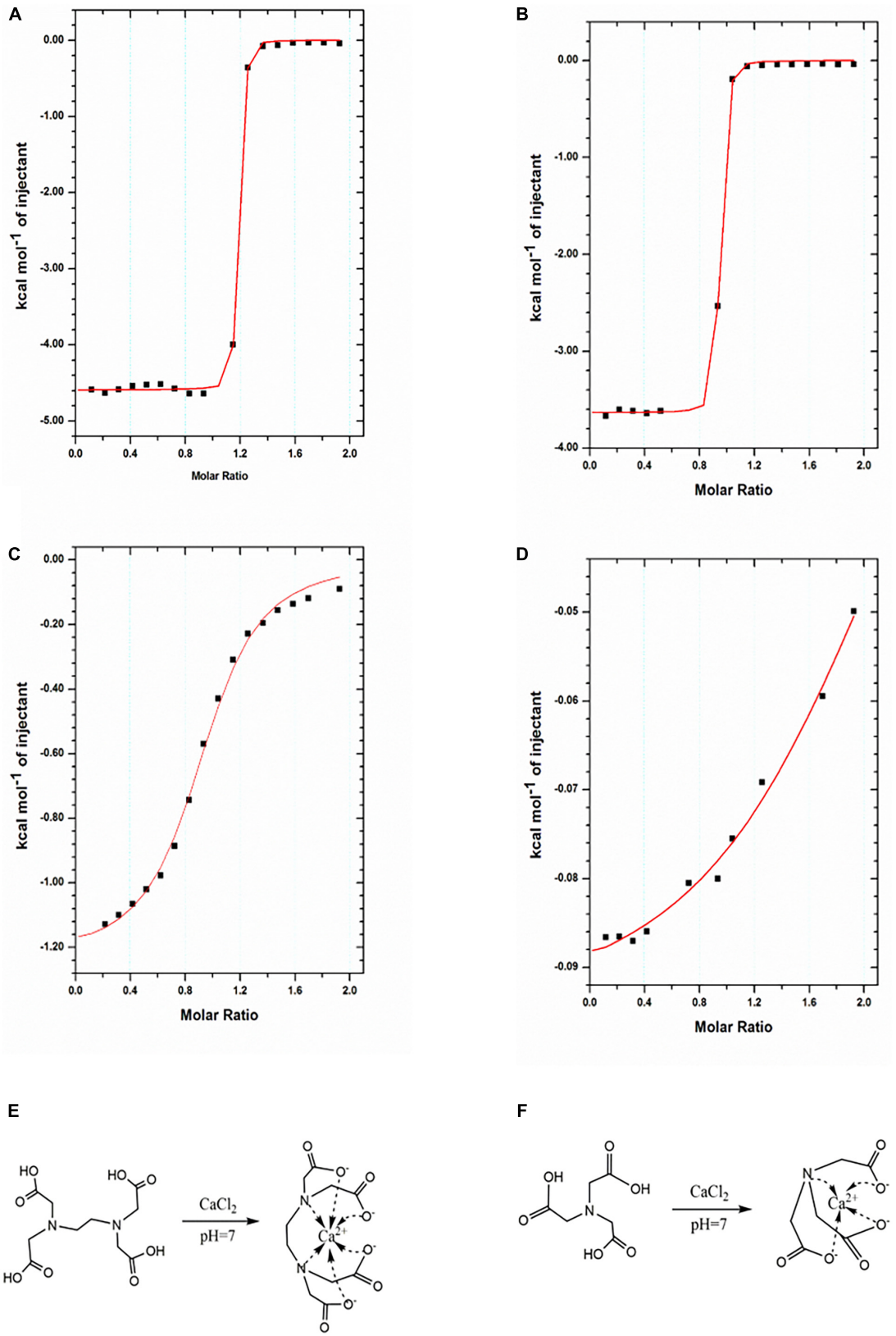

FIGURE 2 | Characterization of binding interactions by ITC. **(A,B)** ITC titration of EDTA (1 mM) with Ca^{2+} ions (10 mM) at 25°C in pH 7 **(A)** and pH 6.5 **(B)**. **(C,D)** NTA (1 mM) with Ca^{2+} ions (10 mM) at 25°C in pH 7 **(C)** and pH 6.5 **(D)**. The reaction schemes for the formation of the Ca-EDTA complex **(E)** and Ca-NTA complex **(F)**.

TABLE 1 | Ca^{2+}-EDTA/NTA binding parameters at 25°C.

	pH	*N*	K_{ITC} (M^{-1})
Ca-EDTA	7	1.14 ± 0.00174	(8.66 ± 1.96) × 10^6
Ca-EDTA	6.5	0.908 ± 0.00153	(3.48 ± 0.646) × 10^6
Ca-NTA	7	0.927 ± 0.00122	(1.95 ± 0.224) × 10^4
Ca-NTA	6.5	2.24 ± 0.0792	(5.49 ± 1.35) × 10^3

of acetic acid in the oil phase (**Figure 1Ei**). The stability of the oil–water interface was broken by the injected PFO through an additional channel (**Figure 1Eii**). Microgels were then immediately transferred from the oil to an aqueous phase consisting of the buffer until the pH of microgels was neutralized (**Figure 1Eiii**). Microgels were finally collected from the water–oil mixture solution by centrifugation (**Figure 1F**). Although a previous study has shown that Ca-EDTA as a calcium source for on-chip gelation can enable continuous production of cell-laden microgels without significantly compromising cell viability (Hati et al., 2016); the detrimental effects on the encapsulated cells of a high concentration of acid to dissociate Ca-EDTA and the long-term cell functionality have not been proved.

Aiming at this, here, we hypothesized that the replacement of Ca-EDTA by Ca-NTA may lead to enhanced biocompatibility of the microfluidic fabrication process since the triggered release of Ca^{2+} ions from NTA can be achieved by less acid due to the lower chelation energy between Ca^{2+} ions and NTA relative to EDTA. To prove this, we compared the equilibrium dissociation constant between Ca^{2+} ions and EDTA vs. NTA molecules using ITC. The ITC measurements monitored the heat change during the titration of EDTA (or NTA) solution with $CaCl_2$ solution at different pH values. Typically, a plot of heat change dependent on the molar ratio of $CaCl_2$ to EDTA (or NTA) can be obtained (**Figure 2**). For compounds with strong reciprocal affinity, the graph typically showed a sharp variation of heat upon the concentration of the titrant until the reaction toward saturation. The molar ratio at the center of the binding isotherm indicated the reaction stoichiometry (N) and the number of binding sites (Rafols et al., 2016). Herein, we observed that the stoichiometry of both Ca-EDTA and Ca-NTA upon the molar ratio of Ca^{2+} ions to EDTA (or NTA) molecules reached 1:1 (**Table 1**). The slope of the linear region of the sharp increase in the calorimetric curve corresponded with K_{ITC} values which represented the dissociation constant. Therefore, a lower K_{ITC} value corresponded with a higher dissociation constant, indicating that the components tend to be dissociated. As shown in **Table 1**, the K_{ITC} value of Ca-NTA (or Ca-EDTA) declined with pH decrease, as evidenced by the K_{ITC} value of 1.95 ± 0.224 × 10^4 M^{-1} at pH 7 decreasing to 8.66 ± 1.96 × 10^6 M^{-1} at pH 6.5. This indicated that lowering the pH can ease the dissociation of the calcium complex and trigger the release of Ca^{2+} ions. Moreover, in the comparison of Ca-NTA and Ca-EDTA, the former combination showed lower K_{ITC} value and thus higher dissociation constant, which suggested that Ca-NTA was more likely to be dissociated at the same pH. These findings confirmed our hypothesis that the release of Ca^{2+} ions can be triggered using less acid from Ca-NTA rather than Ca-EDTA.

On-Chip Formation of Alginate Microgels

We further investigated the influence of two crosslinkers (i.e., Ca-EDTA vs. Ca-NTA) on the fabrication process of alginate microgels, including the concentration of acetic acid to trigger-release Ca^{2+} ions, the on-chip gelation time, and the flow rates of each inputting liquid. We observed that the threshold concentration to trigger the on-chip release of Ca^{2+} ions from Ca-NTA at a fixed aqueous/oil flow rate ratio Q_{aqu}/Q_{oil} = 1/10 (Q_{aqu} = 100 μl/h) was 0.2 v/v‰ (**Figure 3A**), while the threshold concentration of acetic acid for Ca-EDTA was 0.4 v/v‰ (**Figure 3B**). Apparently, the introduction of Ca-NTA as the crosslinker requested less acetic acid for triggering the release of Ca^{2+} ions compared to Ca-EDTA. Moreover, the increase of flow rate ratio Q_{aqu}/Q_{oil} eased the formation of alginate microgels. For instance, alginate microgels can be formed at a considerably low acetic acid concentration of 0.05 v/v‰ by using Ca-NTA as the crosslinker (Q_{aqu}/Q_{oil} = 1:25). This might be attributed to the accumulation of acetic acid dissolved in the oil phase, which enhanced the total amount of acid accessible to the aqueous droplets upon increasing Q_{aqu}/Q_{oil} values. In sum, these results suggested that the use of Ca-NTA instead of Ca-EDTA can ease the preparation of alginate microgels by reducing the desired dose of acetic acid.

The gelation time was important for cell viability (Utech et al., 2015; Hati et al., 2016), fluid stability (Huang et al., 2006), and chip design. We further investigated the time needed to completely gellify alginate droplets. By adjusting the length of the downstream channel after the flow-focusing drop-maker, we can determine the desired minimum gelation time by assessing different morphologies of collected microgels. For chips designed with a rather long downstream channel, alginate microgels with desirable spherical morphology without aggregation can be obtained. By reducing the length of the downstream channel, we can evaluate the morphology of resulting microgels and confirm the threshold gelation time if spherical alginate particles cannot be obtained. We found that Ca-NTA showed a significantly shorter gelation time of 13.67 ± 0.85 ms upon using 1 v/v‰ acetic acid to trigger alginate gelation compared to Ca-EDTA (15.98 ± 0.70 ms) (**Figure 3C**). Upon lowering the acid concentration to 0.4 v/v‰, the gelation time of alginate triggered by Ca-NTA increased to 17.01 ± 1.48 ms compared to that of Ca-EDTA (29.71 ± 1.03 ms) (**Figure 3C**). A previous study by Hati et al. (2016) measured the gelation time of alginate hydrogels using a rheometer; it showed that the gelation time for 3.5 ml of alginate hydrogels was 9.0 ± 3.5 s using Zn^{2+} exchange between EDDA and EDTA to trigger gelation at a relatively mild condition. The gelation time reported here was more than two magnitudes shorter than their microfluidic strategy, which can be attributed to the lower diffusion efficiency measured using a rheometer. Therefore, the present method by using Ca-NTA as a crosslinker considerably reduced the acid concentration needed to trigger Ca^{2+} release but also

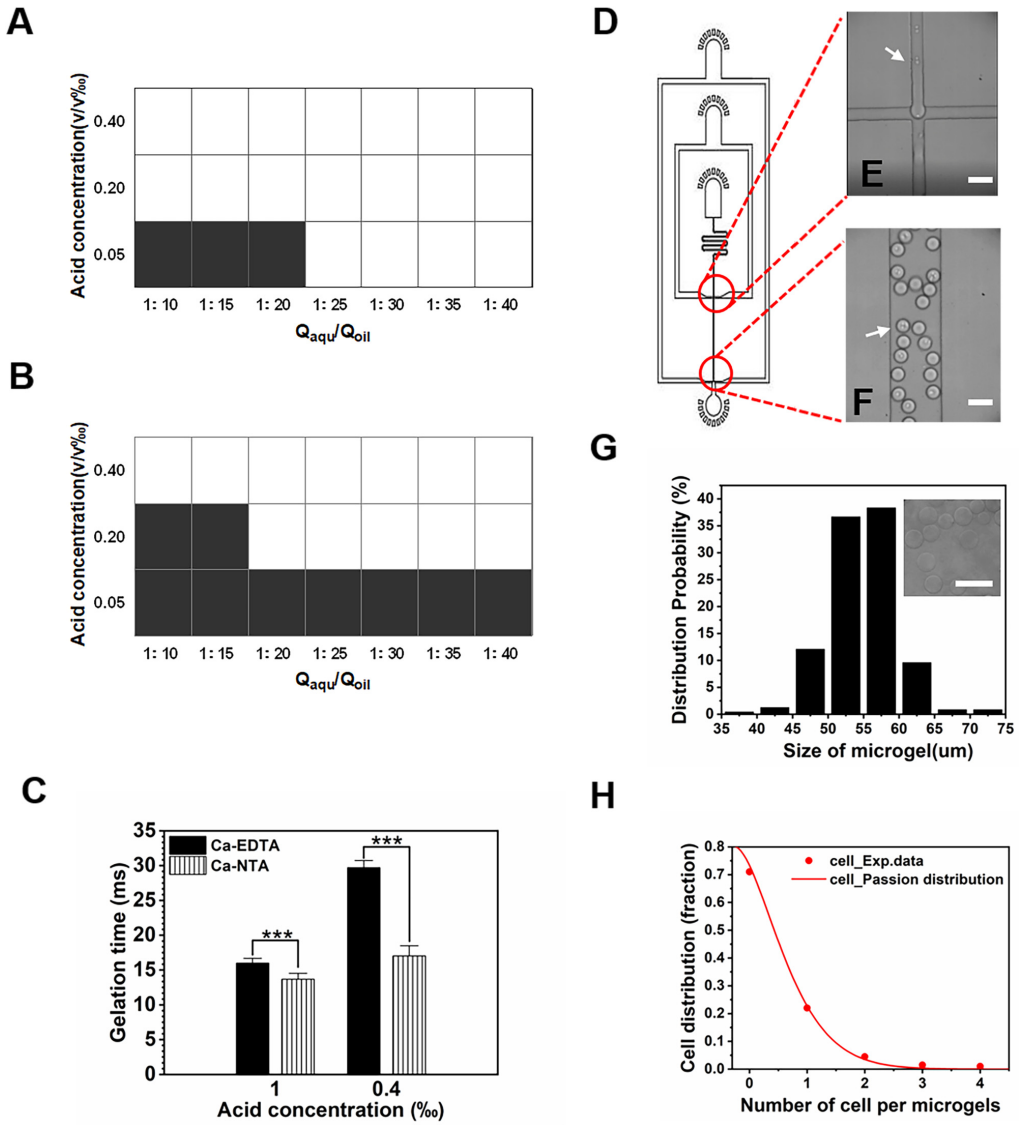

FIGURE 3 | Gelation triggered by different calcium complexes. **(A,B)** Effect of water–oil flow rate ratio (Q_{aqu}/Q_{oil}) and acetic acid concentration on the formation of alginate microgels when **(A)** Ca-NTA and **(B)** Ca-EDTA were used as the crosslinker, respectively. White and black areas indicated complete crosslink and uncrosslink, respectively. If the gelation process can be achieved on-chip, solid-like hydrogel particles can be obtained. Otherwise, only liquid can be collected since the gelation of the droplets cannot be realized within the short time window, for which we considered them as uncrosslinked microgels. **(C)** Gelation time in different acid concentrations where Ca^{2+} ions were chelated in NTA or EDTA. **(D)** AutoCAD design of the microfluidic device for cell encapsulation. **(E,F)** Microscopic images of microchannels **(E)** for formation of alginate cell-laden microgels **(F)**. White arrows indicate cells. **(G,H)** Effect of Ca-NTA on microgel size and cell distribution. **(G)** Size distribution of alginate microgels. **(H)** Cell distribution in the microgels follows the Poisson distribution. Scale bar is 100 μm (***$p < 0.001$).

significantly decreased the gelation time, which can ease the design of microfluidic chip for continuous generation of cell-laden microgels.

We further characterized these cell-laden microgels using the present approach. The cell-laden alginate/Ca-NTA mixture was emulsified into monodisperse droplets (**Figure 3D**). With the use of the chip with a 50-μm channel (**Figure 3E**) and acid concentration of 0.2 v/v‰, cell-laden microgels (**Figure 3F**) ranging in size from 50 to 60 μm were produced (**Figure 3G**). We observed that the distribution of cell numbers in each microgels followed the Poisson distribution (**Figure 3H**) and met with the results from previous studies using microfluidic droplet-based strategies (Koster et al., 2008; An et al., 2020). Of the microgels, 22% contained single cells, while the majority of the microgels (71%) remained empty, and a few droplets contained more than one cell (**Figure 3H**).

Biocompatibility of Microfluidic Fabrication Process

The biocompatibility of the microfluidic fabrication process is the prerequisite for applications of cell-loaded microgels.

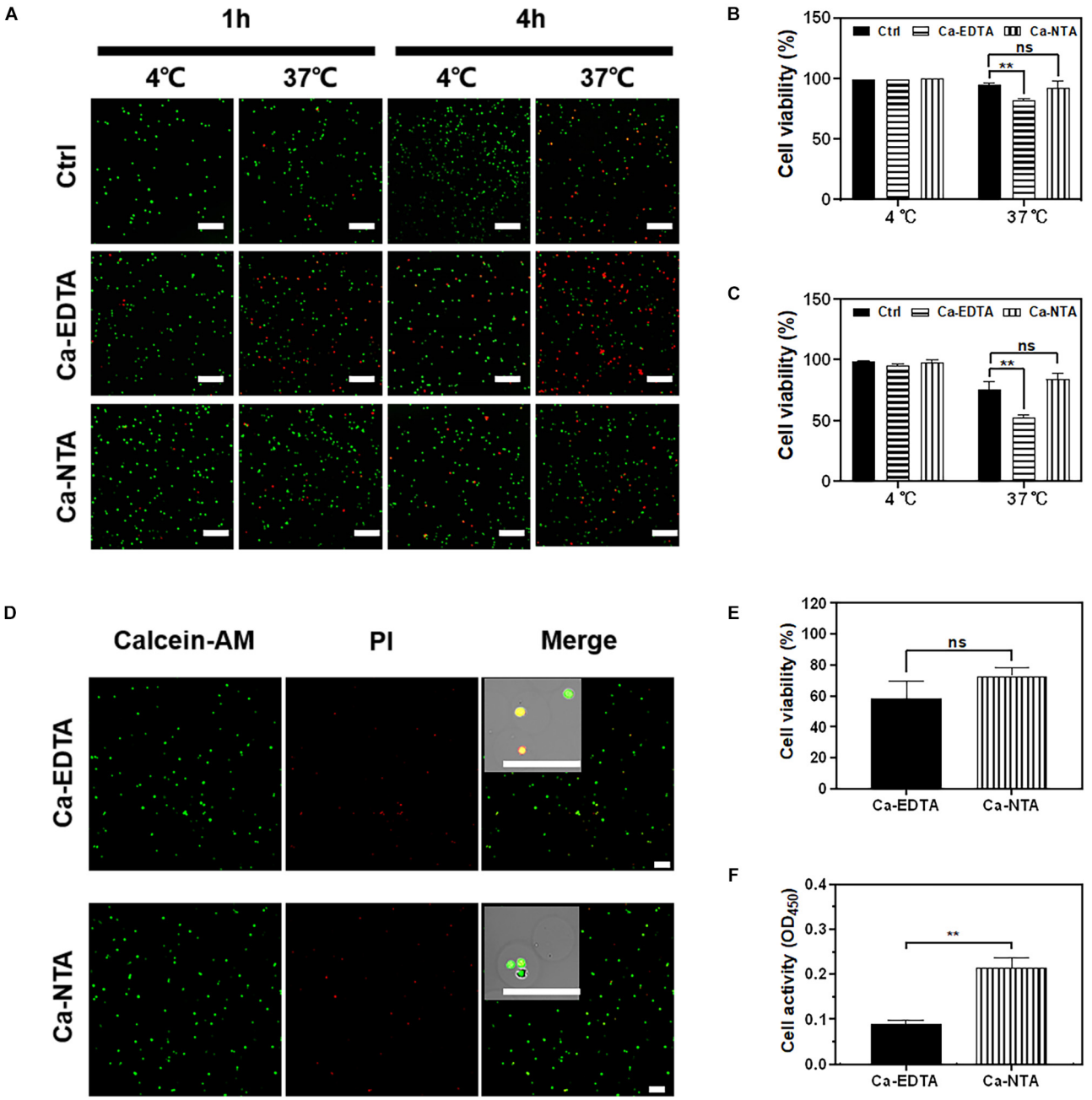

FIGURE 4 | Evaluation of cell viability for microfluidic fabrication process. NIH3T3 fibroblasts were cultured in medium containing 1 wt% Na-alginate and 50 mM Ca-EDTA or Ca-NTA, incubated in a sealed syringe at 4°C and 37°C for 1 and 4 h, respectively. **(A)** The confocal microscopic images of live (green) and dead (red) cells stained by Calcein-AM and ethidium homodimer, respectively. The cells were incubated **(B)** 1 h and **(C)** 4 h. The numbers of live and dead cells were counted with the aid of ImageJ. The viability of NIH3T3 fibroblasts in microgels. To encapsulate cells, Ca-NTA and Ca-EDTA were used as the crosslinker. **(D)** Live (green) and dead (red) cells were stained by calcein-AM and ethidium homodimer, respectively. **(E)** The numbers of live and dead cells from microgels that were triggered by Ca-NTA or Ca-EDTA were counted with the aid of ImageJ. **(F)** Cell activity of encapsulated cells was assessed by CCK-8 assay after 24 h of culture. Scale bar is 200 μm (**$p < 0.01$).

Therefore, the viability and metabolic activity of the cells after the fabrication process were assessed. In typical microfluidic processes for cell encapsulation, cells were mixed with hydrogel precursor solution for hours in a sealed syringe. Therefore, cell viability is frequently compromised due to the lack of nutrients and oxygen. We mimicked this process by mixing cells with alginate precursor and crosslinkers (Ca-EDTA or Ca-NTA) in a sealed syringe and stored at 4 and 37°C,

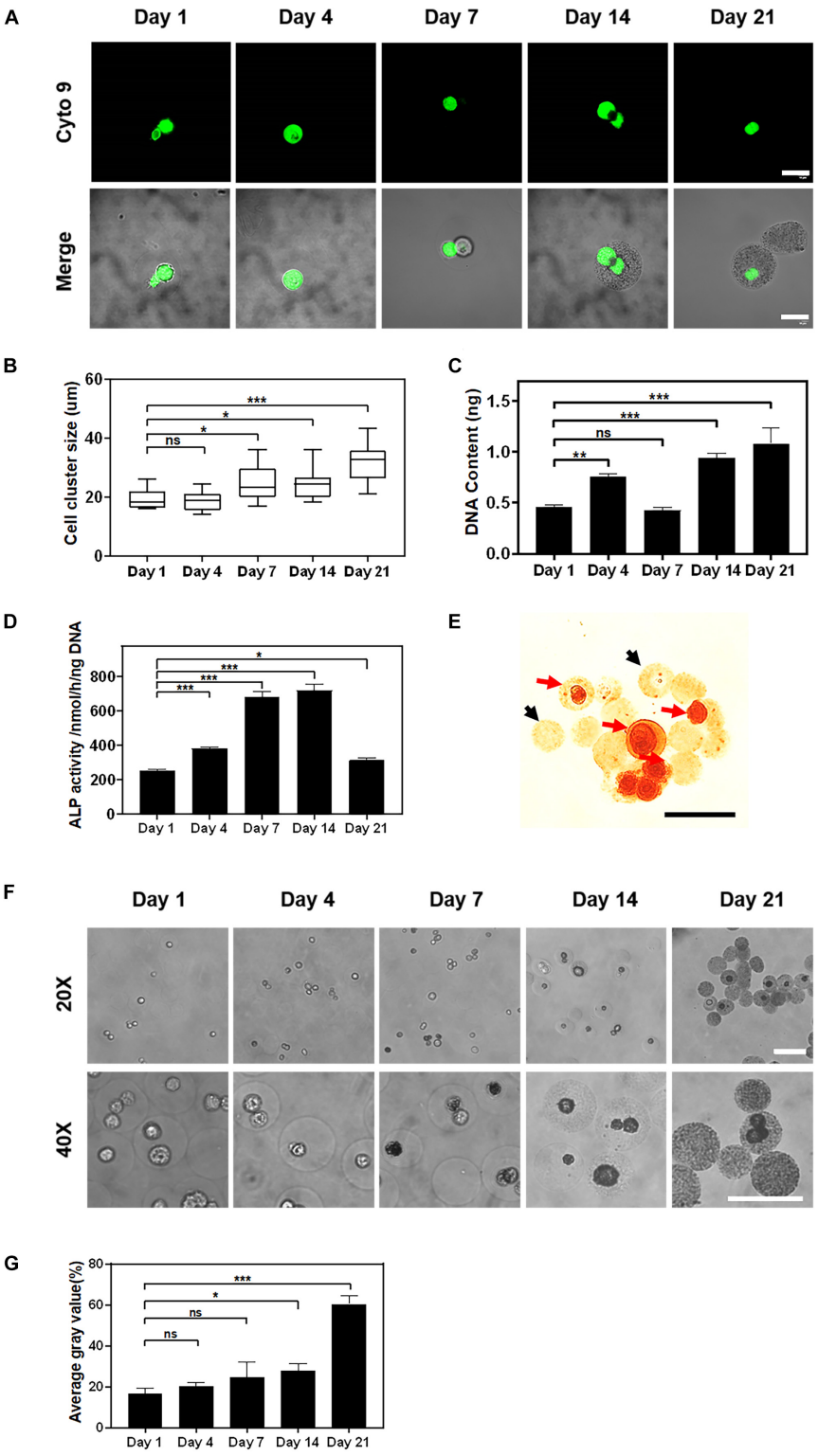

FIGURE 5 | The proliferation and osteogenic differentiation of stem cells encapsulated in alginate using the Ca-NTA complex. **(A)** Confocal microscopic images of MSCs encapsulated in alginate microgel after SYTO 9 nucleus staining (green). Scale bar is 20 μm. **(B)** Quantify the average diameter of cell clusters within the microgels at different time points using ImageJ. **(C)** The cell proliferation was further determined by the DNA content. **(D)** Osteogenic differentiation of MSCs was measured by ALP activity at different time points. **(E)** Cell-laden microgels were stained with 1% Alizarin Red S. The black arrow indicated microgels without cells, and the red arrow indicated cell-laden microgels. **(F)** Light microscopic images of microgels under the phase contrast microscope, and **(G)** the mineralization of the cell-laden microgels was determined based on the average gray value of microgels. Scale bar is 100 μm (ns > 0.05, *p < 0.05, **p < 0.01, ***p < 0.001).

respectively. The NIH3T3 fibroblasts were further observed, and their viability was analyzed after 1 and 4 h of maintenance in the syringe (**Figures 4A–C**). No significant difference in cell viability was observed at a low temperature (4°C) compared to the control group in which cells were suspended and maintained in the medium (**Figures 4B,C**). As a result, cells incubated with alginate precursor and Ca-NTA at 37°C for 1 h (92.33 ± 4.64% vs. 94.33 ± 1.70%) and 4 h (84.00 ± 3.74% vs. 75.67 ± 4.99%) showed no significant difference in cell viability compared to the control group (**Figures 4B,C**). However, cell viability of the Ca-EDTA group (81.67 ± 1.24%) was significantly declined compared to the control (94.33 ± 1.70%) after 1 h and more obviously reduced (52.00 ± 2.16% vs. 75.67 ± 4.99%) after 4 h. These results suggested that cells can be maintained at a low temperature (4°C) for high viability even for several hours. Also, the use of Ca-NTA as the crosslinker had superior biocompatibility than that of Ca-EDTA.

We further evaluated the biocompatibility of microgels produced using Ca-NTA vs. Ca-EDTA as the crosslinker and using different concentrations of the acid (0.2 v/v‰ for Ca-NTA and 0.4 v/v‰ for Ca-EDTA) in the continuous phase (**Figures 4D–F**). We did not observe a significant difference of cell viability prepared using Ca-NTA (72.75 ± 4.60%) and Ca-EDTA (58.25 ± 9.91%) after 1 day of encapsulation (**Figure 4E**). However, the metabolic activity using CCK-8 assay showed that cells prepared using Ca-NTA had twice as high metabolic activity as Ca-EDTA. This indicated that Ca-NTA can provide a more bio-friendly environment for cell encapsulation in alginate microgels.

Viability and Functionality of the Encapsulated Cells

The biological functions of encapsulated cells play a key role in practical applications such as cell therapy and tissue regeneration. Here, we evaluated the biological functions of encapsulated cells by using an osteogenic differentiation model with rat MSCs since it is a typical regeneration model and allogeneic cells are planned to be encapsulated for tissue engineering for further animal study. When MSCs were encapsulated in alginate microgels using Ca-NTA as the crosslinker and cultured in the osteogenic medium (**Figure 5A**), the average diameter of cell clusters within the microgels significantly increased from 19.58 ± 3.50 to 32.20 ± 5.70 μm from 1 to 21 days (**Figure 5B**). These findings indicated a continuous cell division and cell proliferation in microgels. The cell proliferation was further determined by the DNA content. It showed that MSCs proliferated from 1 day (0.46 ± 0.02 ng) to 21 days (1.08 ± 0.12 ng) (**Figure 5C**).

The differentiation of MSCs was further assessed by the ALP activity and the mineralization of encapsulated MSCs. As a potential maker of osteogenic differentiation of MSCs, the ALP activity of encapsulated MSCs increased rapidly after 7 days (684.80 ± 23.40 nmol/h/ng) of *in vitro* culture and peaked by 14 days (721.14 ± 29.54 nmol/h/ng) followed by a sharp decrease afterward (314.07 ± 11.50 nmol/h/ng) (**Figure 5D**). This finding suggested that MSCs encapsulated in alginate microgels underwent the osteogenesis process. The reduction of ALP activity at a later time point was presumed to be due to the mineralization of MSCs as previously reported (Zhang et al., 2019). Further Alizarin Red S staining for calcium deposition in the hydrogel matrix indicated the distribution and formation of calcium-based minerals. To distinguish the mineralization from introduced calcium ions, we used empty microgels as a negative control. The results showed that empty microgels were stained faint yellow while cells in microgels were stained scarlet (**Figure 5E**). This suggested that the mineralization of the microgel matrix was attributed to the osteogenic differentiation of encapsulated MSCs. We further characterized the mineralization process by monitoring the change in opacity of the cell-laden microgels. We observed that cells and microgels transformed from transparent to opaque after 7 days of osteogenic culture (**Figure 5F**). Quantitatively, the degree of opacity did not show a significant difference between 1 day (16.44 ± 2.41%) and 7 days (24.48 ± 6.15%) of culture but exhibited a substantial increase as evidenced by the increase of gray values from 24.48 ± 6.15% at day 7 to 60.40 ± 3.25% at day 21 of culture (**Figure 5G**). To sum up, these findings suggested that MSCs encapsulated in alginate microgels maintained their functionality and committed osteogenic differentiation upon inductive culture. Therefore, the current approach for the preparation of cell-laden alginate microgels by using Ca-NTA as the crosslinker is able to maintain high viability and the long-term functionality of encapsulated cells.

CONCLUSION

We hereby presented an effective and biocompatible method for encapsulating single cells using alginate microgels. The efficiency of triggering the release of calcium ions using Ca-EDTA vs. Ca-NTA was evaluated by characterizing the on-chip gelation time and pH and the equilibrium dissociation constant of both calcium complexes. It demonstrated that Ca-NTA had a higher dissociation constant compared to Ca-EDTA due to the release of calcium ions at a rather neutral pH. Compared to Ca-EDTA, Ca-NTA used as a crosslinker showed significantly higher cell viability and cell metabolic activity for encapsulated cells after the microfluidic process, as well as long-term functionality of encapsulated MSCs evidenced by the osteogenic differentiation model. This biocompatible strategy for cell encapsulation using microfluidic chips offers a powerful tool for future applications of alginate microgels in tissue engineering and cell-based therapies.

DATA AVAILABILITY STATEMENT

All datasets generated for this study are included in the article/supplementary material.

ETHICS STATEMENT

The animal study was reviewed and approved by the Biology and Medical Ethics Committee, Dalian University of Technology.

AUTHOR CONTRIBUTIONS

FS, LY, and HW designed the study. FS and LY performed the experiment and collated the data. CA, HZ, YX, and YuZ helped with the experiments. FS, YaZ, and HW analyzed the data and wrote the manuscript. All authors contributed to the article and approved the submitted version.

FUNDING

This work was granted by the National Key Research and Development Program of China (Nos. 2018YFA0703000 and 2018YFA0703001), the National Natural Science Foundation of China (No. 31870957), the Fundamental Research Funds for the Central Universities of China [No. DUT15RC(3)113] to HW, and the National Natural Science Foundation of China (No. 31900966) to YaZ.

REFERENCES

An, C., Liu, W., Zhang, Y., Pang, B., Liu, H., Zhang, Y., et al. (2020). Continuous microfluidic encapsulation of single mesenchymal stem cells using alginate microgels as injectable fillers for bone regeneration. *Acta Biomater.* 111, 181–196. doi: 10.1016/j.actbio.2020.05.024

Borenstein, J. T., Weinberg, E. J., Orrick, B. K., Sundback, C., Kaazempur-Mofrad, M. R., and Vacanti, J. P. (2007). Microfabrication of three-dimensional engineered scaffolds. *Tissue Eng.* 13, 1837–1844. doi: 10.1089/ten.2006.0156

Burdick, J. A., Mauck, R. L., and Gerecht, S. (2016). To serve and protect: hydrogels to improve stem cell-based therapies. *Cell Stem Cell* 18, 13–15. doi: 10.1016/j.stem.2015.12.004

Caiazzo, M., Okawa, Y., Ranga, A., Piersigilli, A., Tabata, Y., and Lutolf, M. P. (2016). Defined three-dimensional microenvironments boost induction of pluripotency. *Nat. Mater.* 15, 344–352. doi: 10.1038/nmat4536

Campiglio, C. E., Bidarra, S. J., Draghi, L., and Barrias, C. C. (2020). Bottom-up engineering of cell-laden hydrogel microfibrous patch for guided tissue regeneration. *Mater. Sci. Eng. C Mater. Biol. Appl.* 108:110488. doi: 10.1016/j.msec.2019.110488

Choi, C. H., Wang, H., Lee, H., Kim, J. H., Zhang, L., Mao, A., et al. (2016). One-step generation of cell-laden microgels using double emulsion drops with a sacrificial ultra-thin oil shell. *Lab. Chip.* 16, 1549–1555. doi: 10.1039/c6lc00261g

Franco, C. L., Price, J., and West, J. L. (2011). Development and optimization of a dual-photoinitiator, emulsion-based technique for rapid generation of cell-laden hydrogel microspheres. *Acta Biomater.* 7, 3267–3276. doi: 10.1016/j.actbio.2011.06.011

Goh, C. H., Heng, P. W. S., and Chan, L. W. (2012). Alginates as a useful natural polymer for microencapsulation and therapeutic applications. *Carbohyd. Polym.* 88, 1–12. doi: 10.1016/j.carbpol.2011.11.012

Hati, A. G., Bassett, D. C., Ribe, J. M., Sikorski, P., Weitz, D. A., and Stokke, B. T. (2016). Versatile, cell and chip friendly method to gel alginate in microfluidic devices. *Lab. Chip* 16, 3718–3727. doi: 10.1039/c6lc00769d

Holloway, J. L., Ma, H., Rai, R., and Burdick, J. A. (2014). Modulating hydrogel crosslink density and degradation to control bone morphogenetic protein delivery and in vivo bone formation. *J. Control Release* 191, 63–70. doi: 10.1016/j.jconrel.2014.05.053

Hu, Y., Mao, A. S., Desai, R. M., Wang, H., Weitz, D. A., and Mooney, D. J. (2017). Controlled self-assembly of alginate microgels by rapidly binding molecule pairs. *Lab. Chip* 17, 2481–2490. doi: 10.1039/c7lc00500h

Huang, K.-S., Lai, T.-H., and Lin, Y.-C. (2006). Manipulating the generation of Ca-alginate microspheres using microfluidic channels as a carrier of gold nanoparticles. *Lab. Chip* 6, 954–957. doi: 10.1039/b606424h

Kang, A., Park, J., Ju, J., Jeong, G. S., and Lee, S. H. (2014). Cell encapsulation via microtechnologies. *Biomaterials* 35, 2651–2663. doi: 10.1016/j.biomaterials.2013.12.073

Kang, D., Hong, G., An, S., Jang, I., Yun, W. S., Shim, J. H., et al. (2020). Bioprinting of multiscaled hepatic lobules within a highly vascularized construct. *Small* 2020:e1905505. doi: 10.1002/smll.201905505

Kong, H. (2003). Designing alginate hydrogels to maintain viability of immobilized cells. *Biomaterials* 24, 4023–4029. doi: 10.1016/s0142-9612(03)00295-3

Koster, S., Angile, F. E., Duan, H., Agresti, J. J., Wintner, A., Schmitz, C., et al. (2008). Drop-based microfluidic devices for encapsulation of single cells. *Lab. Chip* 8, 1110–1115. doi: 10.1039/b802941e

Kumar Meena, L., Rather, H., Kedaria, D., and Vasita, R. (2019). Polymeric microgels for bone tissue engineering applications – a review. *Intern. J. Polym. Mater. Polym. Biomater.* 69, 381–397. doi: 10.1080/00914037.2019.1570512

Lim, F., and Sun, A. M. (1980). Microencapsulation islets as bioartificial endocrine pancreas. *Science* 210, 908–910. doi: 10.1126/science.6776628

Mao, A. S., Shin, J. W., Utech, S., Wang, H., Uzun, O., Li, W., et al. (2017). Deterministic encapsulation of single cells in thin tunable microgels for niche modelling and therapeutic delivery. *Nat. Mater.* 16, 236–243. doi: 10.1038/nmat4781

Markstedt, K., Mantas, A., Tournier, I., Martinez Avila, H., Hagg, D., and Gatenholm, P. (2015). 3D bioprinting human chondrocytes with nanocellulose-alginate bioink for cartilage tissue engineering applications. *Biomacromolecules* 16, 1489–1496. doi: 10.1021/acs.biomac.5b00188

Moyer, H. R., Kinney, R. C., Singh, K. A., Williams, J. K., Schwartz, Z., and Boyan, B. D. (2010). Alginate microencapsulation technology for the percutaneous delivery of adipose-derived stem cells. *Ann. Plast. Surg.* 65, 497–503. doi: 10.1097/SAP.0b013e3181d37713

Pereira, R., Carvalho, A., Vaz, D. C., Gil, M. H., Mendes, A., and Bartolo, P. (2013). Development of novel alginate based hydrogel films for wound healing applications. *Int. J. Biol. Macromol.* 52, 221–230. doi: 10.1016/j.ijbiomac.2012.09.031

Qin, D., Xia, Y., and Whitesides, G. M. (2010). Soft lithography for micro- and nanoscale patterning. *Nat. Protoc.* 5, 491–502. doi: 10.1038/nprot.2009.234

Rafols, C., Bosch, E., Barbas, R., and Prohens, R. (2016). The Ca(2+)-EDTA chelation as standard reaction to validate isothermal titration calorimeter measurements (ITC). *Talanta* 154, 354–359. doi: 10.1016/j.talanta.2016.03.075

Selimovic, S., Oh, J., Bae, H., Dokmeci, M., and Khademhosseini, A. (2012). Microscale strategies for generating cell-encapsulating hydrogels. *Polymers* 4:1554. doi: 10.3390/polym4031554

Somo, S. I., Khanna, O., and Brey, E. M. (2017). Alginate microbeads for cell and protein delivery. *Methods Mol. Biol.* 1479, 217–224. doi: 10.1007/978-1-4939-6364-5_17

Tan, W. H., and Takeuchi, S. (2007). Monodisperse alginate hydrogel microbeads for cell encapsulation. *Adv. Mater.* 19, 2696–2701. doi: 10.1002/adma.200700433

Utech, S., Prodanovic, R., Mao, A. S., Ostafe, R., Mooney, D. J., and Weitz, D. A. (2015). Microfluidic generation of monodisperse, structurally homogeneous alginate microgels for cell encapsulation and 3D cell culture. *Adv. Healthc. Mater.* 4, 1628–1633. doi: 10.1002/adhm.201500021

Uyen, N. T. T., Hamid, Z. A. A., Tram, N. X. T., and Ahmad, N. (2019). Fabrication of alginate microspheres for drug delivery: a review. *Int. J. Biol. Macromol.* 153, 1035–1046. doi: 10.1016/j.ijbiomac.2019.10.233

Velasco, D., Tumarkin, E., and Kumacheva, E. (2012). Microfluidic encapsulation of cells in polymer microgels. *Small* 8, 1633–1642. doi: 10.1002/smll.201102464

Wan, J. (2012). Microfluidic-based synthesis of hydrogel particles for cell microencapsulation and cell-based drug delivery. *Polymers* 4, 1084–1108. doi: 10.3390/polym4021084

Yao, R., Zhang, R., Luan, J., and Lin, F. (2012). Alginate and alginate/gelatin microspheres for human adipose-derived stem cell encapsulation and differentiation. *Biofabrication* 4:025007. doi: 10.1088/1758-5082/4/2/025007

Yeung, T. W., Ucok, E. F., Tiani, K. A., McClements, D. J., and Sela, D. A. (2016). Microencapsulation in alginate and chitosan microgels to enhance viability of bifidobacterium longum for oral delivery. *Front. Microbiol.* 7:494. doi: 10.3389/fmicb.2016.00494

Yun, H., Kim, K., and Lee, W. G. (2013). Cell manipulation in microfluidics. *Biofabrication* 5:022001. doi: 10.1088/1758-5082/5/2/022001

Zhang, H., Tumarkin, E., Sullan, R. M. A., Walker, G. C., and Kumacheva, E. (2007). Exploring microfluidic routes to microgels of biological polymers. *Macromol. Rapid Commun.* 28, 527–538. doi: 10.1002/marc.200600776

Zhang, L., Chen, K., Zhang, H., Pang, B., Choi, C. H., Mao, A. S., et al. (2018). Microfluidic templated multicompartment microgels for 3D encapsulation and pairing of single cells. *Small* 14:1702955. doi: 10.1002/smll.201702955

Zhang, Y., Yang, W., Devit, A., and van den Beucken, J. (2019). Efficiency of coculture with angiogenic cells or physiological BMP-2 administration on improving osteogenic differentiation and bone formation of MSCs. *J. Biomed. Mater. Res. A* 107, 643–653. doi: 10.1002/jbm.a.36581

Conflict of Interest: The authors declare that the research was conducted in the absence of any commercial or financial relationships that could be construed as a potential conflict of interest.

frontiers in Bioengineering and Biotechnology

REVIEW
published: 29 October 2020
doi: 10.3389/fbioe.2020.575057

Immunomodulation of MSCs and MSC-Derived Extracellular Vesicles in Osteoarthritis

Xige Zhao[1†], Yanhong Zhao[1†], Xun Sun[2], Yi Xing[1], Xing Wang[3,4] and Qiang Yang[2*]*

[1] Stomatological Hospital of Tianjin Medical University, Tianjin, China, [2] Department of Spine Surgery, Tianjin Hospital, Tianjin University, Tianjin, China, [3] Beijing National Laboratory for Molecular Sciences, Institute of Chemistry, Chinese Academy of Sciences, Beijing, China, [4] University of Chinese Academy of Sciences, Beijing, China

Osteoarthritis (OA) has become recognized as a low-grade inflammatory state. Inflammatory infiltration of the synovium by macrophages, T cells, B cells, and other immune cells is often observed in OA patients and plays a key role in the pathogenesis of OA. Hence, orchestrating the local inflammatory microenvironment and tissue regeneration microenvironment is important for the treatment of OA. Mesenchymal stem cells (MSCs) offer the potential for cartilage regeneration owing to their effective immunomodulatory properties and anti-inflammatory abilities. The paracrine effect, mediated by MSC-derived extracellular vehicles (EVs), has recently been suggested as a mechanism for their therapeutic properties. In this review, we summarize the interactions between MSCs or MSC-derived EVs and OA-related immune cells and discuss their therapeutic effects in OA. Additionally, we discuss the potential of MSC-derived EVs as a novel cell-free therapy approach for the clinical treatment of OA.

Keywords: osteoarthritis, MSCs, exosomes, immunomodulatory, macrophage

OPEN ACCESS

Edited by:
Liyuan Zhang,
Harvard University, United States

Reviewed by:
Emilie Velot,
Université de Lorraine, France
Jae-Won Shin,
University of Illinois at Chicago, United States

***Correspondence:**
Xing Wang
wangxing@iccas.ac.cn
Qiang Yang
yangqiang1980@126.com

†These authors have contributed equally to this work

Specialty section:
This article was submitted to Biomaterials, a section of the journal Frontiers in Bioengineering and Biotechnology

Received: *22 June 2020*
Accepted: *21 September 2020*
Published: *29 October 2020*

Citation:
Zhao X, Zhao Y, Sun X, Xing Y, Wang X and Yang Q (2020) Immunomodulation of MSCs and MSC-Derived Extracellular Vesicles in Osteoarthritis. Front. Bioeng. Biotechnol. 8:575057. doi: 10.3389/fbioe.2020.575057

INTRODUCTION

Osteoarthritis (OA) is a chronic degenerative joint disease that affects about 15% of the global population (Loeser, 2013; Hunter and Bierma-Zeinstra, 2019). OA involves not only the knees but also the spine, hands, and temporal–mandibular joints and is characterized by the articular cartilage degradation, synovitis, subchondral bone remodeling, and osteophyte formation. Patients experience aggravating pain and disability, resulting in decreased life quality and a high economic burden. The traditional viewpoint is that OA is a non-inflammatory disease. However, studies have shown that there is a type of chronic, low-grade inflammation in the pathogenesis of OA, which seriously hinders the proliferation of chondrocytes and the deposition of cartilage matrix, resulting in low efficiency of repair (Aspden and Saunders, 2019; Chow and Chin, 2020; Woodell-May and Sommerfeld, 2020). Various immune cells have been identified in the synovium of OA patients. Among them, macrophages, T cells, and B cells are the most abundant (de Lange-Brokaar et al., 2012).

Synovial macrophages (Mφ) are the main immune cells in joints (Fernandes et al., 2020; Wu C. L. et al., 2020). Historically, macrophages have been characterized as classically activated macrophages, or proinflammatory macrophages (M1Mφ), and are activated by interferon-γ (IFN-γ), tissue necrosis factor-α (TNF-α), or pathogen-associated molecular patterns. Once activated, these macrophages secrete proinflammatory cytokines such as interleukin-1 (IL-1), IL-6, IL-12, and inducible nitric oxide synthase. Conversely, anti-inflammatory macrophages

(M2Mφ) are activated by an alternative activation pathway. These macrophages release growth and angiogenic factors such as transforming growth factor-β (TGF-β) and arginase-1 (Arg-1), which down-regulate inflammation and promote remodeling of damaged tissue (Wynn and Vannella, 2016; Oishi and Manabe, 2018). The spatiotemporal distribution of M1 and M2Mφ plays a key role in the orchestration of inflammation and tissue regeneration (Zhang H. Y. et al., 2018; Fernandes et al., 2020). It has been thought that depletion of Mφ can eliminate inflammation and further alleviate the progression of OA. For this reason, Wu et al. used the macrophage Fas-induced apoptosis (MaFIA) transgenic mice. They placed the MaFIA mice on a high-fat diet and induced knee OA and then conditional macrophage exhaustion in synovium tissue. The results showed that OA with obesity was not attenuated by macrophage depletion of both M1 and M2 types. On the contrary, inflammatory cytokine production was intensified, which induced an increase of joint synovitis and cartilage damage (Wu et al., 2017). Given that M1Mφ is involved mainly in the initiation of inflammation, yet M2Mφ is involved mainly in the regression of inflammation, this phenomenon indicated that the failure of transformation from M1Mφ to M2Mφ may result in persistent chronic inflammation. At present, the implications of the alteration of the Mφ polarization state for OA treatment are not clear, but several relevant studies have shown that infiltrative M1Mφ and M2Mφ exert different effects on cells within the joint, thus playing a key role in the orchestration of inflammation and regeneration (Blom et al., 2007; Fahy et al., 2014; Fichadiya et al., 2016; Utomo et al., 2016; Samavedi et al., 2017; Hu et al., 2018; Chen et al., 2020).

T cells are lymphocytes that represent the second main constituents of synovial infiltrates in OA patients. T cells can be broadly divided into helper T cells (T_H cells), cytotoxic T cells (Tc cells), and regulatory T cells (Tregs) according to their different functions, and the first two are collectively known as effector T cells. Previous studies have shown that both $CD4^+$ (mainly differentiated into T_H cells after activation) and $CD8^+$ T-cell subsets (mainly differentiated into Tc cells after activation) have been found at higher levels not only in synovial fluid and membranes but also in peripheral blood (Haynes et al., 2002; Hussein et al., 2008; Labinsky et al., 2020), which suggests that T_H cells and Tc cells are involved in the pathogenesis of OA (Raphael et al., 2015). Specifically, OA synovial tissue exhibits increased levels of T_H1 ($CD4^+IFN\text{-}\gamma^+$ T cells), T_H17 ($CD4^+IL\text{-}17^+$ T cells), and Tc ($CD8^+$ T cells), whereas the synovial fluid has increased levels of T_H1, T_H9 ($CD4^+IL9^+$ T cells) and T_H17 cells. T_H1 produce IL-2, IFN-γ, TNF-α, lymphotoxins, and granulocyte–macrophage colony-stimulating factor Inflammatory cytokines, which exacerbate joint inflammation and recruit more effector T cells to inflammatory tissues, thus causing tissue damage (Li et al., 2017). T_H9 cells preferentially produce IL-9, which is positively correlated with OA index (Qi et al., 2016). T_H17 cells mainly produce IL-17 and IL-23, and the overexpression of the two cytokines promotes the infiltration of the immune cells, secretion of vascular endothelial growth factor, and growth of the blood vessel, thus aggravating cartilage degeneration (Bommireddy and Doetschman, 2007). Tc cells also have been found to significantly shape the pathogenesis of OA; however, the exact role of them response in the biology of OA is still unclear (Hsieh et al., 2013). Under the induction of TGF-β, naive T cells differentiate into Tregs. Tregs are important immunomodulators in many inflammatory and autoimmune diseases, as they inhibit the immune response and maintain immune tolerance by secreting cytokines such as TGF-β, IL-10, and IL-35. Tregs exhibit a decreased response in the pathogenesis of OA (Hori et al., 2003; Bommireddy and Doetschman, 2007). Besides, the role of T_H17/Treg ratio in the immunoregulation of OA has also attracted increasing attention. It was found that if T_H17/Treg ratio is deviated in favor of proinflammatory T_H17 cells, arthritis was exacerbated (Noack and Miossec, 2014; Yang et al., 2018; Min et al., 2019; Peter et al., 2020) (**Figure 1**).

In the case of OA, if the decomposition products of the cartilage matrix are exposed, B cells can be stimulated to produce autoantibodies and activate humoral immunity (Zhu et al., 2020), leading to disturbance of the entire articular environment. In such cases, autoantibodies against cartilage mesothelin, osteopontin, ykl-39, collagen, and proteoglycan have been detected (Ozeki et al., 2016). The harmful effects of autoantibody formation may lie in its diffusion and deposition in articular cartilage as an immune complex, which makes it easy to degrade and destroy. This may stimulate the complement system to clear the complex and become part of the complex pathogenic circuit that causes tissue damage (Modinger et al., 2019) (**Figure 1**).

Therefore, the treatment of OA should focus not only on "cartilage wear" but also on the immune cells that have a major impact on the occurrence and development of OA. Regulating the local inflammatory microenvironment and tissue regeneration microenvironment is important in the treatment of OA. Mesenchymal stem cells (MSCs) with self-renewal capacity and multidifferentiation potential have received much attention as an alternative approach in the management of cartilage degradation (Barry and Murphy, 2013; Fernandez-Pernas et al., 2020). Moreover, MSCs have been shown to possess effective immunomodulatory properties in the treatment of inflammatory diseases (Guillamat-Prats et al., 2017; de Castro et al., 2019; Zhao L. et al., 2019) and are capable of regulating the immune cells that play a pathogenic role in the progression of OA. In recent years, the paracrine effect of MSCs mediated by extracellular vehicles (EVs) has been suggested to explain their curative effect (Kalluri and LeBleu, 2020). Three main types of EVs have been described based on their biogenesis and size: exosomes (30–150 nm in diameter), microvesicles/microparticles, and apoptotic bodies (both considered to be >100 nm). Exosomes are secreted to the extracellular environment through the fusion of multivesicular bodies with the plasma membrane. The last two types of vesicles are released through forward budding of the plasma membrane in living and dying cells, respectively (Bui et al., 2018; Kalluri and LeBleu, 2020). EVs, as a natural and efficient transport carrier, can maintain functional characteristics similar to their parent cells (Bui et al., 2018; Wu X. et al., 2020). This insight has given rise to a new paradigm wherein EVs are collected from MSCs and used to actively regulate complicated communication among

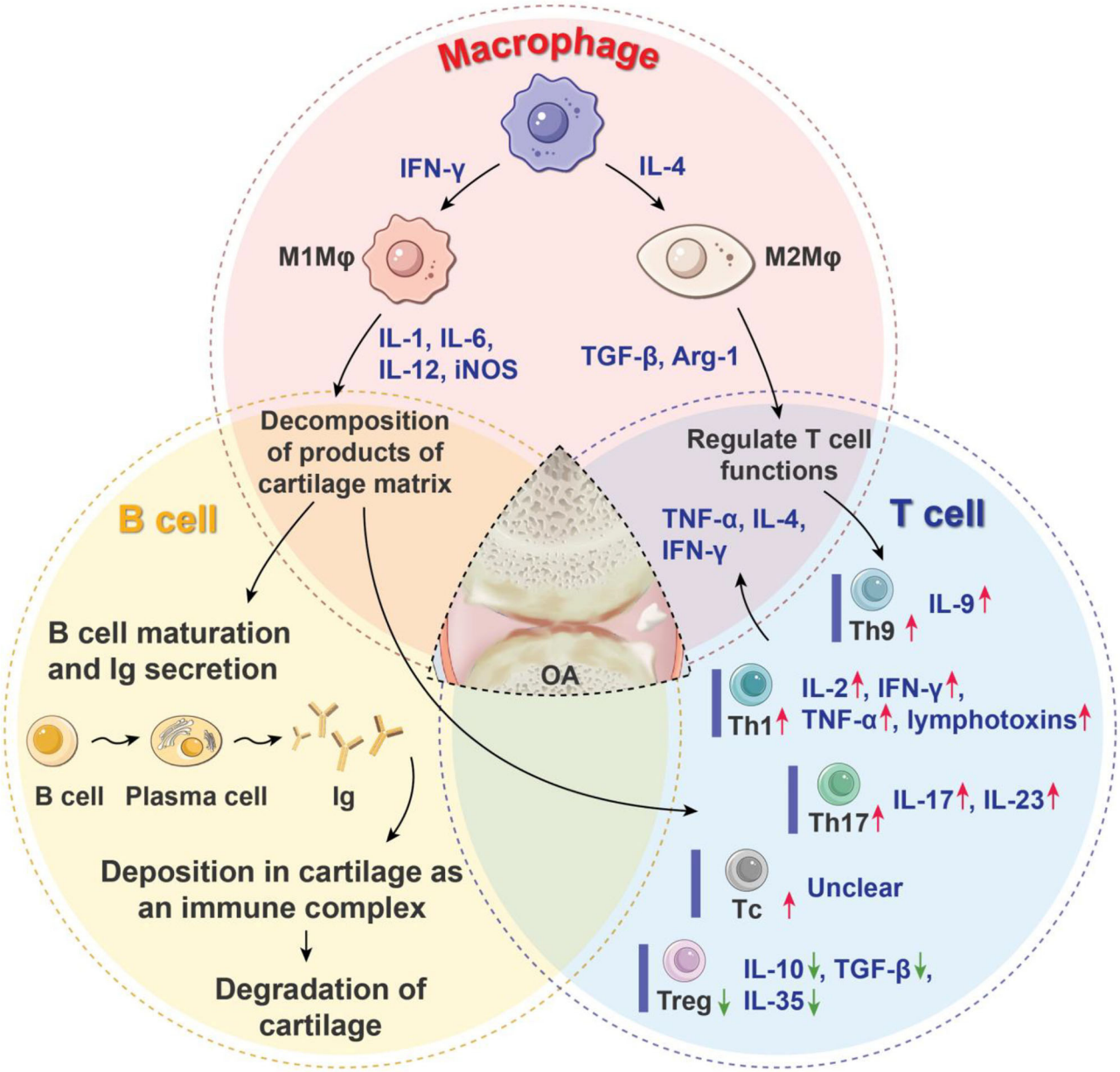

FIGURE 1 | Roles of immune cells in the progression of OA. OA is characterized by the articular cartilage degeneration, synovitis, subchondral bone sclerosis, and osteophyte formation. Macrophages, T cells, and B cells are the three main immune cells that regulate inflammatory processes and the immune response of OA. They form a complex network through coordination or antagonism. Arg-1, arginase-1; IL, interleukin; Ig, immune globulin; IFN-γ, interferon-γ; iNOS, inducible nitric oxide synthase; Mφ, macrophages; OA, osteoarthritis; Tc, cytotoxic T cell; T_H, helper T cell; Treg, regulatory T cell; TGF-β, transforming growth factor-β; TNF-α, tissue necrosis factor-α; red arrow means increased production of proinflammatory cells or mediators; green arrow means decreased production of anti-inflammatory cells or mediators.

components of the immune system (Wang et al., 2018). The cell-free nature of EVs suggests that they may have a more favorable safety profile than cell-based therapies.

Within this review, we summarize and discuss what is known about the interactions of MSCs or MSC-derived EVs with OA-related immune cells and the importance of these interactions in therapeutic strategies for OA.

ROLES OF MSCS IN IMMUNOMODULATION

MSCs have immunomodulatory properties relying on both cell-to-cell contact and paracrine signaling. Furthermore, under the local inflammatory microenvironment, low or high levels of specific toll-like receptor (TLR) ligands may greatly influence the

immunoregulatory characteristics of MSCs and thereby impact the effect of MSC-based therapies (Lei et al., 2011). In the early stage of OA, the molecules produced by damaged tissue or pathogens will be recognized by TLR2/4 (differences by species may exist) on the surface of MSCs, lead to MSCs polarization into MSC1 (Tomchuck et al., 2008). This phenotype can promote the immune response in the early stage of inflammation. This kind of acute inflammatory response after injury can induce the accumulation of inflammatory cells in the damaged area and play a role of automatic debridement, which has characteristics of protecting the joint tissue. However, persistent chronic inflammation is harmful to joints (Huang and Kraus, 2016). Accordingly, in the late stage of inflammation, the high levels of TLR3 ligand lead to MSCs transform to the inflammation-dampening MSC2 phenotype to prevent prolonged damage to joints (Ayala-Cuellar et al., 2019). Failure of transformation in the stage of inflammation abatement during OA is the key to the continuation of the pathological vicious circle. In this case, joint resident MSCs may not be as effective as infused MSCs in restoring immunological and regenerative homeostasis in the degenerative joint. Therefore, in this section, we summarize the major studies investigating the effects of adoptive transferred MSCs during OA or other chronic degenerative diseases with chronic inflammation, focusing mainly on their immunosuppressive properties.

Immunomodulatory Effect of MSCs on Macrophages

MSCs can produce various growth factors, chemokines, and other signaling molecules affecting macrophage polarization, maturation, proliferation, and migration, which have been verified by MSC secretome analyses (Vizoso et al., 2017; Lin and Du, 2018).

Recent studies have revealed the ability of MSCs to regulate macrophage polarization by inducing a transformation from the M1 to the M2 phenotype, thus promoting the healing process (Cho et al., 2014). Abumaree et al. co-cultured "fried egg–like" M1 macrophages with MSCs for 3 days, and the cells gradually turned into "spindle-like" M2 macrophages (Abumaree et al., 2013). This process is accompanied by high-level secretion of IL-10, low levels of IL-12 and IL-1β, and increased phagocytic activity. MSCs can also regulate the immune phenotype of macrophages *in vivo*, which has been demonstrated in a variety of disease models. For example, MSCs can prolong corneal allograft survival by altering M1/M2 polarization and inhibiting the infiltration of antigen-presenting cells (APCs) (Murphy et al., 2016).

At present, the mechanism by which MSCs regulate the phenotypic transformation of macrophages is not fully understood. Several studies have confirmed that MSCs affect macrophage polarization via direct cell contact and cytokines such as IL-10, prostaglandin E2 (PGE2), indoleamine 2,3-dioxygenase (IDO), and TGF-β secreted by MSCs (Park et al., 2018; Shi et al., 2019). IL-10 can promote the inflammatory repair of tissues, reduce inflammatory damage, and promote the transformation of macrophages to M2, which may be one of the main mechanisms of MSC-mediated macrophage transformation (Faulknor et al., 2017). PGE2 is another important anti-inflammatory factor; it can combine with EP2 and EP4 receptors on the surface of macrophages, change the expression of downstream genes, and cause macrophages to transform into the M2 phenotype (Kawahara et al., 2015). The anti-inflammatory effect of macrophages is weakened by using specific PGE2 inhibitors, and the expression of IL-10 and IL-1α in anti-inflammatory cells also significantly decreases (Ylostalo et al., 2012). MSCs can also release IDO, which induces macrophages to transform into the M2 phenotype and release more IL-10. Lee et al. found that after treatment with the IDO-specific inhibitor 1-L-methyl-tryptophan (1-L-MT), the expression of IFN-α increased, and anti-inflammatory effects were significantly inhibited (Lee et al., 2016). TGF-β1 is an important marker for M2 monocytes/macrophages. Liu et al. found that the inflammation was significantly attenuated after TGF-β1 injection in colitis model mice (Jiang and Xu, 2020). Moreover, MSCs have also been reported to induce monocyte maturation directly to M2 macrophages by MSC secretion of IDO, IL-6, and PGE2 (**Figure 2**).

Collectively, these studies show that MSCs can induce macrophages to transform from the M1 to the M2 phenotype, inhibit proinflammatory cytokines, release anti-inflammatory cytokines, reduce joint tissue damage, suppress the progress of inflammation, and promote the repair of inflammatory tissue.

Immunomodulatory Effects of MSCs on T Cells

MSCs Inhibit T-Cell Proliferation

Nitric oxide (NO) secretion by mouse MSCs has been shown to regulate immunosuppression of T-cell responses directly by cell cycle arrest or apoptosis (Sato et al., 2007). Cytokines such as TGF-β and hepatocyte growth factor secreted by MSCs can down-regulate the expression of cyclin D2 and up-regulate the expression of p27kip1 in T cells, resulting in cell cycle arrest in the G1 phase, thus inhibiting T-cell proliferation (Glennie et al., 2005; Kyurkchiev et al., 2014). PGE2 secreted by MSCs can also inhibit T-cell proliferation by decreasing IL-2 and down-regulating IL-2 receptor, leading to impaired DNA binding activity of transcription factors through inhibition of Janus kinase 3 signaling (Burr et al., 2013). Under stimulation by proinflammatory factors such as TNF-α and IFN-γ, MSCs can inhibit the proliferation of T cells and induce the apoptosis of activated T cells by producing IDO (Behm et al., 2020), an iron-containing heme monomer membrane-binding protein that can catalyze the transformation of tryptophan into L-canine uric acid and picolinic acid. Tryptophan is an essential amino acid for the maintenance of T-cell activation and proliferation (Liu et al., 2016). The proliferation of T cells is blocked in the G1 phase if tryptophan concentration is low, resulting in the decrease of T cells. The tryptophan depletion mediated by IDO inhibits only activated T cells, not resting T cells (**Figure 2**).

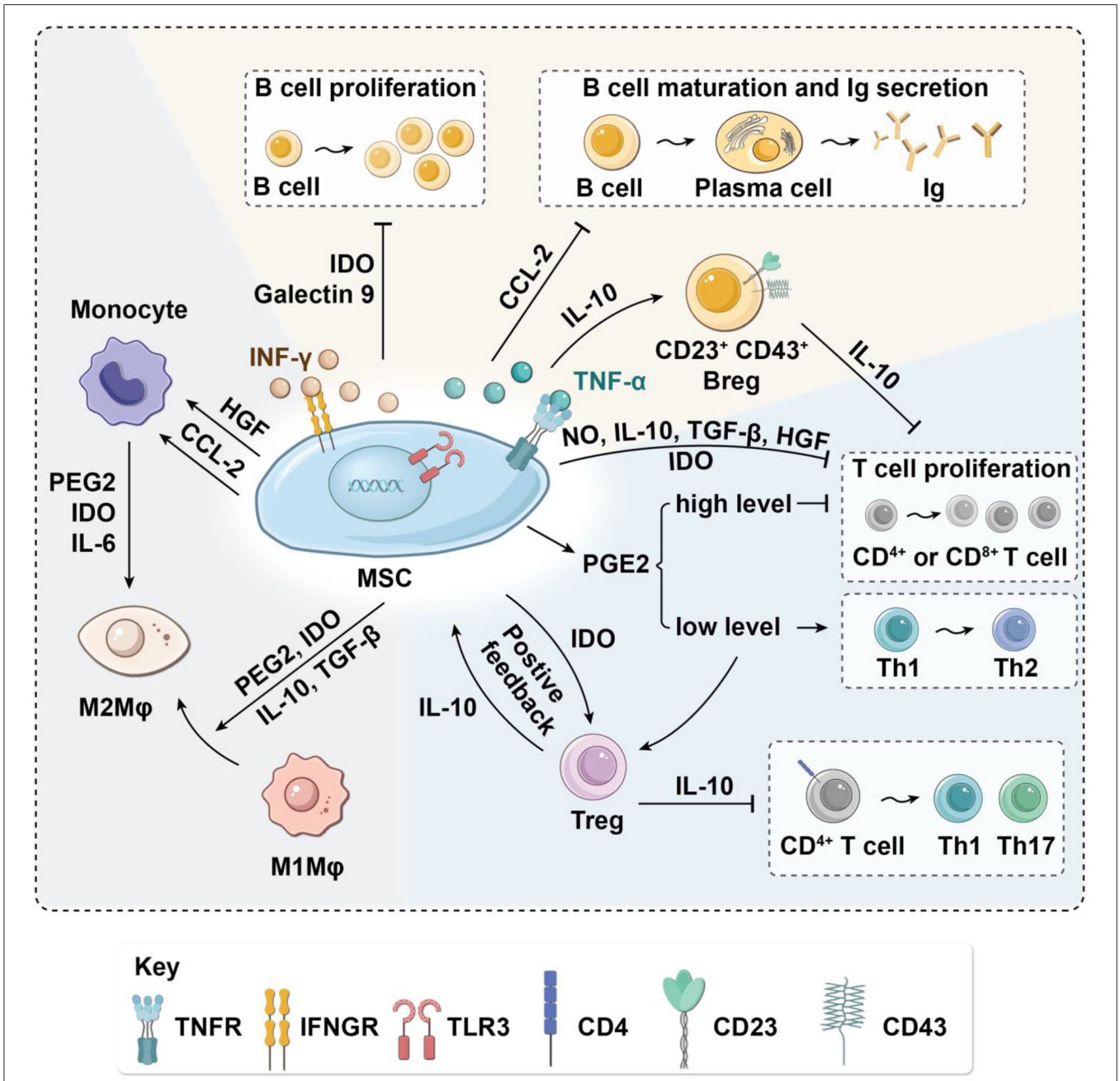

FIGURE 2 | Immunoregulatory effects of MSCs on immune cells in the paracrine manner. MSCs have immunomodulatory effects on OA-related macrophages, T cells, and B cells via the secretion of various cytokines. MSCs suppress macrophage migration and regulate their polarization by inducing transformation from M1 to M2. MSCs inhibit the proliferation of T cells and activation of inflammatory T_H1 and T_H17 cells. In turn, MSCs induce immunosuppressive Tregs. Moreover, MSCs decrease B-cell activation and proliferation and attenuate immunoglobulin production. Arg-1, arginase-1; Breg, regulatory B cell; CCL-2, C-C motif chemokine ligand 2; HGF, hepatocyte growth factor; IDO, indoleamine-2,3-dioxygenase; IL, interleukin; Ig, immune globulin; IFN-γ, interferon-γ; iNOS, inducible nitric oxide synthase; MSC, mesenchymal stem cell; Mφ, macrophages; NO, nitric oxide; OA, osteoarthritis; PGE2, prostaglandin E2; T_H, helper T cell; Treg, regulatory T cell; TGF-β, transforming growth factor-β.

MSCs Modulate T Cell Activation, Differentiation, and Effector Function

Cytokines secreted by MSCs can not only inhibit proliferation and induce apoptosis of T cells but also suppress the activation of naive T cells and change the differentiation process of T-cell subsets. Specifically, MSC-secreted cytokines may inhibit proinflammatory T cells and induce Tregs (Kalinski, 2012; Luz-Crawford et al., 2013; Baharlou et al., 2019; Jimenez-Puerta et al.,

2020) resulting in decreased production of TNF-α and IL-12 and increased production of IL-10. When the concentration of IL-10 in the microenvironment reaches a certain level, soluble human leukocyte antigen-G5 (HLA-G5) will be secreted, attenuating the activation of $CD4^+$ T cells to T_H1 and T_H17 and inducing Treg production (Selmani et al., 2008), thus forming a positive feedback loop (**Figure 2**).

Direct contact between MSCs and T cells also plays an important role in the immune regulation of T cells. The expression of intercellular adhesion molecule-1 and vascular cell adhesion molecule-1 (VCAM-1) is indispensable for MSCs to exert immunosuppressive effects toward T cells via increasing the adhesion between MSCs and T cells (Ren et al., 2010; Ma et al., 2017). In addition, some cell-to-cell contact-dependent mechanisms participate in the immunomodulation of T cells: Fas/FasL signaling pathway activation can induce the apoptosis of inflammatory T cells (Akiyama et al., 2012), Jagged-1/Notch-1 signal activation can promote $CD4^+$ T-cell differentiation into Tregs (Del Papa et al., 2013; Cahill et al., 2015), and programmed death-1/programmed death-1 ligand (PD-1/PD-L1) signaling effectively represses T_H17 differentiation (Kim et al., 2018). Moreover, direct contact between MSCs and T cells requires HLA-G5, which is responsible for both the contact-dependent and paracrine immunosuppressive functions of MSCs (**Figure 3**) (Selmani et al., 2008).

In summary, MSCs inhibit the proliferation of T cells and the activation of inflammatory T_H1 and T_H17 cells. In turn, MSCs induce immunosuppressive Tregs, thus inhibiting the immune response and attenuating inflammation.

Immunomodulatory Effects of MSCs on B Cells

Both secreted factors and cell-to-cell contact are needed for MSC modulation of B cells. Che et al. showed that co-culture with MSCs inhibits the phosphorylation of serine/threonine kinase and p38 mitogen-activated protein kinase in B cells (Che et al., 2012), while promoting the phosphorylation of extracellular response kinase 1/2 (ERK1/2) (Tabera et al., 2008). Another recent study showed that co-culture with MSCs significantly enhances the immunomodulatory activity of B cells by up-regulating IL-10. Chen et al. found that MSCs can induce a new regulatory B-cell (Breg) population characterized by $CD23^+CD43^+$ phenotypes. These $CD23^+CD43^+$ Breg cells significantly inhibit the secretion of proinflammatory cytokines and the proliferation of T cells through the IL-10–dependent pathway (Carreras-Planella et al., 2019a; Chen et al., 2019). Rafei et al. found that MSCs inhibit the expression of transcription factor signal transducer and activator of transcription 3 (STAT3) via chemokine C-C motif chemokine ligand 2 (CCL2) and then induce paired box 5 (PAX5) protein synthesis to inhibit the secretion of immune globulin in plasma cells (Rafei et al., 2008) (**Figure 2**). In addition to the paracrine effect, MSCs also play a contact-dependent immunomodulatory role with B cells. Schena et al. found that when activated by a high concentration of IFN-γ, MSCs can activate the programmed cell death receptor through direct contact and that the PD-1/PD-L1 signaling pathway inhibits the proliferation and maturation of B cells (**Figure 3**) (Schena et al., 2010).

In conclusion, MSCs can inhibit the proliferation of B cells and the differentiation and maturation of plasma cells and the secretion of antibody, while inducing a new Breg population, and attenuate inflammation in osteoarthritic joints.

MSC-DERIVED EVS AS IMMUNOMODULATORY THERAPEUTICS

Immunomodulatory Effects of MSC-Derived EVs on Macrophages

Several studies have shown that MSC-derived EVs can blunt the recruitment of macrophages. For instance, Shen et al. found that MSC-derived EVs express C-C motif chemokine receptor 2, which plays a key role in preventing macrophage accumulation and tissue damage by binding and serving as a decoy to inhibit proinflammatory chemokine CCL2 activity (Shen et al., 2016).

In addition, the therapeutic efficacy of MSC-derived EVs targeting M1/M2 polarization has been studied in various disease models. Zhang et al. found that EVs derived from MSCs have an immunomodulatory effect and can attract M2 macrophages to infiltrate OA cartilage defects and synovium, reduce the infiltration of M1 macrophages, and down-regulate the expression of IL-1β and TNF-α, thereby inhibiting the inflammatory response in OA (Zhang S. et al., 2018). In spinal cord injury (SCI) models, the detection of fluorescence-labeled human umbilical cord MSC (hUC-MSC)–derived EVs after intravenous infusion showed that hUC-MSC–derived EVs migrate to the injury site in a manner similar to hUC-MSCs themselves. Macrophages, especially the M2 subtype, are the primary target of EVs at SCI sites (Lankford et al., 2018). Sun et al. further confirmed that hUC-MSC–derived EVs can induce macrophage polarization from M1 to M2 and down-regulate the release of inflammatory factors, facilitating the repair of SCI (Sun et al., 2018). In an experimental murine model of bronchopulmonary dysplasia, MSC-derived EVs ameliorated hyperoxia-associated inflammation via modulation of lung macrophage phenotype (Willis et al., 2018). Similar immunoregulatory roles of MSC-derived EVs have been established in inflammatory bowel disease (Schena et al., 2010) and diabetic peripheral neuropathy (Fan et al., 2020).

Several studies have further explored the immunoregulatory mechanism in MSC-derived EVs. Zhao et al. found that mouse bone marrow MSC-derived EVs attenuate myocardial ischemia/reperfusion (I/R) injury in mice via shuttling microRNA-182 (miR-182), which targeted TLR4/nuclear factor κB/PI3K/Akt signaling, thereby modifying the polarization status of macrophages (Zhao J. et al., 2019). Another study demonstrated that adipose-derived stem cell (ADSC)–derived EVs facilitate the transportation of EV-enriched active STAT3 into macrophages to regulate polarization to the M2 phenotype through the transactivation of Arg-1 (Zhao et al., 2018). A recent study on cutaneous wound healing showed that miR-223, which is contained in MSC-derived EVs, induces the polarization of macrophages by targeting pknox1 (He et al., 2019).

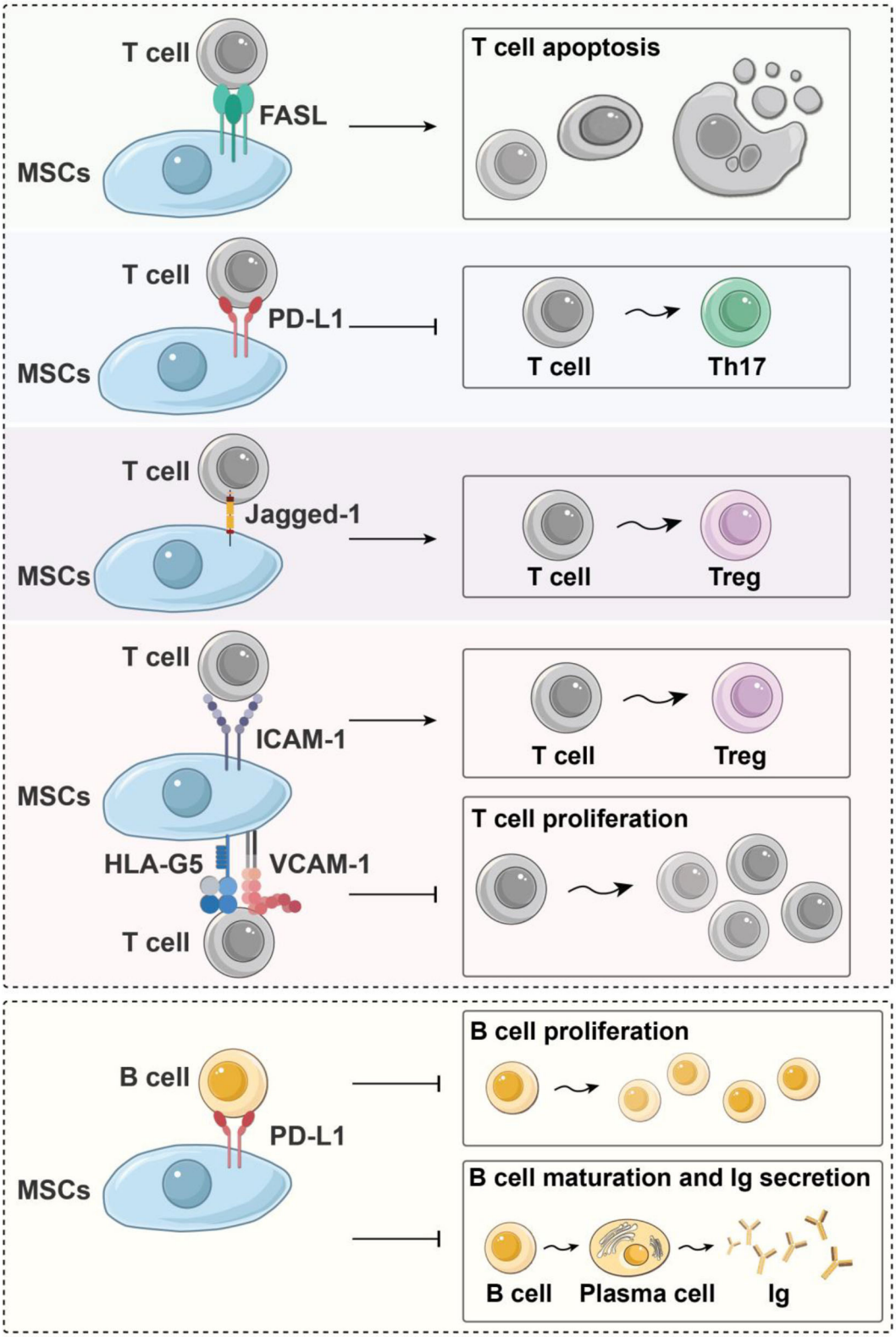

FIGURE 3 | Immunoregulatory effects of MSCs on immune cells in a contact-dependent manner. Fas/FasL signal activation can induce the apoptosis of inflammatory T cells; Jagged-1/Notch-1 signal activation can induce $CD4^+$ T cells to differentiate into Tregs, and PD-1/PD-L1 signaling effectively represses T_H17 differentiation and *(Continued)*

FIGURE 3 | inhibits the proliferation and maturation of B cells. Moreover, HLA-G5, ICAM-1, and VCAM-1 are needed for MSCs to exert their immunosuppressive effects upon T cells. HLA-G5, human leukocyte antigen-G5; ICAM-1, intercellular adhesion molecule-1; Ig, immune globulin; MSC, mesenchymal stem cells; PD-L1, programmed death-1 ligand; T_H, helper T cell; Treg, regulatory T cell; VCAM-1, vascular cell adhesion molecule-1.

Preconditioning MSCs with stimulating factors may increase the therapeutic potential of EVs. Ti et al. found that MSC-derived EVs preconditioned with lipopolysaccharide (LPS-EVs) had a more significant regulatory effect on macrophage polarization. The results of microarray analysis showed that the LPS-EVs mechanism of immunomodulation is associated with the expression of let-7b, which can impede the TLR4 pathway to regulate macrophage polarization (Ti et al., 2015). Song et al. used IL-1β to stimulate hUC-MSCs before administration to septic mice and found that huMSCs transfer miR-146a to macrophages via EVs, thereby promoting the M1-M2 transition. The survival rate of mice in the EV-treated group was decreased after miR-146a inhibition, demonstrating that miR-146a plays a protective role in the treatment of sepsis by MSC-derived EVs (Song et al., 2017). Transfection is another method of MSC modification. Jiang et al. found that miR-30d-5p–overexpressing ADSC-derived EVs prevent cerebral injury by inhibiting autophagy-mediated microglial polarization to M1 via the inhibition of Beclin-1 and autophagy-related gene 5 (ATG5) (Jiang et al., 2018).

These studies indicate that MSC-derived EVs can regulate macrophage polarization in a manner similar to MSCs. Moreover, considering that MSCs have plasticity, the EVs from preconditioned MSCs may possess different characteristics and may obtain better therapeutic effects (**Table 1**).

Immunomodulatory Effects of MSC-Derived EVs on T Cells

The effect of MSC-derived EVs on T cells has been described in several *in vitro* experiments. For example, Chen et al. co-cultured peripheral blood mononuclear cells with MSC-derived EVs and found that EVs induce the transformation of T_H1 cells into T_H2 cells, reduce the potential of T cells to differentiate into T_H17 cells, and increase the content of Tregs (Chen et al., 2016). The regulatory effects of MSC-derived EVs on T cells have also been confirmed in various disease models. Cosenza et al. assessed the immunosuppressive effects of EVs on T cells in a delayed-type hypersensitivity model. The results showed that EVs from MSCs inhibited T-cell proliferation and induced Treg populations in a dose-dependent manner, thereby exerting an immunomodulatory effect on inflammatory arthritis (Cosenza et al., 2018). Zhang et al. further demonstrated that MSC-derived EVs induce the differentiation of naive T cells into Tregs via an APC-mediated pathway *in vitro* and *in vivo* (Zhang B. et al., 2018).

Owing to the plasticity of MSCs and the biological characteristics of EVs, EVs from modified MSCs have also been investigated in the field of inflammatory disease therapy. Riazifar et al. evaluated the role of EVs derived from MSCs stimulated by IFN-γ (IFN-γ-EVs) as a treatment in an experimental autoimmune encephalomyelitis mice model (Riazifar et al., 2019). They demonstrated that EVs decreased neuroinflammation and up-regulated the number of Tregs within the spinal region. Furthermore, RNA sequencing showed that IFN-γ-EVs contained anti-inflammatory RNAs and proteins, and inhibition of these RNAs could partially inhibit the potential of EVs to induce Tregs, suggesting potential for EVs as a cell-free therapy for immune-related diseases. Studies have also investigated molding EVs via lentivirus transfection of MSCs. Wei et al. developed an miR-181–overexpressing MSC-EV system that has strong therapeutic effects on myocardial I/R injury. The miRNA-181a mimic was able to interact with the c-Fos mRNA complex and induce Treg differentiation (Wei et al., 2019).

In conclusion, the immunoregulatory effects of MSC-derived EVs on T cells are manifested mainly in the immunosuppression of effector T cells and the induction of Tregs (**Table 1**).

Immunomodulatory Effects of MSC-Derived EVs on B Cells

MSC-derived EVs also play an immunosuppressive role for B cells and can inhibit the terminal differentiation and maturation of plasma cells (Cosenza et al., 2018). In an OA model induced by collagenase, MSC-derived EVs effectively reduce the clinical symptoms of inflammation. However, treatment with IFN-γ did not affect the immunosuppressive function of EVs before isolation from MSCs (Cosenza et al., 2018).

A large number of studies have shown that EVs derived from MSCs exert effects through horizontal protein transfer, mRNA, and regulatory microRNA. Based on evidence that miRNA may be transferred to target cells, Khare et al. studied changes in activated B-cell mRNA after culture with bone marrow MSC (BMSC)-derived EVs and found that 186 genes were significantly differentially expressed after culture with EVs. The BMSC-derived EVs may inhibit the proliferation and decrease the chemotaxis of B cells by inhibiting the expression of chemokine receptor on B cells (Khare et al., 2018).

However, a recent study showed that the immunomodulatory effect of MSCs on B cells is mediated partially by soluble secreted factors rather than EVs. The authors found that MSC-derived EVs failed to induce naive B cells or reduce memory B cells, unliske the MSCs themselves. Furthermore, MSC-derived EVs induced $CD24^+CD38^+$ B cells to a similar extent compared with MSCs, but these B cells did not produce IL-10 and were therefore not considered true Bregs (Carreras-Planella et al., 2019b).

Do MSC-derived EVs have immunosuppressive effects upon B cells? The roles of EVs in MSC-mediated B-cell immunoregulation merit further investigation (**Table 1**).

TABLE 1 | Effects of MSC-derived EVs on OA-related immune cells.

Disease model	Extracellular vesicle source	Precondition of MSCs	Effects on immune cells	Defined key factors	References
Renal injury	Mouse BMSC	\	Suppress the recruitment and action of macrophages	CCR2	Shen et al., 2016
Osteochondral defects	Human ESC-MSC	\	Induce the infiltration of M2 Mφ and reduce the infiltration of M1 Mφ in the defects	\	Zhang B. et al., 2018
Spinal cord injury	Human UC-MSC	\	Induce Mφ polarization from M1 to M2 and down-regulate the release of inflammatory factors	\	Sun et al., 2018
Experimental bronchopulmonary dysplasia	Mouse BMSC	\	Decrease and increase M1 and M2 Mφ phenotype markers, respectively	\	Willis et al., 2018
IBD	Human BMSC	\	Metallothionein-2 acts as a critical negative regulator of the inflammatory response in Mφs.	Metallothionein-2	Liu et al., 2019
DPN	Mouse BMSC	\	Decrease and increase M1 and M2 Mφ phenotype markers, respectively	miR-17, miR-23a, miR-125b	Fan et al., 2020
Myocardial I/R injury	Mouse BMSC	\	Mediate macrophage polarization from M1 to M2	miR-182	Zhao J. et al., 2019
Obesity-induced inflammation	Mouse ADSC	\	Induce M2 Mφ polarization	Activated STAT3	Zhao et al., 2018
Skin defect	Human jaw BMSC	\	Induce M2 Mφ polarization	miR-223	He et al., 2019
Diabetic cutaneous wounds	Human UC-MSC	Stimulated by LPS	Induce M2 Mφ polarization	let-7b	Ti et al., 2015
Sepsis	Human UC-MSC	Stimulated by IL-1β	Induce M2 Mφ polarization	miR-146a	Song et al., 2017
Middle cerebral artery occlusion	Rat ADSC	Transfection of miR-30d-5p mimic	Transform microglial/macrophage polarization from M1 to M2	miR-30d-5p	Jiang et al., 2018
\	Human BMSC	\	Induce the transformation of T_H1 cells into T_H2 cells, reduce the potential of T cells to differentiate into T_H17 cells and increase the content of Tregs	\	Chen et al., 2016
Arthritis (DTH or CIA induced)	Mouse BMSC	\	Inhibit T-cell proliferation through Treg induction. Suppress plasma cell differentiation and induce Bregs	\	Cosenza et al., 2018
GVHD	Human ESC-MSC	\	Induce the differentiation of naive T cells into Tregs	\	Zhang B. et al., 2018
EAE	Human BMSC	Stimulated by IFN-γ	Suppress T Cell Proliferation and up-regulate the number of Tregs within the spinal	Aggrecan, periostin, HAPLN1	Riazifar et al., 2019
Myocardial I/R injury	Human UC-MSC	Transfection of miR-181 mimic	Induce the differentiation of Tregs	miR-181	Wei et al., 2019
\	Human BMSC	\	Inhibit the proliferation of B cells and decrease the chemotaxis of B cells	CXCL8, MZB1	Khare et al., 2018

ADSC, adipose-derived stem cells; BMSC, bone marrow mesenchymal cells; Breg, regulatory B cell; CCR2, C-C chemokine receptor type 2; CIA, collagen-induced arthritis; CXCL8, C-X-C motif ligand 8; DTH, delayed-type hypersensitivity; EAE, experimental autoimmune encephalomyelitis; ESC-MSC, embryonic stem cell–derived mesenchymal cells; GVHD, graft-vs.-host disease; HAPLN1, hyaluronan and proteoglycan link protein 1; IBD, inflammatory bowel disease; IL, interleukin; IFN-γ, interferon-γ; I/R, ischemia/reperfusion; LPS, lipopolysaccharide; miR, microRNA; Mφ, macrophages; MZB1, marginal zone B and B-1 cell-specific protein; OA, osteoarthritis; OPN, diabetic peripheral neuropathy; STAT, signal transducer and activator of transcription; T_H, helper T cell; Treg, regulatory T cell; UC-MSC, umbilical cord–derived mesenchymal cells.

SUSTAINED DELIVERY OF EVS

One challenge in the application of sustained EV delivery systems is the difficulty of producing EVs in large quantities and with high purity (Yamashita et al., 2018). The typical yield of EVs isolated from 1 mL of medium may be <1 μg EV protein, whereas the effective dose of EVs in mouse models typically ranges from 10 to 100 μg of protein. Humans are expected to require larger therapeutic doses (Willis et al., 2017). The endocytic pathway of target cells is the main route by which EVs exert their biological effects (Mulcahy et al., 2014). However, studies have shown that, regardless of their source and whether they are administered

through direct intravenous injection, subcutaneous injection or any other direct delivery routes, EVs will be quickly cleared from blood circulation and discharged from the body (Smyth et al., 2015; Charoenviriyakul et al., 2017). Therefore, prolonging the half-life of EVs to maximize their local therapeutic effects remains a major challenge.

To overcome this limitation, biomaterials may be utilized in EV encapsulation strategies to deliver EVs in a sustained-release manner. Hydrogels are three-dimensional cross-linked hydrophilic polymers with biological media that swell in water but do not dissolve (Narayanaswamy and Torchilin, 2019). Because hydrogels are biodegradable, biocompatible, and non-toxic, they have received great attention in various fields. Hydrogels can serve as biological drug delivery systems, cell encapsulation matrices, or scaffolds in regenerative medicine (Oliva et al., 2017; Mahdavinia et al., 2018). Hydrogel is considered to be an excellent carrier for EVs and may be capable of effectively delivering EVs to damaged tissues and prolonging their effects (Riau et al., 2019).

Liu et al. developed a photoinduced imine-crosslinking hydrogel glue to load-induced pluripotent stem cell–derived EVs for repairing knee articular cartilage defects, effectively prolonging the activity of stem cell–derived EVs promoting the repair of cartilage defects (Liu et al., 2017). Zhang et al. isolated EVs from human placenta-derived MSCs and combined EVs with chitosan hydrogel to form hydrogel-incorporated EVs (CS-EVs). They evaluated the effects of CS-EVs in endothelial cells using a murine hindlimb ischemia model and found that chitosan hydrogel strongly enhanced the retention of EVs at the target site. CS-EVs had advantageous functions compared with EVs alone, including enhancing angiogenesis, suppressing apoptosis of muscle cells, and attenuating fibrosis (Zhang K. et al., 2018). Henriques-Antunes et al. exploited a light triggerable hyaluronic acid hydrogel for the remote release control of EVs, which is more efficient in regulating EVs release according to the tissue healing dynamics in diabetic chronic wounds. Moreover, this hydrogel can provide antimicrobial activity by incorporating autolytic enzymes such as collagenases and antimicrobial peptides in order to avoid recurrent infection (Henriques-Antunes et al., 2019). Given that the mesh size of the ECM is usually smaller than the size of EVs, understanding how EVs are dispersed is critical to developing these cell-free therapies and stopping disease progression. Recently, Lenzini et al. revealed the diffusion and transport process of EVs in dense ECM by using engineered hydrogel. They confirmed that matrix stress relaxation is a key factor for EVs to overcome the confinement and that water infiltration also plays an essential role in EV deformation and navigation in ECM. These findings bring us closer to designing effective drug delivery systems (Lenzini et al., 2020).

PERSPECTIVE

The current viewpoint of OA is evolving from a simple mechanical joint injury toward a complex organ disease that involves biomechanics, inflammation, and the immune system. Macrophages, T cells, and B cells are the three main immune cells that control the inflammatory processes and immune response in OA. They form a complex network regulation system through coordination and antagonism. For example, T_H2 cells can induce macrophage polarization via cytokines, yet the M2 polarization of macrophages might be involved in the induction of Tregs (Murray, 2017; Phan et al., 2017). Each of these processes overlaps and is also related to the local microenvironment, including trauma, inflammation, and cartilage remodeling. Fully understanding the complex inflammatory network system in OA will facilitate more effective and systematic treatment (**Figure 1**).

Currently, several studies have demonstrated the immunomodulatory effects of MSCs/EVs during OA, but there is still a lack of hard evidence of key factors and related mechanisms. Therefore, we also discussed the immunomodulatory effect of MSCs/EVs in some similar disease models based on chronic degenerative diseases with chronic inflammation hereinabove. We speculate that MSCs/EVs have similar immunomodulatory mechanisms in OA, and these roles need to be further investigated by future research in OA models.

As we have seen, MSCs have been widely used in regenerative therapy and immunotherapy owing to their anti-inflammatory and immunomodulatory effects (Prockop and Oh, 2012). The role of MSCs is to adjust the balance between inflammation and tissue reconstruction to provide the damaged tissue with a relatively stable environment, which is beneficial for tissue repair (Shi et al., 2018). However, direct MSC transplantation has several critical limitations to overcome: (1) the procurement of some stem cells, such as embryonic stem cells, is still controversial; (2) it is difficult to predict the lasting capacity for cell behavior and cell–cell interactions because of aging; (3) the survival rate associated with stem cell transplantation is low; (4) there is immune rejection in some patients; (5) the procedures are typically expensive and have a high risk of infection (Jiang and Xu, 2020). Moreover, as has been noted, MSCs are sensitive to certain microenvironment or inflammatory milieu and undergo specific behavioral modification. The plasticity of MSCs may have a negative impact on direct MSC transplantation. For example, MSCs can switch to MSC1, when induced by exposure to a low level of TLR2/4 ligands *in vivo*, and can then take effect in augmenting the inflammatory response (Tomchuck et al., 2008; Lei et al., 2011).

Therefore, more and more researchers have tended to test the secretory products of MSCs, including MSC-derived EVs in animal models of OA, rather than direct transplanting MSCs themselves. EVs derived from MSCs have been proven to reproduce some benefits of MSC-mediated immunosuppression (Mianehsaz et al., 2019). They can transfer miRNA or other bioactive substances such as cytokines, growth factors, and metabolites to target cells, thus playing the role of immune regulators. Being cell-free particles, EVs can avoid any chance of cell modification, and this guaranteed the stability of soluble bioactive factor types and abundance applied to the degenerative joint. Further knowledge regarding the mechanisms of action for MSCs and EVs in OA will enable individual assessments of the severity of the articular condition. Based on the plasticity of MSCs, it may be possible to obtain EVs with different characteristics prior to application to develop personalized

treatments and increase therapeutic efficacy (Ti et al., 2015; Song et al., 2017; Jiang et al., 2018; Riazifar et al., 2019). However, EV-based therapy has some disadvantages: First, MSCs have numerous contact effects and numerous paracrine effects including EVs; therefore, EVs can reproduce the positive function of MSCs partially, but not all of them. Second, the major drawback of EVs is their rapid clearance, and sustained local delivery of EVs is therefore important (Smyth et al., 2015; Charoenviriyakul et al., 2017). It is also important to determine how to prepare EVs quickly, cheaply, and efficiently. Moreover, as described in *Immunomodulatory Effects of MSC-Derived EVs on B Cells*, a recent study different from previous studies reported no or low functional effects of EVs on B cells (Carreras-Planella et al., 2019b). This discrepancy may be due to a variety of factors, including MSC sources, isolation methods, culture conditions, and/or the use of repeated freeze-thawed EVs. Another possibility is that EVs play a small role in MSC-mediated B-cell immunoregulation, which need further investigation; if that is the case, the appropriate treatment (cell or cell-free) should be selected according to different targeted immune cells.

To sum up, EVs avoid some of the inherent risks of MSC therapies and hold great promise in a range of applications. However, there are still many uncertain aspects of the interactions between MSCs/MSC-derived EVs and immune cells involved in OA, and future studies should further explore and optimize the role of EVs in immunoregulation and enable the efficient application of EVs in clinical therapy.

AUTHOR CONTRIBUTIONS

XW and QY initiated the project and made suggestions and revised the article. XZ, YZ, XS, and YX searched the database, wrote, and finalized the manuscript. All authors reviewed and commented on the entire manuscript.

FUNDING

This work was supported by National Key Research and Development Program of China (2020YFC1107402 and 2019YFC110005), National Natural Science Foundation of China (31300798, 81871782, 51973226, and 31900968), Youth Innovation Promotion Association CAS (No. 2019031), Tianjin Science Fund for Distinguished Young Scholars (18JCJQJC47900), and Research Foundation of the Tianjin Health Bureau (16KG114).

REFERENCES

Abumaree, M. H., Al Jumah, M. A., Kalionis, B., Jawdat, D., Al Khaldi, A., Abomaray, F. M., et al. (2013). Human placental mesenchymal stem cells (pMSCs) play a role as immune suppressive cells by shifting macrophage differentiation from inflammatory M1 to anti-inflammatory M2 macrophages. *Stem Cell Rev. Rep.* 9, 620–641. doi: 10.1007/s12015-013-9455-2

Akiyama, K., Chen, C., Wang, D., Xu, X., Qu, C., Yamaza, T., et al. (2012). Mesenchymal-stem-cell-induced immunoregulation involves FAS-ligand-/FAS-mediated T cell apoptosis. *Cell Stem Cell* 10, 544–555. doi: 10.1016/j.stem.2012.03.007

Aspden, R. M., and Saunders, F. R. (2019). Osteoarthritis as an organ disease: from the cradle to the grave. *Eur Cells Mater.* 37, 74–87. doi: 10.22203/eCM.v037a06

Ayala-Cuellar, A. P., Kang, J. H., Jeung, E. B., and Choi, K. C. (2019). Roles of mesenchymal stem cells in tissue regeneration and immunomodulation. *Biomol. Ther.* 27, 25–33. doi: 10.4062/biomolther.2017.260

Baharlou, R., Rashidi, N., Ahmadi-Vasmehjani, A., Khoubyari, M., Sheikh, M., and Erfanian, S. (2019). Immunomodulatory effects of human adipose tissue-derived mesenchymal stem cells on T cell subsets in patients with rheumatoid arthritis. *Iran. J. Allergy Asthma Immunol.* 18, 114–119. doi: 10.18502/ijaai.v18i1.637

Barry, F., and Murphy, M. (2013). Mesenchymal stem cells in joint disease and repair. *Nat. Rev. Rheumatol* 9, 584–594. doi: 10.1038/nrrheum.2013.109

Behm, C., Blufstein, A., Gahn, J., Nemec, M., Moritz, A., Rausch-Fan, X., et al. (2020). Cytokines differently define the immunomodulation of mesenchymal stem cells from the periodontal ligament. *Cells* 9:1222. doi: 10.3390/cells9051222

Blom, A. B., van Lent, P. L., Libregts, S., Holthuysen, A. E., van der Kraan, P. M., van Rooijen, N., et al. (2007). Crucial role of macrophages in matrix metalloproteinase-mediated cartilage destruction during experimental osteoarthritis: involvement of matrix metalloproteinase 3. *Arthritis Rheum.* 56, 147–157. doi: 10.1002/art.22337

Bommireddy, R., and Doetschman, T. (2007). TGFbeta1 and Treg cells: alliance for tolerance. *Trends Mol. Med.* 13, 492–501. doi: 10.1016/j.molmed.2007.08.005

Bui, T. M., Mascarenhas, L. A., and Sumagin, R. (2018). Extracellular vesicles regulate immune responses and cellular function in intestinal inflammation and repair. *Tissue Barriers* 6, e1431038. doi: 10.1080/21688370.2018.1431038

Burr, S. P., Dazzi, F., and Garden, O. A. (2013). Mesenchymal stromal cells and regulatory T cells: the Yin and Yang of peripheral tolerance? *Immunol. Cell Biol.* 91, 12–18. doi: 10.1038/icb.2012.60

Cahill, E. F., Tobin, L. M., Carty, F., Mahon, B. P., and English, K. (2015). Jagged-1 is required for the expansion of CD4(+) CD25(+) FoxP3(+) regulatory T cells and tolerogenic dendritic cells by murine mesenchymal stromal cells. *Stem Cell Res. Ther.* 6:19. doi: 10.1186/s13287-015-0021-5

Carreras-Planella, L., Monguió-Tortajada, M., Borràs, F., and Franquesa, M. (2019a). Corrigendum: immunomodulatory effect of MSC on B cells is independent of secreted extracellular vesicles. *Front. Immunol.* 10:2413. doi: 10.3389/fimmu.2019.02413

Carreras-Planella, L., Monguió-Tortajada, M., Borràs, F., and Franquesa, M. (2019b). Immunomodulatory effect of MSC on B cells is independent of secreted extracellular vesicles. *Front. Immunol.* 10:1288. doi: 10.3389/fimmu.2019.01288

Charoenviriyakul, C., Takahashi, Y., Morishita, M., Matsumoto, A., Nishikawa, M., and Takakura, Y. (2017). Cell type-specific and common characteristics of exosomes derived from mouse cell lines: yield, physicochemical properties, and pharmacokinetics. *Eur. J. Pharm. Sci.* 96, 316–322. doi: 10.1016/j.ejps.2016.10.009

Che, N., Li, X., Zhou, S. L., Liu, R., Shi, D. Y., Lu, L. W., et al. (2012). Umbilical cord mesenchymal stem cells suppress B-cell proliferation and differentiation. *Cell. Immunol.* 274, 46–53. doi: 10.1016/j.cellimm.2012.02.004

Chen, W., Huang, Y., Han, J., Yu, L., Li, Y., Lu, Z., et al. (2016). Immunomodulatory effects of mesenchymal stromal cells-derived exosome. *Immunol. Res.* 64, 831–840. doi: 10.1007/s12026-016-8798-6

Chen, X., Cai, C., Xu, D., Liu, Q., Zheng, S., Liu, L., et al. (2019). Human mesenchymal stem cell-treated regulatory CD23(+)CD43(+) B cells alleviate intestinal inflammation. *Theranostics* 9, 4633–4647. doi: 10.7150/thno.32260

Chen, Y., Jiang, W., Yong, H., He, M., Yang, Y., Deng, Z., et al. (2020). Macrophages in osteoarthritis: pathophysiology and therapeutics. *Am. J. Transl. Res.* 12, 261–268.

Cho, D. I., Kim, M. R., Jeong, H. Y., Jeong, H. C., Jeong, M. H., Yoon, S. H., et al. (2014). Mesenchymal stem cells reciprocally regulate the M1/M2 balance in mouse bone marrow-derived macrophages. *Exp. Mol. Med.* 46:e70. doi: 10.1038/emm.2013.135

Chow, Y. Y., and Chin, K. Y. (2020). The Role of Inflammation in the Pathogenesis of Osteoarthritis. *Mediators Inflamm.* 2020:8293921. doi: 10.1155/2020/8293921

Cosenza, S., Toupet, K., Maumus, M., Luz-Crawford, P., Blanc-Brude, O., Jorgensen, C., et al. (2018). Mesenchymal stem cells-derived exosomes are more immunosuppressive than microparticles in inflammatory arthritis. *Theranostics* 8, 1399–1410. doi: 10.7150/thno.21072

de Castro, L. L., Lopes-Pacheco, M., Weiss, D. J., Cruz, F. F., and Rocco, P. R. M. (2019). Current understanding of the immunosuppressive properties of mesenchymal stromal cells. *J. Mol. Med.* 97, 605–618. doi: 10.1007/s00109-019-01776-y

de Lange-Brokaar, B. J. E., Ioan-Facsinay, A., van Osch, G. J. V. M., Zuurmond, A. M., Schoones, J., Toes, R. E., et al. (2012). Synovial inflammation, immune cells and their cytokines in osteoarthritis: a review. *Osteoarthr. Cartilage* 20, 1484–1499. doi: 10.1016/j.joca.2012.08.027

Del Papa, B., Sportoletti, P., Cecchini, D., Rosati, E., Balucani, C., Baldoni, S., et al. (2013). Notch1 modulates mesenchymal stem cells mediated regulatory T-cell induction. *Eur. J. Immunol.* 43, 182–187. doi: 10.1002/eji.201242643

Fahy, N., de Vries-van Melle, M. L., Lehmann, J., Wei, W., Grotenhuis, N., Farrell, E., et al. (2014). Human osteoarthritic synovium impacts chondrogenic differentiation of mesenchymal stem cells via macrophage polarisation state. *Osteoarthr. Cartilage* 22, 1167–1175. doi: 10.1016/j.joca.2014.05.021

Fan, B., Li, C., Szalad, A., Wang, L., Pan, W., Zhang, R., et al. (2020). Mesenchymal stromal cell-derived exosomes ameliorate peripheral neuropathy in a mouse model of diabetes. *Diabetologia* 63, 431–443. doi: 10.1007/s00125-019-05043-0

Faulknor, R. A., Olekson, M. A., Ekwueme, E. C., Krzyszczyk, P., Freeman, J. W., and Berthiaume, F. (2017). Hypoxia impairs mesenchymal stromal cell-induced macrophage M1 to M2 transition. *Technology* 5, 81–86. doi: 10.1142/S2339547817500042

Fernandes, T. L., Gomoll, A. H., Lattermann, C., Hernandez, A. J., Bueno, D. F., and Amano, M. T. (2020). Macrophage: a potential target on cartilage regeneration. *Front. Immunol.* 11:111. doi: 10.3389/fimmu.2020.00111

Fernandez-Pernas, P., Barrachina, L., Marquina, M., Rodellar, C., Arufe, M. C., and Costa, C. (2020). Mesenchymal stromal cells for articular cartilage repair: preclinical studies. *Eur. Cell. Mater* 40, 88–114. doi: 10.22203/eCM.v040a06

Fichadiya, A., Bertram, K. L., Ren, G., Yates, R. M., and Krawetz, R. J. (2016). Characterizing heterogeneity in the response of synovial mesenchymal progenitor cells to synovial macrophages in normal individuals and patients with osteoarthritis. *J. Inflamm.* 13:12. doi: 10.1186/s12950-016-0120-9

Glennie, S., Soeiro, I., Dyson, P. J., Lam, E. W., and Dazzi, F. (2005). Bone marrow mesenchymal stem cells induce division arrest anergy of activated T cells. *Blood* 105, 2821–2827. doi: 10.1182/blood-2004-09-3696

Guillamat-Prats, R., Camprubi-Rimblas, M., Bringue, J., Tantinya, N., and Artigas, A. (2017). Cell therapy for the treatment of sepsis and acute respiratory distress syndrome. *Ann. Transl. Med.* 5:446. doi: 10.21037/atm.2017.08.28

Haynes, M. K., Hume, E. L., and Smith, J. B. (2002). Phenotypic characterization of inflammatory cells from osteoarthritic synovium and synovial fluids. *Clin. Immunol.* 105, 315–325. doi: 10.1006/clim.2002.5283

He, X., Dong, Z., Cao, Y., Wang, H., Liu, S., Liao, L., et al. (2019). MSC-derived exosome promotes m2 polarization and enhances cutaneous wound healing. *Stem Cells Int.* 2019:7132708. doi: 10.1155/2019/7132708

Henriques-Antunes, H., Cardoso, M. S. R., Zonari, A., Correia, J., Leal, E. C., Jiménez-Balsa, A., et al. (2019). The kinetics of small extracellular vesicle delivery impacts skin tissue regeneration. *ACS Nano* 13, 8694–8707. doi: 10.1021/acsnano.9b00376

Hori, S., Nomura, T., and Sakaguchi, S. (2003). Control of regulatory T cell development by the transcription factor Foxp3. *Science* 299, 1057–1061. doi: 10.1126/science.1079490

Hsieh, J. L., Shiau, A. L., Lee, C. H., Yang, S. J., Lee, B. O., Jou, I. M., et al. (2013). CD8+ T cell-induced expression of tissue inhibitor of metalloproteinses-1 exacerbated osteoarthritis. *Int. J. Mol. Sci.* 14, 19951–19970. doi: 10.3390/ijms141019951

Hu, T., Xu, H., Wang, C., Qin, H., and An, Z. (2018). Magnesium enhances the chondrogenic differentiation of mesenchymal stem cells by inhibiting activated macrophage-induced inflammation. *Sci. Rep.* 8:3406. doi: 10.1038/s41598-018-21783-2

Huang, Z. Y., and Kraus, V. B. (2016). Does lipopolysaccharide-mediated inflammation have a role in OA? *Nat. Rev. Rheumatol.* 12, 123–129. doi: 10.1038/nrrheum.2015.158

Hunter, D. J., and Bierma-Zeinstra, S. (2019). Osteoarthritis. *Lancet* 393, 1745–1759. doi: 10.1016/S0140-6736(19)30417-9

Hussein, M. R., Fathi, N. A., El-Din, A. M., Hassan, H. I., Abdullah, F., Al-Hakeem, E., et al. (2008). Alterations of the CD4(+), CD8 (+) T cell subsets, interleukins-1beta, IL-10, IL-17, tumor necrosis factor-alpha and soluble intercellular adhesion molecule-1 in rheumatoid arthritis and osteoarthritis: preliminary observations. *Pathol. Oncol. Res.* 14, 321–328. doi: 10.1007/s12253-008-9016-1

Jiang, M., Wang, H., Jin, M., Yang, X., Ji, H., Jiang, Y., et al. (2018). Exosomes from MiR-30d-5p-ADSCs reverse acute ischemic stroke-induced, autophagy-mediated brain injury by promoting M2 microglial/macrophage polarization. *Cell. Physiol. Biochem.* 47, 864–878. doi: 10.1159/000490078

Jiang, W., and Xu, J. Y. (2020). Immune modulation by mesenchymal stem cells. *Cell Prolif.* 53:e12712. doi: 10.1111/cpr.12712

Jimenez-Puerta, G. J., Marchal, J. A., Lopez-Ruiz, E., and Galvez-Martin, P. (2020). Role of mesenchymal stromal cells as therapeutic agents: potential mechanisms of action and implications in their clinical use. *J. Clin. Med.* 9:445. doi: 10.3390/jcm9020445

Kalinski, P. (2012). Regulation of immune responses by prostaglandin E2. *J. Immunol.* 188, 21–28. doi: 10.4049/jimmunol.1101029

Kalluri, R., and LeBleu, V. S. (2020). The biology, function, and biomedical applications of exosomes. *Science* 367:eaau6977. doi: 10.1126/science.aau6977

Kawahara, K., Hohjoh, H., Inazumi, T., Tsuchiya, S., and Sugimoto, Y. (2015). Prostaglandin E2-induced inflammation: Relevance of prostaglandin E receptors. *Biochim. Biophys. Acta* 1851, 414–421. doi: 10.1016/j.bbalip.2014.07.008

Khare, D., Or, R., Resnick, I., Barkatz, C., Almogi-Hazan, O., and Avni, B. (2018). Mesenchymal stromal cell-derived exosomes affect mRNA expression and function of B-lymphocytes. *Front. Immunol.* 9:3053. doi: 10.3389/fimmu.2018.03053

Kim, J. Y., Park, M., Kim, Y. H., Ryu, K. H., Lee, K. H., Cho, K. A., et al. (2018). Tonsil-derived mesenchymal stem cells (T-MSCs) prevent Th17-mediated autoimmune response via regulation of the programmed death-1/programmed death ligand-1 (PD-1/PD-L1) pathway. *J. Tissue Eng. Regen. Med.* 12, e1022–e1033. doi: 10.1002/term.2423

Kyurkchiev, D., Bochev, I., Ivanova-Todorova, E., Mourdjeva, M., Oreshkova, T., Belemezova, K., et al. (2014). Secretion of immunoregulatory cytokines by mesenchymal stem cells. *World J. Stem Cells* 6, 552–570. doi: 10.4252/wjsc.v6.i5.552

Labinsky, H., Panipinto, P. M., Ly, K. A., Khuat, D. K., Madarampalli, B., Mahajan, V., et al. (2020). Multiparameter analysis identifies heterogeneity in knee osteoarthritis synovial responses. *Arthritis Rheumatol.* 72, 598–608. doi: 10.1002/art.41161

Lankford, K. L., Arroyo, E. J., Nazimek, K., Bryniarski, K., Askenase, P. W., and Kocsis, J. D. (2018). Intravenously delivered mesenchymal stem cell-derived exosomes target M2-type macrophages in the injured spinal cord. *PLoS ONE* 13:e0190358. doi: 10.1371/journal.pone.0190358

Lee, S., Zhang, Q., Karabucak, B., and Le, A. (2016). DPSCs from inflamed pulp modulate macrophage function via the TNF-α/IDO axis. *J. Dent. Res.* 95, 1274–1281. doi: 10.1177/0022034516657817

Lei, J. X., Wang, Z., Hui, D. Y., Yu, W. H., Zhou, D. H., Xia, W. J., et al. (2011). Ligation of TLR2 and TLR4 on murine bone marrow-derived mesenchymal stem cells triggers differential effects on their immunosuppressive activity. *Cell. Immunol.* 271, 147–156. doi: 10.1016/j.cellimm.2011.06.014

Lenzini, S., Bargi, R., Chung, G., and Shin, J. W. (2020). Matrix mechanics and water permeation regulate extracellular vesicle transport. *Nat. Nanotechnol.* 15, 217–223. doi: 10.1038/s41565-020-0636-2

Li, Y. S., Luo, W., Zhu, S. A., and Lei, G. H. (2017). T cells in osteoarthritis: alterations and beyond. *Front. Immunol.* 8:356. doi: 10.3389/fimmu.2017.00356

Lin, L. Y., and Du, L. M. (2018). The role of secreted factors in stem cells-mediated immune regulation. *Cell. Immunol.* 326, 24–32. doi: 10.1016/j.cellimm.2017.07.010

Liu, H., Liang, Z., Wang, F., Zhou, C., Zheng, X., Hu, T., et al. (2019). Exosomes from mesenchymal stromal cells reduce murine colonic inflammation via a macrophage-dependent mechanism. *JCI Insight* 4:e131273. doi: 10.1172/jci.insight.131273

Liu, X. L., Yang, Y. L., Li, Y., Niu, X., Zhao, B. Z., Wang, Y., et al. (2017). Integration of stem cell-derived exosomes with in situ hydrogel glue as a promising tissue patch for articular cartilage regeneration. *Nanoscale* 9, 4430–4438. doi: 10.1039/C7NR00352H

Liu, Y. L., Zhang, Y. J., Zheng, X. F., Zhang, X. S., Wang, H. M., Li, Q., et al. (2016). Gene silencing of indoleamine 2,3-dioxygenase 2 in melanoma cells induces apoptosis through the suppression of NAD plus and inhibits *in vivo* tumor growth. *Oncotarget* 7, 32329–32340. doi: 10.18632/oncotarget.8617

Loeser, R. F. (2013). Aging processes and the development of osteoarthritis. *Curr. Opin. Rheumatol.* 25, 108–113. doi: 10.1097/BOR.0b013e32835a9428

Luz-Crawford, P., Kurte, M., Bravo-Alegria, J., Contreras, R., Nova-Lamperti, E., Tejedor, G., et al. (2013). Mesenchymal stem cells generate a CD4+CD25+Foxp3+ regulatory T cell population during the differentiation process of Th1 and Th17 cells. *Stem Cell Res. Ther.* 4, 65. doi: 10.1186/scrt216

Ma, S., Chen, X., Wang, L., Wei, Y., Ni, Y., Chu, Y., et al. (2017). Repairing effects of ICAM-1-expressing mesenchymal stem cells in mice with autoimmune thyroiditis. *Exp. Ther. Med.* 13, 1295–1302. doi: 10.3892/etm.2017.4131

Mahdavinia, G. R., Soleymani, M., Etemadi, H., Sabzi, M., and Atlasi, Z. (2018). Model protein BSA adsorption onto novel magnetic chitosan/PVA/laponite RD hydrogel nanocomposite beads. *Int. J. Biol. Macromol.* 107, 719–729. doi: 10.1016/j.ijbiomac.2017.09.042

Mianehsaz, E., Mirzaei, H. R., Mahjoubin-Tehran, M., Rezaee, A., Sahebnasagh, R., Pourhanifeh, M. H., et al. (2019). Mesenchymal stem cell-derived exosomes: a new therapeutic approach to osteoarthritis? *Stem Cell Res. Ther.* 10:340. doi: 10.1186/s13287-019-1445-0

Min, H. K., Choi, J., Lee, S. Y., Seo, H. B., Jung, K., Na, H. S., et al. (2019). Protein inhibitor of activated STAT3 reduces peripheral arthritis and gut inflammation and regulates the Th17/Treg cell imbalance via STAT3 signaling in a mouse model of spondyloarthritis. *J. Transl. Med.* 17:18. doi: 10.1186/s12967-019-1774-x

Modinger, Y., Rapp, A. E., Vikman, A., Ren, Z. Z., Fischer, V., Bergdolt, S., et al. (2019). Reduced terminal complement complex formation in mice manifests in low bone mass and impaired fracture healing. *Am. J. Pathol* 189, 147–161. doi: 10.1016/j.ajpath.2018.09.011

Mulcahy, L. A., Pink, R. C., and Carter, D. R. (2014). Routes and mechanisms of extracellular vesicle uptake. *J. Extracell Vesicles* 3:24641. doi: 10.3402/jev.v3.24641

Murphy, N., Lynch, K., Lohan, P., Treacy, O., and Ritter, T. (2016). Mesenchymal stem cell therapy to promote corneal allograft survival: current status and pathway to clinical translation. *Curr. Opin. Organ Transplant.* 21, 559–567. doi: 10.1097/MOT.0000000000000360

Murray, P. J. (2017). Macrophage Polarization. *Annu. Rev. Physiol.* 79, 541–566. doi: 10.1146/annurev-physiol-022516-034339

Narayanaswamy, R., and Torchilin, V. P. (2019). Hydrogels and their applications in targeted drug delivery. *Molecules* 24:603. doi: 10.3390/molecules24030603

Noack, M., and Miossec, P. (2014). Th17 and regulatory T cell balance in autoimmune and inflammatory diseases. *Autoimmun. Rev.* 13, 668–677. doi: 10.1016/j.autrev.2013.12.004

Oishi, Y., and Manabe, I. (2018). Macrophages in inflammation, repair and regeneration. *Int. Immunol.* 30, 511–528. doi: 10.1093/intimm/dxy054

Oliva, N., Conde, J., Wang, K., and Artzi, N. (2017). Designing hydrogels for on-demand therapy. *Acc. Chem. Res.* 50, 669–679. doi: 10.1021/acs.accounts.6b00536

Ozeki, N., Muneta, T., Koga, H., Nakagawa, Y., Mizuno, M., Tsuji, K., et al. (2016). Not single but periodic injections of synovial mesenchymal stem cells maintain viable cells in knees and inhibit osteoarthritis progression in rats. *Osteoarthr. Cartilage* 24, 1061–1070. doi: 10.1016/j.joca.2015.12.018

Park, H. J., Kim, J., Saima, F. T., Rhee, K. J., Hwang, S., Kim, M. Y., et al. (2018). Adipose-derived stem cells ameliorate colitis by suppression of inflammasome formation and regulation of M1-macrophage population through prostaglandin E2. *Biochem. Biophys. Res. Commun.* 498, 988–995. doi: 10.1016/j.bbrc.2018.03.096

Peter, J., Sabu, V., Aswathy, I. S., Krishnan, S., Lal Preethi, S. S., Simon, M., et al. (2020). Dietary amaranths modulate the immune response via balancing Th1/Th2 and Th17/Treg response in collagen-induced arthritis. *Mol. Cell. Biochem.* 472, 57–66. doi: 10.1007/s11010-020-03783-x

Phan, A. T., Goldrath, A. W., and Glass, C. K. (2017). Metabolic and epigenetic coordination of T cell and macrophage immunity. *Immunity* 46, 714–729. doi: 10.1016/j.immuni.2017.04.016

Prockop, D. J., and Oh, J. Y. (2012). Mesenchymal stem/stromal cells (MSCs): role as guardians of inflammation. *Mol. Ther.* 20, 14–20. doi: 10.1038/mt.2011.211

Qi, C. L., Shan, Y. X., Wang, J., Ding, F. P., Zhao, D., Yang, T., et al. (2016). Circulating T helper 9 cells and increased serum interleukin-9 levels in patients with knee osteoarthritis. *Clin. Exp. Pharmacol. P* 43, 528–534. doi: 10.1111/1440-1681.12567

Rafei, M., Hsieh, J., Fortier, S., Li, M., Yuan, S., Birman, E., et al. (2008). Mesenchymal stromal cell-derived CCL2 suppresses plasma cell immunoglobulin production via STAT3 inactivation and PAX5 induction. *Blood* 112, 4991–4998. doi: 10.1182/blood-2008-07-166892

Raphael, I., Nalawade, S., Eagar, T. N., and Forsthuber, T. G. (2015). T cell subsets and their signature cytokines in autoimmune and inflammatory diseases. *Cytokine* 74, 5–17. doi: 10.1016/j.cyto.2014.09.011

Ren, G. W., Zhao, X., Zhang, L. Y., Zhang, J. M., L'Huillier, A., Ling, W. F., et al. (2010). Inflammatory cytokine-induced intercellular adhesion molecule-1 and vascular cell adhesion molecule-1 in mesenchymal stem cells are critical for immunosuppression. *J. Immunol.* 184, 2321–2328. doi: 10.4049/jimmunol.0902023

Riau, A. K., Ong, H. S., G.,Yam, H. F., and Mehta, J. S. (2019). Sustained delivery system for stem cell-derived exosomes. *Front. Pharmacol.* 10:1368. doi: 10.3389/fphar.2019.01368

Riazifar, M., Mohammadi, M., Pone, E., Yeri, A., Lässer, C., Segaliny, A., et al. (2019). Stem cell-derived exosomes as nanotherapeutics for autoimmune and neurodegenerative disorders. *ACS Nano* 13, 6670–6688. doi: 10.1021/acsnano.9b01004

Samavedi, S., Diaz-Rodriguez, P., Erndt-Marino, J. D., and Hahn, M. S. (2017). A Three-dimensional chondrocyte-macrophage coculture system to probe inflammation in experimental osteoarthritis. *Tissue Eng. Pt A* 23, 101–114. doi: 10.1089/ten.tea.2016.0007

Sato, K., Ozaki, K., Oh, I., Meguro, A., Hatanaka, K., Nagai, T., et al. (2007). Nitric oxide plays a critical role in suppression of T-cell proliferation by mesenchymal stem cells. *Blood* 109, 228–234. doi: 10.1182/blood-2006-02-002246

Schena, F., Gambini, C., Gregorio, A., Mosconi, M., Reverberi, D., Gattorno, M., et al. (2010). Interferon-γ-dependent inhibition of B cell activation by bone marrow-derived mesenchymal stem cells in a murine model of systemic lupus erythematosus. *Arthritis Rheum.* 62, 2776–2786. doi: 10.1002/art.27560

Selmani, Z., Naji, A., Zidi, I., Favier, B., Gaiffe, E., Obert, L., et al. (2008). Human leukocyte antigen-G5 secretion by human mesenchymal stem cells is required to suppress T lymphocyte and natural killer function and to induce CD4(+)CD25(high)FOXP3(+) regulatory T cells. *Stem Cells.* 26, 212–222. doi: 10.1634/stemcells.2007-0554

Shen, B., Liu, J., Zhang, F., Wang, Y., Qin, Y., Zhou, Z., et al. (2016). CCR2 Positive exosome released by mesenchymal stem cells suppresses macrophage functions and alleviates ischemia/reperfusion-induced renal injury. *Stem Cells Int.* 2016:1240301. doi: 10.1155/2016/1240301

Shi, X., Chen, Q., and Wang, F. (2019). Mesenchymal stem cells for the treatment of ulcerative colitis: a systematic review and meta-analysis of experimental and clinical studies. *Stem Cell Res. Ther.* 10:266. doi: 10.1186/s13287-019-1336-4

Shi, Y., Wang, Y., Li, Q., Liu, K., Hou, J., Shao, C., et al. (2018). Immunoregulatory mechanisms of mesenchymal stem and stromal cells in inflammatory diseases. *Nat. Rev. Nephrol.* 14, 493–507. doi: 10.1038/s41581-018-0023-5

Smyth, T., Kullberg, M., Malik, N., Smith-Jones, P., Graner, M. W., and Anchordoquy, T. J. (2015). Biodistribution and delivery efficiency of unmodified tumor-derived exosomes. *J. Control. Release* 199, 145–155. doi: 10.1016/j.jconrel.2014.12.013

Song, Y., Dou, H., Li, X., Zhao, X., Li, Y., Liu, D., et al. (2017). Exosomal miR-146a contributes to the enhanced therapeutic efficacy of interleukin-1β-primed mesenchymal stem cells against sepsis. *Stem Cells* 35, 1208–1221. doi: 10.1002/stem.2564

Sun, G., Li, G., Li, D., Huang, W., Zhang, R., Zhang, H., et al. (2018). hucMSC derived exosomes promote functional recovery in spinal cord injury mice via attenuating inflammation. *Mater. Sci. Eng. C Mater. Biol. Appl.* 89, 194–204. doi: 10.1016/j.msec.2018.04.006

Tabera, S., Perez-Simon, J. A., Diez-Campelo, M., Sanchez-Abarca, L. I., Blanco, B., Lopez, A., et al. (2008). The effect of mesenchymal stem cells on the

viability, proliferation and differentiation of B-lymphocytes. *Haematologica* 93, 1301–1309. doi: 10.3324/haematol.12857

Ti, D., Hao, H., Tong, C., Liu, J., Dong, L., Zheng, J., et al. (2015). LPS-preconditioned mesenchymal stromal cells modify macrophage polarization for resolution of chronic inflammation via exosome-shuttled let-7b. *J. Transl. Med.* 13:308. doi: 10.1186/s12967-015-0642-6

Tomchuck, S. L., Zwezdaryk, K. J., Coffelt, S. B., Waterman, R. S., Danka, E. S., and Scandurro, A. B. (2008). Toll-like receptors on human mesenchymal stem cells drive their migration and immunomodulating responses. *Stem Cells* 26, 99–107. doi: 10.1634/stemcells.2007-0563

Utomo, L., Bastiaansen-Jenniskens, Y., Verhaar, J., and van Osch, G. J. (2016). Cartilage inflammation and degeneration is enhanced by pro-inflammatory (M1) macrophages *in vitro*, but not inhibited directly by anti-inflammatory (M2) macrophages. *Osteoarthr. Cartilage* 24, 2162–2170. doi: 10.1016/j.joca.2016.07.018

Vizoso, F. J., Eiro, N., Cid, S., Schneider, J., and Perez-Fernandez, R. (2017). Mesenchymal stem cell secretome: toward cell-free therapeutic strategies in regenerative medicine. *Int. J. Mol. Sci.* 18:1852. doi: 10.3390/ijms18091852

Wang, M., Yuan, Q., and Xie, L. (2018). Mesenchymal stem cell-based immunomodulation: properties and clinical application. *Stem Cells Int.* 2018:3057624. doi: 10.1155/2018/3057624

Wei, Z., Qiao, S., Zhao, J., Liu, Y., Li, Q., Wei, Z., et al. (2019). miRNA-181a over-expression in mesenchymal stem cell-derived exosomes influenced inflammatory response after myocardial ischemia-reperfusion injury. *Life Sci.* 232:116632. doi: 10.1016/j.lfs.2019.116632

Willis, G., Fernandez-Gonzalez, A., Anastas, J., Vitali, S., Liu, X., Ericsson, M., et al. (2018). Mesenchymal stromal cell exosomes ameliorate experimental bronchopulmonary dysplasia and restore lung function through macrophage immunomodulation. *Am. J. Respir. Crit. Care Med.* 197, 104–116. doi: 10.1164/rccm.201705-0925OC

Willis, G. R., Kourembanas, S., and Mitsialis, S. A. (2017). Toward exosome-based therapeutics: isolation, heterogeneity, and fit-for-purpose potency. *Front. Cardiovasc. Med.* 4:63. doi: 10.3389/fcvm.2017.00063

Woodell-May, J. E., and Sommerfeld, S. D. (2020). Role of inflammation and the immune system in the progression of Osteoarthritis. *J. Orthop. Res.* 38, 253–257. doi: 10.1002/jor.24457

Wu, C., McNeill, J., Goon, K., Little, D., Kimmerling, K., Huebner, J., et al. (2017). Conditional macrophage depletion increases inflammation and does not inhibit the development of osteoarthritis in obese macrophage fas-induced apoptosis-transgenic mice. *Arthritis Rheumatol.* 69, 1772–1783. doi: 10.1002/art.40161

Wu, C. L., Harasymowicz, N. S., Klimak, M. A., Collins, K. H., and Guilak, F. (2020). The role of macrophages in osteoarthritis and cartilage repair. *Osteoarthr. Cartilage* 28, 544–554. doi: 10.1016/j.joca.2019.12.007

Wu, X., Wang, Y., Xiao, Y., Crawford, R., Mao, X., and Prasadam, I. (2020). Extracellular vesicles: potential role in osteoarthritis regenerative medicine. *J. Orthop. Translat.* 21, 73–80. doi: 10.1016/j.jot.2019.10.012

Wynn, T. A., and Vannella, K. M. (2016). Macrophages in tissue repair, regeneration, and fibrosis. *Immunity* 44, 450–462. doi: 10.1016/j.immuni.2016.02.015

Yamashita, T., Takahashi, Y., and Takakura, Y. (2018). Possibility of exosome-based therapeutics and challenges in production of exosomes eligible for therapeutic application. *Biol. Pharm. Bull.* 41, 835–842. doi: 10.1248/bpb.b18-00133

Yang, Y., Zhang, X., Xu, M., Wu, X., Zhao, F., and Zhao, C. (2018). Quercetin attenuates collagen-induced arthritis by restoration of Th17/Treg balance and activation of Heme Oxygenase 1-mediated anti-inflammatory effect. *Int. Immunopharmacol.* 54, 153–162. doi: 10.1016/j.intimp.2017.11.013

Ylostalo, J. H., Bartosh, T. J., Coble, K., and Prockop, D. J. (2012). Human mesenchymal stem/stromal cells cultured as spheroids are self-activated to produce prostaglandin E2 that directs stimulated macrophages into an anti-inflammatory phenotype. *Stem Cells* 30, 2283–2296. doi: 10.1002/stem.1191

Zhang, B., Yeo, R., Lai, R., Sim, E., Chin, K., and Lim, S. (2018). Mesenchymal stromal cell exosome-enhanced regulatory T-cell production through an antigen-presenting cell-mediated pathway. *Cytotherapy* 20, 687–696. doi: 10.1016/j.jcyt.2018.02.372

Zhang, H. Y., Lin, C. X., Zeng, C., Wang, Z. Y., Wang, H., Lu, J. S., et al. (2018). Synovial macrophage M1 polarisation exacerbates experimental osteoarthritis partially through R-spondin-2. *Ann. Rheum. Dis.* 77, 1524–1534. doi: 10.1136/annrheumdis-2018-213450

Zhang, K., Zhao, X., Chen, X., Wei, Y., Du, W., Wang, Y., et al. (2018). Enhanced therapeutic effects of mesenchymal stem cell-derived exosomes with an injectable hydrogel for hindlimb ischemia treatment. *ACS Appl. Mater. Interfaces* 10, 30081–30091. doi: 10.1021/acsami.8b08449

Zhang, S., Chuah, S. J., Lai, R. C., Hui, J. H. P., Lim, S. K., and Toh, W. S. (2018). MSC exosomes mediate cartilage repair by enhancing proliferation, attenuating apoptosis and modulating immune reactivity. *Biomaterials* 156, 16–27. doi: 10.1016/j.biomaterials.2017.11.028

Zhao, H., Shang, Q., Pan, Z., Bai, Y., Li, Z., Zhang, H., et al. (2018). Exosomes from adipose-derived stem cells attenuate adipose inflammation and obesity through polarizing M2 macrophages and beiging in white adipose tissue. *Diabetes* 67, 235–247. doi: 10.2337/db17-0356

Zhao, J., Li, X., Hu, J., Chen, F., Qiao, S., Sun, X., et al. (2019). Mesenchymal stromal cell-derived exosomes attenuate myocardial ischaemia-reperfusion injury through miR-182-regulated macrophage polarization. *Cardiovasc. Res.* 115, 1205–1216. doi: 10.1093/cvr/cvz040

Zhao, L., Chen, S., Yang, P., Cao, H., and Li, L. (2019). The role of mesenchymal stem cells in hematopoietic stem cell transplantation: prevention and treatment of graft-versus-host disease. *Stem Cell Res. Ther.* 10:182. doi: 10.1186/s13287-019-1287-9

Zhu, W., Zhang, X., Jiang, Y., Liu, X., Huang, L., Wei, Q., et al. (2020). Alterations in peripheral T cell and B cell subsets in patients with osteoarthritis. *Clin. Rheumatol.* 39, 523–532. doi: 10.1007/s10067-019-04768-y

Conflict of Interest: The authors declare that the research was conducted in the absence of any commercial or financial relationships that could be construed as a potential conflict of interest.

frontiers in Bioengineering and Biotechnology

ORIGINAL RESEARCH
published: 26 November 2020
doi: 10.3389/fbioe.2020.600032

Histological and Histomorphometric Evaluation of Applying a Bioactive Advanced Platelet-Rich Fibrin to a Perforated Schneiderian Membrane in a Maxillary Sinus Elevation Model

Liangjing Xin, Shuai Yuan, Zhixiang Mu, Dize Li, Jinlin Song and Tao Chen**

Chongqing Key Laboratory of Oral Diseases and Biomedical Sciences, Chongqing Municipal Key Laboratory of Oral Biomedical Engineering of Higher Education, Stomatological Hospital of Chongqing Medical University, Chongqing, China

Background: Schneiderian membrane (SM) perforation is a major complication of maxillary sinus elevation with simultaneous bone grafting, yet under this scenario there is no standard biomaterial that maximizes favorable tissue healing and osteogenic effects.

Purpose: To compare the effect of advanced platelet-rich fibrin (A-PRF) and collagen membrane (CM) on a perforated SM with simultaneous bone grafting in a maxillary sinus elevation model.

Materials and Methods: After perforation of the SM was established, 24 animals were randomly divided into two groups: (i) group CM: CM and deproteinized bovine bone mineral (DBBM) (n = 12), (ii) group A-PRF: A-PRF and DBBM (n = 12). Radiographic and histological evaluations were performed at 1 and 4 weeks post-operation.

Results: At 1 week, an intact SM was found in group A-PRF. At each time point, the number of inflammatory cells at the perforated site was higher in group CM, and the area of new osteoid formation was significantly greater in group A-PRF ($p < 0.0001$). At 4 weeks, the osteogenic pattern was shown as from the periphery to the center of the sinus cavity in group A-PRF.

Conclusion: The higher elasticity, matching degradability, and plentiful growth factors of A-PRF resulted in a fully repaired SM, which later ensured the two osteogenic sources from the SM to generate significant new bone formation. Thus, A-PRF can be considered to be a useful bioactive tissue-healing biomaterial for SM perforation with simultaneous bone grafting.

Keywords: Schneiderian membrane, advanced platelet-rich fibrin, collagen membrane, perforation, animal models

OPEN ACCESS

Edited by:
Xuetao Shi,
South China University of Technology, China

Reviewed by:
Sergio Alexandre Gehrke,
BioTecnos, Uruguay
Juan Manuel Aragoneses,
University Federico Henriquez y Carvajal, Dominican Republic

****Correspondence:***
Jinlin Song
Songjinlin@hospital.cqmu.edu.cn
Tao Chen
chentao1985@hospital.cqmu.edu.cn

Specialty section:
This article was submitted to Biomaterials, a section of the journal Frontiers in Bioengineering and Biotechnology

Received: *28 August 2020*
Accepted: *23 October 2020*
Published: *26 November 2020*

Citation:
Xin L, Yuan S, Mu Z, Li D, Song J and Chen T (2020) Histological and Histomorphometric Evaluation of Applying a Bioactive Advanced Platelet-Rich Fibrin to a Perforated Schneiderian Membrane in a Maxillary Sinus Elevation Model. Front. Bioeng. Biotechnol. 8:600032. doi: 10.3389/fbioe.2020.600032

INTRODUCTION

Long-term loss of the maxillary posterior teeth often leads to a series of complications, such as maxillary sinus pneumatization and ridge atrophy. These conditions may increase the implant failure rate (Asai et al., 2002; Stricker et al., 2003; Wallace and Froum, 2003; Sorní et al., 2005; Tajima et al., 2013). To manage unfavorable results, clinicians often adopt maxillary sinus floor elevation

to increase the bone volume of the atrophic maxilla and ensure successful implant placement (Schwartz-Arad et al., 2004; Hallman et al., 2005).

However, despite accurate preoperative radiographic investigations and surgical maneuvers, Schneiderian membrane (SM) perforation can occur during the elevation process, and it has a reported incidence of 56% (Aricioglu et al., 2017). Irregular morphology of the maxillary sinus and the fragile characteristics of the SM contribute to this unfavorable outcome (Schwartz-Arad et al., 2004; Misch and Wang, 2008; Schwarz et al., 2015; Wen et al., 2015). The perforation of the SM may lead to severe complications including the suspension of a surgical process, acute maxillary sinusitis, and an unpredictable survival rate of the dental implants (Cho et al., 2001; Timmenga et al., 2003; Proussaefs et al., 2004; Anavi et al., 2008; Becker et al., 2008).

The treatment of the perforation during sinus elevation depends on the perforation size. When the perforation is less than 5 mm (Hernández-Alfaro et al., 2008), the most common repair procedure is to use an absorbable collagen membrane (CM), which minimizes the risk of infection and usually achieves satisfactory clinical results (Aimetti et al., 2001; Proussaefs et al., 2004; Ardekian et al., 2006; Pikos, 2008). Lim et al. (2018) confirmed that the absorbable CM greatly reduced infection in the sinus cavity and could be used as repair material for SM perforation.

Nevertheless, the dense structure of the CM might block the osteogenesis of the SM. The SM is a possible source of osteogenesis in the maxillary sinus (Srouji et al., 2009; Jung et al., 2015; Mu et al., 2020), and the implantation of an absorbable CM might slow new bone formation in the sinus cavity (Gruber et al., 2004; Palma et al., 2006). Although CMs have been widely used to repair SM perforation, it is not clear if the degradation and mechanical properties of the CM are compatible with the repair process. In addition, its high cost and potential foreign body reaction caused by its porcine sources are issues (Schorn et al., 2019).

Platelet-rich fibrin (PRF), as a self-clotted preparation of platelet-concentrated and autologous blood–derived biomaterial, has been advocated in several studies and produced favorable outcomes for SM perforation during maxillary sinus floor elevation (Panda et al., 2014; Zhao et al., 2015). Advanced PRF (A-PRF) is one of several PRF derivatives, produced by a relatively lower speed centrifugation process (Aizawa et al., 2020). Because of this specific preparation process, the three-dimensional fibrin matrix is more porous than that of the original PRF, and more growth factors, leukocytes, and platelets are "trapped" in its fibrin matrix structure (Lundquist et al., 2008; Ghanaati et al., 2014; Nishimoto et al., 2015; Takeda et al., 2015; Masuki et al., 2016). The trapping ensures that significant amounts of growth factors are present and slowly release (Choukroun et al., 2006; Masuki et al., 2016; Isobe et al., 2017). The fibrin matrix with porous structure could mimic the extracellular matrix, creating an optimal environment for cell adhesion and migration (Choukroun et al., 2006; Roy et al., 2011; Pradeep et al., 2012; Ghanaati et al., 2014; Aricioglu et al., 2017). These studies suggest that A-PRF would function not only as a physical membrane for the perforated site but also as a bioactive tissue-healing "factory" to deliver growth factors for soft and hard tissue repair.

Although an animal study (Aricioglu et al., 2017) has demonstrated that PRF could be used as a substitute for CM in repairing SM perforations, no previous studies have focused on the repair capabilities of CM and A-PRF regarding simultaneous bone grafting. We therefore evaluated the effectiveness of A-PRF and CM for SM repair with bone grafting simultaneously in a rabbit model.

MATERIALS AND METHODS

Preparation of A-PRF

A-PRF was prepared as previously described (Aizawa et al., 2020). Briefly, 9 mL of autologous blood was taken from the central ear artery of a rabbit and collected into tubes (Plain BD Vacutainer Tube; Becton, Dickinson and Company, Franklin Lakes, NJ, United States) free from anticoagulant. The samples were produced using a programmed Duo Quattro centrifugation system (Process for PRF, Nice, France) with 200 × *g* for 14 min. Then, three layers emerged in the anticoagulant-free tube. Acellular plasma was separated, and the red blood cells attached to the A-PRF were removed with a knife (**Supplementary Figure S1A**). After eliminating the red blood cells, A-PRF was compressed to a thin film (**Supplementary Figure S1B**) using a compression device (the PRF Box, Process, Nice, France), as shown in **Supplementary Figure S1C**.

Characterization of CM and A-PRF

Scanning Electron Microscopy

CM and A-PRF were both fixed with 2.5% neutralized glutaraldehyde, dehydrated with a series of ethanol solutions and t-butanol, freeze-dried, and then examined under a scanning electron microscope (SEM) (FEI, Quanta 450, United States) with an accelerating voltage of 15 kV.

Mechanical Testing

The compressed A-PRF, moist CM, and the natural SM were selected for mechanical testing. All membranes were cut into 20 × 5-mm (length × width) rectangular strips for mechanical testing of elasticity. The mechanical properties of different membranes were measured at a stretching speed of 1 mm/min with a desktop universal testing machine (E43, MTS Instrument, United States), where the maximum load cell capacity was 100 N under standard ambient conditions at 25°C ± 3°C and 50 ± 25% relative humidity (RH). The elastic modulus was defined as the average slope of the initial part (0–10% strain) of the stress–strain curve.

Animal Model

Animal experiment protocols were approved by the Animal Ethics Committee of Chongqing Medical University (CQHS-IRB-2018-07) and were conducted according to National Institutes of Health guidelines. We used 24 male New Zealand rabbits with weights ranging from 3 to 3.5 kg. After the SM perforation was established, rabbits were randomly divided into

two groups: (i) group CM: CM and deproteinized bovine bone mineral (DBBM) (n = 12), (ii) group A-PRF: A-PRF and DBBM (n = 12). The effect of each group (n = 6, respectively) was assessed at two healing time points that were 1 and 4 weeks post-operation.

Animal Surgery

The placement of the materials on the perforated SM is illustrated in **Figure 1**. All operations were performed under sterile conditions by one surgeon (Liangjing Xin). The 24 rabbits were subjected to the maxillary sinus floor elevation process as previously described (Mu et al., 2020). In detail, the rabbits were anesthetized using 30 mg/kg xylazine hydrochloride (Rompun; Bayer, Seoul, Korea). Surgical sites were shaved and disinfected with an iodine solution. Local anesthesia was used to minimize pain at the surgical site using 2% lidocaine HCl (20 mg/kg; Huons, Sungnam, Korea). An incision was made from the nose to eye level to expose the nasal bone. Symmetrical bone defects were created using a circular drill (drill diameter = 5 mm), and the bone plates were removed. Entering through these openings, the SM was detached and elevated from the bony walls. Afterward, a perforation was made using a blade in a sagittal direction (perforation diameters = 3 mm/half of the extension of osteotomy; Lim et al., 2018). In group CM, an absorbable CM (Bio-Gide; Geistlich Pharma, Wolhusen, Switzerland) was cut into a 10 × 10-mm section and placed onto the perforated SM, extending onto the lateral and medial sinus bone walls. Autologous blood was taken, and A-PRF was obtained according to the protocol above. A-PRF was compressed and cut into 10 × 10-mm pieces and then placed onto the SM perforation correspondingly. All sinus cavities were grafted using a standardized amount (0.2 cc) of DBBM (Bio-Oss; Geistlich Pharma) (**Figure 2**). Finally, the bone defect was covered with a bone plate, and the wound was closed using absorbable monofilament (Vicryl 5-0; Ethicon, MA, United States).

Animals in the 4-week groups were subcutaneously injected with tetracycline (TE, 25 mg/kg; Sigma, St. Louis, MO, United States), calcein (CA, 25 mg/kg; Sigma), and alizarin complexone (AL, 30 mg/kg; Sigma) at the first, second, and third week post-operation, respectively, to observe the osteogenic patterns.

The rabbits were monitored, and antibiotics and analgesics were administered on the first 3 d post-operation.

Sacrifice and Sample Collection

At the 1- and 4-week healing time points, rabbits were euthanized by injection of sodium pentobarbital (Sigma-Aldrich, St. Louis, MO, United States) through the central ear artery. The maxillary sinus samples were collected and processed for micro–computed tomographic (micro-CT) analysis and histological evaluation.

Micro–Computed Tomographic Analysis

The 4-week post-operation maxillary sinus samples were analyzed using a micro-CT (vivaCT80; SCANCO Medical AG, Switzerland). The scanning condition was acquired at a resolution 14.91 μm (130 kV and 60 μA). Three-dimensional reconstruction of the interest areas was performed withμCT80 (SCANCO Medical AG).

Histological Analysis

Half of the specimens in the 4-week groups were obtained and dehydrated in a graded series of ethanol and embedded in methyl methacrylate (M55909; Sigma). Subsequently, the specimens were prepared using the Hard Tissue Sawing System (E200CP; EXAKT Verteriebs, Germany). Tissue slices were observed with a fluorescent microscope (Olympus, Tokyo, Japan) for fluorescent labeling. Finally, the samples were stained with Van Gieson (VG). In addition, the 12 specimens at 1 and 4 weeks post-operation were decalcified and embedded in paraffin. They were then stained with Picro-Sirius red stain for observation of re-epithelialization during SM repair. Hematoxylin-eosin (H&E) staining was used to evaluate early and later inflammatory responses. Aniline blue and osteocalcin immunohistochemical staining (IHC) were also used to assess formation of new bone. Osteoclast activity was observed using tartrate-resistant acid phosphatase (TRAP) staining.

Histomorphometric Analysis

The tissue sections showed that the fracture of the basal bone corresponded to the perforated area of the SM (**Supplementary Figures S2A,B**), and the regions of interest (ROIs) were under the perforated SM area (ROIa) and underneath the CM and A-PRF (ROIb). Histomorphometric calculation of tissue sections, which were stained with H&E, aniline blue, IHC, and TRAP, was conducted using a Olympus Research System Microscope BX51 (Olympus). The healing patterns of the perforated SM were analyzed. For the stained images, histomorphometric analysis included the following parameters:

- Relative proportion of different cells (%): the percentage of pixels (inflammatory cells, fibroblasts, eosinophils) in the ROIa according to H&E staining.
- The area of new osteoid formation (%): blue-stained mineralized tissue area including osteocytes with the use of aniline blue staining, which is described as a percentage of the whole ROI for semiquantitative analysis (ROIa at 4-week groups, ROIb at 1-week groups).
- Relative expression of osteocalcin (%): percentage of pixels associated with deeply stained osteocalcin-positive cells in the ROIa by IHC staining.
- The relative expression of osteoclasts (%): osteoclasts are recognized as the TRAP-positive cells with the use of TRAP staining sections, which are expressed as a percentage of the ROI for semiquantitative analysis (ROIa at 4-week groups, ROIb at 1-week groups).

Statistical Analysis

All data had a normal distribution and were analyzed using SPSS Statistics version 20.0 (IBM Corp., Armonk, NY). Statistical analysis was performed by Student t-tests using GraphPad Software v6 (GraphPad Software, La Jolla, CA, United States), and statistical significance was considered at $p < 0.05$. All data are expressed as the mean ± standard deviation.

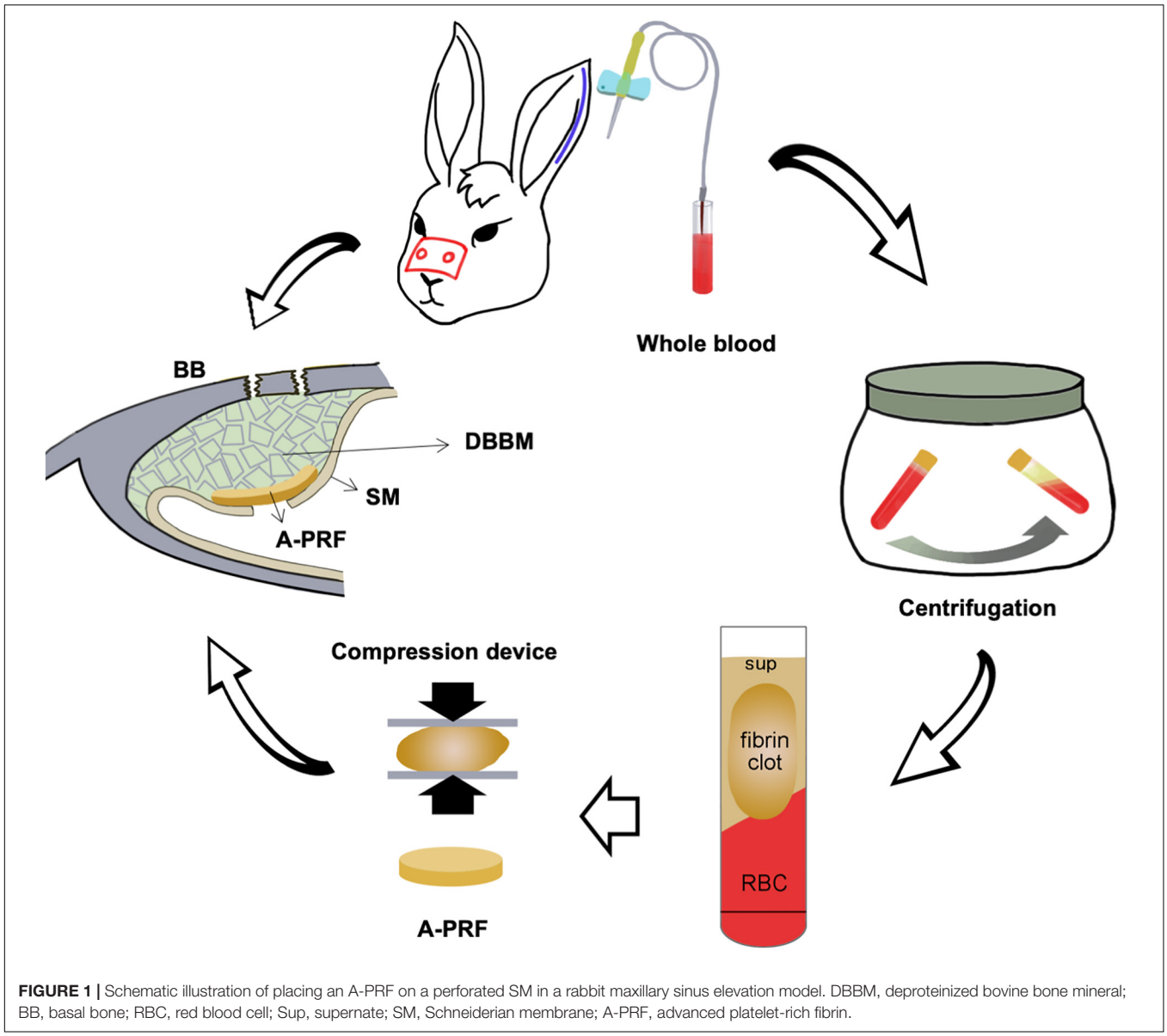

FIGURE 1 | Schematic illustration of placing an A-PRF on a perforated SM in a rabbit maxillary sinus elevation model. DBBM, deproteinized bovine bone mineral; BB, basal bone; RBC, red blood cell; Sup, supernate; SM, Schneiderian membrane; A-PRF, advanced platelet-rich fibrin.

RESULTS

Clinical Findings

All experimental animals undergoing surgical procedures maintained a healthy status throughout the entire experimental period. No complications were observed during the postoperative period.

Characterization of CM and A-PRF

Microstructures of CM and A-PRF were examined by SEM. As shown in **Figure 3A**, the fibrin matrix within A-PRF was thicker and denser than that within the CM. In the cross section, the CM microstructure showed two different layers. Most of the collagen fibers in the front layer were close to each other, indicating a low porosity with a smooth surface. The back layer showed an uneven distribution of collagen fibers, which had a more porous appearance with a rough surface. Collagen fibers were also larger in diameter and arranged in bundles. Nevertheless, both the front and back layers of A-PRF showed reticular and porous microstructures, which were significantly softer and looser than those of CM. The fibronectin was slender and staggered in A-PRF.

Tensile properties among CM, A-PRF, and the natural SM are shown in the stress–strain plot (**Figure 3B**). The yield strain was about 51.2 ± 0.1% in CM, 109.7 ± 0.3% in A-PRF, and 43.3 ± 0.2% in the natural SM. The yield strain in A-PRF was significantly higher than that in CM ($p < 0.0001$), indicating that A-PRF had superior elasticity.

Histological Analysis

A dome-shaped space was observed in the elevated maxillary sinus in two groups (**Supplementary Figures S2A,B**). The DBBM

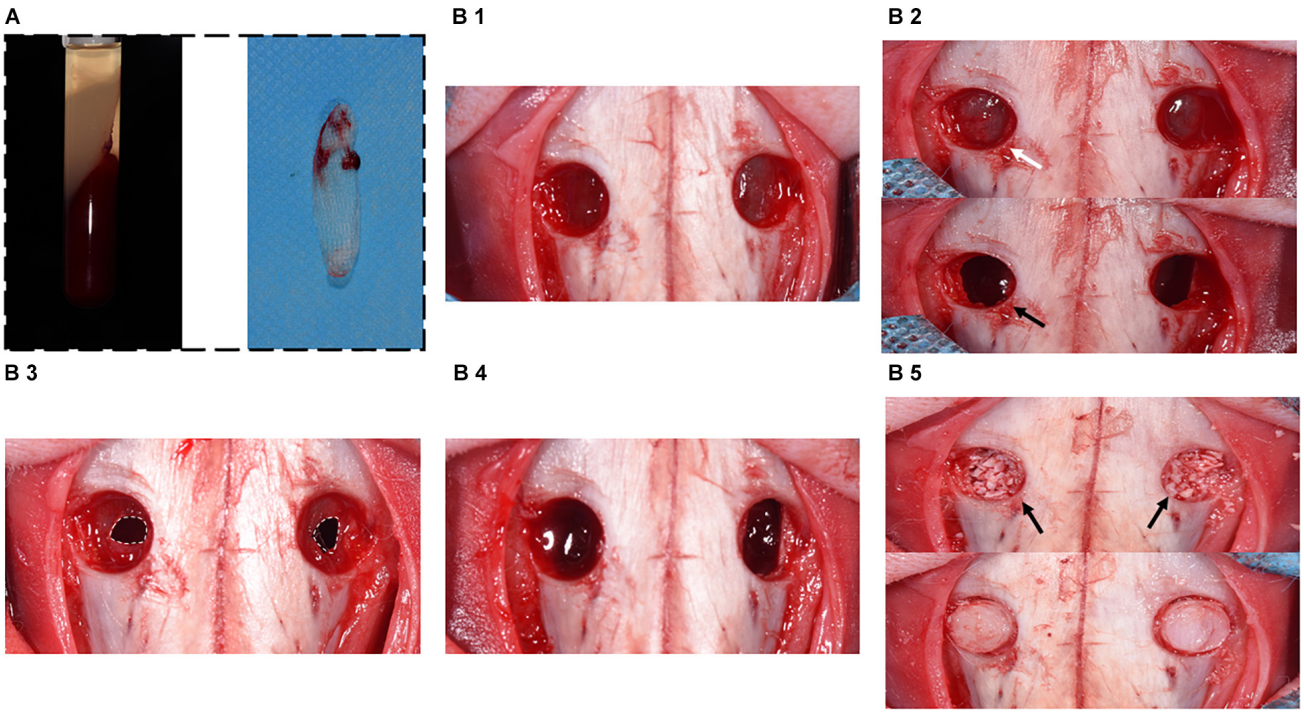

FIGURE 2 | Surgical procedure diagram in a perforated SM model. **(A)** Preparation of A-PRF. **(B1)** Symmetrical bone defects were obtained, and bone plates were acquired correspondingly. **(B2)** SM was detached and elevated from bony walls (marked with white arrow). Rhythmic movement of SM during respiration (black arrow). **(B3)** SM was perforated with a 1-cm incision (marked with the white dotted box). **(B4)** CM or A-PRF was placed onto the perforated SM. **(B5)** The sinuses were filled with DBBM (marked with black arrows). Finally, the bone defects were covered with bone plates.

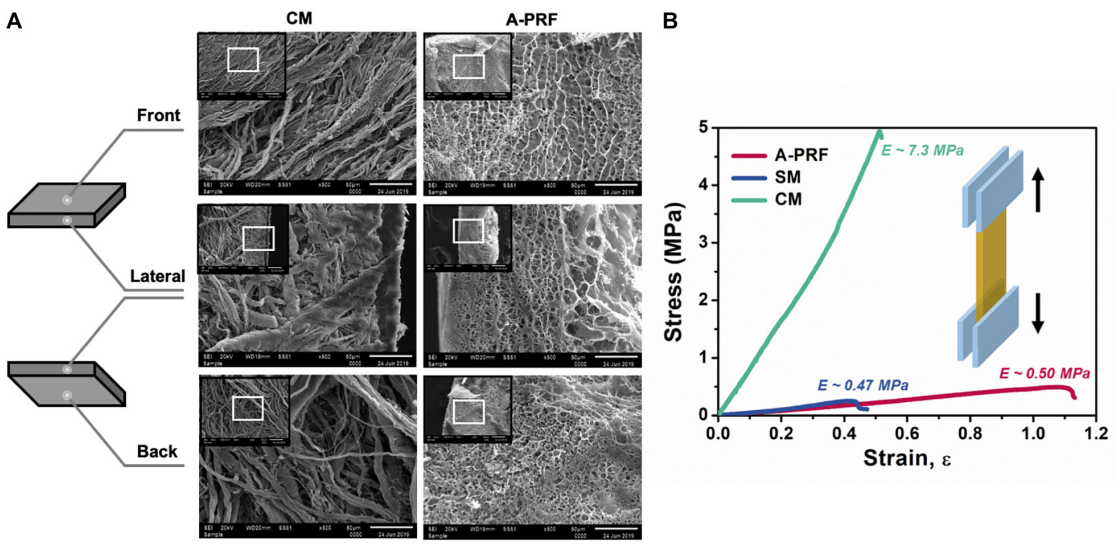

FIGURE 3 | The characterization of CM and A-PRF. **(A)** Representative microstructural images of the freeze-dried CM and A-PRF at different layers (scale bar = 50 μm). **(B)** The representative stress–strain curves of tensile test on CM, A-PRF, and the natural SM. CM, collagen membrane; A-PRF, advanced platelet-rich fibrin; SM, Schneiderian membrane.

was well-distributed within the sinus cavity, and the fracture of the basal bone corresponded exactly to the perforated area. A-PRF was not observed at the repaired site, while CM was found intact under the SM (**Figure 4A**).

H&E staining (**Figure 4B**) revealed an intact SM in group A-PRF, showing that, at the perforated site, a pseudostratified columnar ciliated epithelium facing the sinus cavity comprised a plentiful vascularized lamina propria and a deeper layer of

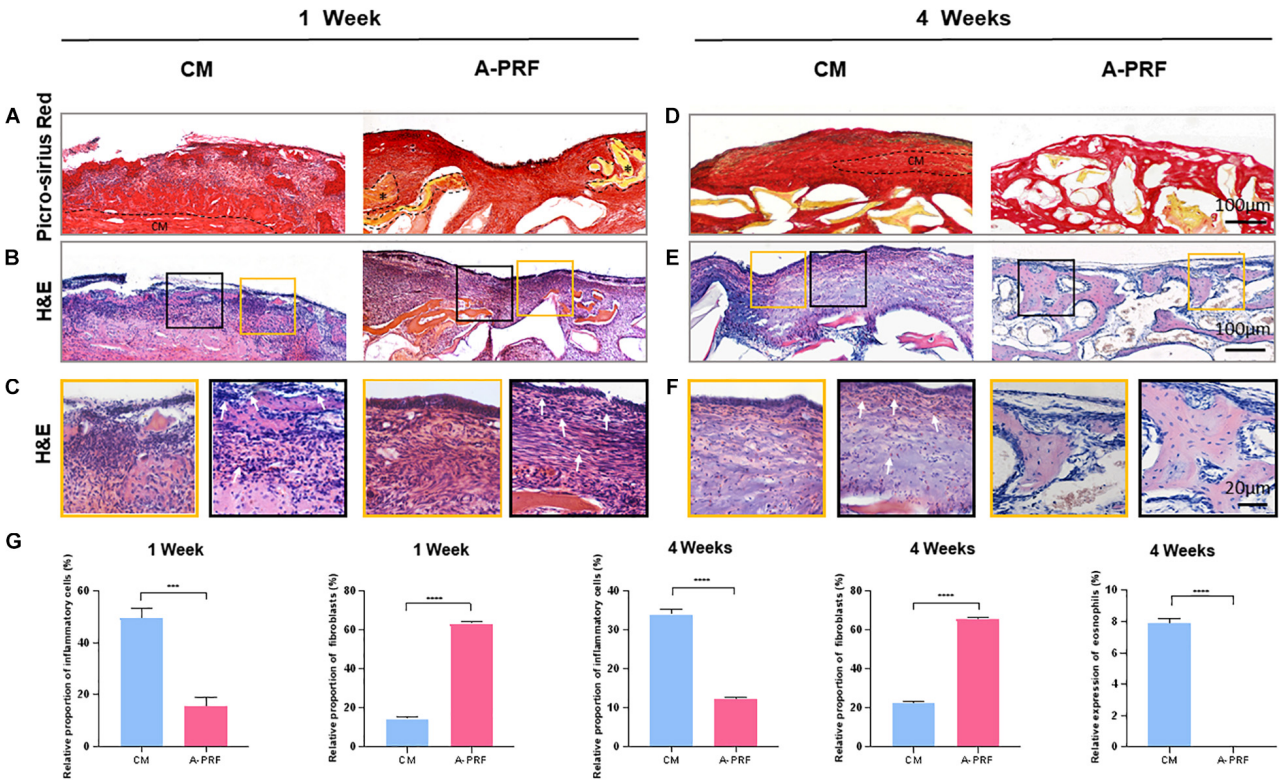

FIGURE 4 | Histological and histomorphometric analysis of soft tissue healing under the perforated SM at 1 and 4 weeks. **(A)** Picro-Sirius red staining on group CM and A-PRF at 1 week post-operation (A-PRF marked with *). **(B)** H&E staining at 1 week post-operation. **(C)** Two ROIs (yellow box and black box) selected to further observe the microscopic components of **(B)**. **(D)** Picro-Sirius red staining at 4 weeks (the dotted box represented the residual CM). **(E)** H&E staining evaluating later inflammatory responses in each group. **(F)** Two ROIs (yellow box and red box) of **(E)**. **(G)** Semiquantitative analysis of the inflammatory reaction at 1 and 4 weeks by measuring the proportion of inflammatory cells, fibroblasts and eosinophils ($n = 3$, $^{***}p < 0.001$, $^{****}p < 0.0001$). CM, collagen membrane; A-PRF, advanced platelet-rich fibrin; ROIs, regions of interest.

periosteum-like components (**Figure 4C**, yellow box); however, this structure was not observed in group CM. In addition, the aggressive infiltration of inflammatory cells (marked with white arrows) was dispersed (**Figure 4C**, black box), suggesting that a severe inflammatory response occurred under the perforated SM in group CM. An increasing number of newborn fibroblasts (spindle-shaped or flat star-shaped with protrusions, marked with white arrows) occurred in group A-PRF at 1 week post-operation (**Figure 4C**, black box). This indicated that the early inflammation stage was replaced by the tissue repair process.

Micro-CT (**Supplementary Figures S2C1–2**) reconstruction was performed to simulate the sinus cavity at 4 weeks post-operation. No leakage of DBBM was observed, and the perforated site was completely repaired.

As shown by Picro-Sirius red staining at 4 weeks post-operation (**Figure 4D**), the CM did not completely degrade, and the newly reconstructed mucosa significantly thickened in group CM because of the inflammatory response (the dotted box represents the residual CM in **Figure 4D**). However, in group A-PRF, the perforated SM repaired with A-PRF was completely degraded. To study the internal mechanism of this phenomenon, H&E staining (**Figure 4E**) was performed on 4-week sections. At high magnification (**Figure 4F**), pseudostratified columnar ciliated epithelium was not observed (yellow box), and a large amount of inflammatory cell infiltration (black box) was observed underneath the SM in group CM. Eosinophils (typical lobulated nuclei, containing eosinophilic granules in the cytoplasm, marked with white arrows) and inflammatory cells formed an infiltration zone surrounding residual non-degraded CM (black box). In contrast, the newly repaired mucosa resembled the natural SM (yellow box) and had a large number of fibroblasts (black box) in group A-PRF.

Based on aniline blue staining (**Figure 5A**), there was little blue-stained mineralized tissue underneath the CM, which showed the least amount of new bone formation at 1 week in group CM. In contrast, the representative histological sections (black arrows) underneath A-PRF revealed a small amount of new bone formation in group A-PRF at an early stage. In TRAP staining (**Figure 5B**), few osteoclasts were seen around the DBBM at 1 week in group CM. However, a few osteoclasts that infiltrated around the DBBM occurred in group A-PRF. Aniline blue staining at 4 weeks post-operation (**Figure 5D**) showed little new bone formation in group CM, while evident blue-stained mineralized tissue was observed under the SM in group A-PRF.

In IHC, group A-PRF exhibited strongly osteocalcin-positive cells under the SM, whereas almost no positive expression

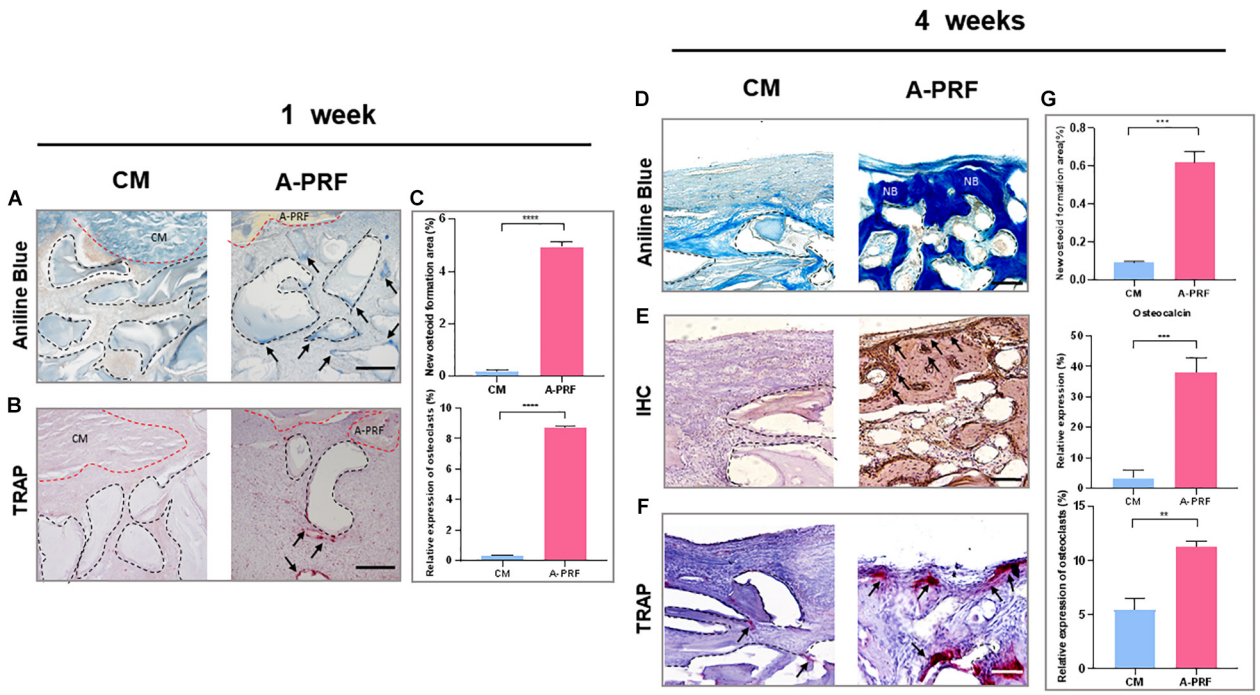

FIGURE 5 | Histological and histomorphometric analysis of new bone formation under SM area at 1 and 4 weeks. **(A)** Aniline blue staining for assessing new bone formation in group CM and A-PRF at 1 week (blue-stained mineralized tissues were marked with black arrows; black dotted boxes represented DBBM, scale bar: 100 μm). **(B)** TRAP staining for the osteoclast activity at 1 week (TRAP-positive cells were marked with black arrows, scale bar: 100 μm). **(C)** Semiquantitative analysis regarding new osteoid formation and the relative expression of osteoclast area at 1 week ($n = 3$, $^{****}p < 0.0001$). Aniline blue staining **(D)**, IHC **(E)**, and TRAP staining **(F)** were performed to further reveal bone remodeling in group CM and A-PRF at 4 weeks (scale bar: 50 μm). **(G)** Semiquantitative analysis regarding new osteoid formation, relative expression of osteocalcin, osteoclast area at 4 weeks post-operation ($n = 3$, $^{**}p < 0.01$, $^{***}p < 0.001$). CM, collagen membrane; A-PRF, advanced platelet-rich fibrin; DBBM, deproteinized bovine bone mineral; NB, new bone.

was shown in group CM (**Figure 5E**). In TRAP staining at 4 weeks (**Figure 5F**), little TRAP-positive cell expression and low osteoclast activity were observed under the SM in group CM. In contrast, many more osteoclasts were detected underneath the SM, suggesting active bone remodeling in group A-PRF.

While distinguishing the osteogenic patterns in each group, a fluorochrome label of new bone mineralization was detected. Weak fluorescence signals were observed in group CM, whereas group A-PRF displayed stronger fluorescence intensity (**Figure 6A**). The fluorescence signals were randomly scattered in the basal bone in group CM (**Figure 6B**, blue box). However, the three-color fluorescence signals were distributed both in the basal bone (**Figure 6B**, blue box) and underneath the SM (**Figure 6B**, pink box) in group A-PRF. VG staining (**Figure 6C**) revealed a large amount of new bone formation near the basal bone in the two groups, whereas the new bone growth was generated from the periphery to the center of the sinus cavity in group A-PRF.

Histomorphometric Analysis

The relative proportion of inflammatory cells was significantly different between group CM and A-PRF (49.37 ± 3.83% vs. 15.43 ± 3.44% at 1 week, $p < 0.001$; 33.87 ± 1.29% vs. 12.23 ± 0.25% at 4 weeks, $p < 0.0001$). The relative proportion of fibroblasts in group A-PRF was measured compared to group CM, which was significant (63.37 ± 1.19% vs. 14.43 ± 1.19% at 1 week, 65.7 ± 0.9% vs. 22.33 ± 1.12% at 4 weeks, $p < 0.0001$). Eosinophils in group A-PRF were significantly fewer than in group CM (0% vs. 7.9 ± 0.3% at 4 weeks, $p < 0.0001$) (**Figure 4G**).

At both healing time points, the percentage of new osteoid formation was significantly greater in group A-PRF compared to group CM (4.93 ± 0.21% vs. 0.18 ± 0.06% at 1 week, $p < 0.0001$; 0.62 ± 0.06% vs. 0.09 ± 0.01% at 4 weeks, $p < 0.001$) (**Figure 5C**). The relative expression of osteocalcin at 4 weeks was significantly different in group A-PRF (37.93 ± 4.91%) and group CM (3.33 ± 2.63%) ($p < 0.001$). In addition, there was a significant difference between group A-PRF and group CM in the relative expression of osteoclasts (8.72 ± 0.06% vs. 0.32 ± 0.01% at 1 week, $p < 0.0001$; 11.27 ± 0.5% vs. 5.43 ± 1.12% at 4 weeks, $p < 0.01$) (**Figure 5G**).

DISCUSSION

Perforation of the SM occurs in the maxillary sinus elevation at a frequency of 10–56% (Pikos, 2008; Nolan et al., 2014; Shiffler et al., 2015; Aricioglu et al., 2017). Although an absorbable CM has been proposed, there is no standard treatment for the repair of SM perforation when the size is less than 5 mm. Most of the following qualities should be present in a proper tissue-healing membrane regarding perforated SM

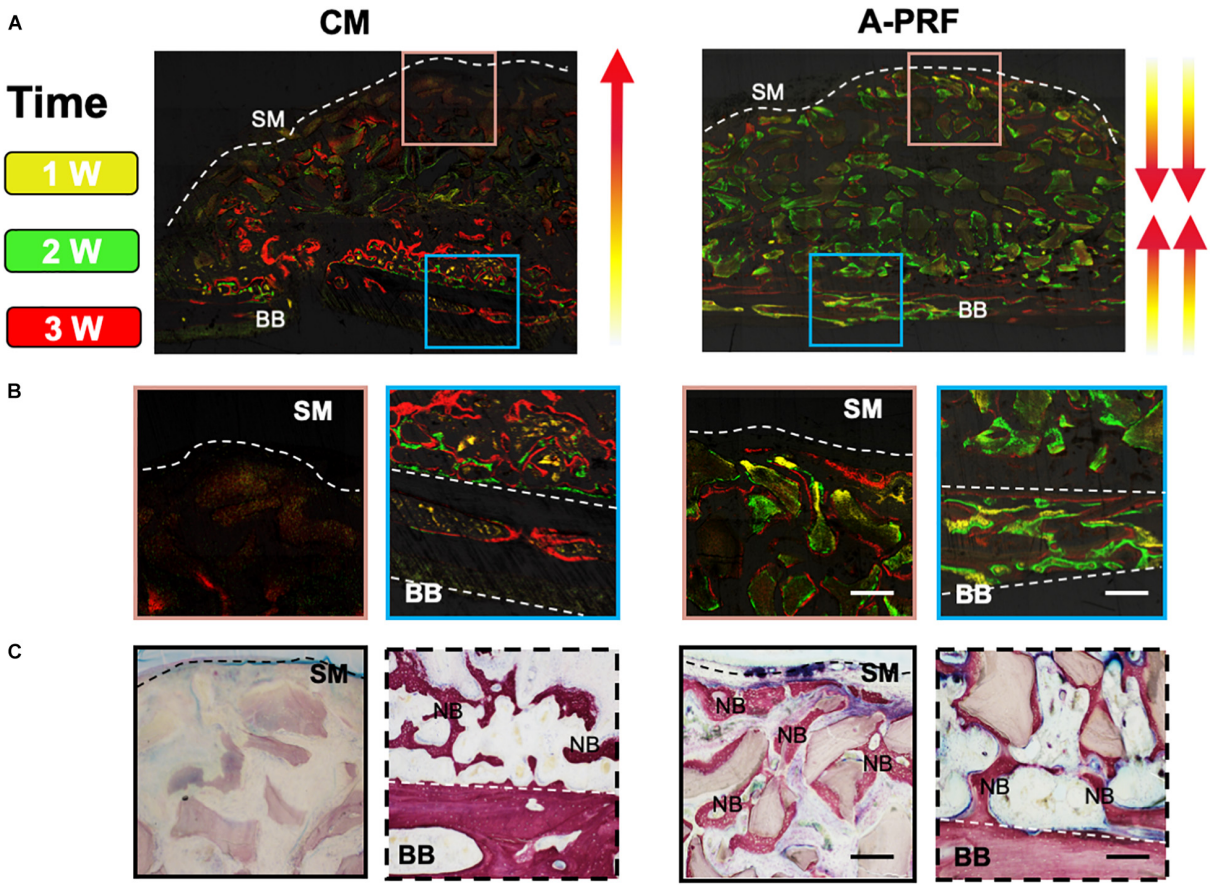

FIGURE 6 | Osteogenic patterns in group CM and group A-PRF at 4 weeks. **(A)** Fluorescent labeling (tetracycline shown as yellow, calcein as green and alizarin red red) of the two groups. **(B)** Magnified images of two ROIs indicating the direction of new bone formation: (1) area underneath the SM (pink box); (2) area near the basal bone (blue box). **(C)** VG staining at 4 weeks. SM, Schneiderian membrane; BB, basal bone; NB, new bone (scale bar: 100 μm).

(Al-Maawi et al., 2019): (a) appropriate mechanical properties allowing combination with natural tissue and providing an intact microenvironment for tissue remodeling; (b) suitable degradative profile matching the neotissue formation; (c) non-immunogenicity allowing integration of the membrane with the host tissue without triggering an overinflammatory effect; (d) being rich in cells and growth factors to provide a bioactive basis through biomaterial-induced tissue reactions.

A CM is a double-layered absorbable barrier membrane that has been widely used in guided bone/tissue regeneration (GBR/GTR) (Rothamel et al., 2005; Dimitriou et al., 2012; Al-Maawi et al., 2019; Schorn et al., 2019). The back layer is exposed to the bony defect, allowing osteogenic cells to immigrate to the repair site, while the front layer is exposed to the soft tissue and used to prevent soft tissue ingrowth (Lang et al., 1994; Schorn et al., 2019). According to SEM images (**Figure 3A**), the large bundles of collagen fibers within the bilayered CM were arranged in a parallel horizontal direction. In contrast, A-PRF was a reticular structure composed of fibronectin. The mechanical properties of barrier membranes are largely related to their microstructure, and proper mechanical properties can facilitate favorable tissue repair (Ghanaati et al., 2014; Masuki et al., 2016; Fujioka-Kobayashi et al., 2017). As shown in the stress–strain curve (**Figure 3**), yield strain was significantly higher in A-PRF than that in CM (109.7 ± 0.3% vs. 51.2 ± 0.1%, $p < 0.0001$), suggesting that the superior elasticity shown in A-PRF was due to its reticular and porous microstructure. Therefore, the superior elasticity of A-PRF avoided secondary perforation caused by breathing movement and overfilling of DBBM in the repair site, which provided a good foundation for perforated SM repair.

As a physical barrier in GBR/GTR, CM maintains its integrity to promote bone tissue ingrowth (Chu et al., 2017). Premature resorption of the CM will cause tissue regeneration failure (e.g., soft tissue ingrowth) and produce a longer treatment period. In contrast, for tissue-healing biomaterials implanted *in vivo*, timely degradation and appropriate immunogenic characteristics are important prerequisites to facilitate the repair process. As shown in **Figure 4A**, there was a crevice in the SM in group CM, while continuous and complete repair of the SM in group A-PRF and A-PRF was not observed at the repair site. These outcomes suggest that the CM was less prone to degradation due to the dense collagen fiber network, whereas the degradation of A-PRF and repair of the perforated SM occurred simultaneously for the porous microstructure of

A-PRF. Although CM has been the preferred clinical choice for GBR/GTR, it has limitations in the process of perforated SM repair. In addition, H&E staining (**Figure 4B**) revealed an intact repaired SM in group A-PRF, showing a pseudostratified columnar ciliated epithelium at the perforated site (**Figure 4C**, yellow box). This structure was similar to a natural SM previously reported (Srouji et al., 2009) and demonstrates the satisfactory tissue repairing ability of A-PRF as applied to a perforated SM. Based on histological images (**Figure 4C**, black box), the number of inflammatory cells in group A-PRF was significantly lower than that in group CM (15.43 ± 3.44% vs. 49.37 ± 3.83%, $p < 0.001$), whereas the fibroblasts were greatly increased compared to group CM at an early stage (63.37 ± 1.19% vs. 14.43 ± 1.19%, $p < 0.0001$) (**Figure 4G**). After *in vivo* implantation of biomaterials, acute inflammation occurs following the initial host–material interaction. This leads to a neutrophil influx at the interface of the perforated SM biomaterials. The neutrophils secrete enzymes to degrade the biomaterials and release chemokines and cytokines to recruit and activate monocytes. The monocytes differentiate into macrophages to enhance their phagocytosis. As a foreign biomaterial, porcine-derived CMs will inevitably trigger host–membrane immune response after implantation, which involves the activation of phagocytic cells. The cell-mediated degradation may be involved in the CM degradation process (Fang et al., 2020), and this overinflammatory state produces an adverse microenvironment for tissue repair. Nevertheless, a cocktail of growth factors with A-PRF, such as transforming growth factor β (TGF-β), platelet-derived growth factor (PDGF), and vascular endothelial growth factor (VEGF), can actively trigger and orchestrate the tissue repair processes (Marx, 2004; Aminabadi, 2008; Peerbooms et al., 2010; Soloviev et al., 2014; Herath et al., 2018). Specifically, TGF-β could regulate macrophage polarization from M1 to M2 phenotypes, which eventually reaches more cells of the tissue repair brigade (Dohan et al., 2006; Nasirzade et al., 2020). Additionally, A-PRF could modulate the inflammatory responses by the nuclear factor κB signal pathway (Nasirzade et al., 2020). Therefore, because of the rich growth factors and non-immunogenic characteristics of A-PRF, a continuous and intact pseudostratified columnar ciliated epithelial structure formed at the perforated site without triggering overinflammation. This provided a proper base for tissue repair at an early stage. At 4 weeks post-operation, an intact pseudostratified columnar ciliated epithelium was not observed in group CM (**Figure 4F**, yellow box). The residual CM was still observed (**Figure 4D**), and an increasing number of inflammatory cells (33.87 ± 1.29%) and eosinophils (7.9 ± 0.3%) appeared under the perforated SM area. This persistent inflammatory state resulted in a persistent allergic reaction (**Figure 4F**, black box) and unfavorable mucosa thickening (**Figure 4F**, yellow box). The perforated SM had been fully integrated, and the A-PRF completely degraded in group A-PRF (**Figure 4**). Overall, the intact microenvironment created by A-PRF with substantial cells and growth factors served as a bioactive barrier through favorable biomaterial-induced tissue reactions for the timely degradation and non-immunogenic characteristics of A-PRF.

SM repair restores the integrity of the SM and also establishes a microenvironment suitable for new bone formation and remodeling after the maxillary sinus floor elevation process. Kuchler et al. (2020) concluded that DBBM cannot perform the function of creeping substitution in an inflammatory microenvironment. However, because of the formation of the overinflammatory microenvironment in group CM, histological examinations at 1 week (**Figure 5A**) showed significantly lower new bone formation (0.18 ± 0.06%), and TRAP staining (**Figure 5B**) revealed lower osteoclast activity (0.32 ± 0.01%) in group CM. Such an overinflammatory microenvironment might hinder the physiological functions of osteoblasts–osteoclasts and delay bone remodeling. Thus, the creeping substitution process could not be operated as scheduled in group CM. In contrast, early osteogenesis began to occur under the SM in group A-PRF (**Figures 5A,B**). As previously noted, bioactive factors in A-PRF suppress inflammation, and the low-inflammatory microenvironment favored continuous self-renewal of the sinus cavity in group A-PRF (Nasirzade et al., 2020; Zhang et al., 2020) and reached a dynamic balance between bone formation and resorption. In addition, the significant amount of growth factors and cytokines within A-PRF also played an essential role in regulating the bone remodeling process (Marx, 2004; Aminabadi, 2008; Peerbooms et al., 2010; Soloviev et al., 2014; Herath et al., 2018). Growth factors (such as PDGF-BB and VEGF) in A-PRF could stimulate neovascularization, which is essential for osteoblasts to promote osteogenic differentiation (Fernández-Barbero et al., 2006). In group A-PRF, we also observed a large amount of new bone formation (0.62 ± 0.06%) and an increasing number of osteoclasts (11.27 ± 0.5%) under the SM, which demonstrated an active creeping substitution and bone reconstruction process (**Figures 5D–F**).

Based on previous studies, there are two sources of osteogenesis in the elevated sinus floor area. One is osteogenesis from the basal bone, and the other is from the SM (Srouji et al., 2009; Mu et al., 2020). **Figures 6B,C** show that the osteogenic pattern of the CM originated solely from the basal bone. However, the dense CM structure caused untimely degradation, which hindered repair of the perforated SM. Even though the CM prevented the ingrowth of soft tissue in GBR/GTR, the residual CM simultaneously blocked one of the osteogenic sources in the sinus cavity. As a result of the closure of the SM (**Figures 6B,C**), the presence of A-PRF established an intact microenvironment with low inflammation that was conducive to bone formation and remodeling. Because of its rich growth factors and matching degradation, and the two osteogenic sources as mentioned above, newly formed bone was induced to grow along both the basal bone to SM and the SM to basal bone directions.

This study revealed that (i) significant SM repair occurred when utilizing A-PRF, and the degradation of A-PRF was matched with the SM repair process at an early stage; (ii) bone remodeling in the sinus cavity was active, and a greater amount of new bone formation occurred under the perforated SM area in the A-PRF group at a later time point. This is the first preclinical study evaluating A-PRF as an alternative to CM for repair of SM perforation with the filling of DBBM simultaneously.

Several clinical studies investigated a potential benefit due to the placement of a blood product membrane to the perforated SM (Oncu and Kaymaz, 2017; Malzoni et al., 2020). Those clinical studies aimed to evaluate the effect of applying a blood product membrane to SM perforation on osseointegration and the survival rate of dental implants. Although there were several published studies using the blood product membrane, studies evaluating the efficacy of A-PRF in the repair of SM perforations regarding simultaneous bone grafting are lacking. In the present study, we have investigated the efficacy of the healing process of perforated SM and osteogenic pattern through histological and histomorphometric evaluation.

The rabbit experimental model was first introduced by Watanabe et al. (1999) to mimic a perforated SM in a human maxillary sinus elevation procedure. The rabbit maxillary sinus cavity is appropriate for maxillary sinus elevation, as the sinus cavity communicates with the nasal cavity through a well-defined ostium (Kim et al., 2012). Although the rabbit sinus cavity shows similarities to the human maxillary sinus, it differs in the number of platelets. Coagulation factors in rabbit blood are more abundant than in human blood, making the healing pattern presented in the rabbit faster than that which occurs in humans (Butterfield et al., 2005). However, because of ethical issues, this procedure has not been adopted clinically. An additional clinical trial, with a larger simple size and a longer time point, should be conducted to verify the effectiveness of A-PRF.

DATA AVAILABILITY STATEMENT

The raw data supporting the conclusions of this article will be made available by the authors, without undue reservation.

ETHICS STATEMENT

The animal study was reviewed and approved by the Animal Ethics Committee of Chongqing Medical University (CQHS-IRB-2018-07).

AUTHOR CONTRIBUTIONS

LX: design, methodology, data analysis, drafting article, validation, animal experiments, and data collection. SY: critical revision of article, statistics, and approval of article. ZM: responsible for the assistance of animal experiments and methodology. DL: responsible for micro-CT and H&E staining. JS: funding acquisition, supervision, conceptualization, and formal analysis. TC: conceptualization, project administration, funding acquisition, methodology, and writing-review and editing. All authors contributed to the article and approved the submitted version.

FUNDING

This work was supported by the National Natural Science Foundation of China (No. 81701031), the Postdoctoral Science Foundation of China (No. 2017M622981), the Chongqing Science and Technology Bureau Foundation (No. cstc2017jcyjBX0019), the Chongqing Special Postdoctoral Science Foundation (No. XmT2018009), and the Chongqing Postgraduate Research and Innovation Project Funding (No. CYS19201).

SUPPLEMENTARY MATERIAL

The Supplementary Material for this article can be found online at: https://www.frontiersin.org/articles/10.3389/fbioe.2020.600032/full#supplementary-material

Supplementary Figure 1 | Clinical pictures of A-PRF. **(A)** The appearance of A-PRF after eliminating the red blood cells. **(B)** A-PRF was compressed to a thin film by using a compression device. **(C)** A compression device of A-PRF.

Supplementary Figure 2 | Histological and radiographic analysis of the whole sinus cavity at 1 and 4 weeks. **(A,B)** The tissue sections showed that the fracture of the basal bone corresponded to the perforated area of the SM (marked with black dotted line). **(C1–C2)** Micro-CT analysis of the maxillary sinus cavity at 4-week post-operation in CM and A-PRF groups.

REFERENCES

Aimetti, M., Romagnoli, R., Ricci, G., and Massei, G. (2001). Maxillary sinus elevation: the effect of macrolacerations and microlacerations of the sinus membrane as determined by endoscopy. *Int. J. Periodont. Restorat. Dent.* 21, 581–589.

Aizawa, H., Tsujino, T., Watanabe, T., Isobe, K., Kitamura, Y., Sato, A., et al. (2020). Quantitative near-infrared imaging of platelets in platelet-rich fibrin (PRF) matrices: comparative analysis of Bio-PRF, Leukocyte-Rich PRF, advanced-PRF and concentrated growth factors. *Int. J. Mol. Sci.* 21:4426. doi: 10.3390/ijms21124426

Al-Maawi, S., Herrera-Vizcaíno, C., Orlowska, A., Willershausen, I., Sader, R., Miron, R. J., et al. (2019). Biologization of collagen-based biomaterials using liquid-platelet-rich fibrin: new insights into clinically applicable tissue engineering. *Materials* 12:3993. doi: 10.3390/ma12233993

Aminabadi, N. A. (2008). Plasma rich in growth factors as a potential therapeutic candidate for treatment of recurrent aphthous stomatitis. *Med. Hypothes.* 70, 529–531. doi: 10.1016/j.mehy.2007.06.037

Anavi, Y., Allon, D. M., Avishai, G., and Calderon, S. (2008). Complications of maxillary sinus augmentations in a selective series of patients. *Oral Surg. Oral. Med. Oral Pathol. Oral Radiol. Endod.* 106, 34–38. doi: 10.1016/j.tripleo.2007.09.021

Ardekian, L., Oved-Peleg, E., Mactei, E. E., and Peled, M. (2006). The clinical significance of sinus membrane perforation during augmentation of the maxillary sinus. *J. Oral Maxillofac. Surg.* 64, 277–282. doi: 10.1016/j.joms.2005.10.031

Aricioglu, C., Dolanmaz, D., Esen, A., Isik, K., and Avunduk, M. C. (2017). Histological evaluation of effectiveness of platelet-rich fibrin on healing of sinus membrane perforations: a preclinical animal study. *J. Craniomaxillofac. Surg.* 45, 1150–1157. doi: 10.1016/j.jcms.2017.05.005

Asai, S., Shimizu, Y., and Ooya, K. (2002). Maxillary sinus augmentation model in rabbits: effect of occluded nasal ostium on new bone formation. *Clin. Oral Implants Res.* 13, 405–409. doi: 10.1034/j.1600-0501.2002.130409.x

Becker, S. T., Terheyden, H., Steinriede, A., Behrens, E., Springer, I., and Wiltfang, J. (2008). Prospective observation of 41 perforations of the Schneiderian

membrane during sinus floor elevation. *Clin. Oral Implants Res.* 19, 1285–1289. doi: 10.1111/j.1600-0501.2008.01612.x

Butterfield, K. J., Bennett, J., Gronowicz, G., and Adams, D. (2005). Effect of platelet-rich plasma with autogenous bone graft for maxillary sinus augmentation in a rabbit model. *J. Oral Maxillofac. Surg.* 63, 370–376. doi: 10.1016/j.joms.2004.07.017

Cho, S. C., Wallace, S. S., Froum, S. J., and Tarnow, D. P. (2001). Influence of anatomy on Schneiderian membrane perforations during sinus elevation surgery: three-dimensional analysis. *Pract. Proced. Aesthet. Dent.* 13, 160–163.

Choukroun, J., Diss, A., Simonpieri, A., Girard, M. O., Schoeffler, C., Dohan, S. L., et al. (2006). Platelet-rich fibrin (PRF): a second-generation platelet concentrate. Part IV: clinical effects on tissue healing. *Oral Surg. Oral. Med. Oral Pathol. Oral Radiol. Endod.* 101, e56–e60.

Chu, C., Deng, J., Sun, X., Qu, Y., and Man, Y. (2017). Collagen membrane and immune response in guided bone regeneration: recent progress and perspectives. *Tissue Eng. Part B Rev.* 23, 421–435. doi: 10.1089/ten.teb.2016.0463

Dimitriou, R., Mataliotakis, G. I., Calori, G. M., and Giannoudis, P. V. (2012). The role of barrier membranes for guided bone regeneration and restoration of large bone defects: current experimental and clinical evidence. *BMC Med.* 10:81. doi: 10.1186/1741-7015-10-81

Dohan, D. M., Choukroun, J., Diss, A., Dohan, S. L., and Dohan, A. J. (2006). Platelet-rich fibrin (PRF): a second-generation platelet concentrate. Part II: platelet-related biologic features. *Oral Surg. Oral. Med. Oral Pathol. Oral Radiol. Endod.* 101, e45–e50.

Fang, J., Liu, R., Chen, S., Liu, Q., Cai, H., Lin, Y., et al. (2020). Tuning the immune reaction to manipulate the cell-mediated degradation of a collagen barrier membrane. *Acta Biomater.* 109, 95–108. doi: 10.1016/j.actbio.2020.03.038

Fernández-Barbero, J. E., Galindo-Moreno, P., Avila-Ortiz, G., Caba, O., Sánchez-Fernández, E., and Wang, H. L. (2006). Flow cytometric and morphological characterization of platelet-rich plasma gel. *Clin. Oral Implants Res.* 17, 687–693. doi: 10.1111/j.1600-0501.2006.01179.x

Fujioka-Kobayashi, M., Miron, R. J., Hernandez, M., Kandalam, U., Zhang, Y., and Choukroun, J. (2017). Optimized platelet-rich fibrin with the low-speed concept: growth factor release, biocompatibility, and cellular response. *J. Periodontol.* 88, 112–121. doi: 10.1902/jop.2016.160443

Ghanaati, S., Booms, P., Orlowska, A., Kubesch, A., Lorenz, J., and Rutkowski, J. (2014). Advanced platelet-rich fibrin: a new concept for cell-based tissue engineering by means of inflammatory cells. *J. Oral Implantol.* 40, 679–689. doi: 10.1563/aaid-joi-d-14-00138

Gruber, R., Kandler, B., Fuerst, G., Fischer, M. B., and Watzek, G. (2004). Porcine sinus mucosa holds cells that respond to bone morphogenetic protein (BMP)-6 and BMP-7 with increased osteogenic differentiation in vitro. *Clin. Oral Implants Res.* 15, 575–580. doi: 10.1111/j.1600-0501.2004.01062.x

Hallman, M., Sennerby, L., Zetterqvist, L., and Lundgren, S. (2005). A 3-year prospective follow-up study of implant-supported fixed prostheses in patients subjected to maxillary sinus floor augmentation with a 80:20 mixture of deproteinized bovine bone and autogenous bone Clinical, radiographic and resonance frequency analysis. *Int. J. Oral Maxillofac. Surg.* 34, 273–280. doi: 10.1016/j.ijom.2004.09.009

Herath, T. D. K., Larbi, A., Teoh, S. H., Kirkpatrick, C. J., and Goh, B. T. (2018). Neutrophil-mediated enhancement of angiogenesis and osteogenesis in a novel triple cell co-culture model with endothelial cells and osteoblasts. *J. Tissue Eng. Regen. Med.* 12, e1221–e1236.

Hernández-Alfaro, F., Torradeflot, M. M., and Marti, C. (2008). Prevalence and management of Schneiderian membrane perforations during sinus-lift procedures. *Clin. Oral Implants Res.* 19, 91–98.

Isobe, K., Watanebe, T., Kawabata, H., Kitamura, Y., Okudera, T., Okudera, H., et al. (2017). Mechanical and degradation properties of advanced platelet-rich fibrin (A-PRF), concentrated growth factors (CGF), and platelet-poor plasma-derived fibrin (PPTF). *Int. J. Implant Dent.* 3:17.

Jung, U. W., Unursaikhan, O., Park, J. Y., Lee, J. S. J., Otgonbold, S. H., and Choi, O. (2015). Tenting effect of the elevated sinus membrane over an implant with adjunctive use of a hydroxyapatite-powdered collagen membrane in rabbits. *Clin. Oral Implants Res.* 26, 663–670. doi: 10.1111/clr.12362

Kim, Y. S., Kim, S. H., Kim, K. H., Jhin, M. J., Kim, W. K., Lee, Y. K., et al. (2012). Rabbit maxillary sinus augmentation model with simultaneous implant placement: differential responses to the graft materials. *J. Periodont. Implant Sci.* 42, 204–211. doi: 10.5051/jpis.2012.42.6.204

Kuchler, U., Dos Santos, G. M., Heimel, P., Stähli, A., Strauss, F. J., Tangl, S., et al. (2020). DBBM shows no signs of resorption under inflammatory conditions. An experimental study in the mouse calvaria. *Clin. Oral Implants Res.* 31, 10–17. doi: 10.1111/clr.13538

Lang, N. P., Hämmerle, C. H., Brägger, U., Lehmann, B., and Nyman, S. R. (1994). Guided tissue regeneration in jawbone defects prior to implant placement. *Clin. Oral Implants Res.* 5, 92–97. doi: 10.1034/j.1600-0501.1994.050205.x

Lim, H. C., Son, Y., Hong, J. Y., Shin, S. I., Jung, U. W., and Chung, J. H. (2018). Sinus floor elevation in sites with a perforated Schneiderian membrane: what is the effect of placing a collagen membrane in a rabbit model? *Clin. Oral Implants Res.* 29, 1202–1211. doi: 10.1111/clr.13385

Lundquist, R., Dziegiel, M. H., and Agren, M. S. (2008). Bioactivity and stability of endogenous fibrogenic factors in platelet-rich fibrin. *Wound Repair. Regen.* 16, 356–363. doi: 10.1111/j.1524-475x.2007.00344.x

Malzoni, C. M. A., Nicoli, L. G., Pinto, G. D. C. D. S., Marcantonio, C., Pigossi, S. C., Zotesso, V. A., et al. (2020). The effectiveness of L-PRF in the treatment of Schneiderian membrane large perforations: long-term follow-up of a case series. *J. Oral Implantol.* doi: 10.1563/aaid-joi-D-20-00044 [Epub ahead of print].

Marx, R. E. (2004). Platelet-rich plasma: evidence to support its use. *J. Oral Maxillofac. Surg.* 62, 489–496. doi: 10.1016/j.joms.2003.12.003

Masuki, H., Okudera, T., Watanebe, T., Suzuki, M., Nishiyama, K., Okudera, H., et al. (2016). Growth factor and pro-inflammatory cytokine contents in platelet-rich plasma (PRP), plasma rich in growth factors (PRGF), advanced platelet-rich fibrin (A-PRF), and concentrated growth factors (CGF). *Int. J. Implant Dent.* 2:19.

Misch, K., and Wang, H. L. (2008). Implant surgery complications: etiology and treatment. *Implant Dent.* 17, 159–168. doi: 10.1097/id.0b013e3181752f61

Mu, Z., Chen, K., Yuan, S., Yihan, L., Yuanding, H., Chao, W., et al. (2020). Gelatin nanoparticle-injectable platelet-rich fibrin double network hydrogels with local adaptability and bioactivity for enhanced osteogenesis. *Adv. Healthc. Mater.* 9:e1901469.

Nasirzade, J., Kargarpour, Z., Hasannia, S., Strauss, F. J., and Gruber, R. (2020). Platelet-rich fibrin elicits an anti-inflammatory response in macrophages in vitro. *J. Periodontol.* 91, 244–252. doi: 10.1002/jper.19-0216

Nishimoto, S., Fujita, K., Sotsuka, Y., Kinoshita, M., Fujiwara, T., Kawai, K., et al. (2015). Growth factor measurement and histological analysis in platelet rich fibrin: a pilot study. *J. Maxillofac. Oral Surg.* 14, 907–913. doi: 10.1007/s12663-015-0768-3

Nolan, P. J., Freeman, K., and Kraut, R. A. (2014). Correlation between Schneiderian membrane perforation and sinus lift graft outcome: a retrospective evaluation of 359 augmented sinus. *J. Oral Maxillofac. Surg.* 72, 47–52. doi: 10.1016/j.joms.2013.07.020

Oncu, E., and Kaymaz, E. (2017). Assessment of the effectiveness of platelet rich fibrin in the treatment of Schneiderian membrane perforation. *Clin. Implant Dent. Relat. Res.* 19, 1009–1014. doi: 10.1111/cid.12528

Palma, V. C., Magro-Filho, O., de Oliveria, J. A., Lundgren, S., Salata, L. A., and Sennerby, L. (2006). Bone reformation and implant integration following maxillary sinus membrane elevation: an experimental study in primates. *Clin. Implant Dent. Relat. Res.* 8, 11–24. doi: 10.2310/j.6480.2005.00026.x

Panda, S., Jayakumar, N. D., Sankari, M., Varghese, S. S., and Kumar, D. S. (2014). Platelet rich fibrin and xenograft in treatment of intrabony defect. *Contemp. Clin. Dent.* 5, 550–554. doi: 10.4103/0976-237x.142830

Peerbooms, J. C., van Laar, W., Faber, F., Schuller, H. M., van der Hoeven, H., and Gosens, T. (2010). Use of platelet rich plasma to treat plantar fasciitis: design of a multi centre randomized controlled trial. *BMC Musculoskelet. Disord.* 11:69. doi: 10.1186/1471-2474-11-69

Pikos, M. A. (2008). Maxillary sinus membrane repair: update on technique for large and complete perforations. *Implant Dent.* 17, 24–31. doi: 10.1097/id.0b013e318166d934

Pradeep, A. R., Rao, N. S., Agarwal, E., Bajaj, P., Kumari, M., and Naik, S. B. (2012). Comparative evaluation of autologous platelet-rich fibrin and platelet-rich plasma in the treatment of 3-wall intrabony defects in chronic periodontitis: a randomized controlled clinical trial. *J. Periodontol.* 83, 1499–1507. doi: 10.1902/jop.2012.110705

Proussaefs, P., Lozada, J., Kim, J., and Rohrer, M. D. (2004). Repair of the perforated sinus membrane with a resorbable collagen membrane: a human study. *Int. J. Oral Maxillofac. Implants* 19, 413–420.

Rothamel, D., Schwarz, F., Sager, M., Herten, M., Sculean, A., and Becker, J. (2005). Biodegradation of differently cross-linked collagen membranes: an experimental study in the rat. *Clin. Oral Implants Res.* 16, 369–378. doi: 10.1111/j.1600-0501.2005.01108.x

Roy, S., Driggs, J., Elgharably, H., Biswas, S., Findley, M., Khanna, S., et al. (2011). Platelet-rich fibrin matrix improves wound angiogenesis via inducing endothelial cell proliferation. *Wound Repair. Regen.* 19, 753–766. doi: 10.1111/j.1524-475x.2011.00740.x

Schorn, L., Handschel, J., Lommen, J., Von Beck, F. P., Depprich, R., Kübler, N., et al. (2019). Evaluation of biocompatibility of different membrane surfaces using unrestricted somatic stem cells. *Vivo* 33, 1447–1454. doi: 10.21873/invivo.11623

Schwartz-Arad, D., Herzberg, R., and Dolev, E. (2004). The prevalence of surgical complications of the sinus graft procedure and their impact on implant survival. *J. Periodontol.* 75, 511–516. doi: 10.1902/jop.2004.75.4.511

Schwarz, L., Schiebel, V., Hof, M., Ulm, C., Watzek, G., and Pommer, B. (2015). Risk factors of membrane perforation and postoperative complications in sinus floor elevation surgery: review of 407 augmentation procedures. *J. Oral Maxillofac. Surg.* 73, 1275–1282. doi: 10.1016/j.joms.2015.01.039

Shiffler, K., Lee, D., Aghaloo, T., Moy, P. K., and Pi-Anfruns, J. (2015). Sinus membrane perforations and the incidence of complications: a retrospective study from a residency program. *Oral Surg. Oral Med. Oral Pathol. Oral Radiol.* 120, 10–14. doi: 10.1016/j.oooo.2015.02.477

Soloviev, D. A., Hazen, S. L., Szpak, D., Bledzka, K. M., Ballantyne, C. M., Plow, E. F., et al. (2014). Dual role of the leukocyte integrin αMβ2 in angiogenesis. *J. Immunol.* 193, 4712–4721. doi: 10.4049/jimmunol.1400202

Sorní, M., Guarinós, J., García, O., and Peñarrocha, M. (2005). Implant rehabilitation of the atrophic upper jaw: a review of the literature since 1999. *Med. Oral Patol. Oral Cir. Bucal.* 10(Suppl. 1), E45–E56.

Srouji, S., Kizhner, T., Ben David, D., Riminucci, M., Bianco, P., and Livne, E. (2009). The Schneiderian membrane contains osteoprogenitor cells: in vivo and in vitro study. *Calcif. Tissue Int.* 84, 138–145. doi: 10.1007/s00223-008-9202-x

Stricker, A., Voss, P. J., Gutwald, R., Schramm, A., and Schmelzeisen, R. (2003). Maxillary sinus floor augmention with autogenous bone grafts to enable placement of SLA-surfaced implants: preliminary results after 15-40 months. *Clin. Oral Implants Res.* 14, 207–212. doi: 10.1034/j.1600-0501.2003.140211.x

Tajima, N., Ohba, S., Sawase, T., and Asahina, I. (2013). Evaluation of sinus floor augmentation with simultaneous implant placement using platelet-rich fibrin as sole grafting material. *Int. J. Oral Maxillofac. Implants* 28, 77–83. doi: 10.11607/jomi.2613

Takeda, Y., Katsutoshi, K., Matsuzaka, K., and Inoue, T. (2015). The effect of concentrated growth factor on rat bone marrow cells in vitro and on calvarial bone healing in Vivo. *Int. J. Oral Maxillofac. Implants* 30, 1187–1196. doi: 10.11607/jomi.3995

Timmenga, N. M., Raghoebar, G. M., van Weissenbruch, R., and Vissink, A. (2003). Maxillary sinus floor elevation surgery. A clinical, radiographic and endoscopic evaluation. *Clin. Oral Implants Res.* 14, 322–328. doi: 10.1034/j.1600-0501.2003.140310.x

Wallace, S. S., and Froum, S. J. (2003). Effect of maxillary sinus augmentation on the survival of endosseous dental implants. A systematic review. *Ann. Periodontol.* 8, 328–343. doi: 10.1902/annals.2003.8.1.328

Watanabe, K., Niimi, A., and Ueda, M. (1999). Autogenous bone grafts in the rabbit maxillary sinus. *Oral Surg. Oral Med. Oral Pathol. Oral Radiol. Endod.* 88, 26–32. doi: 10.1016/s1079-2104(99)70189-7

Wen, S. C., Lin, Y. H., Yang, Y. C., and Wang, H. L. (2015). The influence of sinus membrane thickness upon membrane perforation during transcrestal sinus lift procedure. *Clin. Oral Implants Res.* 26, 1158–1164. doi: 10.1111/clr.12429

Zhang, J., Yin, C., Zhao, Q., Zhao, Z., Wang, J., Miron, R. J., et al. (2020). Anti-inflammation effects of injectable platelet-rich fibrin via macrophages and dendritic cells. *J. Biomed. Mater. Res. A* 108, 61–68. doi: 10.1002/jbm.a.36792

Zhao, J. H., Tsai, C. H., and Chang, Y. C. (2015). Clinical application of platelet-rich fibrin as the sole grafting material in maxillary sinus augmentation. *J. Formos. Med. Assoc.* 114, 779–780. doi: 10.1016/j.jfma.2015.02.009

Conflict of Interest: The authors declare that the research was conducted in the absence of any commercial or financial relationships that could be construed as a potential conflict of interest.

frontiers in Materials

ORIGINAL RESEARCH
published: 09 February 2021
doi: 10.3389/fmats.2020.560372

Recombinant Spider Silk Protein Matrices Facilitate Differentiation of Neural Stem Cells Into Mature and Functional Neurons

*Michalina Lewicka[1], Paola Rebellato[2], Jakub Lewicki[1], Per Uhlén[2], Anna Rising[3,4] and Ola Hermanson[1]**

[1]Department of Neuroscience, Karolinska Institutet, Stockholm, Sweden, [2]Department of Medical Biochemistry and Biophysics (MBB), Karolinska Institutet, Stockholm, Sweden, [3]Swedish University of Agricultural Sciences, Department of Anatomy, Physiology and Biochemistry, Uppsala, Sweden, [4]Department of Neurobiology, Care Sciences and Society, Section for Neurogeriatrics, Karolinska Institutet, Huddinge, Sweden

Neural stem cells (NSCs) show great promise in drug discovery and clinical application. Yet few efforts have been made to optimize biocompatible materials for such cells to be expanded and used in clinical conditions. We have previously demonstrated that NSCs are readily cultured on substrates of certain recombinant spider silk protein without addition of animal- or human-derived components. The question remains however whether this material allows differentiation into functional neurons, and whether such differentiation can take place also when the NSCs are cultured not only upon but also within the biodegradable material. Here we demonstrate that "foam"-like structures generated from recombinant spider silk protein (4RepCT) provided excellent matrices for the generation and multicellular analysis of functional excitatory neurons from NSCs without addition of animal- or human-derived components. NSCs isolated from the cerebral cortices of rat embryos were cultured at either 4RepCT matrices shaped as foam-like structures without coating, or on conventional polystyrene plates coated with poly-L-ornithine and fibronectin. Upon treatment with recombinant proteins including the extracellular signaling factor BMP4 or a combination of BMP4 and the signaling factor Wnt3a, the cortical NSCs cultured in 4RepCT foam-like structures differentiated efficiently into neurons that responded to glutamate receptor agonists, such as AMPA, to the same extent as control cultures. Matrices derived from recombinant spider silk proteins thus provide a functional microenvironment for neural stem cells with little or no animal- or human-derived components and can be employed in the development of new strategies in stem cell research and tissue engineering.

Keywords: neural stem cell, biomaterial, spider silk, 3D cultures, scaffold

OPEN ACCESS

Edited by:
Liyuan Zhang,
Harvard University, United States

Reviewed by:
John George Hardy,
Lancaster University, United Kingdom
Banani Kundu,
University of Minho, Portugal

****Correspondence:***
Ola Hermanson
ola.hermanson@ki.se

Specialty section:
This article was submitted to Biomaterials, a section of the journal Frontiers in Materials

Received: *08 May 2020*
Accepted: *29 December 2020*
Published: *09 February 2021*

Citation:
Lewicka M, Rebellato P, Lewicki J, Uhlén P, Rising A and Hermanson O (2021) Recombinant Spider Silk Protein Matrices Facilitate Differentiation of Neural Stem Cells Into Mature and Functional Neurons. Front. Mater. 7:560372. doi: 10.3389/fmats.2020.560372

Abbreviations: NSCs, neural stem cells; BMP4, Bone Morphogenic protein 4; TuJ1, Neuronal class III B-tubulin; P, poly-L-ornithine; F, fibronectin; ECM, extracellular matrix; 3D, three dimensional; BW, BMP4+Wnt3a.

INTRODUCTION

The microenvironment strongly influences stem cell characteristics in various ways. These effects include changes in differentiation-associated gene expression via epigenetic mechanisms, e.g., chromatin modifications, and related changes in transcriptional activity. Several reports from recent years, from our lab and our colleagues, have demonstrated how substrate characteristics such as stiffness and roughness, and incorporation of specific cell binding motifs influence the differentiation of various types of stem cells in a cell context-specific manner (Teixeira et al., 2007; Discher et al., 2009; Teixeira et al., 2009; Teixeira et al., 2010; Blumenthal et al., 2014). Accordingly, a wide range of alternative solutions for optimization of biomaterials for stem cell research and tissue engineering has been tested during recent years.

Spider silk is an interesting biomaterial (Lewis, 2006; Hardy and Scheibel, 2009; Omenetto and Kaplan, 2010; Rising et al., 2011), due to its extreme mechanical properties (Gosline et al., 1999) combined with local tolerance when implanted in living tissues (Vollrath et al., 2002; Allmeling et al., 2008; Fredriksson et al., 2009; Radtke et al., 2011). A recombinant spider silk protein (4RepCT; consisting of four tandem repeats and the C-terminal domain of the major ampullate spidroin 1) that corresponds to approximately 10% of the native spider silk protein, can be readily produced in *Escherichia coli* (*E. coli*) and spontaneously assembles into films, foams and fibers (Stark et al., 2007; Widhe et al., 2010). 4RepCT matrices provide excellent substrates for human primary fibroblasts (Widhe et al., 2010) and we have demonstrated that this recombinant spider silk protein provides a suitable substrate also for culturing of rodent cortical neural stem cells (NSCs) as these cells proliferate, survive, retain multipotency, and differentiate into multiple cell types efficiently on film structures derived from 4RepCT without any additional coating or animal-derived components (Lewicka et al., 2012). The analysis of differentiation in our previous study was however based on gene expression and immunocytochemistry, and it is still not known whether the differentiated neurons and astrocytes derived from neural stem cells grown on 4RepCT are functional or as to which degree this can be analyzed. As it has been shown repeatedly that the expression of differentiation markers not necessarily correlate with functionality (Andersson et al., 2011) such functional analysis is required before proceeding with transplantations and *in vivo* studies in animals.

MATERIALS AND METHODS

Production of protein matrices: The recombinant miniature spider silk protein 4RepCT was produced in *E. coli* and purified as described previously (Hedhammar et al., 2008). A procedure for depletion of lipopolysaccharides (LPS) was also included (Hedhammar et al., 2010). After purification, the protein solution was sterilized by passage through 0.22 µm filter and concentrated to 3 mg/ml by ultrafiltration (Amicon Ultra, Millipore; unless otherwise stated, all general reagents were supplied by Swedish distributors and suppliers in accordance with the national procurement law) before preparation of foam matrices as previously described (Widhe et al., 2010). Matrices were dried over night under sterile conditions at room temperature (RT) and stored in RT until use. The matrices were washed twice with sterile PBS and pre-incubated with serum-free DMEM:F12 media (Sigma-Aldrich) for 1 h at 37°C with 5% CO_2 before plating the cells. The matrices were prepared in six-well cell culture polystyrene plates or 35 mm in diameter polystyrene plates (Sarstedt). Surface morphology, thickness, diameter, pore size, scanning electron microscopy (SEM), z-stacks, and in-depth analysis of the 4RepCT foam structure have previously been described elsewhere (Widhe et al., 2010).

Neural Stem Cell (NSC) culture: NSCs were harvested from cortices at day E15.5 embryos obtained from pregnant Sprague Dawley rats as described previously (Ilkhanizadeh and Teixeira, 2007; Andersson et al., 2011). Cells were mechanically dissociated followed by culture in serum-free DMEM:F12 media (Gibco) enriched with N2 supplements. After mechanical dissociation, the cells were cultured in serum-free DMEM:F12 media (Gibco) with N2 supplement. The cells were maintained in proliferating, undifferentiated state in this media by adding 10 ng/ml recombinant fibroblast growth factor 2 (FGF2; R&D Systems) every 24th hour and typically passaged once before usage in the experiments. NSCs were then seeded at a density of 10,000 cells/cm^2 and allowed to proliferate for 24–72 h to reach appropriate confluency (50–60%) prior to the experiments. The 4RepCT foams covered ~60% of the surface area of the cell culture dishes before NSCs were applied. NSCs used in positive control experiments were seeded on conventional polystyrene culture plates coated with poly-L-ornithine and fibronectin from bovine plasma (P+F) (Sigma-Aldrich) and uncoated polystyrene dishes served as negative controls to these. Soluble factors were re-supplemented at 24 h and medium replaced at 48 h time intervals. FGF2 was withdrawn from the cell culture media and then replaced with bone morphogenic protein (BMP4; R&D Systems) and/or Wnt3a (R&D Systems) to induce differentiation. All animal experiments were approved by the North Stockholm regional committee for animal research and ethics, Stockholm, Sweden (N284/11).

Immunocytochemistry: After a rinse in Phosphate-Buffered Saline (PBS) (Gibco), the cell cultures were fixed in 10% Formalin (Sigma-Aldrich) for 20 min at RT followed by 3 × 5 min washes with PBS with 0.1% Triton-X 100 (Sigma-Aldrich). Plates were then incubated with the respective primary antibody in PBS with 0.1% Triton-X 100 and 1% bovine serum albumin (BSA; Sigma-Aldrich) overnight at 4°C. The primary antibodies sources and dilutions were as follows: mouse anti-intermediate filament protein nestin (1:500; BD Pharmingen), mouse monoclonal anti-Neuronal Class III B-Tubulin (TuJ1; 1:500; Covance), microtubule associated protein 2 (MAP2; 1:500, Sigma-Aldrich), and rabbit poly-clonal anti-glia fibrillary acidic protein (GFAP; 1:500; DAKO). The cells were subsequently washed 6 × 5 min each with PBS with 0.1% Triton-X 100. Secondary antibodies were incubated in PBS with 0.1% Triton-X 100 and 1% BSA at RT for 1 h. The secondary antibodies were species-specific and labeled with Alexa 594 or Alexa 488 (1:500; Molecular Probes). Lastly, the samples were washed 3 × 5 min each in PBS and mounted with Vectashield

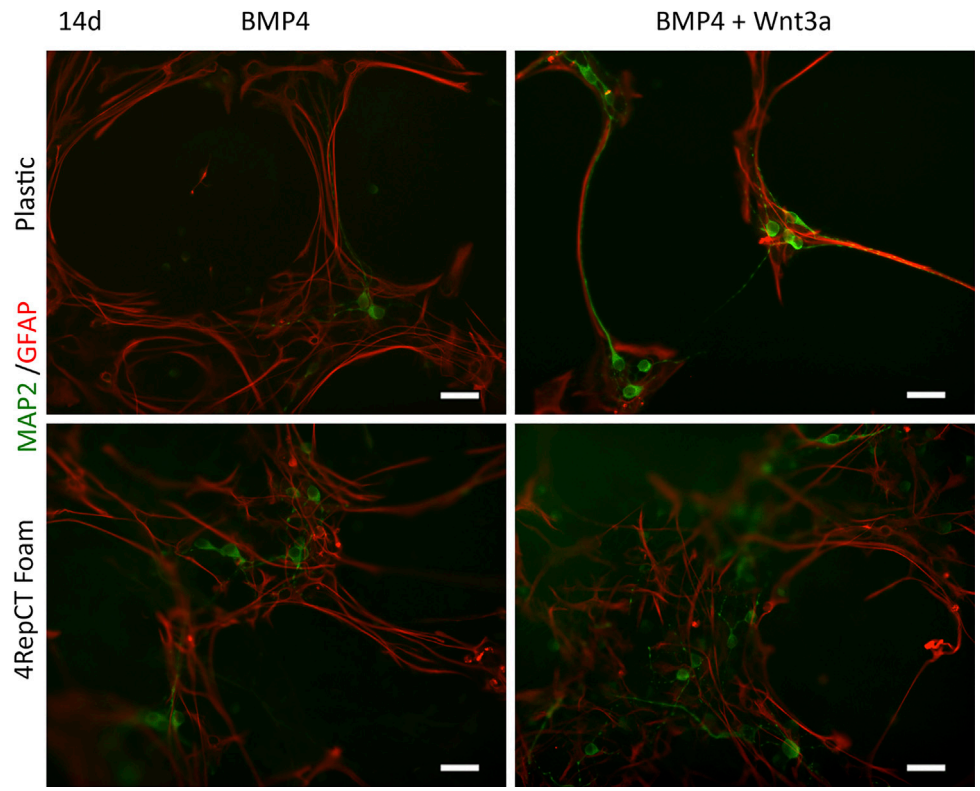

FIGURE 1 | NSCs retained their potential to differentiate into mature post-mitotic neuronal cells on 4RepCT-derived foam-like substrates in response to BMP4 and co-treatment of BMP4 and Wnt3a respectively, in comparison to control cultures expanded on conventional (polystyrene) dishes covered with poly-ornithine and fibronectin. Micrographs demonstrating neuronal cells derived from NSCs after treatment with BMP4 only or co-treatment with BMP4 and Wnt3a when grown on control culture plates or 4RepCT. MAP2-staining (green), GFAP-immunoreactivity (red).

(Vector Laboratories, Inc.). Fluorescent images were acquired with Axioskop software using Zeiss Axioskop2 microscope coupled to an MRm (Zeiss).

Calcium imaging: Cells were loaded with the Ca^{2+}sensitive fluorescence indicator Fluo-3/AM (5 μM, Life Technologies) together with 0.1% Pluronic f-127 (Life Technologies) at 37°C for 20 min in their own medium, and then moved to a Krebs-Ringer buffer containing (in mM) 119.0 NaCl, 2.5 KCl, 2.5 $CaCl_2$, 1.3 $MgCl_2$, 1.0 NaH_2PO_4, 20.0 HEPES (pH 7.4), and 11.0 dextrose. Measurements of intracellular Ca^{2+} were carried out in Krebs-Ringer buffer with or without Ca^{2+} at 37°C using a heat-controlled chamber (Warner Instruments) with a cooled EMCCD QuantEM 512:SC camera (Photometrics) mounted on an upright microscope (Zeiss Axio Examiner.D1) equipped with an W-Plan apochromat 20X/1.0 objective (Carl Zeiss). Excitation at 495 nm was assessed with a filter wheel (Sutter Instrument) at sampling frequency 0.5 Hz. MetaFluor (Molecular Devices) was used to control all devices and to analyze acquired images. The response to AMPA and ATP was determined using MATLAB software (The MathWorks Inc.) as described previously (Uhlén, 2004) considering only increases of more than 30% compared with the baseline as positive response. Drugs were bath-applied following previous protocol (Andersson et al., 2011).

Statistical analysis: Statistical analysis and graphs were performed using the software Prism 4 (Graph Pad). When 2 groups were compared, statistical analysis was performed using two-tailed unpaired *t*-test. When repeated measurements taken at different time points from 2 groups were compared, two-way ANOVA analysis of variance was used. The threshold value for statistical significance (α value) was set at 0.05 ($*p < 0.05$). Data are presented as the mean ± standard error of the mean (SEM) of independent experiments (3–5 experimental series per condition).

RESULTS AND DISCUSSION

4RepCT Foam Structures Provide Efficient Substrates for Neuronal Differentiation of Neural Stem Cells as Assessed by Morphology and Markers

In control cultures, NSCs derived from rat cortex of embryonic day 15 (E15) were cultured in optimal conditions seeded on polystyrene cell culture plates precoated with poly-L-ornithine

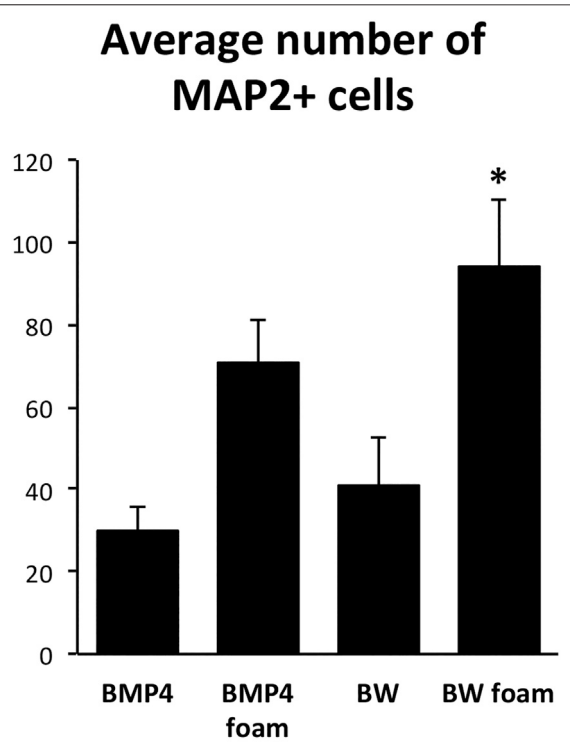

FIGURE 2 | Quantifications of the number of MAP2-positive cells after BMP4 or co-treatment with BMP4 and Wnt3a (BW) of control cultures expanded on conventional (polystyrene) dishes covered with poly-ornithine and fibronectin or 4RepCT-derived foam matrix. *Y* axis represents average number of MAP2-positive cells in 5 micrographs similar to those shown in **Figure 1** from three independent experiments in each condition. The number of MAP2-positive cells in the BW group cultured on the 4RepCT foam matrix was significantly higher than in any other condition. $^*p < 0.05$, error bars represent SEM (standard error mean).

and fibronectin as described in Materials and Methods. This protocol is well-established and widely used for over 2 decades, and provides homogenous cultures of multipotent progenitors (i.e. retaining the potency to differentiate into multiple fates) for a large number of passages (Johe et al., 1996; Jepsen et al., 2007; Andersson et al., 2011; Castelo-Branco et al., 2014). The NSCs expand undifferentiated and self-renew in N2 supplemented medium in the presence of FGF2. In contrast, NSCs grow poorly or not at all on uncoated polystyrene plates or plates coated with either poly-L-ornithine or fibronectin (data not shown and Johe et al., 1996; Teixeira et al., 2009; Lewicka et al., 2012).

After initial expansion of the primary cells, we seeded NSCs after the first passage on 4RepCT foam structures and in control conditions, respectively. NSCs seeded on 4RepCT foam structures attached and proliferated 24–72 h after the first passage into 50–60% confluency (**Figure 1**), indicating that NSC can attach to the 4RepCT protein as previously reported. To investigate if NSCs grown on 4RepCT foam shaped matrices in 3D can differentiate into neurons we exposed the cells to treatment with BMP4 or co-treatment with BMP4 and the signaling factor Wnt3a for 14 days. We have previously shown that BMP4 and BMP4+Wnt3a stimulation induces differentiation of mature, functional glutamate-receptor (GluR)—agonist responsive neuronal cells when NSCs are seeded at relatively high densities (Leao et al., 2010; Andersson et al., 2011). NSCs grown in 3D on 4RepCT foam matrices with pore sizes of around 5–30 μm and exposed to 10 ng/ml BMP4 or BMP4 and Wnt3a every 24 h for 14 days differentiated into neuronal cells positive for the dendritic marker of mature, post-mitotic neurons, microtubule associated protein 2 (MAP2). When analyzing five micrographs per well, we found in average 30 ± 6.4 (BMP4) and 41 ± 12 (BMP4+Wnt3a) MAP2-positive cells in control conditions, and 71 ± 10 (BMP4) and 94 ± 16 (BMP4+Wnt3a) MAP2-positive cells when cultured within the foam 4RepCT (**Figure 2**). Morphological characteristics of cells grown on 4RepCT foam structures were similar to the poly-L-ornithine and fibronectin-coated polystyrene cell culture plates used as controls (**Figure 1**). Virtually all MAP2-negative cells were found to stain positive for the astrocytic marker GFAP (**Figure 1**). NSCs differentiated within 4RepCT 3D foam-like structures thus retained full potential to differentiate into cells expressing neuronal and astrocytic markers, and 4RepCT-derived structures seemed to provide an even better substrate for differentiation than standard culture plates as assessed by MAP2 staining (**Figure 2**).

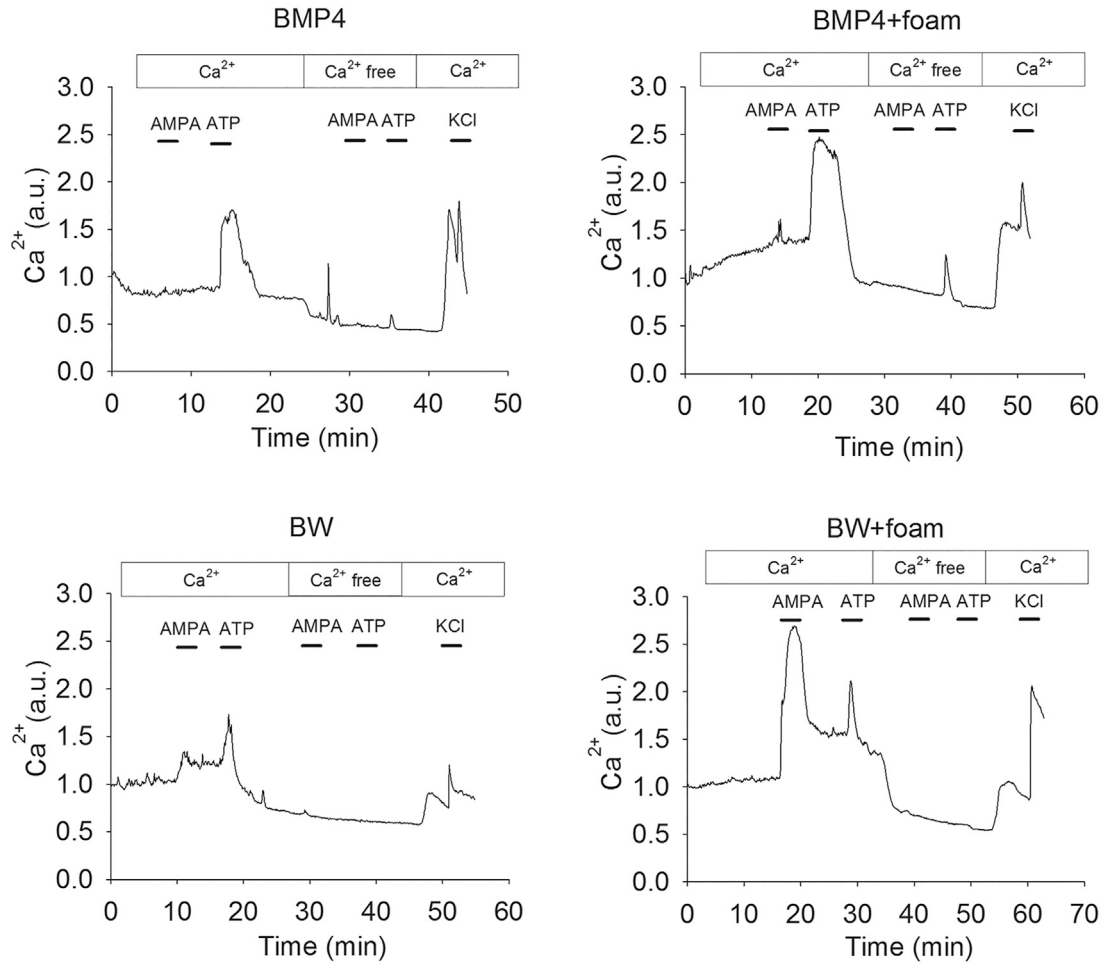

FIGURE 3 | Representative single cell Ca^{2+} response traces after treatment of NSC cultured in control conditions as defined above or 4RepCT-derived foam structures with BMP4 and BMP4+Wnt3a (BW).

4RepCT Foam Structures Provide Efficient Substrates for Differentiation of Neural Stem Cells Into AMPA-Responsive, Functional Neurons

BMP4 and Wnt3a are required for proper development of neurons of the hippocampal formation, a structure of the forebrain essential for learning, and mature hippocampal neurons express receptors for the excitatory neurotransmitter glutamate (Lee et al., 2000; Sur and Rubenstein, 2005). We therefore decided to investigate the functionality of BMP4 vs. BMP4+Wnt3a induced neurons grown in foam 4RepCT matrices by examining their responsiveness to specific glutamate receptor and calcium (Ca^{2+}) signaling agonists. Calcium signaling was measured in NSCs differentiated for 14 days and loaded with the Ca^{2+} sensitive fluorophore Fluo-3/AM.

All cells examined in BMP4 or BMP4+Wnt3a-treated cultures were first shown to respond to KCl depolarization with a rapid increase in the intracellular Ca^{2+} concentration (Supporting Information), indicating that the cultures were functional and healthy. A major advantage of measuring the calcium responses compared to, e.g., electrophysiological analysis (Leao et al., 2010; Tang-Schomer et al., 2014; Chwalek et al., 2015) is that a large number of cells can be analyzed simultaneously and thus populations of different cell types identified. To investigate the functional identity of the cells, we used an established protocol to discriminate between neurons and astrocytes in the BMP4 and BMP4+Wnt3a-treated cells. Astrocytes express mainly the metabotropic P2Y purinoceptors whereas mature neurons express the ionotropic P2X purinoceptors, plus a small population of P2Y receptors that do not affect intracellular Ca^{2+} but mediate slow changes in membrane potential (Illes and Ribeiro, 2004; Rowe et al., 2005; Andersson et al., 2011). Neurons should therefore respond to ATP in the presence, but not absence, of extracellular Ca^{2+}, whereas astrocytes should respond to ATP in both conditions (Rowe et al., 2005; Lin et al., 2007). Cells were further characterized functionally by treatment with the selective ionotropic glutamate receptor (GluR)

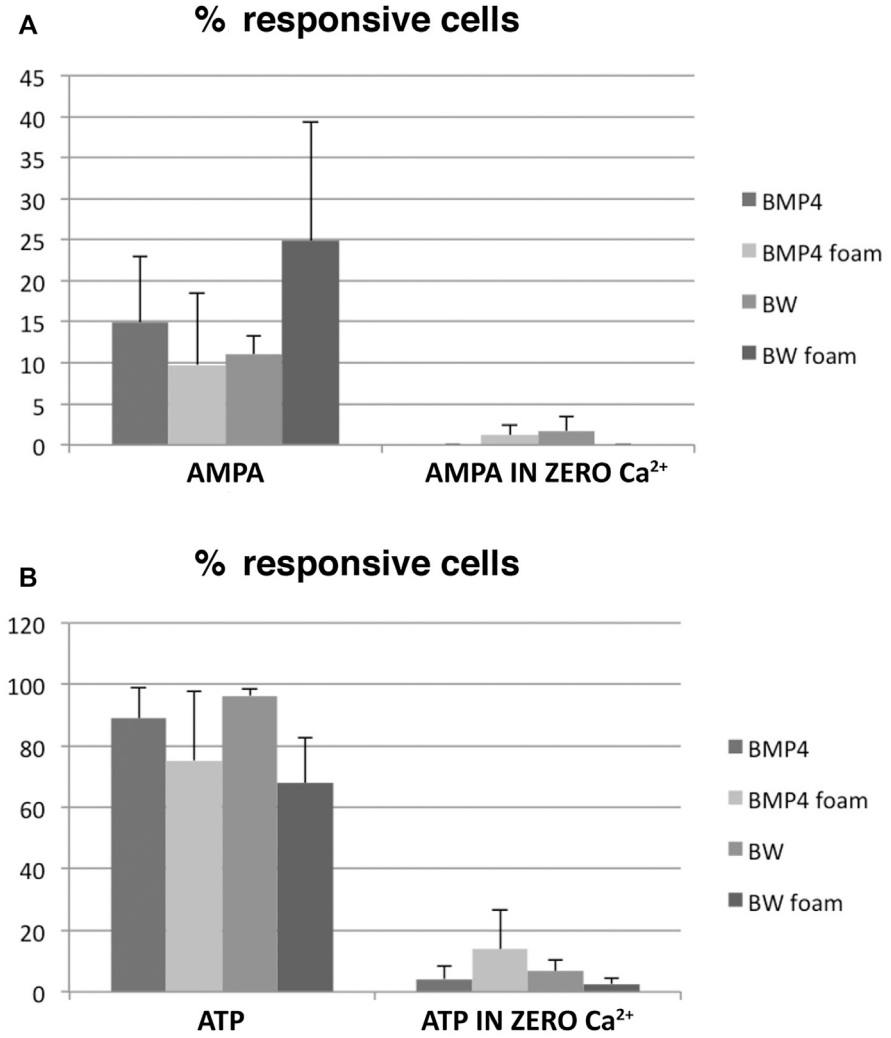

FIGURE 4 | Quantifications of the Ca^{2+} imaging experiments. A large variability was noted, but a substantial fraction of AMPA-responsive neurons was present in the BMP4+Wnt3a (BW)-treated cultures grown in 3D 4RepCT-derived matrices. Each bar represents the means ± SEM (standard error mean; $n > 30$ cells per condition) of single cell Ca^{2+} responses as illustrated in **Figure 3** from $n = 3$ independent experimental series. Statistical analysis was performed using two-tailed unpaired *t*-test after two-way ANOVA analysis of variance was used. The threshold value for statistical significance (α value) was set at 0.05 (*$p < 0.05$). Data are presented as the mean ± standard error of the mean (SEM) of independent experiments (3–5 experimental series per condition). Please see Materials and Methods section for detailed description of the statistical analysis.

agonist AMPA, which, in the presence of extracellular Ca^{2+}, should evoke a transient response in neurons but not in astrocytes. Stimulation of BMP4 and BMP4+Wnt3a-treated cultures with ATP or AMPA in an extracellular medium with or without Ca^{2+} confirmed our previous observations that the NSC-derived cells can be divided into several subsets depending on their distinct Ca^{2+} response patterns. Hence, one subset of cells responded to AMPA and ATP, respectively, with a transient Ca^{2+} increase in the presence but not absence of extracellular Ca^{2+}, other cells responded to both AMPA and ATP in the presence of Ca^{2+}, while another subset of cells only responded to ATP but not AMPA under both conditions. Examples of response curves are depicted in **Figure 3**. Supporting Information contains four micrograph time-lapse movies of around 90 s each representing one c:a 60–70 min experiment in each condition demonstrating the calcium response to ATP, AMPA, and KCl similar to the results from each condition shown in **Figure 3**.

4RepCT Foam Structures Enhance the Differentiation of Neural Stem Cells Into AMPA-Responsive, Functional Neurons

We next performed a quantitative analysis of the multirecordings (>30 cells/recording) of BMP4- and BMP4+Wnt3a-treated NSC-cultures and to which extent ATP-responsive cells also responded to AMPA in the presence or absence of Ca^{2+} in three different

experiments for each condition. The total number of responsive cells as analyzed by ATP-stimulation were between on average 65–95% (**Figure 4B**), of which some also responded in Ca^{2+}-zero conditions, and thus presumably were astrocytes. When analyzing the fraction of cells responding to the glutamate receptor agonist AMPA in the presence of Ca^{2+} specifically, we found that stimulation of cultures co-treated with BMP4+Wnt3a resulted in a transient Ca^{2+} increase in on average 25% of cells grown in 3D 4RepCT foam matrices compared to an average of 10–15% in other conditions (**Figure 4A**). As expected, there were only a very low number of cells responding to AMPA in zero Ca^{2+} conditions (**Figure 4A**).

A substantial variation in responses between the different experiments precluded any statistical analysis, even if the number of experiments would have been increased, but our results clearly demonstrates that the biodegradable, recombinant spider silk substrate 4RepCT permits differentiation by BMP and Wnt3a into functional, glutamate receptor-responsive neurons to an extent at least as efficient as the quintessential NSC culture method.

Most approaches in cell therapy of the central nervous system (CNS) have hitherto been based on delivery of relatively homogenous cell populations to brain structures with limited number of cell types, i.e. substantia nigra or the striatum. However, most parts of the CNS are highly organized with specific functional centers consisting of a larger number of populations with mixed cell types (Zeisel et al., 2015), and due to this highly organized anatomy, 3D-approaches are not only recommended, it is required for continued progress in applied stem cell research and regenerative medicine (Poli et al., 2019). Recombinant spider silk provide several potential advantages over other materials used as matrices and/or over the natural material: 1) it displays mechanical integrity and can be processed into different 3D structures (Stark et al., 2007; Widhe et al., 2010), 2) the production is scalable (Tokareva et al., 2013), 3) the sequence of the proteins can easily be modified to contain also cell binding motifs Wohlrab et al., 2012), 4) recombinant spider silk fibers evoke little inflammatory reaction and are gradually degraded when implanted subcutaneously (Fredriksson et al., 2009; Lucke et al., 2018 and references therein), and 5) the material is chemically defined and of non-animal origin, and thus a possible substrate for long-term, xeno-free cell culture.

Our system has some differences and advantages compared to most published protocols hitherto. First, as previously described, NSCs cultured and differentiated on 4RepCT do not require any additional coating, allowing a xeno-free substrate for organoid cultures as mentioned. In addition, the 4RepCT substrate is transparent allowing analysis of morphological details. Due to this transparency, we could perform calcium analysis after agonist stimulation, and demonstrate the overall efficiency of the differentiation and nature of the differentiated cells and structures of a large proportion of the cells in the cultures. Furthermore, in contrast to many but not all other protocols, our rodent cells have been defined as multipotent and able to differentiate into neurons, astrocytes, and oligodendrocytes in clonal conditions (Jepsen et al., 2007; Castelo-Branco et al., 2014) as well as mesenchymal fates (Andersson et al., 2011) allowing a strict control of the development of the tissue-like structures. Lastly, as the spider silk substrate consists of recombinant protein, it opens up for various possibilities of developing simple protocols for growing neural organoids in GMP-grade environment in the near future.

Here we employed 4RepCT foams in NSCs differentiation in order to successfully identify a defined culture system for NSCs. The 4RepCT foam structure supports NSC attachment, survival, and differentiation into functional neurons in pseudo-3D, and 4RepCT 3D foam implantation has already been successfully applied in animal studies (Fredriksson et al., 2009) as well as transplantation of the NSCs described here (Lundberg et al., 2012), suggesting it to be a promising candidate for future studies of NSC differentiation and formation into functional circuits *in vitro* and for tests for use of NSCs in cell therapy in various animal models of neurological disease *in vivo*.

CONCLUSION

Foam-like structures generated from biodegradable, recombinant spider silk protein (4RepCT) permit differentiation of neural stem cells into functional, AMPA-responsive neuronal circuits without animal- or human-derived components. We propose that matrices generated from recombinant spider silk protein are suitable for development of applications in stem cell research, tissue engineering, and regenerative medicine.

DATA AVAILABILITY STATEMENT

The raw data supporting the conclusions of this article will be made available by the authors, without undue reservation.

ETHICS STATEMENT

The animal study was reviewed and approved by North Stockholm regional committee for animal research and ethics, #284/11.

AUTHOR CONTRIBUTIONS

ML, Neural stem cell culture, immunohistochemistry, calcium imaging, draft development. PR, Calcium imaging, analysis. JL, Neural stem cell culture, analysis, manuscript production. PU, Calcium imaging, supervision, analysis, figure production. AR, Biomaterial generation, biomaterial expertise, manuscript finalisation. OH, Project design, supervision, figure production, manuscript finalisation.

ACKNOWLEDGMENTS

The authors would like to thank the Hermanson lab for valuable discussions and comments on this manuscript. We thank Spiber Technologies AB for providing the 4RepCT matrices. This work was funded by grants from CIMED, StratRegen (SFO to KI), Karolinska Institutets Forskningsstiftelser (2011FoBi023) (to AR), VR-MH (Project Grants to PU, AR, and OH), Karolinska Institutet (TEMA), the Swedish Childhood Cancer Foundation (BCF), the Swedish Cancer Society, and Vinnova (to OH). A previous version of this manuscript has been released as a pre-print at bioRxiv (Lewicka et al., 2019).

SUPPLEMENTARY MATERIAL

The Supplementary Material for this article can be found online at: https://www.frontiersin.org/articles/10.3389/fmats.2020.560372/full#supplementary-material.

REFERENCES

Allmeling, C., Jokuszies, A., Reimers, K., Kall, S., Choi, C. Y., Brandes, G., et al. (2008). Spider silk fibres in artificial nerve constructs promote peripheral nerve regeneration. *Cell Prolif.* 41, 408–420. doi:10.1111/j.1365-2184.2008.00534.x

Andersson, T., Duckworth, J. K., Fritz, N., Lewicka, M., Södersten, E., Uhlén, P., et al. (2011). Noggin and Wnt3a enable BMP4-dependent differentiation of telencephalic stem cells into GluR-agonist responsive neurons. *Mol. Cell. Neurosci.* 47, 10–18. doi:10.1016/j.mcn.2011.01.006

Blumenthal, N. R., Hermanson, O., Heimrich, B., and Shastri, V. P. (2014). Stochastic nanoroughness modulates neuron-astrocyte interactions and function via mechanosensing cation channels. *Proc. Natl. Acad. Sci. USA* 111, 16124–16129. doi:10.1073/pnas.1412740111

Castelo-Branço, G., Lilja, T., Wallenborg, K., Falcão, A. M., Marques, S. C., Gracias, A., et al. (2014). Neural stem cell differentiation is dictated by distinct actions of nuclear receptor corepressors and histone deacetylases. *Stem Cell Reports* 3, 502–515. doi:10.1016/j.stemcr.2014.07.008

Chwalek, K., Tang-Schomer, M. D., Omenetto, F. G., and Kaplan, D. L. (2015). *In vitro* bioengineered model of cortical brain tissue. *Nat. Protoc.* 10, 1362–1373. doi:10.1038/nprot.2015.091

Discher, D. E., Mooney, D. J., and Zandstra, P. W. (2009). Growth factors, matrices, and forces combine and control stem cells. *Science* 324, 1673–1677. doi:10.1126/science.1171643

Fredriksson, C., Hedhammar, M., Feinstein, R., Nordling, K., Kratz, G., Johansson, J., et al. (2009). Tissue response to subcutaneously implanted recombinant spider silk: an *in vivo* study. *Materials* 2, 1908–1922. doi:10.3390/ma2041908

Gosline, J. M., Guerette, P. A., Ortlepp, C. S., and Savage, K. N. (1999). The mechanical design of spider silks: from fibroin sequence to mechanical function. *J. Exp. Biol.* 202, 3295–3303.

Hardy, J. G., and Scheibel, T. R. (2009). Silk-inspired polymers and proteins. *Biochem. Soc. Trans.* 37, 677–681. doi:10.1042/BST0370677

Hedhammar, M., Bramfeldt, H., Baris, T., Widhe, M., Askarieh, G., Nordling, K., et al. (2010). Sterilized recombinant spider silk fibers of low pyrogenicity. *Biomacromolecules* 11, 953–959. doi:10.1021/bm9014039

Hedhammar, M., Rising, A., Grip, S., Martinez, A. S., Nordling, K., Casals, C., et al. (2008). Structural properties of recombinant nonrepetitive and repetitive parts of major ampullate spidroin 1 from Euprosthenops australis: implications for fiber formation. *Biochemistry* 47, 3407–3417. doi:10.1021/bi702432y

Illes, P., and Ribeiro, J. A. (2004). Neuronal P2 receptors of the central nervous system. *Curr. Top. Med. Chem.* 4, 831–838. doi:10.2174/1568026043451032

Ilkhanizadeh, S., and Teixeira, A. I. (2007). Inkjet printing of macromolecules on hydrogels to steer neural stem cell differentiation. *Biomaterials* 28, 3936–3943. doi:10.1016/j.biomaterials.2007.05.018

Jepsen, K., Solum, D., Zhou, T., McEvilly, R. J., Kim, H. J., Glass, C. K., et al. (2007). SMRT-mediated repression of an H3K27 demethylase in progression from neural stem cell to neuron. *Nature* 450, 415–419. doi:10.1038/nature06270

Johe, K. K., Hazel, T. G., Muller, T., Dugich-Djordjevic, M. M., and McKay, R. D. (1996). Single factors direct the differentiation of stem cells from the fetal and adult central nervous system. *Genes Dev.* 10, 3129–3140. doi:10.1101/gad.10.24.3129

Leão, R. N., Reis, A., Emirandetti, A., Lewicka, M., Hermanson, O., and Fisahn, A. (2010). A voltage-sensitive dye-based assay for the identification of differentiated neurons derived from embryonic neural stem cell cultures. *PloS One* 5, e13833. doi:10.1371/journal.pone.0013833

Lee, S. M., Tole, S., Grove, E., and McMahon, A. P. (2000). A local Wnt-3a signal is required for development of the mammalian hippocampus. *Development* 127, 457–467.

Lewicka, M., Hermanson, O., and Rising, A. U. (2012). Recombinant spider silk matrices for neural stem cell cultures. *Biomaterials* 33, 7712–7717. doi:10.1016/j.biomaterials.2012.07.021

Lewicka, M., Rebellato, P., Lewicki, J., Uhlén, P., Rising, A., and Hermanson, O. (2019). Recombinant spider silk protein matrices facilitate multi-analysis of calcuim-signaling in neural stem cell-derived AMPA-responsive neurons. *bioRxiv* 579, 292.

Lewis, R. V. (2006). Spider silk: ancient ideas for new biomaterials. *Chem. Rev.* 106, 3762–3774. doi:10.1021/cr010194g

Lin, J. H., Takano, T., Arcuino, G., Wang, X., Hu, F., Darzynkiewicz, Z., et al. (2007). Purinergic signaling regulates neural progenitor cell expansion and neurogenesis. *Dev. Biol.* 302, 356–366. doi:10.1016/j.ydbio.2006.09.017

Lucke, M., Mottas, I., Herbst, T., Hotz, C., Römer, L., Schierling, M., et al. (2018). Engineered hybrid spider silk particles as delivery system for peptide vaccines. *Biomaterials* 172, 105–115. doi:10.1016/j.biomaterials.2018.04.008

Lundberg, J., Södersten, E., Sundström, E., Le Blanc, K., Andersson, T., Hermanson, O., et al. (2012). Targeted intra-arterial transplantation of stem cells to the injured CNS is more effective than intravenous administration: engraftment is dependent on cell type and adhesion molecule expression. *Cell Transpl.* 21, 333–343. doi:10.3727/096368911X576036

Omenetto, F. G., and Kaplan, D. L. (2010). New opportunities for an ancient material. *Science* 329, 528–531. doi:10.1126/science.1188936

Poli, D., Magliaro, C., and Ahluwalia, A. (2019). Experimental and computational methods for the study of cerebral organoids: a review. *Front. Neurosci.* 13, 162. doi:10.3389/fnins.2019.00162

Radtke, C., Allmeling, C., Waldmann, K. H., Reimers, K., Thies, K., Schenk, H. C., et al. (2011). Spider silk constructs enhance axonal regeneration and remyelination in long nerve defects in sheep. *PloS One* 6, e16990. doi:10.1371/journal.pone.0016990

Rising, A., Widhe, M., Johansson, J., and Hedhammar, M. (2011). Spider silk proteins: recent advances in recombinant production, structure-function relationships and biomedical applications. *Cell. Mol. Life Sci.* 68, 169–184. doi:10.1007/s00018-010-0462-z

Rowe, E. W., Jeftinija, D. M., Jeftinija, K., and Jeftinija, S. (2005). Development of functional neurons from postnatal stem cells *in vitro*. *Stem Cell.* 23, 1044–1049. doi:10.1634/stemcells.2005-0037

Stark, M., Grip, S., Rising, A., Hedhammar, M., Engström, W., Hjälm, G., et al. (2007). Macroscopic fibers self-assembled from recombinant miniature spider silk proteins. *Biomacromolecules* 8, 1695–1701. doi:10.1021/bm070049y

Sur, M., and Rubenstein, J. L. (2005). Patterning and plasticity of the cerebral cortex. *Science* 310, 805–810. doi:10.1126/science.1112070

Tang-Schomer, M. D., White, J. D., Tien, L. W., Schmitt, L. I., Valentin, T. M., Graziano, D. J., et al. (2014). Bioengineered functional brain-like cortical tissue. *Proc. Natl. Acad. Sci. USA* 111, 13811–13816. doi:10.1073/pnas.1324214111

Teixeira, A. I., Duckworth, J. K., and Hermanson, O. (2007). Getting the right stuff: controlling neural stem cell state and fate *in vivo* and *in vitro* with biomaterials. *Cell Res.* 17, 56–61. doi:10.1038/sj.cr.7310141

Teixeira, A. I., Ilkhanizadeh, S., Wigenius, J. A., Duckworth, J. K., Inganäs, O., and Hermanson, O. (2009). The promotion of neuronal maturation on soft substrates. *Biomaterials* 30, 4567–4572. doi:10.1016/j.biomaterials.2009.05.013

Teixeira, A. I., Hermanson, O., and Werner, C. (2010). Designing and engineering stem cell niches. *MRS Bull.* 35, 591–596. doi:10.1038/sj.cr.7310141

Tokareva, O., Michalczechen-Lacerda, V. A., Rech, E. L., and Kaplan, D. L. (2013). Recombinant DNA production of spider silk proteins. *Microb. Biotechnol.* 6, 651–663. doi:10.1111/1751-7915.12081

Uhlén, P. (2004). Spectral analysis of calcium oscillations. *Sci. STKE* 2004 (258), pl15. doi:10.1126/stke.2582004pl15

Vollrath, F., Barth, P., Basedow, A., Engström, W., and List, H. (2002). Local tolerance to spider silks and protein polymers *in vivo*. *In Vivo* 16, 229–234. doi:10.3390/ma2041908

Widhe, M., Bysell, H., Nystedt, S., Schenning, I., Malmsten, M., Johansson, J., et al. (2010). Recombinant spider silk as matrices for cell culture. *Biomaterials* 31, 9575–9585. doi:10.1016/j.biomaterials.2010.08.061

Wohlrab, S., Müller, S., Schmidt, A., Neubauer, S., Kessler, H., Leal-Egaña, A., et al. (2012). Cell adhesion and proliferation on RGD-modified recombinant spider silk proteins. *Biomaterials* 33, 6650–6659. doi:10.1016/j.biomaterials.2012.05.069

Zeisel, A., Muñoz-Manchado, A. B., Codeluppi, S., Lönnerberg, P., La Manno, G., Juréus, A., et al. (2015). Brain structure. Cell types in the mouse cortex and hippocampus revealed by single-cell RNA-seq. *Science* 347, 1138–1142. doi:10.1126/science.aaa1934

Conflict of Interest: The authors declare that the research was conducted in the absence of any commercial or financial relationships that could be construed as a potential conflict of interest.

frontiers in Bioengineering and Biotechnology

ORIGINAL RESEARCH
published: 16 February 2021
doi: 10.3389/fbioe.2021.607709

In vitro and *in vivo* Study on an Injectable Glycol Chitosan/Dibenzaldehyde-Terminated Polyethylene Glycol Hydrogel in Repairing Articular Cartilage Defects

Jianhua Yang[1†], Xiaoguang Jing[2,3†], Zimin Wang[2], Xuejian Liu[3,4], Xiaofeng Zhu[5,6], Tao Lei[7], Xu Li[3], Weimin Guo[3], Haijun Rao[1], Mingxue Chen[3], Kai Luan[2], Xiang Sui[3], Yen Wei[7*], Shuyun Liu[3*] and Quanyi Guo[3*]*

[1] Orthopedics Department, Longgang District People's Hospital of Shenzhen & The Third Affiliated Hospital (Provisional) of The Chinese University of Hong Kong, Shenzhen, China, [2] The Second Affiliated Hospital of Luohe Medical College, Luohe, China, [3] Chinese PLA General Hospital, Institute of Orthopedics, Beijing, China, [4] Department of Orthopedics, Zhengzhou Seventh People's Hospital, Zhengzhou, China, [5] School of Medicine, Jiamusi University, Jiamusi, China, [6] Medical Research Center of Mudanjiang Medical School, Mudanjiang, China, [7] The Key Laboratory of Bioorganic Phosphorus Chemistry and Chemical Biology (Ministry of Education) Department of Chemistry, Tsinghua University, Beijing, China

The normal anatomical structure of articular cartilage determines its limited ability to regenerate and repair. Once damaged, it is difficult to repair it by itself. How to realize the regeneration and repair of articular cartilage has always been a big problem for clinicians and researchers. Here, we conducted a comprehensive analysis of the physical properties and cytocompatibility of hydrogels, and evaluated their feasibility as cell carriers for Adipose-derived mesenchymal stem cell (ADSC) transplantation. Concentration-matched hydrogels were co-cultured with ADSCs to confirm ADSC growth in the hydrogel and provide data supporting *in vivo* experiments, which comprised the hydrogel/ADSCs, pure-hydrogel, defect-placement, and positive-control groups. Rat models of articular cartilage defect in the knee joint region was generated, and each treatment was administered on the knee joint cartilage area for each group; in the positive-control group, the joint cavity was surgically opened, without inducing a cartilage defect. The reparative effect of injectable glycol chitosan/dibenzaldehyde-terminated polyethylene glycol (GCS/DF-PEG) hydrogel on injured articular cartilage was evaluated by measuring gross scores and histological score of knee joint articular-cartilage injury in rats after 8 weeks. The 1.5% GCS/2% DF-PEG hydrogels degraded quickly *in vitro*. Then, We perform *in vivo* and *in vitro* experiments to evaluate the feasibility of this material for cartilage repair *in vivo* and *in vitro*.

Keywords: cartilage defect, glycol chitosan hydrogel, polyethylene glycol, repair, tissue engineering

OPEN ACCESS

Edited by:
Huanan Wang,
Dalian University of Technology, China

Reviewed by:
Xiong Lu,
Southwest Jiaotong University, China
Baolin Guo,
Xi'an Jiaotong University, China

***Correspondence:**
Jianhua Yang
jianhua01@163.com
Yen Wei
weiyen@tsinghua.edu.cn
Shuyun Liu
clear_ann@163.com
Quanyi Guo
doctorguo_301@163.com

†These authors share first authorship

Specialty section:
This article was submitted to Biomaterials, a section of the journal Frontiers in Bioengineering and Biotechnology

Received: *17 September 2020*
Accepted: *18 January 2021*
Published: *16 February 2021*

Citation:
Yang J, Jing X, Wang Z, Liu X, Zhu X, Lei T, Li X, Guo W, Rao H, Chen M, Luan K, Sui X, Wei Y, Liu S and Guo Q (2021) In vitro and in vivo Study on an Injectable Glycol Chitosan/Dibenzaldehyde-Terminated Polyethylene Glycol Hydrogel in Repairing Articular Cartilage Defects. Front. Bioeng. Biotechnol. 9:607709. doi: 10.3389/fbioe.2021.607709

INTRODUCTION

The normal anatomical structure of articular cartilage determines its abilities for regeneration, although repair is very limited once damage occurs (Rai et al., 2017). Achieving regeneration and repair of articular cartilage has been a major problem for clinicians and researchers. Current clinical treatments for cartilage damage include non-steroidal anti-inflammatory drugs, platelet-rich plasma (Laudy et al., 2015), microfractures, autologous chondrocyte implantation, and osteochondral transplantation techniques (Lynch et al., 2015; Oussedik et al., 2015), but in most cases, the results are unsatisfactory. Curative effects occur when the tissue formed by repair is mostly fibrocartilage, rather than hyaline cartilage.

Cartilage tissue engineering provides a new approach for regenerating and repairing articular cartilage defects (Johnstone et al., 2013). Seed cells, scaffold materials, and bioactive factors are three key elements of cartilage tissue engineering. Adipose-derived mesenchymal stem cells (ADSCs) can differentiate into a wide range of tissues and are easy to culture *in vitro*. Numerous studies have confirmed that ADSCs show strong proliferative capacity, strong regulation of immune function, and multi-directional differentiation potential, making them ideal seed cells for cartilage tissue engineering. Recently, the use of ADSCs for cartilage regeneration and repair has gradually increased, and satisfactory results have been achieved (Kasir et al., 2015; Zhang et al., 2017; Pleumeekers et al., 2018).

Hydrogels are three-dimensional grid scaffolds composed of hydrophilic polymers. They have a high water content and similar properties to the natural cartilage extracellular matrix. Hydrogels are considered very suitable for artificial extracellular matrixes in tissue engineering (Yang et al., 2017). Injectable hydrogels can be gelled *in situ* in the defect site after injection (Liu et al., 2017), which offers the advantage that a simple, minimally invasive injection method can be used to simplify complex implant procedures. Research groups have independently developed and prepared injectable ethylene glycol chitosan/dibenzaldehyde-functionalized (GCS/DF)-polyethylene glycol (PEG) hydrogels using chitosan and PEG as raw materials. A previous study showed that PEG-based hydrogels crosslinked by Schiff base has good injectability and promotes self-healing (Zhang et al., 2011). The team designed injectable GCS/DF-PEG-loaded ADSCs to repair articular cartilage defects and simplify cartilage-repair operations, representing an important technological advance. In this study, we conducted a comprehensive analysis of the physical properties and cytocompatibility of hydrogel materials, and their feasibility for tissue engineering cell carriers was evaluated. The *in vivo* findings of our study of repair should serve as a valuable reference in the development of tissue engineering for the treatment of articular cartilage defect. Mechanical testing showed that the hydrogel elastic modulus increased proportionally with DF-PEG concentration. Proliferation experiments with mesenchymal stem cells in hydrogels showed that higher DF-PEG concentrations correlated with slower cell proliferation. Co-culture experiments showed that ADSCs survived well in hydrogels. Eight weeks post-operation, the hydrogel/ADSC repair and pure-hydrogel groups showed better defect repair than the blank-control group, and the hydrogel/ADSC repair group displayed articular cartilage surface, as shown by toluidine blue and red "O" bright green staining. The 1.5% GCS/4% DF-PEG hydrogel showed good injectability, self-healing properties, and biocompatibility and provided a good cell proliferation microenvironment. GCS/DF-PEG hydrogels functioned as cell carriers for ADSC transplantation, enabling articular-cartilage defect treatment. The simple operation showed efficacy compared to the blank group. Hydrogel composition and structure should be improved in future for improved cartilage-repair effect.

MATERIALS AND METHODS

Hydrogel Fabrication

Preparation of GCS/DF-PEG Hydrogels

GCS powder was dissolved with stirring in deionized water to a concentration of 1.5% (mass/vol) and sterilized using a 0.22 μm filter. Dialdehyde-functionalized PEG powder was dissolved in deionized water, with stirring, and sterilized using a 0.22 μm filter. GCS solution was mixed with an equal volume of sterile dialdehyde-functionalized PEG solution and shaped in a 96-well plate to obtain a GCS/DF-PEG hydrogel, as described (Li et al., 2017). Briefly described as: PEG2000 (3.26 g, 1.63 mmol), 4-formylbenzoic acid (0.98 g, 6.52 mmol), and DMAP (0.050 g) were dissolved in 100 mL of dry THF, followed by the addition of DCC (1.68 g, 8.15 mmol) under a nitrogen atmosphere. The system was stirred at 20°C for 18 h; then, the white solid was filtered. The polymer was obtained as a white solid after repeated dissolution in THF and precipitation in diethyl ether for three times. Upon drying, 3.00 g of dialdehyde-functionalized PEG (DF-PEG) was obtained in 79.8% yield.

Electron Microscopy-Based Detection of the Porosity of GCS/DF-PEG Hydrogels

The hydrogel sample prepared above was dehydrated using a vacuum freeze dryer for 24 h, a cross-section was collected, and the sample was cut into 0.5–1.0 mm flakes. The sheet was placed in a vacuum chamber, uniformly coated with a thin layer of gold, and then loaded into a field-emission scanning electron microscope for topographical imaging (Liu et al., 2017).

Different Mass Fractions of Aldehyde-Functionalized, GCS/DF-PEG Hydrogel in *in vitro*-Degradation Experiments

Using the methods described above, we prepared a 1.5% GCS (mass/vol) solution and dialdehyde -functionalized PEG solutions with mass fractions of 2, 4, and 8%. Then, 80 μL of GCS solution was mixed with each of the three dialdehyde-functionalized PEG solutions in equal volumes to obtain three different dialdehyde-functionalized PEG-crosslinked GCS/DF-PEG hydrogels. Each group of hydrogels was prepared according to the same specifications, immersed in phosphate-buffered saline (PBS) (pH 7.4, 37°C) and 5% CO_2, and observed over the

course of 4 weeks. For each group, three pieces were collected each week, water droplets were absorbed to the surface of a rubber block with absorbent paper, the mass was measured with a balance, and then used immediately before degradation occurred. After 5, 7, 14, 21, and 28 days, the degradation rate for each group of hydrogels was calculated as follows: degradation rate = (quality before degradation–quality after degradation)/mass before degradation × 100% (Qi et al., 2018).

Determination of the Elastic Modulus of Different Dialdehyde-Functionalized PEG-Crosslinked GCS/DF-PEG Hydrogels

The 1.5% GCS solution (mass/vol) was mixed with equal volumes of 2, 4, or 8% dialdehyde-functionalized PEG solution, followed by shaping into cylindrical hydrogel blocks. Subsequently, each hydrogel was cut into three pieces and then each set of hydrogel blocks was placed flat on a measuring table. The position of the measuring head was adjusted, such that it came into close contact with the rubber block, after which the rubber block was slowly pressed (0.01 mm/s). The pressing distance was 20% of the total height. The pressure was measured in real time, and the data were analyzed to draw the force curve and calculate the modulus of elasticity (Sun et al., 2017). The shear-thinning and self-healing properties of the hydrogels are characterized in the supplementary information.

Isolation and Culture of ADSCs

ADSCs were isolated and cultured as follows. SD rats were sacrificed and placed in 75% ethanol for 10–15 min after cervical dislocation. The subcutaneous adipose tissue in the bilateral inguinal region was excised, visible blood vessels in the tissues were removed, and the tissue was washed two or three times with PBS. The tissue was transferred to a sterile penicillin vial, cut into a paste, 0.1% type-II collagenase and magnetic beads were added, and the tissue was digested by stirring. After 30 min, the digestion was terminated by adding low-sugar Dulbecco's modified Eagle's medium (DMEM) containing 10% fetal bovine serum. A filter was used to remove large undigested tissue blocks, the filtrate was centrifuged at 1,700 r/min for 5 min, the supernatant was discarded, and the cells were resuspended in low-glucose DMEM supplemented with 10% fetal bovine serum. The cells were transferred to a culture flask and incubated at 37°C with 5% CO_2; after 24 h, the culture medium was replaced for the first time, and then the culture medium was changed every other day. The cells were subcultured 1:3 when they reached 80–90% confluency.

Biosynthesis of Hydrogels on ADSCs

Determining the Survival Rate of ADSCs in GCS/DF-PEG Hydrogels

The survival of ADSCs in GCS/DF-PEG hydrogels was evaluated by dead–live staining, using DMEM containing 10% fetal bovine serum. Sterile solutions of 3% GCS (mass/vol) and dialdehyde-functionalized PEG (mass fraction, 4%) were prepared. A suspension of passage-2 ADSCs (10×10^9 cells/L) was mixed with an equal volume of sterile 4% dialdehyde-functionalized PEG solution and transferred into a focusing dish. After allowing the mixture to stand until it completely gelatinized, appropriate medium was added to the confocal dish, which was placed in a 37°C, 5% CO_2 incubator, and stained with LIVE/DEAD stain on day 1 or 5. The cells were then imaged with a laser confocal microscope.

Detecting ADSC Proliferation in GCS/DF-PEG Hydrogels

The CCK-8 Cell Counting Kit was used to evaluate the proliferation of ADSCs in different mass fractions of dialdehyde-functionalized PEG-crosslinked GCS/DF-PEG hydrogels. An aseptic solution of 3% GCS solution (mass/vol) was mixed with suspended ADSCs, and 80 μL of the resulting cell suspension was mixed with an equal volume of 2, 4, or 8% dialdehyde-functionalized PEG. The resulting solution was stirred evenly, and gel-shaped hydrogels were formed in 96-well plates. After fully gelatinizing, 150 μL of DMEM supplemented with 10% fetal bovine serum was added to each well at 37°C, 5% CO_2 incubator. In the same manner, 80 μL of 1.5% GCS solution (with a cell mass fraction of 1.5%) was mixed with a 2, 4, or 8% dialdehyde-functionalized PEG solution, as done in the aforementioned three experiments. The first, third, fifth, and seventh days were chosen as experimental observation points, using three sets of duplicate wells at each time point in each group. At each time point, the medium in the well was replaced with 150 μL of CCK-8 solution, the plates were incubated for 4 h in a 37°C incubator, and then the CCK-8 solution in each well was transferred to another 96-well plate. The absorbance of each well was quickly measured at 450 nm in the dark using a microplate reader, after which a histogram was obtained and analyzed (Tsukamoto et al., 2017).

Hydrogel Combined With ADSCs for Repairing Articular-Cartilage Defects in Rats

Surgical Operation

Four experimental groups were studied, and five SD rats were randomly assigned to each group (**Table 1**). Preoperative anesthesia was performed with 10% chloral hydrate. Subsequently, the right knee joint was opened patella valgus by medial patellar approach and thigh pulley, and a full-thickness cartilage defect with a diameter of 2 mm and depth of 2 mm was made with a corneal circumcision at the knee joint. In the experimental group, the ADSCs and hydrogel complex were transplanted into the site by injection; in the conditional-control group, only the hydrogel was transplanted into the defect site by injection; no defect was made in the blank-control group. In the positive-control group, only the skin was cut and no cartilage

TABLE 1 | Experimental group treated by different biomaterials.

Groups	Treatments
Experimental group	GCS/DF-PEG/ADSCs
Condition control group	GCS/DF-PEG
Blank control group	Defect open-ended
Sham	No cartilage defect

defect was made. The joint capsule and skin were sutured layer-by-layer using sterile nylon suture.

CatWalk Joint-Repair Function Evaluation

A catwalk gait analyzer was used to analyze the gait scores of SD rats at 8 weeks following surgery. The average footprint strength and average footprint area were analyzed to evaluate the recovery of limb walking function.

Histological Evaluation of Articular Cartilage-Repair Effects

Rats were euthanized 8 weeks after surgery, and knee joint specimens were obtained for gross examination and scored according to the International Rehabilitation Association (ICRS) general observation system (**Table 1**). The repair area of the truncated defect was intercepted, soaked in 10% paraformaldehyde for 24 h, then decalcified with 4% ethylenediamine tetraacetic acid, decalcified for 45 days, embedded in paraffin, and 4-μm thick sections were prepared. The sections were subjected to staining with hematoxylin and eosin (HE), toluidine blue, and modified red O bright green to observe the regenerative repair of cartilage structures and glycosaminoglycan contents.

Statistical Analysis

The experimental data were statistically analyzed by SPSS 7.0 software. All the data were recorded in a $x \pm s$ format, and the inter-group comparison was based on one-way ANOVA. In the experiment, $P < 0.05$ was in the experiment.

RESULTS

General and Electron Microscopic Views of GCS/DF-PEG Hydrogels

As suggested by their molecular and structural formulas, GCS and dialdehyde-functionalized PEG are rapidly gelled by dynamic chemical bonds, which facilitate easy operation. Gel formation was observed 3–5 min after mixing the GCS solution with the dialdehyde-functionalized PEG solution at room temperature (**Figure 1**). As shown in **Figure 2A**, the rubber block could be easily passed through a 2 ml syringe, with hydrogels prepared with lower PEG concentrations being easier to push out. As shown in **Figure 2B**, the broken hydrogel block could be self-healed into a whole piece after being placed in a humid environment for approximately 10 min, with hydrogels prepared with lower PEG concentrations gelling more readily. After the hydrogel was freeze-dried using a vacuum, analysis by scanning electron microscopy showed that it had a porous structure with a pore size of 200–400 μm and good pore connectivity.

In vitro Degradation of GCS/DF-PEG Hydrogels

In vitro degradation-rate curves for three groups of GCS/DF-PEG hydrogels with different mass fractions of dialdehyde-functionalized PEG cross-linking are shown in **Figure 3**. The degradation rate of the gels increased over time, and the degradation rates of the 2, 4, and 8% aldehyde-functionalized PEG hydrogels were 50.67, 23.32, and 18.3% after

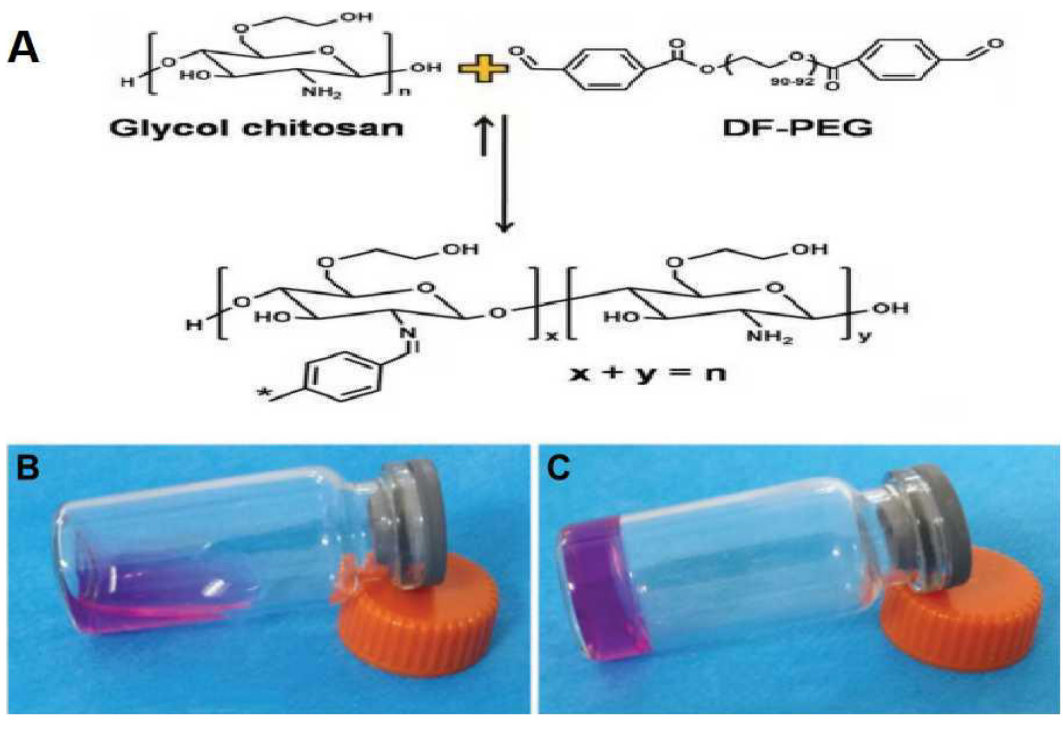

FIGURE 1 | Hydrogel gelation principle and morphology before and after gelation. **(A)** The principle of hydrogel gelation. **(B)** Hydrogel morphology before gelation. **(C)** Hydrogel morphology after gelation.

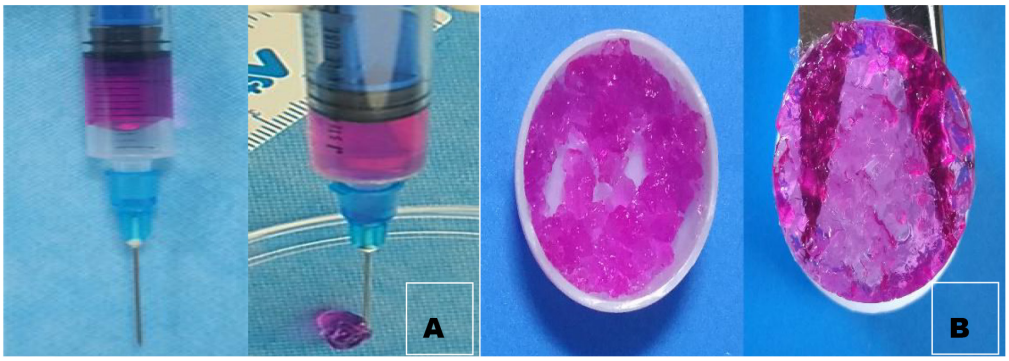

FIGURE 2 | Injectability observation **(A)** and self-healing observation of hydrogel. **(B)** We can see from the graph that the broken hydrogel can self-heal one piece.

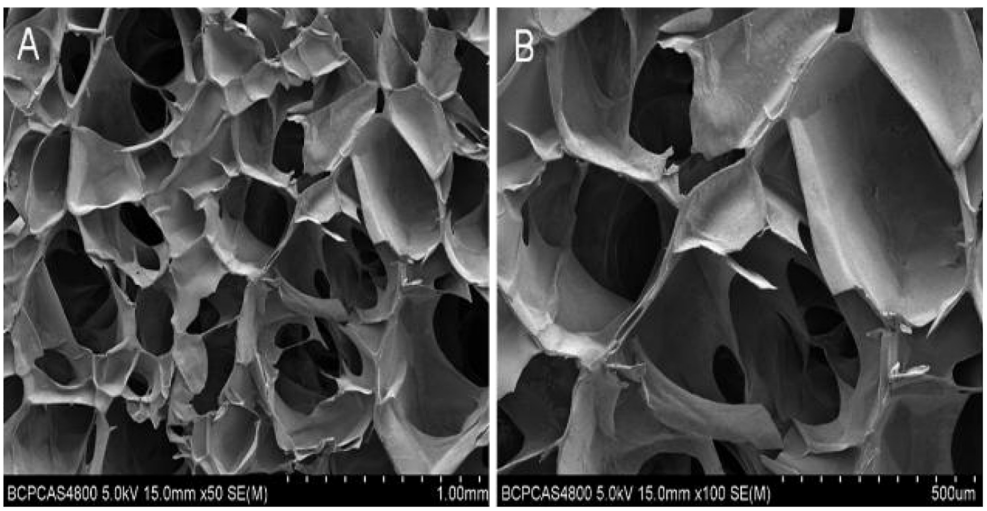

FIGURE 3 | Electron microscopic view of hydrogel. **(A)** Electron microscopic view of hydrogel with low magnification. **(B)** Electron microscopic view of hydrogel with high magnification.

4 weeks, respectively. **Figure 4A** shows that the degradation rate of a hydrogel in the 2%-mass fraction, dialdehyde-functionalized PEG group was significantly faster than those of the other two groups.

GCS/DF-PEG Hydrogel Elastic Modulus Testing

The mechanical test results were accurately recorded, using the elastic modulus formula with the 2, 4, and 8% dialdehyde-functionalized PEG hydrogel. The elastic moduli were 13.48, 22.21, and 33.19 kPa, respectively. **Figure 4B** shows that the elastic moduli of the GCS/DF-PEG hydrogels increased with increasing mass fractions of dialdehyde-functionalized PEG.

Live–Dead Staining of ADSCs in GCS/DF-PEG Hydrogels

The ADSCs in the hydrogels were subjected to live–dead staining and observed by laser confocal microscopy. The living cells showed green fluorescence, and the dead cells showed red fluorescence. **Figure 4C** shows that the ADSCs in the hydrogel were spherical, and the confocal microscopy results showed that the green fluorescence was stronger than the red fluorescence during the same day, that the number of cells increased on the fifth day compared with the first day, and that the survival rate was above 90%. Thus, the ADSCs survived and proliferated well within the hydrogel.

Proliferation of ADSCs in GCS/DF-PEG Hydrogels

The CCK-8 method was used to determine the proliferation of ADSCs in GCS/DF-PEG hydrogels with different mass fractions of dialdehyde-functionalized PEG cross-linking. The absorbance values of the control groups did not change significantly ($P > 0.05$) over time. The ADSCs in each experimental group showed significantly increased proliferation ($P < 0.05$). **Figure 4D** shows ADSC proliferation in the 2%-mass fraction, dialdehyde-functionalized PEG hydrogel. The proliferation rates of ADSCs on the 3rd, 5th, and 7th days were significantly faster in 2%-mass fraction, dialdehyde-functionalized PEG hydrogels than in the 4 and 8% groups ($P < 0.05$). No significant difference was

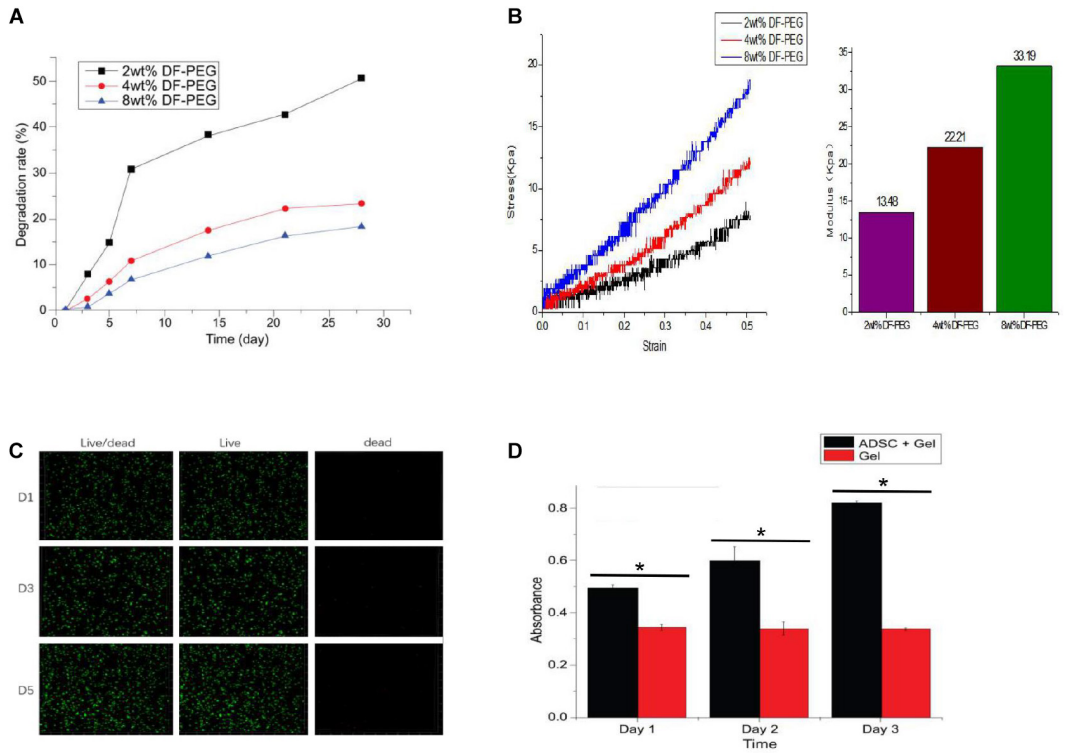

FIGURE 4 | Degradation of hydrogels with different PEG cross-linking concentrations **(A)**, Mechanical testing of different PEG cross-linked hydrogels **(B)**, Inactivated staining of ADSCs in 4% PEG hydrogel **(C)**, and Proliferation assay of ADSCs in 4% PEG hydrogel **(D)**. *$P < 0.05$.

observed in the proliferation rate of ADSCs in the alcohol group ($P > 0.05$).

Catwalk Gait Analysis

Catwalk gait analysis (**Figure 5A**) was performed with the rats at 8 weeks post-operation to evaluate the recovery of post-operative limb functions. The footprint pressure map shows that the postoperative footprint pressure gradually recovered. However, the degree of recovery of the hydrogel-composite ADSC group was significantly better ($P < 0.05$) than that of the simple hydrogel group and blank-control group. This finding indicates that the auto-function recovery of the hydrogel-complexed ADSC group was fastest and that the recovery effect was the best.

General View

Based on the general appearance (**Figure 5A–D**), no signs of knee infection, degenerative changes, or inflammation were found. At 8 weeks post-operation, the regenerated and repaired tissue showed a whitish color The repaired tissue in the experimental group was similar to articular cartilage, well fused with adjacent cartilage, and the contour of the femoral block was restored (smooth articular surface without cracks). After repair, the knee joint tissue in the blank-control group was slightly irregular, partially restored to the contour of the femoral block, and the margin of the defect was slightly gapped. In the defect-control group, the contour of the femur block did not recover, the defect area was clearly visible and slightly enlarged, and the knee joint was visible as a whole. The scores of each group were evaluated according to the ICRS general observation-evaluation system (**Figure 5C**). The following scores were found: ADSCs/hydrogel group (experimental group): 10, hydrogel repair group (conditional-control group): 8.4, blank-control group: 5.4, positive-control group (**Figure 5D**): 11. The scores in the experimental group were significantly higher than those in the hydrogel-transplantation group and the blank-control group ($P < 0.05$).

Organizational Evaluation

Histological staining of SD rats at 8 weeks after knee joint cartilage-defect repair is shown in **Figure 6**. In the experimental group, hydrogel-ADSCs were used to repair cartilage defects of the knee joint. After 8 weeks, HE staining showed that the defect area had thicker new tissue regeneration, and the boundary between the regeneration/repair area and the surrounding cartilage was not obvious. Toluidine blue staining showed that the repaired area was filled with a large amount of neonatal cartilage and cartilage-like tissue. Neonatal chondrocytes are similar in structure to normal hyaline chondrocytes, and numerous cartilage lacunae are present in the regenerative area. Improved safranin-O bright-green staining showed a significant amount of repair, based on proteoglycans in the area.

For the conditional-control group, we used hydrogels to repair the cartilage defect of the knee joint. HE staining revealed regeneration with new tissues growing in the defect

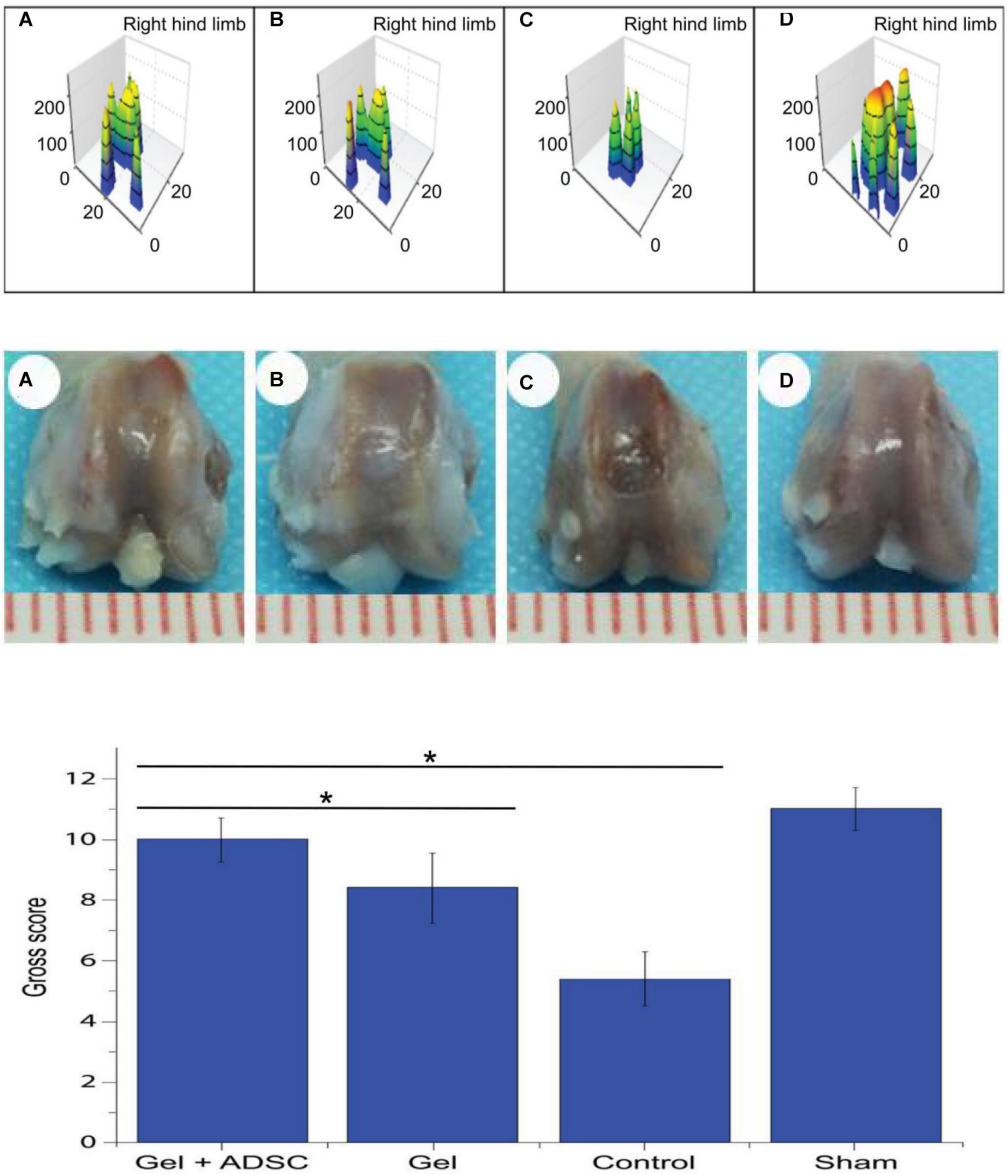

FIGURE 5 | Catwalk gait detection at 8 weeks postoperatively in SD rats. **(A)** ADSCs/hydrogel group; **(B)** pure hydrogel group; **(C)** blank sputum group; **(D)** positive control group (Upper); General view of the 8-week postoperative knee articular cartilage defect repair in SD rats. **(A)** ADSCs/hydrogel group; **(B)** pure hydrogel group; **(C)** blank sputum group; **(D)** positive control group (Middle) and General view score of 8 weeks after repair of knee articular cartilage defects in SD rats (Lower). $^*P < 0.05$.

areas, although the regenerated tissue was thinner than in the experimental group, and the boundary between the regeneration/repair area and the surrounding cartilage was clearly visible. Toluidine blue staining showed that the repaired area was filled with a small amount of new cartilage and cartilage-like tissue, and the cartilage lacuna in the regeneration area was not obvious, when compared with the experimental group. Improved safranin-O bright-green staining showed repair with a low level of proteoglycans in the area. In the defect-setting group, HE staining did not show obvious tissue regeneration in the defect areas, and it was not closely attached to the subchondral bone. Subchondral bone leakage was visible in some areas. Toluidine blue staining showed that the repaired area was filled with fibrous tissue, and the modified safranin was improved. Safranin-O, bright-green staining showed repair and the presence of almost no proteoglycans in the region.

DISCUSSION

The natural structure of articular cartilage lacks blood vessels, lymphatic vessels, and nerves, resulting in the inability to provide sufficient cells for efficient self-healing of cartilage in the defect

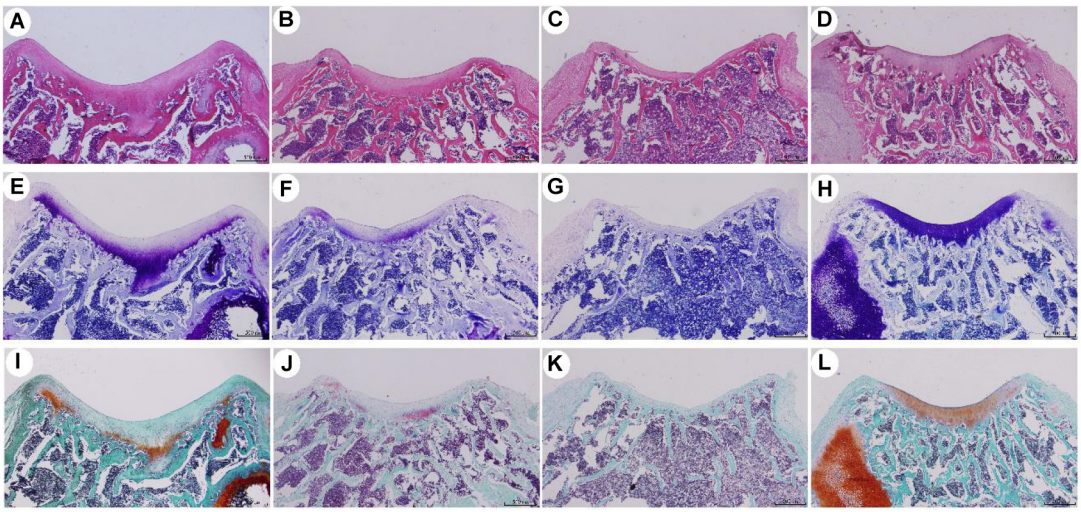

FIGURE 6 | Histological staining of SD rats after knee joint cartilage defect repair for 8 weeks. **(A,E,I)** were ADSCs/hydrogel group; **(B,F,J)** were pure hydrogel groups; **(C,G,K)** were blank group; **(D,H,L)** were positive control groups. **(A–D)** is HE staining; **(E–H)** is toluidine blue staining; **(I–L)** is safranin O staining.

area. In this study, from the perspective of tissue engineering, an injectable chitosan hydrogel was used to transplant ADSCs into the articular cartilage-defect area for articular cartilage regeneration and repair. Attempts were made to establish a feasible method for developing osteoarthritis by injection-mode stem cell transplantation to delay articular cartilage injury.

The use of mesenchymal stem cells as cartilage tissue-engineering seed cells for cartilage regeneration/repair *in vitro* and *in vivo* is gradually increasing. Mesenchymal stem cells are widely available and can be extracted from adipose tissue, placenta, bone, deciduous teeth, and synovial tissue, among other tissues, and are therefore referred to as different types of mesenchymal stem cells. Among them, ADSCs have multi-differentiation potential, can be cultured *in vitro*, have low immunogenicity, and can be acquired from various sites in the body (Huang et al., 2013; Chen et al., 2014; de Girolamo et al., 2015; Ansari et al., 2017; Liao et al., 2017; Liu et al., 2017). As well as a high acquisition rate (adipose tissue can provide more ADSCs than bone marrow). The availability of more stem ADSCs (∼5,000 cells per gram of tissue, compared to 100–1,000 bone marrow-derived stem cells) is preferable for many researchers. ADSCs secrete large amounts of cytokines and growth factors, such as hepatocyte growth factor, interleukin-6, macrophage colony-stimulating factor, transforming growth factor beta 1 (TGF-β1), and tumor necrosis factor-alpha (TNF-α), which support tissue remodeling and inhibit apoptosis. Previous reports have shown that ADSCs exhibit multi-line plasticity (multi-directionality) with the ability to differentiate into multiple cell types (derived from three germ layers: mesoderm, endoderm, and ectoderm). Articular cartilage belongs to connective tissue and is evolved in the embryonic mesoderm. *In vitro* studies of ADSCs cultured in the presence of insulin growth factor, bone morphogenetic protein, and TGF-β can express Sox-9, proteoglycan, cartilage oligomeric matrix protein, chondroitin sulfate, and type II collagen. The expression of cartilage matrix-associated protein was increased. A large number of ADSCs was used for cartilage tissue engineering *in vitro* and *in vivo* to obtain satisfactory results (Im, 2016; Tabatabaei Qomi and Sheykhhasan, 2017).

Biomaterials play important roles in cartilage tissue engineering, providing not only a carrier for cells and factors, but also a good microenvironment for cell proliferation, phenotype development, and differentiation, which in turn promotes the regeneration of articular cartilage. In addition, the preservation of biological materials is a focus of tissue engineering researchers. Different forms of biological materials have different properties. At present, the cartilage-repair materials used in tissue engineering include hydrogels, freeze-dried materials, woven materials, electrospun materials, and composite materials. Hydrogel materials have been used in cartilage tissue engineering because of their high water content (similar to articular cartilage) and good biocompatibility. Injectable hydrogels are an important class of hydrogels because they can be easily bolused with syringes. The encapsulated cells can be filled into cartilage defects of any shape; thus, they have large clinical research potential, are widely used in cartilage tissue engineering (Liu et al., 2017), and have supported a major direction for preparing cartilage-repair hydrogel materials in recent years. Injectable hydrogels typically retain large amounts of water, have good permeability to nutrients and metabolites, and exhibit good biocompatibility. They can be administered using minimally invasive procedures and can be used to properly fill irregularly shape defects (Liao et al., 2017). In addition, cells and bioactive molecules can be uniformly incorporated into the hydrogel. Injectable hydrogels, due to their physical properties similar to extracellular matrix, may serve as a suitable platform to support osteoblast survival, proliferation, and differentiation, and promote articular-cartilage tissue regeneration. In addition, self-healing hydrogel has been widely used quite successfully combined with diversified fields, such as magnesium ions

mediated fibrocartilaginous interface regeneration (Chen et al., 2020), photothermal therapy of infected full-thickness skin wounds (He et al., 2020), and hepatocellular carcinoma therapy by using pH-responsive drug delivery system (Qu et al., 2017).

The GCS/DF-PEG hydrogels used in this experiment relied on the natural material chitosan (GCS) and the synthetic polymer material PEG (DF-PEG) to form a gel through the dynamic Schiff base chemical bond. It was found experimentally that the injectable hydrogel easily passed through a 26-G syringe and exhibited good injectability. In this study, the injectability and self-healing experiments confirmed that the hydrogel could be easily pushed out of a syringe needle and had strong injectability. After 5–10 min, the scattered hydrogel particles protruding through the syringe aggregate into a whole hydrogel, which is consistent with the strong self-healing properties of hydrogels The presence of chemical bonds, the three-dimensional system of the hydrogel in a state of dynamic equilibrium, and the formation of non-constant chemical bonds between the molecules inside the hydrogel enable a self-healing function. To determine the appropriate method for tissue engineering-hydrogel formulation, based on previous experimental studies, we prepared a 1.5 wt% GCS/2 wt% DF-PEG hydrogel, a 1.5 wt% GCS/4 wt% DF-PEG hydrogel, and a 1.5wt% GCS/8wt% DF-PEG hydrogel. Through degradation experiments, we found that increasing DF-PEG concentrations were associated with a higher modulus of elasticity of the hydrogel. Previous studies have shown that when the hydrogel elastic modulus is 20 KPa, stem cells differentiate into hyaline cartilage and produce extracellular matrix characteristic of cartilage. Based on the experimental results of the comprehensive degradation test and the elastic modulus test of the hydrogel, we used 1.5% GCS/4% DF-PEG hydrogels for the tissue engineering cartilage-repair experiments.

We tested the cytotoxicity and porosity of hydrogels comprised of 1.5 wt% GCS and 4 wt% DF-PEG to further study the feasibility of using it in cartilage-repair applications. The electron microscopy images showed that the GCS/DF-PEG hydrogel had a good pore size of 200–400 um and good void connectivity. Our method of hydrogel production produced ice crystals during lyophilization and, thus, the hydrogel material did not show a true void state. However, it is possible to form numerous microtubule structures inside the hydrogel, which can facilitate the transportation of oxygen and various nutrients in culture medium, and to smoothly discharge harmful substances generated by cell metabolism. The live–dead-staining results showed that the ADSCs grew well in GCS/DF-PEG hydrogel. The spherical three-dimensional growth state in hydrogels is similar to the natural state of ADSCs in the body. This finding also confirmed that the chitosan constituting the hydrogel material has good biocompatibility with the PEG component, and can potentially be used as a cell-transplantation material in tissue engineering.

In this study, GCS/DF-PEG hydrogels containing ADSCs were transplanted into fresh cartilage-defect area by injection. Compared with a traditional stent graft, the operation is simple, and the stent material is not needed in the early stage. Trimming and shaping can adapt to defects of various shapes. Cell transplantation using a hydrogel can facilitate a higher concentration of cells in the cartilage injury area and provide a good microenvironment for cell growth and proliferation. After 8 weeks, Catwalk gait analysis showed that the experimental group had a significant recovery of the limb walking function, compared with the blank-placement group, but it still did not reach the walking function in the normal group. Compared with the simple hydrogel-transplantation group, we found that HE, toluidine blue, and red O staining were darker in the defect area of regenerated tissue, and more cartilage lacuna were seen in the repaired tissue. Soft lower bone leakage was observed in the defect-placement group, and the defect degeneration was characterized by toluidine blue and negative red O. These findings indicated that ADSCs and GCS/DF-PEG hydrogel complexes transplanted into the cartilage defect area showed obvious cartilage regeneration. Comprehensive *in vivo* experiments, gross observations, and measurements of walking function indicated that transplanting a GCS/DF-PEG hydrogel containing ADSCs into a fresh cartilage-defect area can achieve cartilage regeneration and repair, although it was still difficult to generate cartilage (needed for complete regeneration and repair).

CONCLUSION

In this study, we explored the use of glycol chitosan/dibenzaldehyde-terminated polyethylene glycol (GCS/DF-PEG) hydrogel to transplant Adipose-derived mesenchymal stem cells (ADSCs) in cartilage regeneration and repair experiments. Although satisfactory results were obtained *in vivo*, there are still some shortcomings. A repair time of 8 weeks in the body is somewhat short, and the long-term effects of the repair method are uncertain. It is hoped that the long-term effect of repair can be detected by prolonging the repair time. Secondly, the mechanism of repairing cartilage damage using this kind of stem cell transplantation method is not clear. It may be that the differentiation of ADSCs into chondrocytes will enable the regeneration of cartilage or promote the cartilage-regeneration ability of host cells. This topic will be the subject of our next experimental study.

DATA AVAILABILITY STATEMENT

The original contributions presented in the study are included in the article/supplementary material, further inquiries can be directed to the corresponding author/s.

ETHICS STATEMENT

The animal study was reviewed and approved by the treatment of animals conforms to the Guiding Opinions on Treating Animals Promulgated by the Ministry of Science and Technology. Written informed consent was obtained from the owners for the participation of their animals in this study.

AUTHOR CONTRIBUTIONS

JY, XJ, QG, SL, and YW carried out the concepts, design, definition of intellectual content, literature search, data acquisition, data analysis, and manuscript preparation. ZW, XL, and XZ provided assistance for data acquisition, data analysis, and statistical analysis. TL, XL, WG, and HR carried out he literature search, data acquisition, and manuscript editing. MC, KL, and XS performed the manuscript review. All authors have read and approved the content of the manuscript.

FUNDING

This study was funded by Shenzhen Longgang District Science and technology innovation Commission (LGKCYLWS201800 0198), the National Key R&D Program of China (2019YFC0110600), and the National Natural Science Foundation of China (21134004 and 81772319). This work was supported by PLA General Hospital Customer Research Institute, Jiamusi University, Longgang District Hospital, Shenzhen, Tsinghua University and all experimental participants.

REFERENCES

Ansari, S., Diniz, I. M., Chen, C., Aghaloo, T., Wu, B. M., Shi, S., et al. (2017). Alginate/hyaluronic acid hydrogel delivery system characteristics regulate the differentiation of periodontal ligament stem cells toward chondrogenic lineage Journal of materials science. *Mater. Med.* 28:162. doi: 10.1007/s10856-017-5974-8

Chen, B. J., Liang, Y. P., Bai, L., Xu, M. G., Zhang, J., Guo, B. L., et al. (2020). Sustained release of magnesium ions mediated by injectable self-healing adhesive hydrogel promotes fibrocartilaginous interface regeneration in the rabbit rotator cuff tear model. *Chem. Eng. J.* 396:125335. doi: 10.1016/j.cej.2020.125335

Chen, C. H., Shyu, V. B., Chen, J. P., and Lee, M. Y. (2014). Selective laser sintered poly-epsilon-caprolactone scaffold hybridized with collagen hydrogel for cartilage tissue engineering. *Biofabrication* 6:015004. doi: 10.1088/1758-5082/6/1/015004

de Girolamo, L., Niada, S., Arrigoni, E., Di Giancamillo, A., Domeneghini, C., Dadsetan, M., et al. (2015). Repair of osteochondral defects in the minipig model by OPF hydrogel loaded with adipose-derived mesenchymal stem cells. *Regen. Med.* 10, 135–151. doi: 10.2217/rme.14.77

He, J. H., Shi, M. T., Liang, Y. P., and Guo, B. L. (2020). Conductive adhesive self-healing nanocomposite hydrogel wound dressing for photothermal therapy of infected full-thickness skin wounds. *Chem. Eng. J.* 394:124888. doi: 10.1016/j.cej.2020.124888

Huang, S. J., Fu, R. H., Shyu, W. C., Liu, S. P., Jong, G. P., Chiu, Y. W., et al. (2013). Adipose-derived stem cells: isolation, characterization, and differentiation potential. *Cell Transplant.* 22, 701–709. doi: 10.3727/096368912X655127

Im, G. I. (2016). Regeneration of articular cartilage using adipose stem cells. *J. Biomed. Mater. Res. Part A* 104, 1830–1844. doi: 10.1002/jbm.a.35705

Johnstone, B., Alini, M., Cucchiarini, M., Dodge, G. R., Eglin, D., Guilak, F., et al. (2013). Tissue engineering for articular cartilage repair–the state of the art. *Euro. Cell. Mater.* 25, 248–267. doi: 10.22203/ecm.v025a18

Kasir, R., Vernekar, V. N., and Laurencin, C. T. (2015). Regenerative engineering of cartilage using adipose-derived stem cells. *Regen. Eng. Transl. Med.* 1, 42–49. doi: 10.1007/s40883-015-0005-0

Laudy, A. B., Bakker, E. W., Rekers, M., and Moen, M. H. (2015). Efficacy of platelet-rich plasma injections in osteoarthritis of the knee: a systematic review and meta-analysis. *Br. J. Sports Med.* 49, 657–672. doi: 10.1136/bjsports-2014-094036

Li, Y., Zhang, Y., Shi, F., Tao, L., Wei, Y., and Wang, X. (2017). Modulus-regulated 3D-cell proliferation in an injectable self-healing hydrogel. *Colloids Surf. B Biointerfaces* 149, 168–173. doi: 10.1016/j.colsurfb.2016.10.021

Liao, J., Wang, B., Huang, Y., Qu, Y., Peng, J., and Qian, Z. (2017). Injectable alginate hydrogel cross-linked by calcium gluconate-loaded porous microspheres for cartilage tissue engineering. *ACS Omega* 2, 443–454. doi: 10.1021/acsomega.6b00495

Liu, M., Zeng, X., Ma, C., Yi, H., Ali, Z., Mou, X., et al. (2017). Injectable hydrogels for cartilage and bone tissue engineering. *Bone Res.* 5:17014. doi: 10.1038/boneres.2017.14

Lynch, T. S., Patel, R. M., Benedick, A., Amin, N. H., Jones, M. H., and Miniaci, A. (2015). Systematic review of autogenous osteochondral transplant outcomes. *Arthroscopy* 31, 746–754. doi: 10.1016/j.arthro.2014.11.018

Oussedik, S., Tsitskaris, K., and Parker, D. (2015). Treatment of articular cartilage lesions of the knee by microfracture or autologous chondrocyte implantation: a systematic review. *Arthroscopy* 31, 732–744. doi: 10.1016/j.arthro.2014.11.023

Pleumeekers, M. M., Nimeskern, L., Koevoet, J. L. M., Karperien, M., Stok, K. S., and van Osch, G. (2018). Trophic effects of adipose-tissue-derived and bone-marrow-derived mesenchymal stem cells enhance cartilage generation by chondrocytes in co-culture. *PLoS One* 13:e0190744. doi: 10.1371/journal.pone.0190744

Qi, C., Liu, J., Jin, Y., Xu, L., Wang, G., Wang, Z., et al. (2018). Photo-crosslinkable, injectable sericin hydrogel as 3D biomimetic extracellular matrix for minimally invasive repairing cartilage. *Biomaterials* 163, 89–104. doi: 10.1016/j.biomaterials.2018.02.016

Qu, J., Zhao, X., Ma, P. X., and Guo, B. (2017). pH-responsive self-healing injectable hydrogel based on N-carboxyethyl chitosan for hepatocellular carcinoma therapy. *Acta Biomater.* 58, 168–180. doi: 10.1016/j.actbio.2017.06.001

Rai, V., Dilisio, M. F., Dietz, N. E., and Agrawal, D. K. (2017). Recent strategies in cartilage repair: a systemic review of the scaffold development and tissue engineering. *J. Biomed. Mater. Res. Part A* 105, 2343–2354. doi: 10.1002/jbm.a.36087

Sun, A. X., Lin, H., Fritch, M. R., Shen, H., Alexander, P. G., DeHart, M., et al. (2017). Chondrogenesis of human bone marrow mesenchymal stem cells in 3-dimensional, photocrosslinked hydrogel constructs: effect of cell seeding density and material stiffness. *Acta Biomater.* 58, 302–311. doi: 10.1016/j.actbio.2017.06.016

Tabatabaei Qomi, R., and Sheykhhasan, M. (2017). Adipose-derived stromal cell in regenerative medicine: a review. *World J. Stem Cells* 9, 107–117. doi: 10.4252/wjsc.v9.i8.107

Tsukamoto, J., Naruse, K., Nagai, Y., Kan, S., Nakamura, N., Hata, M., et al. (2017). (*) Efficacy of a self-assembling peptide hydrogel, SPG-178-Gel, for bone regeneration and three-dimensional osteogenic induction of dental pulp. *Stem Cells Tissue Eng. Part A* 23, 1394–1402. doi: 10.1089/ten.TEA.2017.0025

Yang, J., Zhang, Y. S., Yue, K., and Khademhosseini, A. (2017). Cell-laden hydrogels for osteochondral and cartilage tissue engineering. *Acta Biomater.* 57, 1–25. doi: 10.1016/j.actbio.2017.01.036

Zhang, J., Du, C., Guo, W., Li, P., Liu, S., Yuan, Z., et al. (2017). Adipose tissue-derived pericytes for cartilage. *Tissue Eng. Curr. Stem Cell Res. Ther.* 12, 513–521. doi: 10.2174/1574888X12666170321111211

Zhang, Y., Tao, L., Li, S., and Wei, Y. (2011). Synthesis of multiresponsive and dynamic chitosan-based hydrogels for controlled release of bioactive molecules. *Biomacromolecules* 12, 2894–2901. doi: 10.1021/bm200423f

Conflict of Interest: The authors declare that the research was conducted in the absence of any commercial or financial relationships that could be construed as a potential conflict of interest.

frontiers in Bioengineering and Biotechnology

REVIEW
published: 03 May 2021
doi: 10.3389/fbioe.2021.660145

Hydrogel Scaffolds to Deliver Cell Therapies for Wound Healing

Dharshan Sivaraj†, Kellen Chen†, Arhana Chattopadhyay, Dominic Henn, Wanling Wu, Chikage Noishiki, Noah J. Magbual, Smiti Mittal, Alana M. Mermin-Bunnell, Clark A. Bonham, Artem A. Trotsyuk, Janos A. Barrera, Jagannath Padmanabhan, Michael Januszyk and Geoffrey C. Gurtner**

Division of Plastic and Reconstructive Surgery, Department of Surgery, Stanford University School of Medicine, Stanford, CA, United States

OPEN ACCESS

Edited by:
Liyuan Zhang,
Harvard University, United States

Reviewed by:
Rajendra Kumar Singh,
Institute of Tissue Regeneration Engineering (ITREN), South Korea
Daniel Alge,
Texas A&M University, United States

***Correspondence:**
Geoffrey C. Gurtner
ggurtner@stanford.edu
Kellen Chen
kellenchen@stanford.edu

† These authors have contributed equally to this work and share co-first authorship

Specialty section:
This article was submitted to Biomaterials, a section of the journal Frontiers in Bioengineering and Biotechnology

Received: *28 January 2021*
Accepted: *07 April 2021*
Published: *03 May 2021*

Citation:
Sivaraj D, Chen K, Chattopadhyay A, Henn D, Wu W, Noishiki C, Magbual NJ, Mittal S, Mermin-Bunnell AM, Bonham CA, Trotsyuk AA, Barrera JA, Padmanabhan J, Januszyk M and Gurtner GC (2021) Hydrogel Scaffolds to Deliver Cell Therapies for Wound Healing. Front. Bioeng. Biotechnol. 9:660145. doi: 10.3389/fbioe.2021.660145

Cutaneous wounds are a growing global health burden as a result of an aging population coupled with increasing incidence of diabetes, obesity, and cancer. Cell-based approaches have been used to treat wounds due to their secretory, immunomodulatory, and regenerative effects, and recent studies have highlighted that delivery of stem cells may provide the most benefits. Delivering these cells to wounds with direct injection has been associated with low viability, transient retention, and overall poor efficacy. The use of bioactive scaffolds provides a promising method to improve cell therapy delivery. Specifically, hydrogels provide a physiologic microenvironment for transplanted cells, including mechanical support and protection from native immune cells, and cell–hydrogel interactions may be tailored based on specific tissue properties. In this review, we describe the current and future directions of various cell therapies and usage of hydrogels to deliver these cells for wound healing applications.

Keywords: hydrogel, cell therapy, wound healing, fibrosis, stem cell

INTRODUCTION

Skin acts as a critical protective barrier against external agents (Saghazadeh et al., 2018). After cutaneous injury, such as from a burn or cut, the normal skin structure is disrupted, and the resultant wound progresses through a coordinated cascade ("wound healing") of molecular and cellular processes to restore or replace the damaged tissue (Reinke and Sorg, 2012; Gonzalez et al., 2016).

To improve outcomes after cutaneous injury, researchers have investigated the use of cellular therapies to treat wounds, utilizing a wide array of cell types such as fibroblasts, endothelial cells, platelets, myeloid cells, and stem cells. Several products utilizing adult cells are also already commercially available including Dermagraft® and Apligraf® (Gentzkow et al., 1996; Edmonds, 2009). Multipotent stem cells have become an increasingly attractive choice for cell-based therapy due to their proliferative potential, differentiation capacity, and ability to secrete trophic factors and extracellular matrix (ECM) components important for wound healing (You and Han, 2014). The primary limitation with delivering cell therapies into cutaneous wounds has been low viability and transient engraftment of the transplanted cells. In order to maximize cell viability, a supportive microenvironment must be established to improve survival of these transplanted cells (Kamoun et al., 2017).

Biological scaffolds, such as hydrogels, provide an ideal, physiochemical mimetic of native ECM that can be utilized as a delivery vehicle for cells (Geckil et al., 2010). Hydrogels are

hydrophilic gels with a three-dimensional structure that rapidly swell in water to form a semi-solid. The water content of hydrogel matrices exceeds 90%, ideal for hydrating and maintaining a supportive environment within the wound bed that accelerates angiogenesis, increases breakdown of dead tissue, prevents cell and tissue death, and even alleviates pain (Field and Kerstein, 1994). The biophysical and biochemical properties of the hydrogel can be tuned to adjust the microenvironment to support a variety of cell types (Farhat et al., 2019).

In this review, we detail the use of hydrogels to deliver stem cells for wound healing. We first discuss the advantages and disadvantages of delivering various cell types to improve wound healing. We then discuss the use of bioactive scaffolds and hydrogels to deliver these cells, including technical considerations, such as material selection for hydrogel synthesis, maintaining cell viability during hydrogel gelation, tailoring hydrogel–cell interactions, and preventing cell entrapment by modifying porosity and degradation. Finally, we provide our view of the most promising cell and hydrogel candidates for wound healing and discuss future strategies to accelerate wound healing and improve the quality of tissue repair.

OVERVIEW OF WOUND HEALING

Wound healing proceeds through three sequential phases of inflammation, new tissue formation, and remodeling (**Figure 1**). Immediately after injury, blood and lymphatic fluid enters the wound site, activating coagulation pathways to facilitate platelet aggregation and achieve hemostasis (Gonzalez et al., 2016). During inflammation, inflammatory cells such as neutrophils and monocytes are recruited from the circulation to decontaminate the wound site through phagocytosis of cellular debris and bacteria (Guo and Dipietro, 2010; Schultz et al., 2011). Monocytes may differentiate into macrophages, a heterogenous and highly plastic cell population that may further differentiate into pro- or anti-inflammatory subtypes and are believed to be critical mediators of the cellular response during all stages of soft tissue injury (Gurtner et al., 2008). During new tissue formation, keratinocytes migrate over the injury to initiate re-epithelialization, fibroblasts and myofibroblasts deposit collagen and granulation tissue, and myofibroblasts contract and facilitate bringing the wound edges closer together (Schultz et al., 2011). In the remodeling phase (final and longest stage), wound contraction peaks and collagen is continually synthesized and reorganized (Gonzalez et al., 2016). These phases occur in a carefully coordinated fashion, and aberrancies in this tightly regulated process result in delayed or impaired wound healing (Gurtner et al., 2008).

CLINICAL SIGNIFICANCE OF WOUND HEALING

Abnormalities in wound healing can either lead to "over healing," resulting in excessive fibrosis, or "under healing," leading to a chronic, non-healing wound (Frykberg and Banks, 2015).

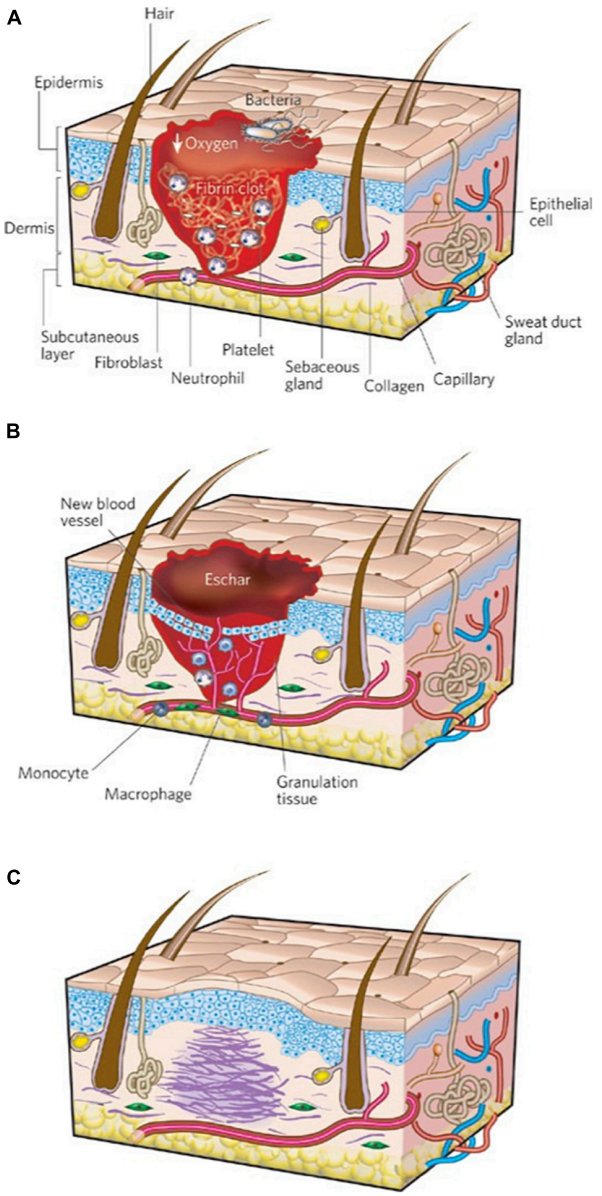

FIGURE 1 | Three stages of wound repair. The three phases of wound repair consist of **(A)** inflammation, **(B)** new tissue formation, and **(C)** remodeling. **(A)** The inflammatory phase lasts until about 48 h after injury. Depicted is a skin wound at about 24–48 h after injury. The wound is characterized by a hypoxic (ischemic) environment in which a fibrin clot has formed. Bacteria, neutrophils, and platelets are abundant in the wound. Normal skin appendages (such as hair follicles and sweat duct glands) are still present in the skin outside the wound. **(B)** New tissue formation occurs about 2–10 days after injury. Depicted is a skin wound at about 5–10 days after injury. The majority of cells from the previous stage of repair have migrated from the wound, and new blood vessels now populate the area. An eschar (scab) has formed on the surface of the wound, and the migration of epithelial cells can be observed under the eschar. **(C)** Remodeling lasts for a year or longer. Depicted is a skin wound about 1–12 months after repair. Disorganized collagen has been laid down by fibroblasts that have migrated into the wound and contracted the wound. The re-epithelialized wound is slightly higher than the surrounding surface, and the healed region does not contain normal skin appendages. Figure adapted with permission from Figure 1 of Gurtner et al. (2008).

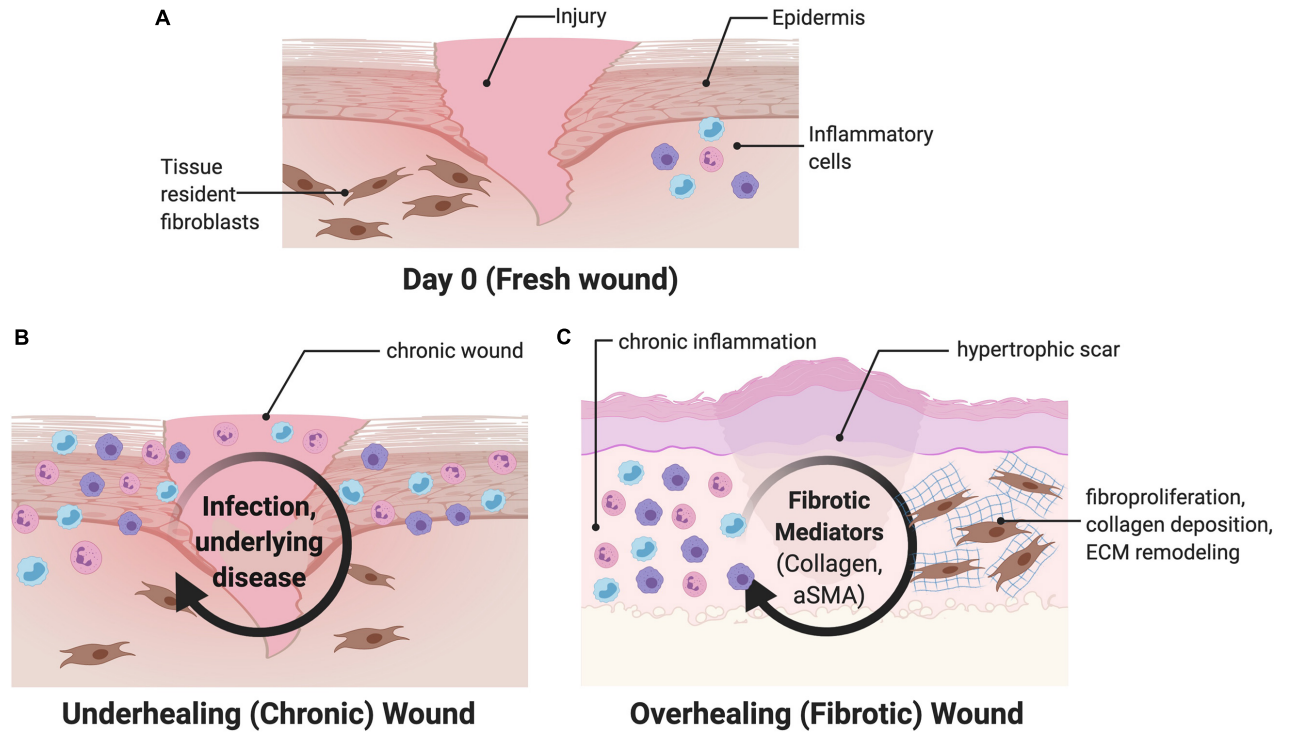

FIGURE 2 | Overview of wound healing. **(A)** After an initial wound, both circulating and tissue resident cells are recruited to the wound, including fibroblasts and inflammatory cells. **(B)** Chronic wounds are characterized by interruptions and subsequent prolongation of the wound healing process. **(C)** Fibrotic wounds are characterized by upregulation of myofibroblast differentiation and increased collagen production and may be driven by mechanical signaling. aSMA, alpha smooth muscle actin.

Infection, chronic inflammation, or vascular dysfunction delay wound closure and generate chronic wounds including arterial and venous ulcers, diabetic wounds, and pressure-related ulcers (**Figures 2A,B**) (Demidova-Rice et al., 2012; Frykberg and Banks, 2015; Xiang et al., 2019). Chronic wounds constitute a source of significant morbidity for the aging global population and a sizeable economic burden to the healthcare system (Jarbrink et al., 2017), with tens of billions of dollars spent annually on wound treatment (Nussbaum et al., 2018). Treatment of chronic wounds involves debridement of all necrotic tissue and selection of appropriate wound dressings that take into account the level of moisture, amount of wound exudate, presence of infection, and quality of the wound bed (Dabiri et al., 2016). In general, traditional topical therapies are geared toward facilitating a clean, moist environment conducive to healing.

In contrast, large surface area injuries such as burns almost always result in excessive fibrosis and hypertrophic scar (HTS) formation, which compromise normal function and result in severe morbidity to those affected (Berman et al., 2008; Gurtner et al., 2008). These scars are characterized by upregulation of myofibroblast differentiation, characterized by increased alpha smooth muscle actin (aSMA) signaling, and increased collagen production, driven by increased mechanotransduction (**Figure 2C**) (Wong et al., 2011a; Ma et al., 2018). Human fetuses display the ability to regenerate skin wounds without scar formation, unlike in adults, where scars develop from most skin wounds through the partial contributions of fibrotic and regenerative processes. The underlying mechanisms determining the fibrotic or regenerative fates of healing wounds remain unclear.

Management of patients with severe wounds is a long-term process that must address the local wound as well as the systemic, psychologic, and social consequences of the injury (Atiyeh et al., 2007; Chua et al., 2016; Zhu et al., 2016). Currently there are no standardized therapeutic treatment options for patients to address either excessive fibrosis or chronic wound formation. The use of some therapeutic agents, such as cytokine-based approaches, lacks strong scientific evidence, and many are based on case studies with mixed success (Meier and Nanney, 2006; Block et al., 2015; Rose and Chan, 2016). Newer cell-based therapies that target the underlying cellular and molecular processes of wound healing may provide a promising improvement for wound care.

CELL BASED THERAPIES

Cellular therapy refers to the transplantation of cells to replace or repair damaged tissue. Although therapeutics may come in the form of small molecules, biologics (e.g., antibodies, growth factors, cytokines, hormones), or cells, only cells may sense the cues in the wound healing environment and respond in complex fashions (Fischbach et al., 2013). Cells respond to the environmental cues, make decisions (proliferation, increased

secretion, etc.), and then provide precise, dynamic control over extended time periods (Fischbach et al., 2013). When utilizing cell therapies, researchers must be sure that the complex benefits from delivering cells are required, instead of simpler small molecules and biologics that provide controlled, static treatments.

These cells may be autologous or allogeneic and can even be engineered to express unique ligands and target-specific receptors (Zakrzewski et al., 2019; Srifa et al., 2020). While autologous cells are well-tolerated at the injury site, harvesting enough cells can be challenging, and both time and money are required to expand and culture a sufficient quantity of cells needed for the therapy. Allogeneic cells are easier to obtain and manufacture, but the immune response is a potential impediment (Chidgey et al., 2008). Interestingly, some recent studies have found that transplantation of xenogeneic cells may attenuate fibrosis; however, this has not yet been fully explored for human therapy (Cargnoni et al., 2009). In the context of wound healing, many different cell types have been transplanted into wound beds including keratinocytes, fibroblasts, platelets, bone marrow derived mesenchymal stromal cells, and adipose derived stromal cells (You and Han, 2014). Broadly, stem cells appear to be the most promising cell-based therapy currently under investigation due to their low immunogenicity, secretion of trophic factors, and ability to differentiate into a wide range of cell types. Here, we discuss these cells in the context of cell therapies (**Table 1**).

Non-stem Cell-Based Therapies

Many past studies have investigated the ability of fully differentiated adult cells to improve wound healing. Keratinocytes, both allogeneic and autologous, have been used to cover wounds for over three decades (You and Han, 2014). They can be harvested from a skin biopsy and expanded in culture to form a large sheet of epidermis that improves wound closure and epithelialization (You and Han, 2014; da Silva et al., 2019). However, keratinocytes are themselves unable to produce a robust extracellular matrix (You and Han, 2014), and their efficacy appears to be significantly reduced in chronic wounds compared to acute wounds. Thamm et al. (2015) found that acute wound exudate supported keratinocyte proliferation over longer time intervals, while chronic wound exudate continually suppressed keratinocyte proliferation and migration.

Fibroblasts are mesenchymal cells crucial to the healing process and have frequently been explored as a potential cell-based therapy. Unlike keratinocytes, fibroblasts directly deposit extracellular matrix proteins such as collagens or proteoglycans. In a study using autologous fibroblasts seeded on a hyaluronic acid sheet to treat facial defects following skin cancer resection, all recipients healed with minimal scar formation (You and Han, 2014). By contrast, allogeneic fibroblast treatments have shown less promise, as any cell cryopreservation reduces viability by almost 50% and inhibits protein production by 70–98% (You and Han, 2014). Macrophages and monocytes have also been found to improve murine wound healing, although they did not improve the quality of the healed tissue in terms of tensile strength, scar formation, or collagen density in this study (Hu et al., 2017).

Apligraf® and Dermigraft® are tissue engineered products used in the clinic that contain living human cells (keratinocytes and fibroblasts, respectively) seeded within an ECM matrix (Gentzkow et al., 1996; Edmonds, 2009). Clinical trial studies demonstrate that use of these seeded scaffolds improved healing outcomes, such as wound closure, compared to control wounds. However, none of these studies compared the effects of the seeded scaffolds to unseeded scaffolds, and additional studies have found that the seeded cells are rejected and degraded within 1–2 weeks (Griffiths et al., 2004). While the use of each of these fully differentiated cell types provides some benefits, no one cell type provides all the necessary functions needed during wound healing, including producing ECM, promoting angiogenesis, and re-epithelialization. Furthermore, these allogeneic cell types may produce immune sensitization (Trainor et al., 2014).

Benefits of Stem Cell Therapies Compared to Fully Differentiated Cells

Stem cells maximize the benefits of cell therapies by having reduced immunogenicity and increased therapeutic benefit, including stimulation of re-epithelialization and wound closure, ECM production, and angiogenesis (da Silva et al., 2019). MSCs can differentiate into many cell types and secrete trophic factors that promote healing (Dabiri et al., 2013; Hu et al., 2018). MSCs can be readily isolated from multiple tissue types and have been shown to accelerate and enhance wound healing by secreting beneficial cytokines, recruiting macrophages, inducing angiogenesis, and restoring sebaceous glands and hair follicles (Isakson et al., 2015; Kosaric et al., 2019). MSCs have immunosuppressive properties by releasing PGE2, galectin-1, HLA-G5, and indoleamine 2,3-dioxygenase (IDO) (Nagamura-Inoue and He, 2014), and low immunogenic characteristics, characterized by a lack of HLA-DR and low expression of MHC Class I molecules (Nagamura-Inoue and He, 2014). Additionally, even after up to 20–30 rounds of division, MSCs retain stem-like properties (You and Han, 2014; Li et al., 2015).

Adipose-derived stromal cells (ASCs) are a subtype of MSCs studied extensively for wound healing. ASCs are easily obtained in large quantities via liposuction and surgical excision of fat tissue, with any given amount of adipose tissue yielding up to 40 times more stem cells than the same amount of bone marrow (Hassan et al., 2014). ASCs have been shown to improve wound healing by promoting angiogenesis, secreting paracrine signaling molecules and extracellular matrices, and differentiating along multiple cell lineages (**Figure 3A**) (Tartarini and Mele, 2015). ASCs secrete factors such as TGF-β, VEGF, KGF, FGF2, PDGF, HGF, IGF, fibronectin, and type I collagen, which enhance epithelial migration and dermal fibroblast proliferation (Kim et al., 2009; Hassan et al., 2014; Tartarini and Mele, 2015). ASCs cultured in acute wound fluid demonstrated increased proliferation and migration, necessary to increase cell numbers and facilitate wound closure during the early phases of healing. Meanwhile, ASCs cultured in chronic wound fluid showed increased expression of VEGF, bFGF, and MMP9, factors necessary to promote angiogenesis and mediate fibroblast growth (Koenen et al., 2015). These findings demonstrate

TABLE 1 | Cell therapies tested for wound healing.

Cell type	Benefits	Limitations	Citations
Keratinocytes	– May be harvested from a skin biopsy and expanded in culture to form a large sheet of epidermis that improves wound closure and epithelialization	– Unable to produce a robust extracellular matrix – Efficacy reduced in chronic wounds compared to acute wounds	Gentzkow et al., 1996; You and Han, 2014; Thamm et al., 2015; da Silva et al., 2019
Fibroblasts	– Directly deposit extracellular matrix proteins – Shown to treat facial defects following skin cancer resection with minimal scar formation	– Allogeneic fibroblast treatments have shown reduction in cell cryopreservation viability by almost 50% and inhibits protein production by 70–98%	Edmonds, 2009; You and Han, 2014
Macrophages and monocytes	– Improves rate of murine wound healing in both wild-type and diabetic mice, with no adverse effect on the quality of repair. – Increased angiogenesis in mice	– Did not improve the quality of the healed tissue in terms of tensile strength, scar formation, or collagen density	Hu et al., 2017
ASCs	– Easily obtained in large quantities – Shown to improve wound healing by promoting angiogenesis, secreting paracrine signaling molecules and extracellular matrices, and differentiating along multiple cell lineages – Multifaceted ability to respond to the changing wound healing phases	– No consensus on a common isolation protocol that is clinically feasible, and which would ensure reproducible results	Strioga et al., 2012; Hassan et al., 2014; Koenen et al., 2015; Bertozzi et al., 2017; Moon et al., 2019
Bone marrow MSCs (BM-MSCs)	– Capacity to differentiate into multiple cell types – Reduce inflammation by diminishing cytokine expression and inflammatory cell chemotaxis – Promote neovascularization and recruit endogenous stem cells to the wound site	– High donor site morbidity and low yield – Require *ex vivo* expansion prior to their application – Harvesting BM-MSCs is painful with donor site morbidity	Chen et al., 2009; Kim and Suh, 2010; Lian et al., 2014; You and Han, 2014; Isakson et al., 2015; Li et al., 2015; Tartarini and Mele, 2015; Liu et al., 2017; Pittenger et al., 2019
Umbilical cord-derived MSCs (UC-MSCs)	– Easily derived from the umbilical cord – Great rate of self-renewal – Primitive stem cells, with greater proliferative and immunosuppressive capabilities compared to other MSCs	– Requires significant *ex vivo* expansion over time – Suffer from extensive phenotypic drift	Nagamura-Inoue and He, 2014

the multifaceted ability of ASCs to respond to the changing wound healing phases.

Bone marrow MSCs (BM-MSCs) are found in the bone marrow stroma and are capable of differentiating into osteoblasts, adipocytes, myoblasts, and neurons (**Figure 3B**) (Lian et al., 2014; You and Han, 2014). BM-MSCs can also differentiate into multiple types of skin cells, such as keratinocytes, endothelial, pericytes, and monocytes, to release cytokines and hematopoietic factors including VEGF, angiopoietin-1, IGF-1, EGF, KGF, and stromal derived factor-1 (SDF-1) (Kim and Suh, 2010; Liu et al., 2017). BM-MSCs also reduce inflammation by reducing cytokine expression and inflammatory cell chemotaxis (Li et al., 2015). Chen et al., treated wounds with BM-MSCs and observed a decrease in $CD45^+$ leukocytes, $CD3^+$ lymphocytes, and $CD8^+$ T-cells in an excisional wound mouse model (Chen et al., 2009; Li et al., 2015). Moreover, BM-MSCs promote neovascularization and recruit endogenous stem cells to the wound site, thereby accelerating the healing process (Lian et al., 2014).

Harvest of BM-MSCs is typically derived from bone marrow aspirate from the iliac crest, which is painful, associated with donor site morbidity, and often results in insufficient cell yield (Isakson et al., 2015; Tartarini and Mele, 2015). Early *in vitro* and animal studies of BM-MSCS quickly transitioned into human clinical trials for a multitude of clinical applications (Pittenger et al., 2019). Unfortunately, the clinical application of BM-MSCs has been limited by two factors. First, harvesting BM-MSCs is a painful process for patients to undergo and carries the risk of donor site morbidity (Isakson et al., 2015). Second, BM-MSCs require *ex vivo* expansion prior to their application due to the relatively low yields acquired after isolation. During cell expansion, MSCs are cultured on flat, unphysiological, and stiff materials such as tissue culture plastic or glass. These stiff substrates promote upregulation of a series of mechanotransduction genes, with increasing culture time leading to increased differentiation into osteogenic phenotypes (Yang et al., 2014). However, these substrates do not recapitulate the native cellular environment, in which cells are receiving signals in all three dimensions from native ECM (Caliari and Burdick, 2016). Yang et al. (2014) found that hMSCs possess a "mechanical memory," in which hMSCs cultured for a longer time on plastic demonstrated higher mechanotransduction activation (through the YAP pathway) and osteogenic phenotypes, even after they had been seeded into more physiologic, soft hydrogels. Increased time in culture and increased passages will also influence cell phenotype, shape, morphology, and transcription (Yao et al., 2006), and the exact stiffness of the culture substrate will also affect factors such as secretion of growth factors and proliferation (Ogle et al., 2020).

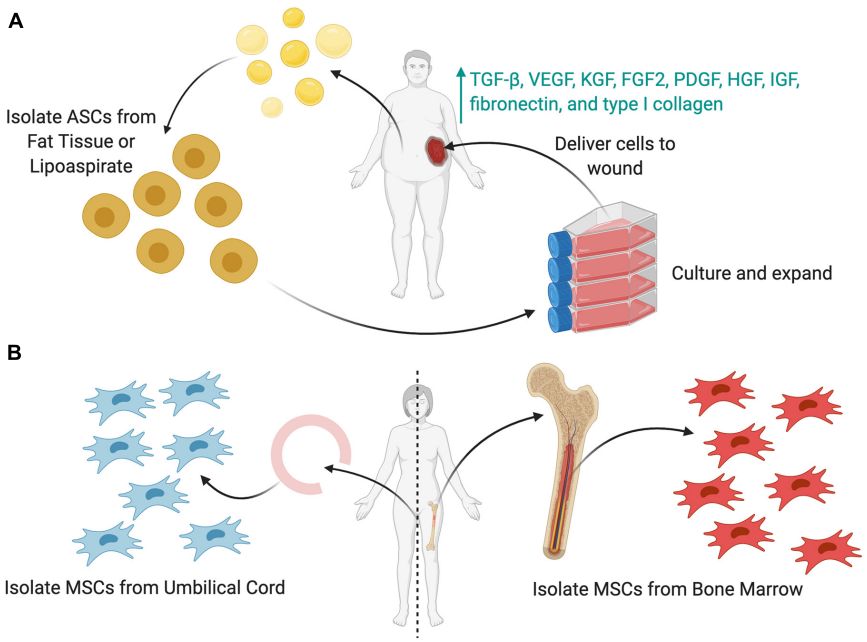

FIGURE 3 | Sources of stem cells to be used as cellular therapies. **(A)** Adipose-derived stem cells (ASCs) can be harvested from either lipoaspirate or fat tissue. These cells (or MSCs) can then be cultured *in vitro*, expanded in number, and then delivered to the wound as a cell therapy. To enhance the cell delivery, several delivery techniques (shown later) may be used. **(B)** Mesenchymal stromal cells (MSCs) can be harvested from either the umbilical cord or the bone marrow.

For wound healing, we have found that about 250,000 cells should be delivered to a 0.5 cm^2 wound (Barrera et al., 2021; Srifa et al., 2020), and others have found that about 1–3 million cells per kg are needed for systemic injection of MSCs in human clinical trials (Capelli et al., 2015). Overall, these would require at least two cell passages to properly expand cell levels for therapy.

Umbilical cord-derived MSCs (UC-MSCs) can be harvested from cord blood and umbilical vein subendothelium, as well as the perivascular zone, intravascular zone, and sub-amnion of the Wharton jelly (**Figure 3B**) (Nagamura-Inoue and He, 2014). These are easily derived from the umbilical cord, which is generally discarded after birth and readily available (Nagamura-Inoue and He, 2014). UC-MSCs have a gene expression profile similar to that of embryonic stem cells and possess a greater rate of self-renewal compared to BM-MSCs, allowing for ease of harvest and expansion. UC-MSCs express markers such as CD13, CD29, CD73, CD90, CD105, and HLA-ABC and produce three times more collagen than BM-MSCs (Nagamura-Inoue and He, 2014). Additionally, they are more primitive stem cells, with greater proliferative and immunosuppressive capabilities compared to other MSCs. Although UC-MSCs are easier to collect and maintain viability *in vitro* longer than BM-MSCs, BM-MSCs may be initially isolated in higher quantities (up to fivefold more from explanted BM compared to an explanted umbilical cord) (Capelli et al., 2015). Thus, UC-MSCs require significantly more *ex vivo* expansion over time, leading to more phenotypic drift that reduces their therapeutic efficacy over time faster (Nagamura-Inoue and He, 2014; Isakson et al., 2015).

From a practical standpoint, ASCs are the most easily accessible and can be isolated in large quantities with minimal patient morbidity (Bertozzi et al., 2017). To date, only a few clinical trials have studied ASCs in the context of wound healing; however, the preliminary results appear promising (Moon et al., 2019). Both ASCs and BM-MSCs have important similarities, such as multi-lineage potential, morphology, telomerase activity, gene expression, and similar cell surface markers such as CD10, CD13, CD29, CD44, CD54, CD71, CD90, CD105, CD106, CD117, and STRO-1 (Hassan et al., 2014; Isakson et al., 2015). Although there exist some differences between ASCs and BM-MSCs, their common secretion profiles, angiogenic potential, gene expression profiles, and clinical data support the use of both BM-MSCs and ASCs in wound healing (Strioga et al., 2012). Certain wound pathologies may favor the use of one cell population over the other, so additional research will be required to further clarify the specific advantages and disadvantages for each situation.

Potential for Engineered-Cell Therapies

New cell-based therapy approaches that utilize genome editing have also opened new and exciting avenues to treat previously intractable diseases. Transducing hematopoietic stem cells of β-thalassemia patients with a functional β-globin locus has been shown to eliminate the need for long-term red-cell infusions in a subset of patients with severe β-thalassemia (Thompson et al., 2018). Moreover, genetically modifying autologous patient-derived T cells with a chimeric antigen receptor (CAR) leads to impressive response rates in patients with hematologic malignancies (Raje et al., 2019). Precise genome editing via new

CRISPR-based technologies may allow for targeted knock-out or knock-in of genes that are key regulators of signaling pathways involved in wound healing (Adli, 2018). For example, gene editing of MSCs could increase their secretion of growth factors such as PDGF and VEGF that are beneficial to wound healing by increasing angiogenesis (Srifa et al., 2020). As the field of gene editing grows, these new techniques could be used to further boost the potential of stem cell delivery, making these already beneficial cell types even more efficient. These early studies point to the promising future potential for genetic engineering platforms to develop novel cellular therapies that both accelerate as well as improve the quality of wound healing.

CELL DELIVERY METHODS

Although many cells show promising capabilities in wound healing, these beneficial effects can be limited by the efficacy of the delivery. Injection-based delivery of stem cells suspended in solution results in rapid cell death, low viability, and transient engraftment (Rustad and Gurtner, 2012; Rustad et al., 2012; Tartarini and Mele, 2015; Ma et al., 2018). Wu et al. (2007) injected BM-MSCs into an excisional wound model and found that engraftment dropped from 28% at 7 days to 7.6% at 14 days and then 2.5% at 28 days. Low viability and transient engraftment may be due to factors such as high shear stresses during injection, lack of extracellular matrix to bind and interact with upon injection, leakage from the site, mechanical washout of cells, or exposure of cells to inflammation and reactive oxygen species (ROS) present within the wound (Li and Mooney, 2016). Optimization of the cell delivery method can maximize cell-tissue interactions to both elicit the most effective responses and promote viability of stem cells in a hostile wound microenvironment (Falanga et al., 2007) (**Table 2**).

Biomaterial Scaffolds for Cell Delivery in Wound Healing

Biologic scaffolds may serve as a delivery vehicle that remains viable, stable, and uncompromised within the harsh environment of the wound bed to maximize the potential of delivered cells. These 'biomaterials' have ECM structures similar to physiologic tissue where cells can be seeded to improve viability and retention. Biomaterials may broadly be defined as any '*material intended to interface with biological systems to evaluate, treat, augment, or replace any tissue, organ or function of the body*' (Williams, 2009). These biomaterials may be procured with techniques such as decellularization or immunomodulation of existing tissue (Ott et al., 2008); electrospinning, which mimics extracellular matrix structure; or triphasic culture, which mimics physiologic orthopedic interfaces (Spalazzi et al., 2006). These materials may be further modified through microtopography to provide signal cues for cellular differentiation (Downing et al., 2013).

"Decellularizing" native organs involves using a series of detergents and washes to remove all cellular material from the organ but retain most of the remaining extracellular matrix (Ott et al., 2008). The matrix can be re-seeded with a patient's own cells to mitigate rejection of the resultant implanted organ. Ott et al. (2008) demonstrate proper contractile and pump function of decellularized murine and rat hearts re-seeded with new cells. Sullivan et al. (2012) similarly re-seeded decellularized kidneys with renal cells. For cell therapies, some have decellularized tissue such as porcine small intestine submucosa to re-seed them with cells such as tenocytes to treat rotator cuff defects (Chen et al., 2007). Milan et al. (2016) decellularized human skin samples and re-seeded them with human umbilical cord perivascular cells (HUCPVCs) to find that these cell-seeded scaffolds could improve wound closure and upregulate angiogenesis in a murine model. The HUCPVCs served as an alternative source of MSCs with higher proliferative rate and better cell yield. Cumulatively, these findings demonstrate that decellularized matrices could be successfully used as a vehicle to deliver cells to wounds.

One of the most commonly studied biomaterials is poly(dimethylsiloxane) (PDMS), a silicone material that is bio-inert and easy to produce. Various studies have found that cells seeded on top of these materials will attach and proliferate normally (Schaffer et al., 1994). Furthermore, these silicone membranes can foster both viability and proliferation of seeded ASCs (Razavi and Thakor, 2018). The ability to treat and coat silicone and other biomaterials remains an attractive method to promote differentiation and growth, and these parameters may be tuned to optimize proper cell growth.

The choice of polymer influences cell growth and differentiation through both growth factors and the stiffness of the matrix (Gilpin and Yang, 2017; Kargozar et al., 2020). For example, Poly(lactic-co-glycolic acid) (PLGA) has been extensively studied as one of the most widely used polymers for materials science engineering applications (Uematsu et al., 2005), including for cartilage and bone regeneration. Sadeghi-Avalshahr et al. (2017) seeded fibroblasts and keratinocytes in a scaffold made of a PLGA-collagen mix for dermal tissue engineering using electrospinning, a complicated process that produces physiologic ECM matrix structure with a low yield strength. Yang et al. (2018) recently created a biodegradable, inorganic MnO_2 3D nanoscaffold with a tunable, wide range of biodegradation times, upregulated ECM-protein binding affinities, highly efficient drug loading, and tunable drug release schedules. While they showed that their scaffold enhanced stem cell transplantation, differentiation, and drug delivery, their 3D nanoscaffolds also required a complex methodology to synthesize.

Advantages of Hydrogel Scaffolds to Deliver Cell Therapies

While scaffolds developed with synthetic polymers or from decellularization can produce ECM constructs with high tunability and physiologic tissue structure, they require difficult methodology and testing to procure and develop, with elevated cost, excessive cellular adhesion, and slow scaffold degradation rates. Many of those scaffolds were designed to completely replace a damaged organ, meaning that any seeded cells within the constructs remain there over long time periods instead of leaving the construct to enter a wound. Using these scaffolds for wound

TABLE 2 | Different scaffolds to deliver cell therapies for wound healing.

Delivery method	Benefits	Limitations	Citations
Alginate hydrogel	– Mechanical properties of hydrogel can be tuned – Establish a robust microenvironment for cells	– Limited long-term stability in physiologic conditions – Must be modified with an adhesive ligand	Percival and McCarty, 2015; Aderibigbe and Buyana, 2018; Salehi et al., 2020; Zhang and Zhao, 2020; Zhang et al., 2020
Collagen hydrogel	– Primary organic constituent of native ECM – Highly biocompatible and cytocompatible, amenable to cell adhesion without modification	– Damage to its covalent cross-links upon extraction weakens hydrogels, which can then disintegrate on handling or under the pressure of surrounding tissues *in vivo*.	Helary et al., 2012; Chattopadhyay and Raines, 2014; Chen et al., 2018; Stoica et al., 2020
Fibrin hydrogel	– Natural role as a matrix involved in hemostasis and wound healing – Can trigger encapsulated cells to secrete ECM components and reparative growth factors	– Fibrin can be especially susceptible to protease-mediated degradation	Ahmed et al., 2007; Janmey et al., 2009; Moreno-Arotzena et al., 2015; Murphy et al., 2017
Hyaluronic acid (HA) hydrogel	– Chemical tunability – Favorable mechanical properties, biocompatibility, and biodegradation capacity	– In modifications like cross-linked HA-aldehyde or HA-amine derivatives, there are disadvantages: the modification procedure involves many synthesis and purification steps, and the crosslinking chemistries that occur upon mixing are hard to control and yield inconsistent gels	Baier Leach et al., 2003; Silva et al., 2016
Poly(dimethylsiloxane) (PDMS)	– Fosters viability and proliferation of seeded ASCs	– Poor biocompatibility	Schaffer et al., 1994; Razavi and Thakor, 2018
Poly-(ethylene glycol) (PEG)	– Versatility in chemical modification and ability to finely tune mechanical properties	– Synthesized in combination with natural polymers or biomimetic peptides as lack the biochemical properties for cellular interaction	Zhu and Marchant, 2011
Poly(lactic-co-glycolic acid) (PLGA)	– Extensively studied – One of the most widely used polymers for materials science engineering applications	– Poor biocompatibility – Challenging to fixate within wound bed	Uematsu et al., 2005; Sadeghi-Avalshahr et al., 2017
Poly(methyl methacrylate) (PMMA)	– Highly crosslinked gels possess longer degradation times	– In general, highly crosslinked gels possess longer degradation times	Henderson et al., 2010
Pullulan-collagen hydrogel	– Best approximate the porous ultrastructure of native reticular ECM – Easy engineering of the mechanical properties – Able to support the growth of multiple cell types – Minimal rejection and favorable biomaterial-tissue integration	– It is possible that the hydrogel microenvironment is hypoxic	Wong et al., 2011b; Rustad et al., 2012
Gelatin hydrogel	– Excellent biocompatibility – Ease of chemical modification	– Accelerated biodegradation compared to other hydrogels – Variation between synthesized bathes – Weak mechanical properties	Kang and Park, 2021

care would be especially disadvantageous due to the need to clean and debride the wounds every several days.

For wound care specifically, an ideal therapy would address concerns such as desiccation (loss of moisture from the wound), long term storage, bacterial infection, preventing debilitating scar formation, and promoting proper skin regeneration (growth of skin appendages, such as hair follicles, and other cutaneous glands) within the wound (**Figure 4**). Over the past decade, there has been increasing evidence that therapeutic hydrogels may address many of these concerns and promote natural skin regeneration, based on strong and promising laboratory and preclinical research findings. These dressings can be kept lyophilized (dry), making them lightweight, portable, and shelf stable. In the clinic, they can be simply unpackaged and soaked in saline to re-hydrate it, providing coverage across and preventing desiccation of the wound to facilitate healing.

Hydrogels have a unique set of properties which make them an ideal candidate for wound dressings. Their high

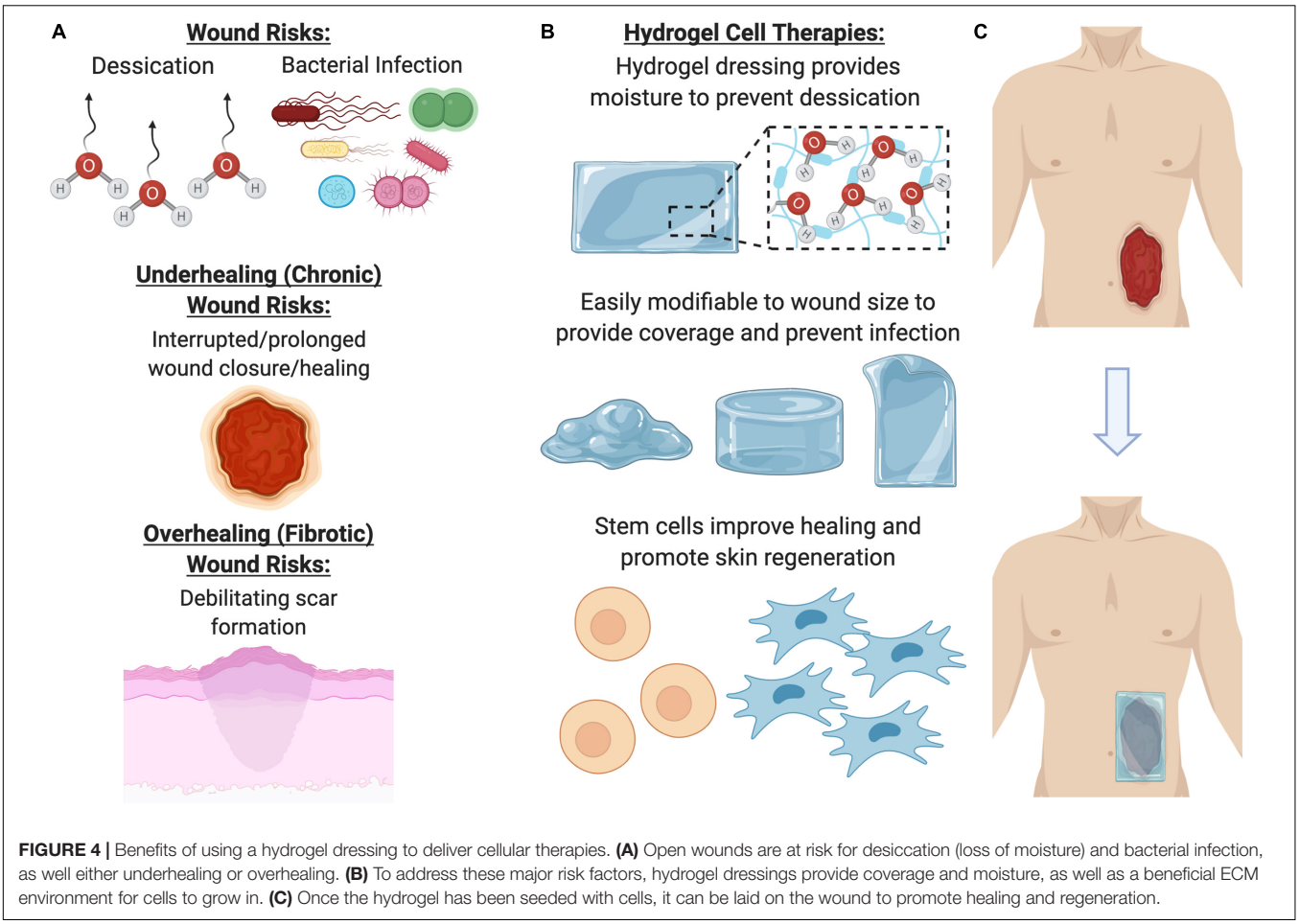

FIGURE 4 | Benefits of using a hydrogel dressing to deliver cellular therapies. **(A)** Open wounds are at risk for desiccation (loss of moisture) and bacterial infection, as well either underhealing or overhealing. **(B)** To address these major risk factors, hydrogel dressings provide coverage and moisture, as well as a beneficial ECM environment for cells to grow in. **(C)** Once the hydrogel has been seeded with cells, it can be laid on the wound to promote healing and regeneration.

water content confers physical similarity and biocompatibility to body tissues and maintains a moist environment around the wound interface (Kamoun et al., 2017; Youngblood et al., 2018). Hydrogel elasticity, mechanical properties, non-adhesion properties, and structural similarity to natural tissue also improve biocompatibility after implantation (da Silva et al., 2019). Hydrogels can be used as a supportive scaffold to deliver therapeutic cells safely to the wound site and shield the delivered cells from immune system attack while retaining permeability to therapeutic, signaling, and metabolic factors (Nafea et al., 2011). The hydrogel microenvironment can be tightly modified to support cells by adjusting numerous biophysical and biochemical properties, such as hydrogel–cell interactions, cell adhesion, microstructure, and degradability (Xu et al., 2020). Common hydrogel sources for wound healing include natural polymers like collagen, alginates, gelatin, and hyaluronic acid, as well as synthetic compounds such as polyethylene glycol and polyurethane (Liu et al., 2017).

Current Clinical Use of Hydrogel Scaffolds and Cellular Therapies

Hydrogels can be commercially obtained as a sheet, gel, or saturated gauze, and some hydrogel products are already being used for wound care from companies such as Medline, McKesson, 3M, ConvaTec, Derma Sciences, or Smith & Nephew. These hydrogels are easy to use and apply to the wound surface. A secondary dressing is required over these hydrogels to secure them in place, which may be useful to prevent infection. For an infected, dry wound, physicians may also use hydrogels with antimicrobial silver incorporated within them, such as Silvasorb from Medline (Das et al., 2015). While these hydrogels are beneficial for most types of wounds, they are rarely used on already moist wounds, such as venous leg ulcers, as they may cause a high amount of output drainage and exudate from the site that further impedes healing by slowing down cell growth or degrading the tissue matrix structure (Murakami et al., 2010). Excess output draining may also promote inflammation or bacterial contamination. Overapplication of these hydrogels may also macerate or soften the skin surrounding the wound and reduce their integrity. Usually, these hydrogels are changed every 3 days, so production of these scaffolds must be simple, quick, and inexpensive to be commercially appealing for physicians.

While hydrogels have become commonplace within the clinic, the use of these hydrogels to house and deliver cells has not been FDA approved. It seems likely that combining the most efficient cell type—stem cells—with the most efficient bioactive scaffold for wound healing—hydrogels—would result

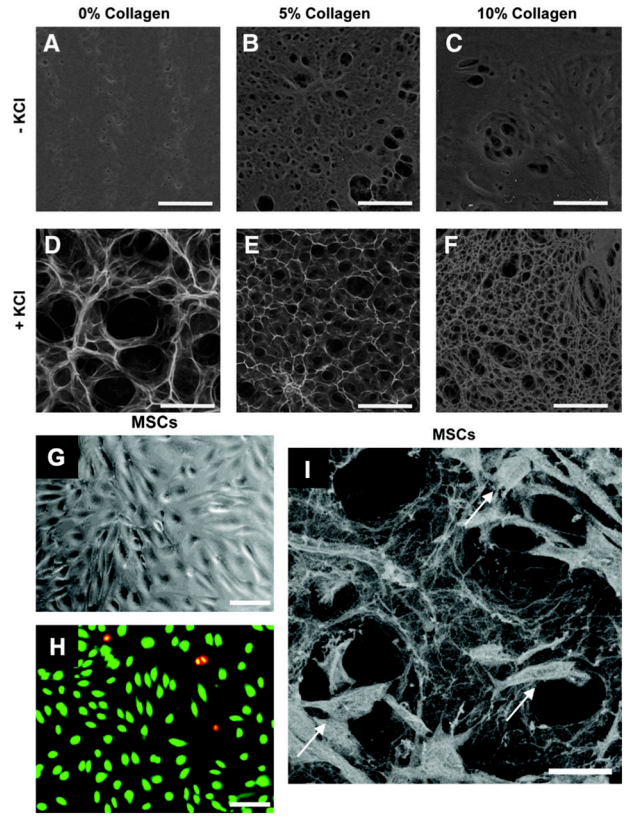

FIGURE 5 | Pullulan-collagen hydrogel can be easily modified across a wide range of factors and provides biocompatibility with stem cells. **(A–F)** Scanning electron microscopy (SEM) imaging demonstrates that varying collagen and KCl concentrations significantly alters the porosity of the hydrogels. Hydrogels fabricated with KCl showed increased porosity, while increasing collagen concentrations decreased porosity. Scale bar 100 μm. **(G,H)** Brightfield imaging and fluorescent imaging of live (green) dead (red/yellow) stain shows successful *in vitro* cellular incorporation of MSCs in the hydrogels. Scale bar 50 μm. **(I)** SEM shows MSCs (arrows) viably incorporated within the pullulan-collagen hydrogels. Scale bar 25 μm. Figures adapted with permission from Figures 2, 6 of Wong et al. (2011b).

in the most effective and beneficial therapy for wound care (da Silva et al., 2019).

Designing Hydrogels for Cell Delivery

There are several technical considerations when designing a hydrogel for therapeutic cell delivery in wound healing. The most common method to incorporate cells within ECM scaffolds is through cellular encapsulation, in which cells are first suspended within a liquid precursor solution. Prior to hydrogel encapsulation, this liquid solution is buffered to the appropriate osmolarity to prevent cell lysis (Caliari and Burdick, 2016). The encapsulation process must be mild to not adversely impact cell viability. Hydrogels may also be pre-formed without cells, and then cells may be seeded on top of the hydrogels. The chemistry and structure of the hydrogel for both methods should facilitate cell proliferation and/or differentiation (Nicodemus and Bryant, 2008), and facilitating migration is especially important to promote seeded cells to crawl into the hydrogel matrix structure.

Hydrogels formed via gelation mechanisms require crosslinking of polymer chains by covalent, ionic, or physical bonds (Caliari and Burdick, 2016). Cells may become entrapped within hydrogels due to their micrometer size, as the three-dimensional structure of hydrogels contains a mesh size usually smaller than the size of the cell (nanometer scale) (Bae et al., 2014; Li and Mooney, 2016). Increasing hydrogel porosity will allow for more space to increase diffusion of nutrients, growth factors, trophic factors, and secreted ECM components from the surrounding medium to other cells throughout the matrix (Seliktar, 2012). More dense mesh size (nanoscale) will increase the concentration of cell–matrix interactions, which in turn promotes focal adhesion contacts and increased cellular adhesion. However, more porous structures (micro-scale) will facilitate migration throughout or even out of the construct into the wound area (**Figures 5A–F**; Wong et al., 2011b). Porosity of the ECM can be modulated with methods such as sacrificial beads, particle annealing, or addition or subtraction of potassium chloride (KCl) salt. Hwang et al. pre-formed scarified gelatin beads and mixed them with alginate to create hydrogels. The gelatin beads dissolved at physiologic temperatures, resulting in a porous alginate hydrogel (Hwang et al., 2010). Alison et al. (2019) also utilized these methods by coating corn oil droplets with silica nanoparticles and mixing these droplets together. After a drying process, the corn oil dissolved, leaving either a porous silica structure, and porosity could be modulated by modifying the size of the initial corn oil droplets (Alison et al., 2019). Griffin et al. (2015) created poly(ethylene) glycol–vinyl sulfone (PEG–VS) spherical particles and annealed them together to create microporous hydrogel materials. 3D printing may also be used to help create porous structures (Alison et al., 2019).

There are numerous factors which influence hydrogel degradation around encapsulated cells, including the cell type, hydrogel chemistry, and number of degradable linkages (Wong et al., 2011b,c; Rustad et al., 2012; Kosaraju et al., 2016). Biodegradable hydrogels formed from physical or ionic crosslinks are often degraded by a combination of hydrolysis or enzyme-mediated processes. In many cases, the degradation profile and rate can be controlled by adjusting parameters of the crosslinked structure. For instance, Wong et al. (2011b) cross-linked pullulan-collagen matrices with sodium trimetaphosphate (STMP) to increase strength and decrease degradation rate and found that the ratio of pullulan to collagen ECM affected the strength of STMP cross-linking. Henderson et al. (2010) and others have used ionic cross-linking, submerging their poly(methyl methacrylate) (PMMA) hydrogels into solutions with Zinc, Calcium, Nickel, Cobalt, and Copper. If hydrogel degradation occurs too quickly, the hydrogel-cell construct will dissolve before therapeutic benefit has been derived. If degradation occurs too slowly, a buildup of secreted factors may accumulate around encapsulated cells and negatively influence their function. In general, highly crosslinked gels possess longer degradation times. Cell mediated enzymatic degradation of hydrogels often occurs in hydrogels synthesized from natural biopolymers (e.g., hyaluronic acid-based hydrogels primarily

degrade from cell-secreted enzymes like hyaluronidase). Short amino acid sequences, which are susceptible to enzymatic cleavage, may also be incorporated within the crosslinking of gels to accelerate degradation (Kong et al., 2004).

Ultimately, there are a multitude of technical considerations to account for when designing the optimal hydrogel for cell delivery. In order to successfully transition this therapy into the clinic, the process must be easily scaled for manufacturing and accepted by surgeons, patients, and healthcare providers. Cells pre-encapsulated within hydrogels may be hard to maintain viability, and these cells may also secrete factors that slowly degrade the hydrogel material properties. Seeding premade hydrogels with cells is especially clinically translatable, since cells could be cultured separately and then added to the hydrogel at the point of care. In addition, the un-seeded hydrogel must be easy to handle and encourage rapid cell seeding (Garg et al., 2014). Accounting for these technical considerations is crucial to facilitate the successful transition of hydrogel-cell therapies from laboratory research through FDA approval and into the clinical setting (**Figure 4**).

Types of Hydrogels to Deliver Cells for Wound Healing

The base materials used for hydrogel construction for wound healing applications can generally be divided into two categories: natural polymers and synthetic polymers. The advantage of synthetic polymers such as poly-(ethylene glycol) [PEG] lie in their versatility for chemical modification and subsequent ability to finely tune the mechanical properties (Zhu and Marchant, 2011). However, since synthetic hydrogels lack the biochemical properties for cellular interaction, they are often synthesized in combination with natural polymers or biomimetic peptides. Examples of biocompatible natural polymers include chitosan, hyaluronic acid, heparin, alginate, fibrin, and collagen. The mechanical and biochemical properties of these materials are able to facilitate key functions for tissue regeneration including cell adhesion and migration (Zhu and Marchant, 2011).

Hyaluronic acid (HA) is a biocompatible glycosaminoglycan found in the extracellular matrix of connective and generally synthesized through bacterial fermentation, although it may also be sourced from animal products such as rooster combs. HA-based biomaterials degrade *in vivo* in response to hyaluronidase and have been used for a multitude of biomedical applications, since they possess several attractive hydrogel properties due to chemical tunability (Baier Leach et al., 2003). HA can also be modified to present functional groups, enabling a variety of crosslinking chemistries to produce a variety of different hydrogel types, including two-dimensional films, injectable materials, and three-dimensional free-swelling hydrogels. Silva et al. (2016) recently utilized HA-based, spongy hydrogels seeded with hASCs for application in a diabetic mouse full-thickness wound model and their results showed accelerated wound closure and neoinnervation. This study and others have illustrated the favorable mechanical properties, biocompatibility, and biodegradation capacity of HA based hydrogels for application in wound healing.

Alginate is a cationic biopolymer obtained from brown algae that has been utilized for hydrogel synthesis and previously used in multiple biomedical applications, including in wound healing (Salehi et al., 2020; Zhang and Zhao, 2020). Alginate forms physically crosslinked hydrogels in the presence of divalent cations (Percival and McCarty, 2015; Aderibigbe and Buyana, 2018), and the mechanical properties of the resulting hydrogel can be tuned by varying the polymer count, molecular weight, and concentration of cations capable of crosslinking. To enable cell attachment, alginate must be modified with an adhesive ligand, in contrast to other natural hydrogels like collagen and fibrin which do not require modification to support cell adhesion (Aderibigbe and Buyana, 2018; Tavakoli and Klar, 2020). One important drawback of an alginate-based hydrogel is its limited long-term stability in physiologic conditions, as these hydrogels can be dissolved due to ion exchange reactions with monovalent cations in the environment (Lee and Mooney, 2012). Zhang et al. (2020) recently developed sodium/alginate hydrogels to encapsulate human umbilical cord derived MSCs (hUC-MSCs). Their results showed that their alginate-based hydrogel established a robust microenvironment for hUC-MSCs to exert their therapeutic effects *in vivo*.

Gelatin has been investigated as a potentially promising polymer backbone for hydrogel synthesis due to its biocompatibility, biodegradability, and ease of chemical modification (Kang and Park, 2021). This material is conventionally extracted from porcine, bovine, or fish collagen. In the context of wound healing, gelatin-based hydrogels have gained attention as a promising substrate to synthesize *in situ* forming hydrogels. Various crosslinking strategies have been developed to synthesize gelatin-based hydrogels that do not dissolve at body temperature. These include thermal gelation, EDC reactions, Schiff base reactions, and enzyme-mediated crosslinking, among others (Campiglio et al., 2019; Zhang et al., 2019). Eke et al. (2017) successfully encapsulated ASCs within a UV-crosslinked biodegradable gelatin/HA hydrogel to accelerate wound healing. They showed that over 90% of ASCs encapsulated within their gelatin hydrogels survived after 21 days. Limitations of gelatin-based hydrogels include weak mechanical properties, variation between synthesized batches, and accelerated biodegradation compared to other hydrogel types.

Fibrin is a natural polymer formed during wound coagulation that is formed via the cleavage of fibrinogen by the serine protease thrombin (Janmey et al., 2009; Murphy et al., 2017). Fibrin molecules interact primarily through a series of disulfide bonds, although Factor XIIIa provides additional crosslinking and is also activated by thrombin (Moreno-Arotzena et al., 2015). Fibrin's natural role as a matrix involved in hemostasis and wound healing makes it a promising vehicle for cell delivery, and fibrin can trigger encapsulated cells to secrete extracellular matrix components and reparative growth factors important in wound healing. However, fibrin can be especially susceptible to protease-mediated degradation (Ahmed et al., 2007).

Poly-(ethylene glycol) [PEG] is one of the most commonly used synthetic polymers for hydrogel synthesis due to its biocompatibility and hydrophilicity. PEG provides a

relatively inert hydrogel base for the introduction of chemical modifications to promote cell–cell interactions. The precursor PEG may be modified with a variety of functional groups, including thiols, amines, and acrylates, which adds high customization and versatility when creating PEG hydrogels. Multiple research groups have developed PEG-based hydrogels for cell delivery and tissue regeneration in a variety of biomedical applications. Dong et al. (2017) developed a (PEG)-gelatin hydrogel derived from multifunctional PEG-based hyperbranched polymer and a thiolated gelatin, which could encapsulate and support murine ASCs. A murine wound healing study showed that the hydrogel significantly improved cell retention, enhanced angiogenesis, and accelerated wound closure. Griffin et al. (2015) also created synthetic, microporous annealed particle (MAP) hydrogels made of PEG–VS and found that these hydrogels promoted wound closure faster than non-porous hydrogels made of the same material. A followup study utilizing these PEG MAP hydrogels demonstrated that hMSCs could be encapsulated and incorporated within the hydrogels, and that further modification of functional groups could improve proliferation and cell function (Xin et al., 2020). This study and others suggest that PEG–based hydrogels can regulate stem cell behaviors in 3D culture and deliver cells for wound healing.

Collagen is the primary organic constituent of native ECM, making it a highly promising material for hydrogel synthesis and cell encapsulation (Chattopadhyay and Raines, 2014). Collagen hydrogels are generally composed of primarily type I collagen; however, other constituents such as glycosaminoglycans as well as type II and III collagen may also be incorporated (Helary et al., 2012; Stoica et al., 2020). These hydrogels are highly biocompatible and cytocompatible, amenable to cell adhesion without modification (Chattopadhyay and Raines, 2014). Collagen hydrogels are formed by raising the temperature and pH of solubilized collagen to initiate fibril self-assembly. If solubilized collagen is mixed with a cellular suspension before self-assembly, this can initiate an easy method to facilitate cellular encapsulation (Chen et al., 2018).

Pullulan Collagen Hydrogels

Our group has engineered novel pullulan-collagen hydrogels with tunable, soft biomechanical properties and biocompatibility for cell-based therapy encapsulation. To develop a soft, biocompatible hydrogel that recapitulates the three-dimensional organization of the native ECM, we combined pullulan, a linear homopolysaccharide produced by the fungus *Aureobasidium pullulans* with type I collagen. This material was crosslinked with sodium trimetaphosphate under alkaline conditions, and potassium chloride salt (KCl) was used as a porogen for in-gel crystallization (Wong et al., 2011b). These unique engineered hydrogels provide several key advantages over traditional materials. First, pullulan-collagen hydrogels best approximate the porous ultrastructure of native reticular ECM based on comparison of fiber length and crosslink distance using a network extraction analysis. Moreover, altering the concentration of the collagen:pullulan ratio enables engineering of the mechanical properties such as hydrogel stiffness and effective porosity with relative ease. Additionally, we have conducted both *in vitro* and *in vivo* tests to demonstrate the biocompatibility of pullulan-collagen hydrogels. In *in vitro* settings, these hydrogels are able to support the growth of multiple cell types including fibroblasts, endothelial cells, and mesenchymal stromal cells, with minimal cytotoxicity (**Figures 5G–I**; Wong et al., 2011a). Further, in a murine subcutaneous implantation model, this bioscaffold demonstrates retention of reticular architecture and cellular infiltration, indicating minimal rejection and favorable biomaterial-tissue integration. In both humanized excisional wound and murine burn models, we found improvements in early wound healing in excisional wounds treated with hydrogels compared to untreated wounds (Barrera et al., 2021). The hydrogel-treated wounds not only healed faster, but also displayed reduced long-term fibrosis as evidenced by a reduction in myofibroblast activation. Specifically, cells such as fibroblasts may migrate into the soft hydrogel environment during healing. The ECM has low stiffness and could provide structural cues to these cells to become less fibrotic and more regenerative (Wong et al., 2011a).

By using capillary forces, cells can also be optimally seeded into hydrogels at the point of care. First, a cellular suspension is placed on top of a hydrophobic surface (parafilm wax paper); a dry hydrogel is then placed on top of this suspension, resulting in active absorption of cells into the pores of the scaffold through capillary, hydrophobic, and entropic forces (Garg et al., 2014). We compared this seeding method against centrifugal seeding or direct injection of cells into hydrogels. Scanning electron microscopy (SEM) showed that capillary force seeding had the most optimal seeding time and efficiency, as well as long-term cell survival and stability of hydrogel structure. Engrafted ASCs and MSCs were found to have over 96% viability within the hydrogels, indicating a beneficial environment conducive to cell growth, and the data suggested that the hydrogel preserved ASCs in a quiescent state and created a functional niche for this stem cell population, with concomitant maintenance of full cellular differentiation capacity (**Figures 5G–I**). Garg et al. (2014) also showed that ASC-hydrogels could significantly improve healing in murine burns, increasing wound vascularity and pro-angiogenic cytokine expression and decreasing scar formation.

Adipose-derived stromal cells seeded in the pullulan-collagen hydrogels improved healing in a murine burn model (Barrera et al., 2021). Burn wounds on the dorsum of mice were treated with either ASC-seeded or unseeded hydrogels (controls). Wounds treated with ASC-hydrogels had significantly reduced wound closure time, reduced scarring, reconstructed collagen networks, more wound vascularity, upregulation of pro-angiogenic cytokines such as *Cxcl12* and *Vegfa*, and downregulation of the fibrotic marker *Timp1*. The ASC-hydrogel group did significantly better across multiple experiments suggesting their superiority and additive therapeutic benefit in wound healing.

This enhanced delivery mechanism was further validated using a highly potent subset of ASCs with enhanced regenerative potential (Rennert et al., 2016). This subpopulation was identified with high specificity using two surface markers, DPP4 and CD55, which also expressed increased levels of general stem cell markers

(CD34 and CD73) and genes associated with embryonic stem cells (GGT1). The regenerative potential of the $DPP4^{+}/CD55^{+}$ ASCs was then tested in a diabetic murine excisional wound healing model (Rustad et al., 2012). Briefly, two 6 mm-thickness cutaneous wounds were excised on either side of the midline of the murine dorsum, with each wound stented with silicone rings sutured in place to prevent wound contraction. Following wounding, a total of 5×10^5 cells in 200 ml of saline was placed on 4 mm hydrogel disks. The ASC-hydrogel treatment demonstrated enhanced time to closure, and improved dermal recovery as compared to control. These findings suggest that this subpopulation of ASCs may have increased regenerative and wound healing potential (Rocchi et al., 2010; Rugg-Gunn et al., 2012; Kannan et al., 2014).

We further validated the biomimetic pullulan-collagen hydrogel scaffold in its ability to deliver bone marrow-derived MSCs in a murine excisional wound healing model (Rustad et al., 2012). Rustad et al. (2012) demonstrated that wounds treated with MSC-hydrogels had increased secretion of angiogenic cytokines and expression of transcription factors associated with maintenance of pluripotency and self-renewal (*Oct4, Sox2, Klf4*) as compared to controls. Wounds treated with MSC-seeded hydrogels also showed significantly accelerated healing and a return of skin appendages. Wounds treated with MSC-seeded hydrogels demonstrated significantly enhanced angiogenesis, which was associated with increased levels of VEGF and other angiogenic cytokines within the wounds. These data suggest that biomimetic hydrogels provide a functional niche capable of augmenting MSC regenerative potential and enhancing wound healing, further supporting the beneficial, additive abilities of pullulan-collagen hydrogel scaffolds for wound repair and regeneration.

FUTURE DIRECTIONS

In this review, we have discussed the wide range of benefits associated with cell-based therapies for wound healing. There is substantial evidence that delivering cells to an injury site provides benefits and improvements to healing. Furthermore, the use of stem cells (both ASCs and MSCs) may be especially beneficial, due to these cells' abilities to differentiate into the multitude of cell types needed in healthy tissue (**Figure 6**). Genetic engineering of these patient derived cells to enhance their therapeutic efficacy and instill novel cellular functions also represent a promising avenue for further investigation.

For tissue engineering, many researchers have explored methods to incorporate cells within extracellular matrices, with techniques ranging from materials science chemistry, decellularization, 3D printing, and electrospinning, to best create a physiologic ECM milieu for cell incorporation. While these techniques may be especially useful in cases where tissue must be replaced (heart, tendon, and liver), external wounds require therapies that provide both coverage and moisture to promote a proper healing environment, and soft hydrogels provide these baseline levels of beneficial healing. Cells seeded within these hydrogels adhere to the extracellular scaffold, but the adhesions are minimal enough so that cells may still detach and leave the hydrogel to enter the wound bed and encourage healing. This contrasts with other bioactive scaffolds that over promote

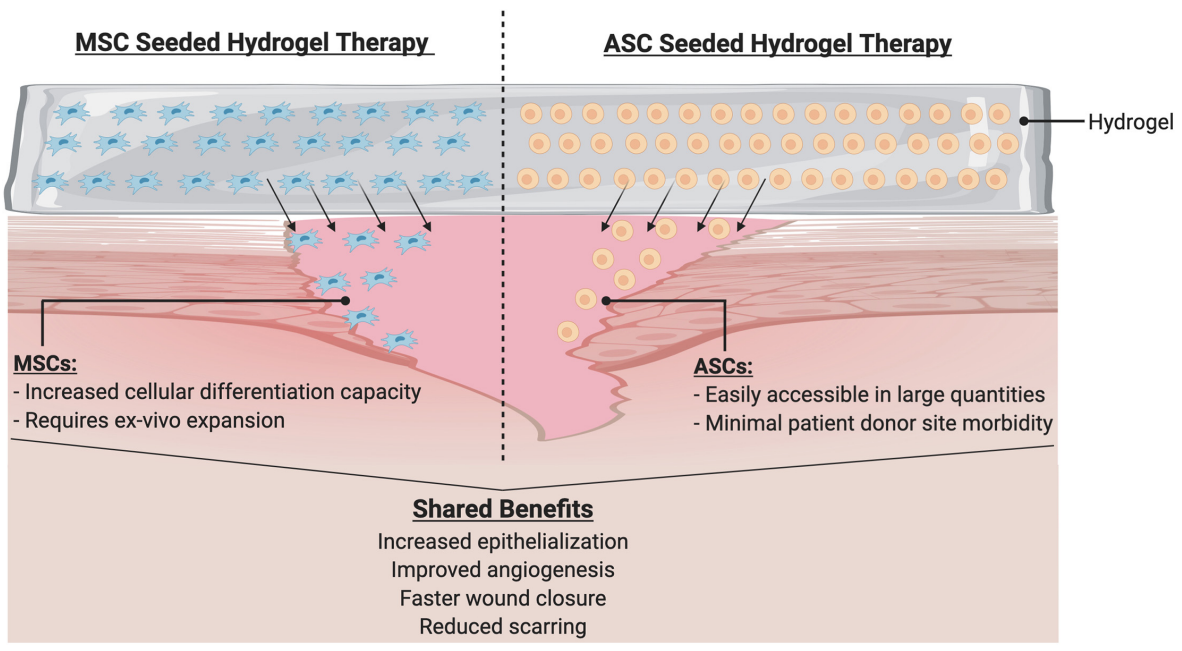

FIGURE 6 | Hydrogel with cellular therapy promotes wound healing. Hydrogel delivery system serves as a physiologic milieu to encapsulate cells to ensure efficient delivery to wound site. Cells such as MSCs or ASCs may be seeded into the hydrogels. Upon application to the wound, cells migrate into the wound to initiate a cascade of beneficial phenotypes.

adhesion so that cells remain within the scaffolds even at long time points.

Utilizing capillary forces, both ASCs and MSCs can be easily seeded within these hydrogels to improve viability and pro-regenerative phenotypes. This relatively straightforward seeding method can be readily translated for bedside application, as hydrogels and cells can be kept separately until just prior to application. It is likely that modifications to timing and frequency of the cellular treatment may improve these effects, as earlier or more frequent treatment may further reduce inflammation, fibrosis, and scarring, or further promote angiogenesis for healing. While a wide range of studies have explored cellular delivery or the use of hydrogels, additional work will be required to further optimize the parameters for these techniques. Further refinement and testing of these strategies in large animal models will also be helpful to eventually bring this technology to the bedside and facilitate clinical translation.

AUTHOR CONTRIBUTIONS

DS, KC, AC, DH, WW, CN, NM, SM, AM-B, CB, AT, JB, JP, MJ, and GG wrote the manuscript. All the authors contributed to the article and approved the submitted version.

ACKNOWLEDGMENTS

Some figures created with BioRender.com.

REFERENCES

Aderibigbe, B. A., and Buyana, B. (2018). Alginate in wound dressings. *Pharmaceutics* 10:42. doi: 10.3390/pharmaceutics10020042

Adli, M. (2018). The CRISPR tool kit for genome editing and beyond. *Nat. Commun.* 9:1911.

Ahmed, T. A., Griffith, M., and Hincke, M. (2007). Characterization and inhibition of fibrin hydrogel-degrading enzymes during development of tissue engineering scaffolds. *Tissue Eng.* 13, 1469–1477. doi: 10.1089/ten.2006.0354

Alison, L., Menasce, S., Bouville, F., Tervoort, E., Mattich, I., Ofner, A., et al. (2019). 3D printing of sacrificial templates into hierarchical porous materials. *Sci. Rep.* 9:409.

Atiyeh, B. S., Gunn, S. W., and Hayek, S. N. (2007). Military and civilian burn injuries during armed conflicts. *Annals Burns Fire Disasters* 20, 203–215.

Bae, H., Chu, H., Edalat, F., Cha, J. M., Sant, S., Kashyap, A., et al. (2014). Development of functional biomaterials with micro- and nanoscale technologies for tissue engineering and drug delivery applications. *J. Tissue Eng. Regen. Med.* 8, 1–14. doi: 10.1002/term.1494

Baier Leach, J., Bivens, K. A., Patrick, C. W. Jr., and Schmidt, C. E. (2003). Photocrosslinked hyaluronic acid hydrogels: natural, biodegradable tissue engineering scaffolds. *Biotechnol. Bioeng.* 82, 578–589. doi: 10.1002/bit.10605

Barrera, J., Trotsyuk, A. A., Maan, Z. N., Bonham, C. A., Larson, M. R., Mittermiller, P. A., et al. (2021). Adipose-derived stromal cells seeded in pullulan-collagen hydrogels improve healing in murine burns. *Tissue Eng Part A*. Online ahead of print.

Berman, B., Viera, M. H., Amini, S., Huo, R., and Jones, I. S. (2008). Prevention and management of hypertrophic scars and keloids after burns in children. *J. Craniofacial Surg.* 19, 989–1006. doi: 10.1097/scs.0b013e318175f3a7

Bertozzi, N., Simonacci, F., Grieco, M. P., Grignaffini, E., and Raposio, E. (2017). The biological and clinical basis for the use of adipose-derived stem cells in the field of wound healing. *Ann. Med. Surg. (Lond).* 20, 41–48. doi: 10.1016/j.amsu.2017.06.058

Block, L., Gosain, A., and King, T. W. (2015). Emerging therapies for scar prevention. *Adv. Wound Care (New Rochelle).* 4, 607–614. doi: 10.1089/wound.2015.0646

Caliari, S. R., and Burdick, J. A. (2016). A practical guide to hydrogels for cell culture. *Nat. Methods* 13, 405–414. doi: 10.1038/nmeth.3839

Campiglio, C. E., Contessi Negrini, N., Fare, S., and Draghi, L. (2019). Cross-Linking strategies for electrospun gelatin scaffolds. *Materials (Basel)* 12:2476. doi: 10.3390/ma12152476

Capelli, C., Pedrini, O., Valgardsdottir, R., Da Roit, F., Golay, J., and Introna, M. (2015). Clinical grade expansion of MSCs. *Immunol. Lett.* 168, 222–227. doi: 10.1016/j.imlet.2015.06.006

Cargnoni, A., Gibelli, L., Tosini, A., Signoroni, P. B., Nassuato, C., Arienti, D., et al. (2009). Transplantation of allogeneic and xenogeneic placenta-derived cells reduces bleomycin-induced lung fibrosis. *Cell Transplant.* 18, 405–422. doi: 10.3727/096368909788809857

Chattopadhyay, S., and Raines, R. T. (2014). Review collagen-based biomaterials for wound healing. *Biopolymers* 101, 821–833. doi: 10.1002/bip.22486

Chen, J. M., Willers, C., Xu, J., Wang, A., and Zheng, M. H. (2007). Autologous tenocyte therapy using porcine-derived bioscaffolds for massive rotator cuff defect in rabbits. *Tissue Eng.* 13, 1479–1491. doi: 10.1089/ten.2006.0266

Chen, K., Vigliotti, A., Bacca, M., McMeeking, R. M., Deshpande, V. S., and Holmes, J. W. (2018). Role of boundary conditions in determining cell alignment in response to stretch. *Proc. Natl. Acad. Sci. U S A.* 115, 986–991. doi: 10.1073/pnas.1715059115

Chen, L., Tredget, E. E., Liu, C., and Wu, Y. (2009). Analysis of allogenicity of mesenchymal stem cells in engraftment and wound healing in mice. *PLoS One* 4:e7119. doi: 10.1371/journal.pone.0007119

Chidgey, A. P., Layton, D., Trounson, A., and Boyd, R. L. (2008). Tolerance strategies for stem-cell-based therapies. *Nature* 453, 330–337. doi: 10.1038/nature07041

Chua, A. W., Khoo, Y. C., Tan, B. K., Tan, K. C., Foo, C. L., and Chong, S. J. (2016). Skin tissue engineering advances in severe burns: review and therapeutic applications. *Burns Trauma* 4:3.

da Silva, L. P., Reis, R. L., Correlo, V. M., and Marques, A. P. (2019). Hydrogel-Based strategies to advance therapies for chronic skin wounds. *Annu. Rev. Biomed. Eng.* 21, 145–169. doi: 10.1146/annurev-bioeng-060418-052422

Dabiri, G., Damstetter, E., and Phillips, T. (2016). Choosing a wound dressing based on common wound characteristics. *Adv. Wound Care (New Rochelle)* 5, 32–41. doi: 10.1089/wound.2014.0586

Dabiri, G., Heiner, D., and Falanga, V. (2013). The emerging use of bone marrow-derived mesenchymal stem cells in the treatment of human chronic wounds. *Expert Opin. Emerg. Drugs* 18, 405–419. doi: 10.1517/14728214.2013.833184

Das, A., Kumar, A., Patil, N. B., Viswanathan, C., and Ghosh, D. (2015). Preparation and characterization of silver nanoparticle loaded amorphous hydrogel of carboxymethylcellulose for infected wounds. *Carbohydr Polym.* 130, 254–261. doi: 10.1016/j.carbpol.2015.03.082

Demidova-Rice, T. N., Hamblin, M. R., and Herman, I. M. (2012). Acute and impaired wound healing: pathophysiology and current methods for drug delivery, part 1: normal and chronic wounds: biology, causes, and approaches to care. *Adv. Skin Wound Care* 25, 304–314. doi: 10.1097/01.asw.0000416006.55218.d0

Dong, Y., Melanie Rodrigues, S. A., Li, X., Kwon, S. H., Kosaric, N., and Khong, S. et al. (2017). Injectable and tunable gelatin hydrogels enhance stem cell retention and improve cutaneous wound healing. *Adv. Funct. Mater.* 27:1606619. doi: 10.1002/adfm.201606619

Downing, T. L., Soto, J., Morez, C., Houssin, T., Fritz, A., Yuan, F., et al. (2013). Biophysical regulation of epigenetic state and cell reprogramming. *Nat. Mater.* 12, 1154–1162. doi: 10.1038/nmat3777

Edmonds, M. (2009). Apligraf in the treatment of neuropathic diabetic foot ulcers. *Int. J. Low Extrem Wounds* 8, 11–18. doi: 10.1177/1534734609331597

Eke, G., Mangir, N., Hasirci, N., MacNeil, S., and Hasirci, V. (2017). Development of a UV crosslinked biodegradable hydrogel containing adipose derived stem

cells to promote vascularization for skin wounds and tissue engineering. *Biomaterials* 129, 188–198. doi: 10.1016/j.biomaterials.2017.03.021

Falanga, V., Iwamoto, S., Chartier, M., Yufit, T., Butmarc, J., Kouttab, N., et al. (2007). Autologous bone marrow-derived cultured mesenchymal stem cells delivered in a fibrin spray accelerate healing in murine and human cutaneous wounds. *Tissue Eng.* 13, 1299–1312. doi: 10.1089/ten.2006.0278

Farhat, W., Hasan, A., Lucia, L., Becquart, F., Ayoub, A., and Kobeissy, F. (2019). Hydrogels for advanced stem cell therapies: a biomimetic materials approach for enhancing natural tissue function. *IEEE Rev. Biomed. Eng.* 12, 333–351. doi: 10.1109/rbme.2018.2824335

Field, C. K., and Kerstein, M. D. (1994). Overview of wound healing in a moist environment. *Am. J. Surg.* 167:2S.

Fischbach, M. A., Bluestone, J. A., and Lim, W. A. (2013). Cell-based therapeutics: the next pillar of medicine. *Sci. Transl. Med.* 5:179s7.

Frykberg, R. G., and Banks, J. (2015). Challenges in the treatment of chronic wounds. *Adv. Wound Care (New Rochelle)* 4, 560–582. doi: 10.1089/wound.2015.0635

Garg, R. K., Rennert, R. C., Duscher, D., Sorkin, M., Kosaraju, R., Auerbach, L. J., et al. (2014). Capillary force seeding of hydrogels for adipose-derived stem cell delivery in wounds. *Stem Cells Transl. Med.* 3, 1079–1089. doi: 10.5966/sctm.2014-0007

Geckil, H., Xu, F., Zhang, X., Moon, S., and Demirci, U. (2010). Engineering hydrogels as extracellular matrix mimics. *Nanomedicine (Lond)* 5, 469–484. doi: 10.2217/nnm.10.12

Gentzkow, G. D., Iwasaki, S. D., Hershon, K. S., Mengel, M., Prendergast, J. J., Ricotta, J. J., et al. (1996). Use of dermagraft, a cultured human dermis, to treat diabetic foot ulcers. *Diab. Care* 19:350. doi: 10.2337/diacare.19.4.350

Gilpin, A., and Yang, Y. (2017). Decellularization strategies for regenerative medicine: from processing techniques to applications. *Biomed. Res. Int.* 2017:9831534.

Gonzalez, A. C., Costa, T. F., Andrade, Z. A., and Medrado, A. R. (2016). Wound healing - a literature review. *An Bras Dermatol.* 91, 614–620.

Griffin, D. R., Weaver, W. M., Scumpia, P. O., Di Carlo, D., and Segura, T. (2015). Accelerated wound healing by injectable microporous gel scaffolds assembled from annealed building blocks. *Nat. Mater.* 14, 737–744. doi: 10.1038/nmat4294

Griffiths, M., Ojeh, N., Livingstone, R., Price, R., and Navsaria, H. (2004). Survival of apligraf in acute human wounds. *Tissue Eng.* 10, 1180–1195. doi: 10.1089/ten.2004.10.1180

Guo, S., and Dipietro, L. A. (2010). Factors affecting wound healing. *J. Dent. Res.* 89, 219–229.

Gurtner, G. C., Werner, S., Barrandon, Y., and Longaker, M. T. (2008). Wound repair and regeneration. *Nature* 453, 314–321.

Hassan, W. U., Greiser, U., and Wang, W. (2014). Role of adipose-derived stem cells in wound healing. *Wound Repair Regen.* 22, 313–325. doi: 10.1111/wrr.12173

Helary, C., Zarka, M., and Giraud-Guille, M. M. (2012). Fibroblasts within concentrated collagen hydrogels favour chronic skin wound healing. *J. Tissue Eng. Regen. Med.* 6, 225–237. doi: 10.1002/term.420

Henderson, K. J., Zhou, T. C., Otim, K. J., and Shull, K. R. (2010). Ionically cross-linked triblock copolymer hydrogels with high strength. *Macromolecules* 14, 6193–6201. doi: 10.1021/ma100963m

Hu, M. S., Borrelli, M. R., Lorenz, H. P., Longaker, M. T., and Wan, D. C. (2018). Mesenchymal stromal cells and cutaneous wound healing: a comprehensive review of the background, role, and therapeutic potential. *Stem Cells Int.* 2018:6901983.

Hu, M. S., Walmsley, G. G., Barnes, L. A., Weiskopf, K., Rennert, R. C., Duscher, D., et al. (2017). Delivery of monocyte lineage cells in a biomimetic scaffold enhances tissue repair. *JCI Insight.* 5:2.

Hwang, C. M., Sant, S., Masaeli, M., Kachouie, N. N., Zamanian, B., Lee, S. H., et al. (2010). Fabrication of three-dimensional porous cell-laden hydrogel for tissue engineering. *Biofabrication* 2:035003. doi: 10.1088/1758-5082/2/3/035003

Isakson, M., de Blacam, C., Whelan, D., McArdle, A., and Clover, A. J. (2015). Mesenchymal stem cells and cutaneous wound healing: current evidence and future potential. *Stem Cells Int.* 2015:831095.

Janmey, P. A., Winer, J. P., and Weisel, J. W. (2009). Fibrin gels and their clinical and bioengineering applications. *J. R. Soc. Interface* 6, 1–10. doi: 10.1098/rsif.2008.0327

Jarbrink, K., Ni, G., Sonnergren, H., Schmidtchen, A., Pang, C., Bajpai, R., et al. (2017). The humanistic and economic burden of chronic wounds: a protocol for a systematic review. *Syst. Rev.* 6:15.

Kamoun, E. A., Kenawy, E. S., and Chen, X. (2017). A review on polymeric hydrogel membranes for wound dressing applications: PVA-based hydrogel dressings. *J. Adv. Res.* 8, 217–233. doi: 10.1016/j.jare.2017.01.005

Kang, J. I., and Park, K. M. (2021). Advances in gelatin-based hydrogels for wound management. *J. Mater. Chem. B* 9, 1503–1520. doi: 10.1039/d0tb02582h

Kannan, N., Nguyen, L. V., and Eaves, C. J. (2014). Integrin beta3 links therapy resistance and cancer stem cell properties. *Nat. Cell Biol.* 16, 397–399. doi: 10.1038/ncb2960

Kargozar, S., Singh, R. K., Kim, H. W., and Baino, F. (2020). "Hard" ceramics for "Soft" tissue engineering: paradox or opportunity? *Acta Biomater.* 115, 1–28. doi: 10.1016/j.actbio.2020.08.014

Kim, J. Y., and Suh, W. (2010). Stem cell therapy for dermal wound healing. *Int. J. Stem Cells* 3, 29–31. doi: 10.15283/ijsc.2010.3.1.29

Kim, W. S., Park, B. S., Park, S. H., Kim, H. K., and Sung, J. H. (2009). Antiwrinkle effect of adipose-derived stem cell: activation of dermal fibroblast by secretory factors. *J. Dermatol. Sci.* 53, 96–102. doi: 10.1016/j.jdermsci.2008.08.007

Koenen, P., Spanholtz, T. A., Maegele, M., Sturmer, E., Brockamp, T., Neugebauer, E., et al. (2015). Acute and chronic wound fluids inversely influence adipose-derived stem cell function: molecular insights into impaired wound healing. *Int. Wound J.* 12, 10–16. doi: 10.1111/iwj.12039

Kong, H. J., Alsberg, E., Kaigler, D., Lee, K. Y., and Mooney, D. J. (2004). Controlling degradation of hydrogels via the size of cross-linked junctions. *Adv. Mater.* 16, 1917–1921. doi: 10.1002/adma.200400014

Kosaraju, R., Rennert, R. C., Maan, Z. N., Duscher, D., Barrera, J., Whittam, A. J., et al. (2016). Adipose-Derived stem cell-seeded hydrogels increase endogenous progenitor cell recruitment and neovascularization in wounds. *Tissue Eng. Part A* 22, 295–305. doi: 10.1089/ten.tea.2015.0277

Kosaric, N., Kiwanuka, H., and Gurtner, G. C. (2019). Stem cell therapies for wound healing. *Expert Opin. Biol. Ther.* 19, 575–585.

Lee, K. Y., and Mooney, D. J. (2012). Alginate: properties and biomedical applications. *Prog. Polym Sci.* 37, 106–126. doi: 10.1016/j.progpolymsci.2011.06.003

Li, D., Wang, A., Liu, X., Meisgen, F., Grunler, J., Botusan, I. R., et al. (2015). MicroRNA-132 enhances transition from inflammation to proliferation during wound healing. *J. Clin. Invest.* 125, 3008–3026. doi: 10.1172/jci79052

Li, J., and Mooney, D. J. (2016). Designing hydrogels for controlled drug delivery. *Nat. Rev. Mater.* 1:16071.

Lian, X., Bao, X., Al-Ahmad, A., Liu, J., Wu, Y., Dong, W., et al. (2014). Efficient differentiation of human pluripotent stem cells to endothelial progenitors via small-molecule activation of WNT signaling. *Stem Cell Rep.* 3, 804–816. doi: 10.1016/j.stemcr.2014.09.005

Liu, W., Ma, K., Kwon, S. H., Garg, R., Patta, Y. R., Fujiwara, T., et al. (2017). The abnormal architecture of healed diabetic ulcers is the result of FAK degradation by calpain 1. *J. Invest. Dermatol.* 137, 1155–1165. doi: 10.1016/j.jid.2016.11.039

Ma, K., Kwon, S. H., Padmanabhan, J., Duscher, D., Trotsyuk, A. A., Dong, Y., et al. (2018). Controlled delivery of a focal adhesion kinase inhibitor results in accelerated wound closure with decreased scar formation. *J. Invest. Dermatol.* 138, 2452–2460. doi: 10.1016/j.jid.2018.04.034

Meier, K., and Nanney, L. B. (2006). Emerging new drugs for scar reduction. *Expert Opin. Emerg. Drugs* 11, 39–47. doi: 10.1517/14728214.11.1.39

Milan, P. B., Lotfibakhshaiesh, N., Joghataie, M. T., Ai, J., Pazouki, A., Kaplan, D. L., et al. (2016). Accelerated wound healing in a diabetic rat model using decellularized dermal matrix and human umbilical cord perivascular cells. *Acta Biomater.* 45, 234–246. doi: 10.1016/j.actbio.2016.08.053

Moon, K. C., Suh, H. S., Kim, K. B., Han, S. K., Young, K. W., Lee, J. W., et al. (2019). Potential of allogeneic adipose-derived stem cell-hydrogel complex for treating diabetic foot ulcers. *Diabetes* 68, 837–846.

Moreno-Arotzena, O., Meier, J. G., Del Amo, C., and García-Aznar, J. M. (2015). Characterization of fibrin and collagen gels for engineering wound healing models. *Materials (Basel)* 8, 1636–1651. doi: 10.3390/ma8041636

Murakami, K., Aoki, H., Nakamura, S., Nakamura, S., Takikawa, M., Hanzawa, M., et al. (2010). Hydrogel blends of chitin/chitosan, fucoidan and alginate

as healing-impaired wound dressings. *Biomaterials* 31, 83–90. doi: 10.1016/j.biomaterials.2009.09.031

Murphy, K. C., Whitehead, J., Zhou, D., Ho, S. S., and Leach, J. K. (2017). Engineering fibrin hydrogels to promote the wound healing potential of mesenchymal stem cell spheroids. *Acta Biomater.* 64, 176–186. doi: 10.1016/j.actbio.2017.10.007

Nafea, E. H., Marson, A., Poole-Warren, L. A., and Martens, P. J. (2011). Immunoisolating semi-permeable membranes for cell encapsulation: focus on hydrogels. *J. Control Release* 154, 110–122. doi: 10.1016/j.jconrel.2011.04.022

Nagamura-Inoue, T., and He, H. (2014). Umbilical cord-derived mesenchymal stem cells: their advantages and potential clinical utility. *World J. Stem Cells* 6, 195–202. doi: 10.4252/wjsc.v6.i2.195

Nicodemus, G. D., and Bryant, S. J. (2008). Cell encapsulation in biodegradable hydrogels for tissue engineering applications. *Tissue Eng. Part B Rev.* 14, 149–165. doi: 10.1089/ten.teb.2007.0332

Nussbaum, S. R., Carter, M. J., Fife, C. E., DaVanzo, J., Haught, R., Nusgart, M., et al. (2018). An Economic Evaluation of the Impact, Cost, and Medicare Policy Implications of Chronic Nonhealing Wounds. *Value Health* 21, 27–32. doi: 10.1016/j.jval.2017.07.007

Ogle, M. E., Doron, G., Levy, M. J., and Temenoff, J. S. (2020). Hydrogel culture surface stiffness modulates mesenchymal stromal cell secretome and alters senescence. *Tissue Eng. Part A* 26, 1259–1271. doi: 10.1089/ten.tea.2020.0030

Ott, H. C., Matthiesen, T. S., Goh, S. K., Black, L. D., Kren, S. M., Netoff, T. I., et al. (2008). Perfusion-decellularized matrix: using nature's platform to engineer a bioartificial heart. *Nat. Med.* 14, 213–221. doi: 10.1038/nm1684

Percival, S. L., and McCarty, S. M. (2015). Silver and alginates: role in wound healing and biofilm control. *Adv. Wound Care* 4, 407–414. doi: 10.1089/wound.2014.0541

Pittenger, M. F., Discher, D. E., Peault, B. M., Phinney, D. G., Hare, J. M., and Caplan, A. I. (2019). Mesenchymal stem cell perspective: cell biology to clinical progress. *NPJ Regen. Med.* 4:22.

Raje, N., Berdeja, J., Lin, Y., Siegel, D., Jagannath, S., Madduri, D., et al. (2019). Anti-BCMA CAR T-Cell therapy bb2121 in relapsed or refractory multiple myeloma. *N. Engl. J. Med.* 380, 1726–1737.

Razavi, M., and Thakor, A. S. (2018). An oxygen plasma treated poly(dimethylsiloxane) bioscaffold coated with polydopamine for stem cell therapy. *J. Mater. Sci. Mater. Med.* 29:54.

Reinke, J. M., and Sorg, H. (2012). Wound repair and regeneration. *Eur. Surg. Res.* 49, 35–43.

Rennert, R. C., Januszyk, M., Sorkin, M., Rodrigues, M., Maan, Z. N., Duscher, D., et al. (2016). Microfluidic single-cell transcriptional analysis rationally identifies novel surface marker profiles to enhance cell-based therapies. *Nat. Commun.* 7:11945.

Rocchi, A., Manara, M. C., Sciandra, M., Zambelli, D., Nardi, F., Nicoletti, G., et al. (2010). CD99 inhibits neural differentiation of human Ewing sarcoma cells and thereby contributes to oncogenesis. *J. Clin. Invest.* 120, 668–680. doi: 10.1172/jci36667

Rose, L. F., and Chan, R. K. (2016). The burn wound microenvironment. *Adv. Wound Care (New Rochelle)* 5, 106–118. doi: 10.1089/wound.2014.0536

Rugg-Gunn, P. J., Cox, B. J., Lanner, F., Sharma, P., Ignatchenko, V., McDonald, A. C., et al. (2012). Cell-surface proteomics identifies lineage-specific markers of embryo-derived stem cells. *Dev. Cell* 22, 887–901. doi: 10.1016/j.devcel.2012.01.005

Rustad, K. C., and Gurtner, G. C. (2012). Mesenchymal stem cells home to sites of injury and inflammation. *Adv. Wound Care (New Rochelle)* 1, 147–152. doi: 10.1089/wound.2011.0314

Rustad, K. C., Wong, V. W., Sorkin, M., Glotzbach, J. P., Major, M. R., Rajadas, J., et al. (2012). Enhancement of mesenchymal stem cell angiogenic capacity and stemness by a biomimetic hydrogel scaffold. *Biomaterials* 33, 80–90. doi: 10.1016/j.biomaterials.2011.09.041

Sadeghi-Avalshahr, A., Nokhasteh, S., Molavi, A. M., Khorsand-Ghayeni, M., and Mahdavi-Shahri, M. (2017). Synthesis and characterization of collagen/PLGA biodegradable skin scaffold fibers. *Regen. Biomater.* 4, 309–314. doi: 10.1093/rb/rbx026

Saghazadeh, S., Rinoldi, C., Schot, M., Kashaf, S. S., Sharifi, F., Jalilian, E., et al. (2018). Drug delivery systems and materials for wound healing applications. *Adv. Drug Deliv. Rev.* 127, 138–166. doi: 10.1016/j.addr.2018.04.008

Salehi, M., Ehterami, A., Farzamfar, S., Vaez, A., and Ebrahimi-Barough, S. (2020). Accelerating healing of excisional wound with alginate hydrogel containing naringenin in rat model. *Drug Deliv. Transl. Res.* 11, 142–153. doi: 10.1007/s13346-020-00731-6

Schaffer, J. L., Rizen, M., L'Italien, G. J., Benbrahim, A., Megerman, J., Gerstenfeld, L. C., et al. (1994). Device for the application of a dynamic biaxially uniform and isotropic strain to a flexible cell culture membrane. *J. Orthop. Res.* 12, 709–719. doi: 10.1002/jor.1100120514

Schultz, G. S., Chin, G. A., Moldawer, L., and Diegelmann, R. F. (2011). "Principles of wound healing," in *Mechanisms of Vascular Disease: A Reference Book for Vascular Specialists*, eds R. Fitridge and M. Thompson (Adelaide (AU): University of Adelaide Press).

Seliktar, D. (2012). Designing cell-compatible hydrogels for biomedical applications. *Science* 336, 1124–1128. doi: 10.1126/science.1214804

Silva, L. P., Pirraco, R. P., Santos, T. C., Novoa-Carballal, R., Cerqueira, M. T., Reis, R. L., et al. (2016). Neovascularization induced by the hyaluronic acid-based spongy-like hydrogels degradation products. *ACS Appl. Mater. Interfaces* 8, 33464–33474. doi: 10.1021/acsami.6b11684

Spalazzi, J. P., Doty, S. B., Moffat, K. L., Levine, W. N., and Lu, H. H. (2006). Development of controlled matrix heterogeneity on a triphasic scaffold for orthopedic interface tissue engineering. *Tissue Eng.* 12, 3497–3508. doi: 10.1089/ten.2006.12.3497

Srifa, W., Kosaric, N., Amorin, A., Jadi, O., Park, Y., Mantri, S., et al. (2020). Cas9-AAV6-engineered human mesenchymal stromal cells improved cutaneous wound healing in diabetic mice. *Nat. Commun.* 11:2470.

Stoica, A. E., Chircov, C., and Grumezescu, A. M. (2020). Hydrogel dressings for the treatment of burn wounds: an up-to-date overview. *Materials (Basel)* 25:13.

Strioga, M., Viswanathan, S., Darinskas, A., Slaby, O., and Michalek, J. (2012). Same or not the same? comparison of adipose tissue-derived versus bone marrow-derived mesenchymal stem and stromal cells. *Stem Cells Dev.* 21, 2724–2752. doi: 10.1089/scd.2011.0722

Sullivan, D. C., Mirmalek-Sani, S. H., Deegan, D. B., Baptista, P. M., Aboushwareb, T., Atala, A., et al. (2012). Decellularization methods of porcine kidneys for whole organ engineering using a high-throughput system. *Biomaterials* 33, 7756–7764. doi: 10.1016/j.biomaterials.2012.07.023

Tartarini, D., and Mele, E. (2015). Adult stem cell therapies for wound healing: biomaterials and computational models. *Front. Bioeng. Biotechnol.* 3:206. doi: 10.3389/fbioe.2015.00206

Tavakoli, S., and Klar, A. S. (2020). Advanced hydrogels as wound dressings. *Biomolecules* 11:10.

Thamm, O. C., Koenen, P., Bader, N., Schneider, A., Wutzler, S., Neugebauer, E. A., et al. (2015). Acute and chronic wound fluids influence keratinocyte function differently. *Int. Wound J.* 12, 143–149. doi: 10.1111/iwj.12069

Thompson, A. A., Walters, M. C., Kwiatkowski, J., Rasko, J. E. J., Ribeil, J. A., Hongeng, S., et al. (2018). Gene therapy in patients with transfusion-dependent beta-thalassemia. *N. Engl. J. Med.* 378, 1479–1493.

Trainor, N., Pietak, A., and Smith, T. (2014). Rethinking clinical delivery of adult stem cell therapies. *Nat. Biotechnol.* 32, 729–735. doi: 10.1038/nbt.2970

Uematsu, K., Hattori, K., Ishimoto, Y., Yamauchi, J., Habata, T., Takakura, Y., et al. (2005). Cartilage regeneration using mesenchymal stem cells and a three-dimensional poly-lactic-glycolic acid (PLGA) scaffold. *Biomaterials* 26, 4273–4279. doi: 10.1016/j.biomaterials.2004.10.037

Williams, D. F. (2009). On the nature of biomaterials. *Biomaterials* 30, 5897–5909. doi: 10.1016/j.biomaterials.2009.07.027

Wong, V. W., Rustad, K. C., Akaishi, S., Sorkin, M., Glotzbach, J. P., Januszyk, M., et al. (2011a). Focal adhesion kinase links mechanical force to skin fibrosis via inflammatory signaling. *Nat. Med.* 18, 148–152. doi: 10.1038/nm.2574

Wong, V. W., Rustad, K. C., Galvez, M. G., Neofytou, E., Glotzbach, J. P., Januszyk, M., et al. (2011b). Engineered pullulan-collagen composite dermal hydrogels improve early cutaneous wound healing. *Tissue Eng. Part A* 17, 631–644. doi: 10.1089/ten.tea.2010.0298

Wong, V. W., Rustad, K. C., Glotzbach, J. P., Sorkin, M., Inayathullah, M., Major, M. R., et al. (2011c). Pullulan hydrogels improve mesenchymal stem cell delivery into high-oxidative-stress wounds. *Macromol. Biosci.* 11, 1458–1466.

Wu, Y., Chen, L., Scott, P. G., and Tredget, E. E. (2007). Mesenchymal stem cells enhance wound healing through differentiation and angiogenesis. *Stem Cells* 25, 2648–2659. doi: 10.1634/stemcells.2007-0226

Xiang, J., Wang, S., He, Y., Xu, L., Zhang, S., and Tang, Z. (2019). Reasonable glycemic control would help wound healing during the treatment of diabetic foot ulcers. *Diab. Ther.* 10, 95–105. doi: 10.1007/s13300-018-0536-8

Xin, S., Gregory, C. A., and Alge, D. L. (2020). Interplay between degradability and integrin signaling on mesenchymal stem cell function within poly(ethylene glycol) based microporous annealed particle hydrogels. *Acta Biomater.* 101, 227–236. doi: 10.1016/j.actbio.2019.11.009

Xu, X., Xia, X., Zhang, K., Rai, A., Li, Z., Zhao, P., et al. (2020). Bioadhesive hydrogels demonstrating pH-independent and ultrafast gelation promote gastric ulcer healing in pigs. *Sci. Transl. Med.* 26:12.

Yang, C., Tibbitt, M. W., Basta, L., and Anseth, K. S. (2014). Mechanical memory and dosing influence stem cell fate. *Nat. Mater.* 13, 645–652.

Yang, L., Chueng, S. D., Li, Y., Patel, M., Rathnam, C., Dey, G., et al. (2018). A biodegradable hybrid inorganic nanoscaffold for advanced stem cell therapy. *Nat. Commun.* 9:3147.

Yao, L., Bestwick, C. S., Bestwick, L. A., Maffulli, N., and Aspden, R. M. (2006). Phenotypic drift in human tenocyte culture. *Tissue Eng.* 12, 1843–1849.

You, H. J., and Han, S. K. (2014). Cell therapy for wound healing. *J. Korean Med. Sci.* 29, 311–319.

Youngblood, R. L., Truong, N. F., Segura, T., and Shea, L. D. (2018). It's all in the delivery: designing hydrogels for cell and non-viral gene therapies. *Mol. Ther.* 26, 2087–2106.

Zakrzewski, W., Dobrzynski, M., Szymonowicz, M., and Rybak, Z. (2019). Stem cells: past, present, and future. *Stem Cell Res. Ther.* 10:68.

Zhang, L., Liu, J., Zheng, X., Zhang, A., Zhang, X., and Tang, K. (2019). Pullulan dialdehyde crosslinked gelatin hydrogels with high strength for biomedical applications. *Carbohydr. Polym.* 216, 45–53.

Zhang, M., and Zhao, X. (2020). Alginate hydrogel dressings for advanced wound management. *Int. J. Biol. Macromol.* 162, 1414–1428.

Zhang, Z., Li, Z., Li, Y., Wang, Y., Yao, M., Zhang, K., et al. (2020). Sodium alginate/collagen hydrogel loaded with human umbilical cord mesenchymal stem cells promotes wound healing and skin remodeling. *Cell Tissue Res.* 383, 809–821.

Zhu, J., and Marchant, R. E. (2011). Design properties of hydrogel tissue-engineering scaffolds. *Expert Rev. Med. Dev.* 8, 607–626.

Zhu, Z., Ding, J., and Tredget, E. E. (2016). The molecular basis of hypertrophic scars. *Burns Trauma.* 4:2.

Conflict of Interest: The authors declare that the research was conducted in the absence of any commercial or financial relationships that could be construed as a potential conflict of interest.

Advantages of publishing in Frontiers

OPEN ACCESS
Articles are free to read for greatest visibility and readership

FAST PUBLICATION
Around 90 days from submission to decision

HIGH QUALITY PEER-REVIEW
Rigorous, collaborative, and constructive peer-review

TRANSPARENT PEER-REVIEW
Editors and reviewers acknowledged by name on published articles

Frontiers
Avenue du Tribunal-Fédéral 34
1005 Lausanne | Switzerland

Visit us: www.frontiersin.org
Contact us: frontiersin.org/about/contact

REPRODUCIBILITY OF RESEARCH
Support open data and methods to enhance research reproducibility

DIGITAL PUBLISHING
Articles designed for optimal readership across devices

FOLLOW US
@frontiersin

IMPACT METRICS
Advanced article metrics track visibility across digital media

EXTENSIVE PROMOTION
Marketing and promotion of impactful research

LOOP RESEARCH NETWORK
Our network increases your article's readership